I, Qionger He, declare that the work presented in this thesis is my own. Where information has been derived from other sources, I confirm that this has been indicated in the thesis.

Rebound potentiation: long-term potentiation of inhibitory transmission at cerebellar interneuron-Purkinje cell synapses

A thesis submitted for the Degree of Doctor of Philosophy at UCL

By

Qionger He, B.Sc.(Hons.)

Department of Neuroscience,
Physiology and Pharmacology,
UCL
Gower Street, London
WC1E 6BT

ProQuest LLC
789 East Eisenhower Parkway
P.O. Box 1346
Ann Arbor, MI 48106-1346

ASTRACT

Rebound potentiation (RP) is triggered by strong climbing fibre (CF) stimulated depolarization of postsynaptic Purkinje cells (PC) in the cerebellum. Subsequent Ca^{2+} influx through the activation of voltage gated calcium channels (VGCC) and further Ca^{2+} release from intracellular stores synergise to activate Ca^{2+} dependent kinase pathway resulting in the manifestation of a persistent enhancement of γ aminobutryic acid type A receptor ($GABA_AR$) mediated current between presynaptic interneurons (IN) and postsynaptic PCs.

In our study, we first discovered that different profiles for RP can be elicited using different latencies between the formation of whole cell configuration and stimulus application. This is possibly due to the disruption of the innate physiological state of the PC, but also unveiled a possible early and phase of RP.

We confirmed that the induction and maintenance of RP depends on Ca^{2+}/Camodulin-dependent kinase II (CaMKII), and revealed a role for protein tyrosine kinase (PTK) by applying a selection of inhibitors (CaMKIINtide and genistein). These two kinases may work through two inter-dependent pathways, αCaMKII mediated potentiation of inhibition appeared to be dependent on the PTK activity.

Suppression of RP by inhibitors of exocytosis revealed that $GABA_AR$ insertion is the underlying mechanism of rebound potentiation, which may occur downstream of receptor phosphorylation by kinases.

Using transgenic mice, we verified that the α1 subunit is essential for mediating the phasic inhibition observed in PC; and that β2 subunit containing receptors underlie the large amplitude, fast rise time miniature inhibitory postsynaptic currents (mIPSC). They are also implicated in the induction of RP as β2-/- animals exhibited impaired RP. Thirdly, mutation of two tyrosine residues (Y365 Y367), on the γ2 subunit known to be phosphorylated by PTK, delivered a rebound depression (RD) of inhibition. Hence, we conclude that these two tyrosine residues determine the polarity of the plasticity.

Taken overall, the phenomenon of RP involves at least two protein kinases and it is manifest by the insertion of $GABA_ARs$ at inhibitory synapses.

ACKNOWLEDGEMENT

I would like to express my gratitude to my supervisor, Prof. Trevor G. Smart, for his help and guidance throughout my study. I am also grateful for the support I received from colleagues, in particular Dr. Ian C. Duguid, for introducing me to the world of rebound potentiation, and Dr. Phil Thomas, Dr Catriona Houston, Dr. Megan Wilkins, Dr Martin Mortensen, Dr Alastair Hosie, Ms Helena De Sliva and Mr Mike Lumb, for performing the genotyping on transgenic mice.

I would also like to thank Dr Verena Tretter, for the generous gift of the $\gamma 2$ subunit mutant mice.

My friends and fellow students at UCL have also played a huge part in my life as a PhD student. I would like to thank Miss Rugina Ali, Dr Jan Hendrich, Mr Toby Collins and Miss Tanya small, in particular.

Finally, I would like to dedicate my work to my parents. This work was funded by the Medical Research council.

CONTENTS:

Chapter 3

CHARACTERISATION OF REBOUND POTENTIATION

Chapter 4

PHOSPHORYLATION SIGNALLING PATHWAYS FOR REBOUND POTENTIATION

List of Figures

Chapter 1

Chapter 2

Chapter 3

Chapter 4

Chapter 5

Chapter 6

List of Tables

Abbreviation

2-AG, 2-arachidonoylglycerol; **AC,** adenylate cyclase; **aCSF,** artificial cerebrospinal fluids; **AHP,** after-hyperpolarisation; **AID,** autoinhibitory domain; **AMPA,** α-amino-3-hydroxy-5-methyl-4-isoxazolepropionic acid; **AKAP**, A-kinase anchoring protein; **AP-1/2,** clathrin adaptor protein 1/2; **ARF,** ADP-ribosylation factor; **BAPTA,** 1,1-Bis(2-aminophenoxy)ethane-*N,N,N',N'*-tetraacetic acid; **BC,** basket cell; **BDNF,** brain-derived neurotrophic factor; **BZ,** benzodiazepine; **BFA,** Brefeldin A; **BIG2,** brefeldin A-inhibited GDP/GTP exchange factor 2; **GEF,** GDP-GTP exchange factor; **BoNT-B,** Botulinum toxin light chain B; **CB1,** cannabinoid receptor 1; **CBD,** calmdolin binding domain; **CD4**, cluster of

differentiation molecule 4; **CaM,** calmodulin; **CaMKII,** Calcium/Calmodulin-dependent protein kinase; **CF,** climbing fibre; **CMZ,** Calmidazolium; **CNS,** central nervous system; **DARPP-32,** dopamine- and cAMP-regulated phosphoprotein; **DCN,** deep cerebellar nuclei; **DPI,** depolarisation induced potentiation of inhibition; **DSI,** depolarisation induced suppression of inhibition; **EGTA,** Ethylene glycol-bis(2-aminoethylether)- *N,N,N',N'*-tetraacetic acid; **EPSC,** excitatory postsynaptic current; **ER,** endoplasmic reticulum; **FITC,** fluorescein-isothiocyanate; **GABA,** γ-aminobutyric acid; **$GABA_AR$,** $GABA_A$ receptor; **$GABA_BR$,** $GABA_B$ receptor; **GABARAP,** $GABA_AR$ associated protein; **GAD 65**, GABA biosynthesis enzyme glutamic acid; **GAT-1,** GABA transporter-1; **GC,** granule cell; **GCL,** Granule cell layer of cerebellum; **GDP-β-S,** Guanosine 5′-[β-thio]diphosphate; **GluR1/2/δ2,** glutamate receptor (AMPA) subunit 1/2/δ2; **GODZ,** Golgi apparatus specific protein; **GRIF-1,** $GABA_AR$ interacting factor-1; **HAP-1,** Huntingtin-Associated protein 1; **HEK,** human embryonic cell; **HEPES,** 4-(2-hydroxyethyl)-1-piperazineethanesulfonic acid; **ICL,** intracellular loop; **IN,** interneuron; **LTD,** long term depression; **LTP,** long term potentiation; **MAP,** microtubule-associated proteins; **MAPK,** mitogen-activated protein kinase; **MF,** mossy fibre; **mGluR1,** metabotropic glutamate receptor 1; **m/sIPSC,** miniature/spontaneous inhibitory postsynaptic current; **ML,** molecular layer of cerebellum; **NEM** *N*-ethylmaleimide; **NMDA**, N-methyl-D-aspartic acid; **NR2A/B,** NMDA receptor subunit 2A/B; **NSF,** *N*-ethylmaleimide sensitive factor; **NSNA,** Non-Stationary Noise Analysis; **ODA,** okadaic acid; **PC,** Purkinje cell; **PCL,** Purkinje cell layer of cerebellum; **PF,** parallel fibre; **PI3K,** phosphatidylinositol 3-kinase; **PKA,** cAMP-dependent protein kinase; **PKB/C,** protein kinases B/C; **PKG,**

cGMP-dependent protein kinase; **PLC,** phospholipase C; **Plic1/2,** protein that link integrin-associated protein with the cytoskeleton 1/2; **PMCA pump** , plasma membrane Ca^{2+}–ATPase pump; **PP1/2,** protein phosphatase 1/2; **PP2B,** protein phosphatase 2B, calcineurin; **PRIP-1/2,** PLC-related inactive protein type 1/2; **PSD** postsynaptic density; **PTK,** protein tyrosine kinase; **PTP,** protein tyrosine phosphatase; **PV,** parvalbumin; **Rab; RACK,** receptor for activatied C kinase; **RP,** rebound potentiation; **RyR1-3,** ryanodine-sensitive receptor 1-3; **SC,** stellate cell; **SCS,** salicylidene salicylhydrazide; **SERCA,** sarco-endoplasmic reticulum Ca^{2+}–ATPase pump ; **siRNA,** short interference RNA; **TM,** transmembrane domain; **TGN,** trans-Golgi Network; **TRITC,** tetramethylrhodamine isothiocyanate; **VGCC,** voltage gated calcium channel; **wt,** wild-type mice.

For more specific abbreviations, refer to text.

Aim

The aim of this thesis study is to understand the mechanisms that underlie the phenomenon of RP. There are three major objectives.

Firstly, to clarify which intracellular signalling pathways lead to the enhancement of inhibitory synaptic transmission during RP. In particular, identifying the kinases involves in RP.

Secondly, what is the cellular mechanism underlying RP. For example, is $GABA_AR$ channel function affected, or is there a change in the number of active cell surface $GABA_ARs$.

Finally, this study addresses which types of $GABA_AR$ subunits are expressed in PCs and how these are involved in the manifestation of RP.

Chapter 1

Introduction

1.1 Cerebellum: anatomical and functional basis

1.1.1 Cerebellum: overview

Taking up 10% of the total brain volume, a full understanding of cerebellar function remains a challenge, as it receives sensory input but gives no discrimination. Cerebellar function was conventionally thought to underlie voluntary movement, gait, posture, speech, and motor tasks, with potential cognitive implications (Rapoport et al., 2000). In spite of this, cerebellar lesions cause jerky, erratic, and uncoordinated movements, but no lasting paralysis due to its recuperative ability (Ghez et al. 1991).

The cerebellum has the highest neuronal density in the central nerve system (CNS), accommodating more than half of the total neuron in the brain. Located at the posterior cranial cortex, anchored by cerebellar peduncles, dorsal to pons and medulla, it receives inputs from many areas of the neuraxis and projects to descending motor pathways, including the red nucleus of the brain stem, the primary cortex (via dorsal thalamus) and the premotor cortex (Fig 1.1). The three pairs of cerebellar peduncles, inferior, middle *(brachium pontis)* and superior *(brachium conjunctivum)*, connect the cerebellum to the brain cortex. The inferior and middle peduncles confer the majority of sensory information from afferent fibres. Morphologically, two rostral-caudal grooves divide the cerebellum into three parts: a narrow midline vermis (derived from corpus cerebelli), and two expansive lateral hemispheres unique to mammals. The auricles give rise to the most lateral

flocculus (also present in non-mammals). The cerebellar cortex is highly convoluted, with folia and fissures, further separating the cerebellum into three lobes and ten recognised lobules (Ghez et al., 1991).

Three functional divisions make up the cerebellum: the spinocerebellum, the cerebrocerebellum and the vestibulocerebellum. They receive inputs from various regions and send outputs to the four different bilaterally-paired deep cerebellar nuclei (DCN) neurons, which in turn connect to lower motor centres. DCN neurons receive inputs from the principle neurons of the cerebellum, the PC. The three functional divisions share the same precisely arranged internal neuronal organisation: the outermost molecular layer, the Purkinje cell layer, and the innermost Granule cell layer (Fig 1.2).

Fig 1.1. The anatomical structure of cerebellum, functional divisions and inputs (Modified from Ghez., 1991)

1.1.2 The molecular layer (ML)

This outer layer contains mostly axons and processes from neurons in the inner core of the cerebellum. PC dendrites extend into the ML and receive multiple inputs. Parallel fibres (PF), bifurcated from the ascending granule cell axons, run perpendicular to the long axis of the folium and synapse with thousands of PCs and interneurons, where they release glutamate as the neurotransmitter. CF, originated from the inferior olive, entwines with the PC dendrites in a 1:1 ratio, although one CF makes multiple synapses with a target PC. The CF-PC synapse is known to be the

strongest excitatory connection in the CNS, with ~1500 release sites, and triggers powerful depolarisations in PCs via α-amino-3-hydroxy-5-methyl-4-isoxazolepropionic acid (AMPA) receptor activation. As a result, complex spikes arise with a fast Na^+ component and a slower multiple Ca^{2+}, Na^+ current in PCs, accompanied by large Ca^{2+} transient in the dendritic tree (Daniel et al., 1998; Maeda et al., 1999; Stuart and Hausser, 1994). The ML also contains the bodies of interneuron basket cells (BC) and stellate cells (SC). The latter lie in the outer molecular layer and synapse onto the distal PC dendrites. The inhibition from SCs is less powerful and only influences the integration of local synaptic activities where its axon terminates (Ghez et al., 1991). On the other hand, BCs lie closer to the border of the molecular and Purkinje cell layers, synapsing in the somatodendritic region. The BC-PC synapse is one of the strongest inhibitory synapses, with ability to turn-off PC spike firing (Fig 1.2).

Fig 1.2 The neurons of cerebellum and the internal circuit. The box insert shows the presumed $GABA_AR$ subunits expression in each cell type. (Modified from Haines *et al.*, 1997)

Bergmann glial cell processes span the entire thickness of the ML, with somata aligning with PCs. Their extended radial fibres enwrap synapses on PCs dendrites. They provide important guidance for young granule cell migration away from the external granule cell layer. They also support neuronal survival and functioning (Grosche et al., 2002).

1.1.3 The Purkinje Cell layer

In the middle of the cerebellum, lies the single uniform layer of large (50-80μm) PC cell bodies. They are the sole output neurons of the cerebellum, utilising the inhibitory neurotransmitter γ-aminobutyric acid (GABA) to suppress the firing of DCN neurons. PCs extend an elaborate dendritic tree into the ML. This planar, fan-shaped dendritic tree receives synaptic terminals, concentrated mainly on the secondary and tertiary dendrites. The development of spines depends on the presence of spontaneous electrical activity received from the inferior olive via the CFs, giving rise to smooth branchlets and spiny branchlets (Harvey et al., 2005). The PC axons descend into the granule cell layer and may form recurrent collaterals before reaching the cerebellar nuclei as cerebellar corticonuclear fibres (Ghez., 1991).

1.1.4 The Granule cell Layer (GCL)

The small (5-8μm) but abundant interneuron, granule cells (GC), extend four dendrites, which ramify in the vicinity of their cell bodies. Their axons bifurcate into ML and synapse with PCs on the spiny branchlets and with ML interneurons, where they convey excitatory transmission. The larger (18-25μm) Golgi cells also inhabit the GCL, located close to PC soma with dendrites shooting up to the ML. Their axons synapse with granule cells within the GCL to inhibit their activities, indirectly dampening PC excitation. Minor interneurons, the GABAergic/glycinergic Lugaro cells, reside just below PCs with dendrites confined within the GCL. They innervate PCs, Golgi cells and interneurons in the ML. Globular cells have both their axons and dendrites in the ML (Simat et al., 2007). The excitatory interneuron, unipolar brush cells are unevenly distributed in the GCL,

forming intracortical rosettes and glomeruli with mossy fibre (MF) terminals, in which they synapse with granule cells and other brush cells to amplify the excitatory effects of the afferent MFs (Dino et al., 2000).

1.1.5 Afferent and efferent subdivisions of Cerebellum

In the cerebellum, two large fibre bundles carry the majority of afferent projections: the inferior and middle cerebellar peduncles. The largest afferent inputs, the MFs, are derived from four sources: the limbic function associated spinocerebellar pathway, from the spinal cord and the external cuneate nuclei, projecting to the anterior lobe (lobules I-V) with in the vermis; the vision related pontocerebellar projection, terminating in lobule VI and VII, relaying information for the planning, initiation and timing of movements; vestibulocerebellar projections, regulating the vestibular reflexes; and reticulocerebellar projections (Ghez., 1991). In general, descending pontocerebellar MFs are ipsilateral while the rest, ascending fibre projections are contralateral. MF terminals form rosettes and glomeruli, encompassing glutamergic synapses with granule cells (Voogd and Glickstein, 1998).

The other major afferents, the CFs, cross the midline at the base of the brainstem into the inferior peduncle then transverse the GCL to synapse onto the proximal smooth branchlets of PCs. The olivecerebellar projection displays parasagittal band organisation, with specific connection to the matching PCs. This connection undergoes developmental activity dependent elimination to sculpt the innervations of mature PCs in adults (Armstrong and Hawkes, 2000).

MF and CF collaterals also project directly onto the cerebellar and vestibular nuclei, overlapping with the ipsilaterally terminated PC axons (Ito, 2001).

1.1.6 Development of morphology and electrical behaviour of PCs

The function of the cerebellum in posture and balance control, fine coordination of motor movement, ocular adaptation and learning of conditioned behaviour, is widely regarded (Middleton and Strick, 1998). PCs integrate multimodal afferent inputs and coordinate the execution of commands.

PCs exhibit two types of excitatory currents, mainly mediated by postsynaptic AMPAR. CF stimulation triggers an all-or-none excitatory current in the PCs. It is estimated that each PC arbour, on average contains 111 CF terminal branches, running a total length of 1535 μm, yielding 288 varicosities, each creating 1-6 synapses with the stubby spines on primary, secondary and tertiary dendrites (Strata and Rossi, 1998). This potentially creates up to 1500 release sites between a CF-PC pair. The majority of these synapses (88%) are confined to the two distal compartments of the dendrites. PF inputs typically form 80000~200000 synapses with PCs on the distal dendrites, generating a smooth synaptic current in proportion to the stimulation strength (Konnerth et al., 1990; Strata and Rossi, 1998).

These two excitatory inputs evoke separate firing patterns of PC. High frequency (> 100Hz) spontaneous simple spikes occur in response to multiple PF excitations during movement. Fast simple spikes are solely mediated by the somatic voltage dependent Na^+ currents. The more intense

singular CF stimulation, generates complex spikes with frequency of 1-2Hz on average. They are shaped by AMPAR mediated depolarisation and subsequent Na^+ action potential, which initiates in the axonal region and passively spreads into the dendritic tree (Khaliq and Raman, 2005; Stuart and Hausser, 1994). Complex spikes consist of a large amplitude Na^+ dependent action potential, followed by high frequency oscillatory spikelets. The spikelets are triggered by activation of dendritic AMPARs, which depolarise PCs to the threshold for voltage gated Ca^{2+} channels (VGCC), generating reverberating Ca^{2+} currents in the dendrites (Llinas and Sugimori, 1980). The Ca^{2+} currents in turn activate both Ca^{2+} dependent large (BK) and small conductance (SK) K^+ channels resulting in the spike after-hyperpolarisation (AHP) (Edgerton and Reinhart, 2003). This prolongs Ca^{2+} induced K^+ hyperpolarisation, serving as a regulatory mechanism, keeping the orderly firing of PCs, by counterbalancing the fast Na^+ action potential, as well as a secondary slow non-inactivating Na^+ current (Llinas and Sugimori, 1980). The complex spikes originated from CF-PC activity may provide a periodic clock for the coordinated movement or the long-term modification of cerebellar activities (Kitazawa and Wolpert, 2005).

The structural and functional development of PCs starts postnatally and rapidly reaches completion in three stages. During the early postnatal (P0~9) stage, PCs exhibit short multipolar dendrites and immature Na^+-spike discharges. Between the second and third postnatal weeks (P12~18), their maturation accelerates and repetitive Na^+-Ca^{2+} bursts emerge, accompanied with the expansion of the dendritic tree. The last stage between P18 to P90, cell outputs undergo final refinements. In the first postnatal week, L-type Ca^{2+} channels dominate in the somatic region, and account for > 60% of the

Ca^{2+} influx, underlying the low-threshold spike bursts at the onset of depolarising current injections. The second week sees an increase of P/Q- (predominantly in the dendrites) and R type Ca^{2+} channels, the former instigates the Ca^{2+} - Na^{+} bursts at the end of the second postnatal week. High threshold P/Q type channel expression is maintained into adulthood and constitutes ~90% of all Ca^{2+} currents. These currents also terminate the Ca^{2+} - Na^{+} spikes by subsequent activation of Ca^{2+} - activated K^{+} currents, participating in the fast AHP following mature Na^{+} currents. The levels of L and N type Ca^{2+} channels decrease with age, and each contributes to ~5% of the Ca^{2+} currents in mature PCs. Low threshold T type Ca^{2+} channels are present at all ages (Llinas and Sugimori, 1980).

The appearance of Ca^{2+} - Na^{+} bursts and Ca^{2+} spikes alters the intrinsic conductance pattern of the soma-dendritic region, and may contribute to age-dependent changes in information processing, as a basis of learning and memory formation. Increase in proficiency of postural balance control, general locomotor activity and limbic coordination, as well as eye blinking response takes place between the second and third postnatal week, coinciding with the peak growth of PC dendrites. Associative learning only materializes after full maturation of PC input-output relations. Final refinement of distal dendrites lasts up to two mouths, and may contribute to high resolution tuning of cell outputs or higher order synaptic plasticity (McKay and Turner, 2005).

The synchronous and rhythmic CF inputs originate from the inferior olive, suggesting that they may serve as a motor timing device and an error detector during movement (Hansel and Linden, 2000). On the other hand, PF

inputs drive feed-forward inhibition onto PCs through interneurons, sharply curtailing excitatory postsynaptic potentials (EPSPs) to increase the precision of the resultant action potentials. This feed-forward inhibition limits the summation of EPSPs to a narrow window of 1-2 ms, and inhibits asynchronous EPSPs for up to 30 ms. This microcircuitry orchestrates synaptic integration and temporal precision for the coincidental detection of CF and PF triggered spikes in PCs, ensuing the deliverance of PF LTD (Mittmann et al., 2005).

The inhibitory inputs PCs receive come from interneurons, BC and SC (Eccles et al., 1966). BCs and SCs have different rates of maturation. Between P9-11, SC differentiation is still on-going, hence most inhibitory currents are presumably from functional BCs. From the age of P12-15, the ML expands and functional SCs emerge. Mature PCs exhibit a broad range of IPSC amplitudes of up to 2nA, in response to spontaneously firing presynaptic interneurons (Vincent and Marty, 1996). The size of spontaneous inhibitory postsynaptic currents (sIPSC) amplitude is a function of the proximity of the presynaptic inputs. The larger amplitude, more variable sIPSCs originate from BC inputs (Vincent and Marty, 1996). Concerted multivescular release occurs at both BC and SC terminals, raising the prospect of regenerative Ca^{2+} signals in the presynaptic terminals in response to action potential firing (Auger et al., 1998). Action potential-independent miniature IPSCs also exhibited unusually large amplitudes (mean amplitude > 100pA), with a frequency around 4 Hz and highly skewed amplitude distribution (Llano et al., 2000). These large amplitude mIPSCs (lamIPSCs) are also believed to result from by multivesicular release of neurotransmitter vesicles controlled by presynaptic ryanodine-

sensitive Ca^{2+} stores. The BC terminals are particularly enriched with these Ca^{2+} stores and yield extremely synchronized, fast rise-time postsynaptic mIPSCs with amplitudes in the nanoamp range (Conti et al., 2004).

1.2 $GABA_AR$ structure, function and distribution

The majority of fast inhibitory transmission in the brain is mediated by GABA activated $GABA_A$ receptors ($GABA_AR$). These receptors facilitate the fast inhibitory currents in mature neurons by the opening of ligand-gated anion channels upon GABA binding, allowing Cl^- and partially HCO_3^- ions across the membrane (Bormann, 2000a; Farrant and Nusser, 2005). In juveniles, the $GABA_AR$ mediated transmission is excitatory, due to the HCO_3^- permeability and an outward Cl^- gradient, which is gradually reversed by the expression of K^+-Cl^- co-transporter KCC2 (Ben Ari, 2002; Obata et al., 1978)

Slow inhibitory transmission is manifested by metabotropic $GABA_B$ receptors coupled to $G_{i/o}$ protein/cAMP pathway, and inhibits the VGCCs to suppress the presynaptic release of neurotransmitter. In addition $GABA_B$ receptors can hyperpolarise the membrane potential by increasing K^+ conductance (Dutar and Nicoll, 1988; Mehta and Ticku, 1999).

Dysfunctional GABAergic transmission could lead to neurological and mental disorders such as epilepsy, anxiety, Angelman's syndrome and schizophrenia (Luscher and Keller, 2004). The pivotal function of $GABA_AR$ receptor makes it an important target for therapeutic drugs such as benzodiazepines, barbiturates, neurosteroids, ethanol, some anticonvulsants and general anaesthetics (Mehta and Ticku, 1999).

1.2.1 $GABA_AR$ structure and subunits

Structurally, $GABA_AR$ belongs to the pentameric Cys-loop ligand-gated ion channel superfamily. Other members include nicotinic acetylcholine, $5HT_3$ and glycine receptors (Schofield et al., 1987; Smith and Olsen, 1995). To date, 19 $GABA_AR$ subunit genes have been identified: α(1-6), β(1-3), γ(1-3), δ, ϵ, θ, π, ρ(1-3), with an estimated average molecular weight around 50,000 daltons (Barnard et al., 1998; Bonnert et al., 1999; Korpi et al., 2002; Whiting et al., 1999). Although individual subunits can form homomeric channels when expressed in *Xenopus* oocytes, only the ρ subunit is known to form homomeric channels *in vivo,* expressed predominantly in the retina (Bormann, 2000; Drew C.A., 1984). Alternative splicing adds to receptor subunit diversity. The most well known is the two splice variants of the γ2 subunits, the longer isoform γ2L subunit has 8 extra amino acids inserted at position 338-345 (Moss and Smart, 1996). Additional splice variants were discovered amongst other subunits, such as the α6 and β2 subunits, although their functions remain unclear (Mehta and Ticku, 1999).

Each receptor subunit contains an extracellular N terminal domain, with various glycosylation sites, and a disulphide Cys-Cys bridge. This is followed by four hydrophobic transmembrane domains TM1-4, with TM2 forming the lining of the integral ion channel (Barnard et al., 1987). On the cytosolic side is a large intracellular loop (ICL) linking the TM3 and TM4, which contains various consensus sites for phosphorylation in the β and γ subunits (McDonald and Moss, 1997; Moss and Smart, 1996). The C terminal is predicted to end on the extracellular side of the membrane (Fig 1.3) (Luscher and Keller, 2004).

Receptor subunits co-assemble into hetero-pentamers. Despite the potential for significant diversity of receptor subtypes, in reality, the extent of different subunit combinations is likely to be less than 30 (Whiting et al., 1995).

The most common naturally-occurring $GABA_AR$ consists of two copies of α and β subunits, with one copy of the γ subunit. The δ subunit substitutes for the γ subunit in some receptors. Both α and γ subunits are required for benzodiazepine (BZ) sensitivity, with α subunits further conferring the specificity of the binding for different classes of BZs. For example, the α1 subunit-containing receptors have sensitivity for Class I BZ, owing to a glycine at position 201 near the N-terminal, which is replaced with a glutamate in α2, 3, and 5 subunit, with Class II BZs specificity (Luddens et al., 1995). The BZ binding site is believed to localize at the border between α and γ subunits (Zezula et al., 1996).

High affinity GABA binding sites are postulated to reside at the interface between α and β subunits (Pregenzer et al., 1993; Zezula et al., 1996). Between the disulphide loop and TM1 in the β2 subunit, two domains modulate GABA mediated activation, as mutation of Tyr 157 or Tyr 195 to Phe, and Thr160 or Thr202 to Ser, reduced binding affinity for GABA (Amin and Weiss, 1993; Smith and Olsen, 1995)

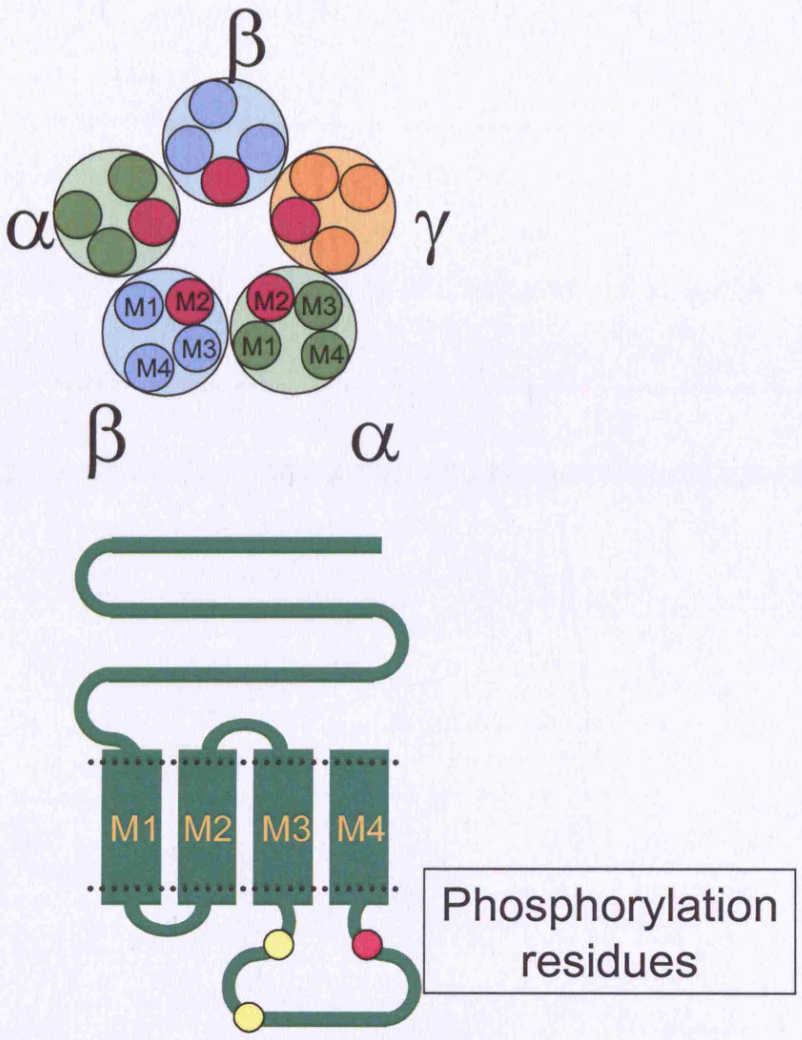

Fig 1.3. The topology of the $GABA_AR$. Top: the oligomeric assembly of 5 $GABA_AR$ subunits in the most common composition in the CNS. Bottom: membrane topology of a single subunit. The major ICL contains multiple phosphorylation sites.

1.2.2 $GABA_AR$ subunit expression and distribution in the cerebellum

In situ hybridisation identified α1 as the most prevalent subunit in the brain followed by α2 and α3 subunits (Laurie et al., 1992b). Immunohistochemistry confirmed the α1 subunit expression was highest in the cerebellum, and the opposite was observed in hippocampus where α1

subunit levels were low and α2-5 subunits dominated (Pirker et al., 2000). The α2-5 subunits were thought to be absent from cerebellum, although some evidence suggested that α2 and α3 subunits may be expressed in juvenile cerebellum (Takayama and Inoue, 2004). The α6 subunit has only been identified in cerebellar granule cells to participate in both phasic and tonic inhibition (Khan et al., 1996a; Nusser et al., 1998). The β1 and β3 subunit distributions follow the order of hippocampus > cortex > cerebellum, whilst the β2 subunit expression is somewhat different, with the pattern of cerebellum > cortex > hippocampus (Gutierrez et al., 1994; Laurie et al., 1992a; Pirker et al., 2000). The γ2 subunit is the most abundant γ isoform expressed in the cerebellum, with γ2L greater than γ2S level (Gutierrez et al., 1994; Khan et al., 1996b). The expression of δ subunits is high in the cerebellar granule cell layer, exclusively mediating tonic inhibition in the GCs (Nusser et al., 1998); the ρ subunits, although predominantly distributed in the retina, can also be found in PCs (Harvey et al., 2006; Mehta and Ticku, 1999).

The majority of $GABA_A$Rs are confined to the somatodendritic and axon initial segment areas, with the exception of some α2 subunit-containing receptors, recently identified at mossy fibre terminals in the hippocampus (Bergersen et al., 2003; Ruiz et al., 2003). Distinct subtypes of $GABA_A$R may be targeted to different subcellular locations on the cell membrane, giving rise to divergent responses to the same input, namely phasic and tonic inhibitions. Phasic inhibition results from synaptic receptor mediated IPSCs; tonic inhibition appears slow and continuous, mainly relying on extrasynpatic receptors to set the threshold of excitability and govern neuronal firing. Phasic currents in the cerebellum are mediated by receptors

primarily composed of γ2 subunits associating with α1-3 and β2 subunits (Brickley et al., 1999). Selective deletion of the γ2 subunit gene dramatically reduced the postsynaptic receptor clusters and lowered miniature post synaptic inhibitory current (mIPSC) amplitudes (Lorez et al., 2000). Tonically active extrasynaptic δ subunit-containing receptors exhibit incomplete desensitization and high affinity for the antagonist, SR95531, compared to γ2 subunit containing synaptic receptors. These extrasynaptic receptors are activated by ambient ('spillover') GABA (Stell and Mody, 2002). Expression of δ subunits in the cerebellar granule cells is dependent on the level of α6 subunits as they show preferential co-assembly (Jones et al., 1997). The competition between γ2 and δ subunits for α and β binding partners is evident as target disruption of δ subunits led to enhanced γ2 subunit levels in the cerebellum and forebrain, but a reduction in the α4 subunit levels, which is known to associate with the δ subunits at extrasynpatic sites (Peng et al., 2002; Tretter et al., 2001). The δ subunit mediated tonic inhibition is also present in the dentate gyrus granule cells (Stell et al., 2003).

Single $GABA_AR$ channel conductances are best represented by studies from cerebellar granule cells, where subunit diversity is high. Three conductance states, 28, 17, and 12pS, have been reported, arising from four possible receptor subtypes: α1β2/3γ2, α6β2/3γ2, α6β2/3δ, α1/6β2/3γ2. Synaptic single channel conductances appear to display a more uniform conductance level, equivalent to the highest extrasynaptic conductance (~30pS). It is likely that the synaptic channels will always comprise of γ2 subunit-containing receptors (Brickley et al., 1999). The γ2 subunit is believed to associate with $GABA_A$ receptor associated protein (GABARAP)

and gephyrin, which are scaffolding proteins involved in the clustering of $GABA_AR$ in the synapses (Wang et al., 1999). The $\alpha5$ subunit is identified to be expressed extrasynaptically (Brunig et al., 2002a; Caraiscos et al., 2004), although a synaptic subset of $\alpha5$ subunit-containing receptors can also be found in cultured hippocampal neurons (Christie et al., 2002).

In cerebellar PCs, the majority of receptors adopt the stoichimetry of $(\alpha1)_2(\beta2)_2(\gamma2)_1$ (Poltl et al., 2003). This receptor composition binds class I BZs, such as β-carbolines, CL 218872 and zolpidem (Bureau and Olsen, 1990; Olsen et al., 1990; Yakushiji et al., 1993). The lack of Zn^{2+} sensitivity confirmed the presence of the $\gamma2$ subunits (Smart et al., 1991; Zempel and Steinbach, 1995). *In situ* hybridisation detected mRNA of only $\alpha1$, $\beta2/3$, $\gamma2$ subunits in the mature PCs (Laurie et al., 1992b; Nadler et al., 1994). In the PC soma where most of inhibitory inputs received are of basket cell origin, intense punctate staining for $\alpha1$ subunits was observed (Fritschy et al., 1992). This intensity was reduced in the dendritic area (Pirker et al., 2000; Sassoe-Pognetto et al., 2000). Gephyrin, required for the surface expression of $GABA_AR$, was only co-stained with the $\alpha1$ subunit in the dendritic areas and not the soma (Sassoe-Pognetto et al., 2000). The expression of the $\alpha1$ subunit was first observed at P7, followed by a robust increase at P10 in the soma, declining in adults as the subunit migrated to cell processes. Colocalisations of $\alpha1$ and $\alpha3$ subunits were sometimes observed in the soma (Fritschy et al., 1992). The expression of the $\alpha3$ subunit is rather controversial, while some studies showed sparse staining on the soma, and intense punctate staining colocalising with gephyrin in the proximal dendrites (inner half of molecular) and at stellate cells terminals (Pirker et al., 2000), others showed a complete lack of $\alpha3$ subunit expression (Fritschy

et al., 1992). Developmental regulation may account for this discrepancy, as one study reported the disappearance of the α3 subunit together with the α2 subunit in the first postnatal week (Takayama and Inoue, 2004). Diffuse α2 subunit staining was also identified in the molecular layer, whilst the α5 subunit expression was found to be scattered throughout the cerebellum (Pirker et al., 2000).

The β1 subunit exhibited a diffuse staining pattern, mainly in the ML. The predominant β2 subunit was moderately stained on both PC soma and dendrites (Pirker et al., 2000). By comparison, β2/3 subunits showed staining only in the ML, IGL, and not on the soma of PCs (Nadler et al., 1994). This conflicts with electrophysiological evidence, and may result from lower sensitivity of immunofluorescence in detecting β subunits. mRNA expressions for β2/3 subunits increases by 2-3 fold in the cerebellum after the age of P4 (Laurie et al., 1992b)

Staining for the γ1 subunit appeared on the PC soma (Pirker et al., 2000), whereas the dominating γ2 subunit was found diffusely in the molecular layer, strongly colocalised with gephyrin (Sassoe-Pognetto et al., 2000). The γ2 subunit started to appear at P7, increased rapidly during P10-P14, maintained throughout development thereafter (Somogyi et al., 1996). Both splice variants coexisted, but γ2L was in excess and colocalised with α and β subunits (Gutierrez et al., 1994a; Khan et al., 1996b). *In situ* hybridisation indicated low levels of γ1 and γ3 subunits were present in the cerebellum (Laurie et al., 1992b), which dramatically increased in the first postnatal week, but declined after P14. Some diffuse γ3 subunit staining was also present in the PC soma and the ML (Pirker et al., 2000).

$GABA_AR$ subunits were also detected in the other cell types in the cerebellum (Fig 1.2). α1, β2, γ2 and equal levels of γ2L and γ2S subunits were found on BCs and SCs (Laurie et al., 1992b). Granule cells possess a rich repertoire of $GABA_AR$ subunits, initially expressing α1-3, β2/3 and γ2 subunits. Developmental progression substantially increases the level of α1, β2/3, γ2 subunits, with the incorporation of new subunits α6 and δ (Wisden et al., 1996).

1.2.3 Trafficking of $GABA_AR$

Embedded within the large intracellular loop between TM3 and TM4 of β and γ subunits are multiple putative interaction sites for scaffolding and trafficking. These postsynaptic proteins and their associated cytoskeletons are essential for the accumulation and clustering of $GABA_AR$ at postsynaptic membranes (Essrich et al., 1998). Hence β and γ, but not α subunits, have functional significance in the trafficking of $GABA_AR$ (Chen et al., 2005; Luscher and Keller, 2004).

Gephyrin

Gephyrin is a 93-kDa protein highly enriched in the subsynaptic compartment of both GABAergic and glycinergic synapses. It contains an N- and a C-terminal domain, linked by 14 amino acids sequence resembling a repeated motif of microtubule-associated protein MAP2 and Tau. This sequence promotes tubulin polymerization, enabling tubulin binding to gephyrin. The gephyrin-dynein motor interaction is of particular interest, in the recruitment and clustering of $GABA_AR$ (Luscher and Keller, 2004; Maas et al., 2006). Gephyrin has the ability to form a cell-type specific hexagonal

protein lattice, providing structural support for receptors at the membrane. Through high affinity binding to cytoskeleton tubulins and microtubules, gephyrin is the primary candidate for $GABA_AR$ trafficking and clustering.

In the brain, gephyrin is considered a marker for $GABA_AR$ (Brunig et al., 2002a; Christie et al., 2002; Essrich et al., 1998; Sassoe-Pognetto et al., 2000). Immunofluorescent imaging and immunoelectron microscopy showed gephyrin expression was colocalised with postsynaptic $GABA_ARs$. However, the direct interaction of gephyrin with $GABA_AR$ remained obscure (Meyer et al., 1995). Evidence supports a reliance of gephyrin expression on $\gamma 2$ subunits (Essrich et al., 1998; Schweizer et al., 2003), and deletion of $\gamma 2$ subunits disrupted the trafficking and clustering of synaptic $GABA_AR$. In the cerebellum, deletion of the $\gamma 2$ subunit led to the complete disappearance of gephyrin and punctate $\alpha 1$ subunit staining. Disruption of gephyrin with antisense olgionucleotides also markedly reduced punctate staining of $GABA_ARs$ in hippocampal cultures, signifying the importance of gephyrin for clustering $GABA_ARs$ (Essrich et al., 1998).

A direct binding of $\alpha 2$ subunits with gephyrin, facilitating the targeting of $\alpha 2$ subunit-containing synaptic receptors to the axon initial segment and dendrites in hippocampal pyramidal neurons has been reported (Tretter et al., 2008). This binding requires a hydrophobic motif consisting of amino acids 336-347 in the major ICL of the $\alpha 2$ subunits. With the inclusion of this motif, surface expression of synaptic $\alpha 2$ subunits was enhanced (Kneussel et al., 2001; Tretter et al., 2008). The high homology within the α subunit family means it is likely this motif may be present in other α isoforms to mediate their surface expression.

Despite the almost complete loss of γ2 and α2 containing surface receptor clusters in hippocampal neurons of gephyrin knockout mice, resulting in reduction in mean mIPSC amplitude, normal levels of functional receptor expression could still be seen, emphasizing compromised synaptic localization only. The $GABA_AR$ clusters opposite presynaptic terminals were only partially reduced. Similar results were achieved with siRNA disruption of gephyrin expression (Kneussel et al., 1999; Levi et al., 2004). Therefore, initial synthesis and clustering of $GABA_ARs$ seemed to be gephyrin-independent. The role of gephyrin may be focused on aggregation and stabilisation of readily clustered receptors, as receptors assembled in the absence of gephyrin tend to be more mobile in the plasma membrane (Kneussel et al., 1999; Luscher and Keller, 2004). During development, gephyrin association with β3 and γ2 subunits was sometimes found at extrasynaptic sites, conversely some synaptic gephyrin stains were not accompanied by β3 or γ2 subunits. This postulates a gephyrin-independent mechanism in targeting synaptic $GABA_AR$ in the hippocampus (Danglot et al., 2003).

BIG2

Excitatory and inhibitory postsynaptic domains do not usually share common scaffold proteins, with the exception of brefeldin A-inhibited GDP/GTP exchange factor 2 (BIG2). It is a high molecular weight (200kDa), Sec7 domain-containing GDP-GTP exchange factor (GEF), promoting the GDP-GTP exchange on Class I members of the ADP-ribosylation factor (ARF) family of small GTPase (ARF1 and 3). ARF activation by GDP/GTP exchange initiates budding of Golgi apparatus, directing protein passage through the trans-Golgi network (TGN), and

exiting via exocytotic pathways. BIG2 selectively interacts with β subunits of $GABA_A$Rs with high affinity, at an 18 amino acids sequence in the large ICL, to promote the exit of β subunit-containing $GABA_A$Rs from endoplasmic reticulum (ER) (Charych et al., 2004). The subcellular location of BIG2 was mostly concentrated on the TGN in the soma, also in vesicle-like synaptic structures in the proximal dendritic regions, and microtubules in the axons. They sometimes colocalise with $GABA_A$R in the intracellular compartments, implicating a role in delivering newly-assembled $GABA_A$R by recruiting clathrin/AP-1 coat complexes (Charych et al., 2004; Chen and Olsen, 2007; Luscher and Keller, 2004).

Dystrophin-glycoprotein

Another multiprotein complex at inhibitory synapses, Dystrophin-glycoprotein, stabilises a subset of $\alpha 1/\alpha 2$ subunit-containing $GABA_A$R in the cerebral cortex, hippocampus and cerebellum (Knuesel et al., 1999). Their expression appears after the clustering of $GABA_A$R and gephyrin, and thus they may only function as regulatory mechanisms (Brunig et al., 2002b).

GABARAP

The assembly and delivery of various $GABA_A$R subtypes to differential synaptic locations in distinct trafficking vesicles is a sophisticated process. An important molecule is the GABARAP, a 13.9kDa polypeptide protein that binds selectively to the $\gamma 1$, $\gamma 2$ (both L and S) subunits, on a conserved

18 amino acids sequence in their large ICL. *In vivo* association between GABARAP and native $GABA_AR$s has been identified (Wang et al., 1999). The C-terminal of GABARAP exhibits similarity to ubiquitin, with amino acids 35-52 implicated in the binding to $GABA_AR$. GABARAP also shares sequence and structural homology to light chain-3 of microtubule-associated proteins (MAPs) 1A, 1B, and is postulated to be a member of the MAP family complex (Wang et al., 1999). The highly positively-charged regions in GABARAP may take part in binding to tubulin *in vivo*. GABARAP also contains a hydrophobic domain, with the potential to regulate the $\gamma 2$ subunit interaction and the availability of free GABARAP for tubulin binding. This region binds vesicular trafficking factor N-ethylmaleimide-sensitive factor (NSF) (Coyle et al., 2002; Nymann-Andersen et al., 2002), widely regarded as a regulator of general membrane fusion events and a central molecule in intracellular trafficking. GABARAP association with NSF is thought to enhance the ATPase activity of NSF required in the recycling of SNARE protein for vesicle fusion (Chen and Olsen, 2007). Recent work has discovered competitive binding of GABARAP and $GABA_AR$ β subunits to NSF. Unlike the GABARAP-NSF interaction, the β subunits-NSF interaction is reliant on ATP, thus has potential physiological relevance. A direct interaction of NSF with residues 395-415 of $GABA_AR$ $\beta 2/3$ subunits was identified by co-immunoprecipitation, confined to the plasma membrane. By this association, NSF down-regulates $GABA_AR$ surface expression and restricts membrane receptor insertion without affecting endocytosis (Goto et al., 2005).

The functions of GABARAP and its homolog, Golgi-associated transport factor enhancer of 16kDa (GATE-16), are postulated to direct the intra Golgi

vesicular transport, and guide general trafficking between different types of vesicular organelles (Chen and Olsen, 2007; Wang and Olsen, 2000). When co-expressed, GABARAP enhanced the surface expression of γ2 subunit-containing $GABA_A$Rs and GABAergic currents in *Xenopus* oocytes and cultured hippocampal neurons. However, in QT6 cells, GABARAP mediated preferential clustering of γ2 containing receptors over αβ containing receptor, was coupled with a simultaneous reduction in GABA affinity, alterations in $GABA_A$R channel kinetics, and possibly conductance (Boileau et al., 2005; Chen et al., 2000; Chen et al., 2005; Everitt et al., 2004). Curiously, GABARAP knockout mice did not exhibit a deficit in punctate $GABA_A$R synaptic localization (O'Sullivan et al., 2005), and GABARAP immunoreactivity did not overlap with that for γ2 subunits or gephyrin at the majority of inhibitory synapses, but concentrated at perinuclear regions in cultured hippocampal cells (Leil et al., 2004). Hence it was thought that main function of GABARAP was to deliver $GABA_A$Rs to the synaptic membrane, the anchoring of such receptors may require another molecule (Leil et al., 2004).

PRIP-1, 2

One of GABARAP's binding partners, is the phopholipase C-related catalytically inactive protein-1 and 2 (PRIP-1, 2), a family of novel proteins which also bind inositol 1,4,5-trisphosphate (IP_3), and structurally resemble phospholipase Cγ, without the catalytic activity. PRIP-1 is the predominant isoform found in PCs and GCs of the cerebellum. They have similar distribution pattern to $GABA_A$Rs, though they tend to colocalise with GABARAP in intracellular punctates rather than with surface $GABA_A$Rs (Chen and Olsen, 2007). PRIP proteins control subunit-dependent targeting

of $GABA_ARs$, particularly promoting the trafficking of the $\gamma 2$ subunits. A double knockout of PRIP 1 and 2 reduced GABARAP and $\gamma 2$ subunit surface expression, but increased overall levels of α/β containing receptors. It now appears that the formation of $\beta 3$-GABARAP-PRIP-1 trimeric complex is crucial for the facilitative role of PRIP1 in $\gamma 2$ subunit trafficking, as supported by the compromised surface trafficking of $\gamma 2$ subunit-containing receptors by disruption of the $\beta 3$-PRIP-1 interaction. The hypothesis is that through the interaction with PRIP, the $\beta 3$ subunits recruit GABARAP, spatially and temporally, to be delivered to the $\gamma 2$ subunits, in order for receptor trafficking to take place (Mizokami et al., 2007). The β subunit interaction with PRIP was thought to partake in the constitutive and partially phospho-dependent, clathrin-mediated internalisation of β subunit-containing $GABA_AR$. Clathrin heavy chain, $\mu 2$ and $\beta 2$ subunits of adaptor protein AP2, protein phosphatase 1 and 2A (PP1, PP2A), and PRIP-1 form complex and co-internalise with $GABA_AR$, before undergoing degradation in lysosomes (Kanematsu et al., 2007).

Plic-1 and 2

Ubiquitin-like 67-kDa proteins that link integrin-associated protein with the cytoskeleton (Plic-1 and 2), stabilise $GABA_ARs$ at all locations through direct interactions with the major ICL (residues 346-355) of α (1, 2, 3, 6) and β subunits. This function is thought to be achieved by interfering with ubiquitin-mediated degradation of proteasome substrates, rather than receptor internalisation. Plic-1, 2 share 33% homology with ubiqutin. By binding to $GABA_AR$ subunits, Plic-1 inhibits their poly-ubiquitination (Bedford et al., 2001; Luscher and Keller, 2004). Plic-1 expression is

enriched beneath inhibitory synapses, colocalised with $GABA_AR$ β2/3 subunits at intracellular clusters, within or just below cell surface, also on clathrin-coated pits and Golgi apparatus. Evidence of reduced $GABA_AR$ cell surface numbers, by Plic1 dominant negative peptides, confirmed a role of Plic1 in membrane trafficking of $GABA_AR$. Plic1 is believed to enhance the half-life of internalised $GABA_ARs$, to prevent constitutive proteasome degradation, thus increasing the availability of $GABA_ARs$ to be reinserted. This function may also apply to unassembled $GABA_AR$ subunits in the ER and aid subunit maturation to produce functional receptors (Bedford et al., 2001).

GODZ

Only the γ subunits of $GABA_AR$ possess five cysteine residues between C359 to C380 in their major ICL, all subjected to palmitoylation. Four of which interact with a Golgi apparatus specific protein (GODZ) (Luscher and Keller, 2004). Palmitoylation of the γ subunits is initiated upon GODZ binding, and controls receptor clustering and stability on the surface. Post-translational palmitoylation may enhance $GABA_AR$ interaction with the cytoskeleton and gephyrin, to increase receptor clustering. This covalent modification may also stabilise surface $GABA_ARs$ by incorporation into lipid rafts (Keller et al., 2004; Luscher and Keller, 2004). In cultured neurons, GODZ was found on one face of Golgi apparatus (transport vesicle sorting side), suggesting an involvement in the secretory pathway of the γ2 subunit-containing receptors, though GODZ does not appear to co-immunoprecipitate in the synapse with the γ2 subunit , nor with gephyrin (Keller et al., 2004).

HAP-1

Huntingtin-Associated protein 1 (HAP-1) interacts with the β1 subunit of $GABA_AR$s. It is predominantly found in dendrites, axons, perinuclear compartments such as endosomes and tubulovesicular structures. HAP-1 partially colocalises with and stabilizes $GABA_AR$ in these intracellular compartments, facilitating receptor recycling and endocytic sorting. Functionally, HAP-1 enhances $GABA_AR$ activity in the hypothalamus and controls GABA stimulated feeding behaviour. It is also vital in early brain development (Kittler et al., 2004).

GRIF-1

The β2 subunit interacts with $GABA_AR$ interacting factor-1 (GRIF-1), a hydrophilic protein with the ability to homo- or hetero-dimerise. It is a homologue of HAP-1, and presumed to affect receptor trafficking. GRIF-1 regulates mitochondrial trafficking, which may in turn organise receptor vesicle transportation to ensure synaptic strength during development and plasticity (Chen and Olsen, 2007).

Postsynaptic insertion of $GABA_AR$ can be modulated by multiple pathways, often featuring phosphorylation. Insulin mediated recruitment of $GABA_AR$s to the synapses is known to involve β2 subunit phosphorylation of Ser410 by serine/threonine kinase Akt (protein kinase B, PKB), downstream of phosphatidylinositol 3-kinase (PI3K) (Wan et al., 1997b; Wang et al., 2003b). BDNF activated receptor tyrosine kinase, TrkB, also modulates $GABA_AR$ surface expression and contributes to neuronal development (Brunig et al., 2001; Cheng and Yeh, 2003). Mature rat hippocampal CA1 neurons responded to BDNF-TrkB-phospholipase Cγ

(PLCγ) modulation with a reduction in α1-3-subunit containing surface $GABA_AR$s and in mIPSC amplitude, whereas younger CA1 neurons (P6) exhibited an enhancement of excitatory GABAergic transmission under BDNF modulation through Ca^{2+} influx induced Ca^{2+}/Camodulin dependent kinase II (CaMKII) (Mizoguchi et al., 2003; Tanaka et al., 1997).

Besides direct insertion of $GABA_AR$, lateral movement of receptors from extrasynaptic locations into the synapses is another major mechanism to increase the number of synaptic receptors and promote GABAergic transmission. $GABA_AR$ diffusion within the plane of the membrane has been reported in hippocampal pyramidal neurons (Thomas et al., 2005). This process is much more rapid than conventional importation of receptors from intracellular sites. Whether this diffusive behaviour contributes to synaptic plasticity remains, as yet, unknown.

The removal of receptors in the synapses by endocytosis is a key limiting factor for surface receptor numbers. Constitutive recycling of $GABA_AR$s and agonist-induced internalization occur between plasma membranes and intracellular endosome compartments via clathrin-coated pits (Jalilian Tehrani and Barnes, 1997; Kittler et al., 2000a). In heterologous expression systems and neuronal preparations, $GABA_AR$s containing $\alpha1\beta2\gamma2$, in contrast to $\alpha1\beta2$, were constitutively endocytosed to perinuclear compartments via the intact microtubule cytoskeleton and recycled. The role of the $\gamma2$ subunit in basal endocytosis has been demonstrated in PKC-induced receptor internalization (Connolly et al., 1999; Kittler et al., 2000a). The addition of the $\gamma2$ subunits appeared to target $\alpha\beta$ receptors into a later

endosomal compartment, subjected to slow recycling in recombinant systems (Luscher and Keller, 2004).

Clathrin adaptor protein AP2 (composed of α, β2, μ2 and σ2 adaptin subunits) is a major component of the endocytotic machinery. AP2 μ2 subunit interacts with $GABA_AR$ β and γ subunits on a di-leucine motif and a YECL motif respectively, in the large ICL, consequently recruiting them into clathrin-coated pits (Kittler et al., 2000b; Kittler et al., 2008). Co-localisation of AP2 with a subset of $GABA_AR$ was found on numerous membrane sites in cultured hippocampal neurons. The di-leucine motif conserved on the β subunits is of particular importance (Herring et al., 2003). This atypical AP2 binding motif (401-410 KTHLRRRSSQLK) incorporates the conserved regulatory phosphorylation site Ser408/409 on the β3 subunits, which inhibits the AP2 binding upon phosphorylation. This molecular switch of AP2-mediated clathrin-dependent endocytosis of $GABA_AR$ was also found on the γ2 subunits on tyrosines Y365 and Y367. Both switches regulate the stability of surface receptors of different subtypes (Kittler et al., 2005; Kittler et al., 2008). Disruption of clathrin-coated pits enhanced GABAergic currents (Herring et al., 2003; Kittler et al., 2000a). Clathrin-independent endocytosis for $GABA_ARs$ also exists and had been reported in HEK cells (Cinar and Barnes, Jr., 2001).

Fig 1.4 The postsynaptic protein apparatus at GABAergic synapses. (Chen and Olsen, 2007)

1.2.4 Modulation of $GABA_A$Rs by phosphorylation

Phosphorylation of individual subunits is a major determinant of $GABA_A$R channel function, such as desensitization rate, mean channel open time and open probability, as well as trafficking.

All β and $\gamma 2$ subunits contain consensus sites in their major ICL between TM3 and TM4 for phosphorylation by serine/threonine kinases and tyrosine kinases. Utilizing *in vitro* GST-fusion protein encoded with the major intracellular domains of individual subunits, it was found that the conserved serine residues in all β subunits can be phosphorylated by PKA, PKB (Akt), PKC, PKG and CaMKII (Brandon et al., 2000; McDonald and

Moss, 1994; McDonald and Moss, 1997; Wang et al., 2003b). Tyrosine phosphorylation of the β subunits by protein tyrosine kinases, in particular Src kinase is also present (Brandon et al., 2001; Moss et al., 1995; Wan et al., 1997a), although the major tyrosine phosphorylation occurs on the $\gamma 2$ subunit .

Phosphorylation sites on the β subunits include the conserved serine residues located within the sequence RRRXSLQK, (X=A for $\beta 1,2$, and X=S in $\beta 3$), at position S409 in $\beta 1$, S408/409 in $\beta 3$, and S410 in $\beta 2$ subunit (McDonald and Moss, 1994; McDonald and Moss, 1997). The outcome of phosphorylation is subunit- and cell-type specific. In recombinant systems, PKA phosphorylation of $\beta 1$ and $\beta 3$ subunits results in inhibition and potentiation in GABAergic responses, respectively (McDonald et al., 1998; Moss et al., 1992b). The negative modulation by S408 in $\beta 3$ is interconvertible with $\beta 1$, mutation of $\beta 1$ A408 to serine delivered a PKA dependent increase of GABA currents (McDonald et al., 1998). PKA modulation is mediated via A-kinase anchoring protein (AKAP79/150) which connects PKA with $\beta 1/3$ subunits. The $\beta 2$ subunit appears to have no affinity for AKAP and is not subjected to PKA phosphorylation in recombinant systems (Brandon et al., 2003). In physiological systems, PKA activity triggered cell specific inhibition of GABA-activated currents in the spinal cord, cerebellar granule cells and hippocampal pyramidal neurons (Poisbeau et al., 1999; Porter et al., 1990). The opposite was observed in hippocampal dentate granule, cerebellar Purkinje, and olfactory bulb granule cells (Kano and Konnerth, 1992; Kapur and MacDonald, 1996; Nusser et al., 1999).

PKC phosphorylation of Ser409/410 in the β1/2 subunits, Ser408/409 of the β3 subunits, and Ser327/343 the in γ2L subunits, in recombinant systems, are known to inhibit $GABA_AR$ function (Kellenberger et al., 1992; Krishek et al., 1994). In cortical neurons, the β3 subunits are basally phosphorylated by PKC on Ser408/409, and the removal of this basal phosphorylation enhanced GABAergic currents, unmasking a suppressive effect of PKC phosphorylation (Brandon et al., 2000). PKC, via its βII isoform, directly binds to the β3 subunit of $GABA_ARs$ (Brandon et al., 1999). Indirect targeting of PKC to $GABA_AR$ subunits can also occur in the presence of the receptor for activated C-kinase (RACK-1) (Brandon et al., 2002; Kittler and Moss, 2003). Both PKA and PKC mediated β3 phosphorylation can be counteracted by PP1(α)-dephosphorylation (McDonald et al., 1998; Terunuma et al., 2004). PKC is also known to be the downstream effector of BDNF-mediated modulation of $GABA_ARs$. A switch in the phosphorylation state of the β3 subunits underlies BDNF-induced biphasic modulation of $GABA_AR$ function (Jovanovic et al., 2004). The function of PKC phosphorylation in regulating the surface number of $GABA_ARs$ is unclear. While one study revealed PKC phosphorylation decreased surface expression of $GABA_ARs$ (Brunig et al., 2001), another showed the removal of PKC activity had no discernible effect on surface receptor numbers in cortical neurons, despite the increase in whole cell GABA currents (Brandon et al., 2000).

Ca^{2+}/Camodulin dependent kinase II (CaMKII) has an additional phosphorylation site on the β1 and β3 subunits, at Ser384 and Ser383, respectively (McDonald and Moss, 1997). In synaptosomal membranes, CaMKII phosphorylation increased the binding of muscimol to $GABA_ARs$,

indicative of an increase in the availability of functional receptors with unaltered GABA affinity (Churn and DeLorenzo, 1998). Direct enhancement of GABA mediated Cl^- currents was also achieved by either injection of thiophosphorylated CaMKII in acutely-isolated spinal cord neurons (Wang et al., 1995), or increasing $[Ca^{2+}]$ in cortical neurons (Aguayo et al., 1998). Similarly, preactivated αCaMK-II potentiated the whole-cell GABA currents from cultured rat cerebellar granule neurons and recombinant $GABA_A$Rs expressed in neuroblastoma, NG108-15 cells, although the potentiation was only manifest on the $\alpha1\beta3(\gamma2)$ receptors, not the $\alpha1\beta2(\gamma2)$ receptors (Houston and Smart, 2006).

The γ2 subunit is pivotal in the trafficking and clustering of $GABA_A$Rs at synapses. Its major ICL encompasses several sites for serine/threonine phosphorylation by PKA, PKC and CaMKII. Phosphorylation substrates, Ser327, Ser348, and Thr350 are present on both splice variants, γ2S and γ2L. An extra PKC phosphorylation site, Ser343, resides within the 8 extra amino acids on γ2L (Moss et al., 1992a). Ser327 undergoes basal phosphorylation, which is reversed upon calcineurin binding to the major ICL of the γ2 subunits. This may bear importance in sustaining the suppression of $GABA_A$R function, during excitatory LTP in the hippocampus (Wang et al., 2003a). Protein tyrosine Src kinase phosphorylation of the two adjacent tyrosines Tyr 365, Tyr367 (in γ2S and Tyr373, Tyr375 in γ2L) is critical to the normal functioning of $GABA_A$Rs. Phosphorylation of these two residues increases the opening probability of recombinant $GABA_A$R channels, co-assembled with $\alpha1\beta1$ or $\alpha1\beta2$ subunits (Moss et al., 1995). Constitutive phosphorylation of these two residues was believed to be restricted by protein tyrosine phosphatases (Brandon et al.,

2001). Src kinase also binds $GABA_AR$ β subunits, and phosphorylates the $\beta1$ subunit on Tyr384 and Tyr386 with no apparent functional outcome (Moss et al., 1995). Notably, GABA currents via $\beta2/\beta3$ containing receptors were positively regulated by PTK $^{pp60c\text{-}}$Src phosphorylation in the spinal dorsal horn and medulla neurons (Wan et al., 1997a). To summarise, tyrosine phosphorylation of β subunits (in particular $\beta2$), has a separate effect to that of phosphorylation of $\gamma2$ subunits (Moss et al., 1995).

A connection between the CaMKII and PTK activity is also evident from using $\alpha1\beta3\gamma2$ transfected NG108-15 cells. GABAergic current was enhanced by direct injection of αCaMKII, phosphorylating Ser383 on the $\beta3$ subunit. This increase has a component attributed to PTK phosphorylation of Tyr365 and Tyr367 on $\gamma2$ subunits. The potentiation was only fully ablated after inhibition of both CaMKII and PTK, or by mutation of $\beta3^{S383A}$ and $\gamma2^{Y365,\ 367F}$. This discovery signifies that the phosphorylation of $GABA_ARs$ can be amplified by CaMKII activation of PTK (Houston et al., 2007).

Table 1.1 Kinases and their phosphorylation sites on individual $GABA_AR$ subunits
(Modified from Moss and Smart, 1996).

1.3 Ca^{2+} -Calmodulin dependent Kinase-II and synaptic plasticity of the cerebellum

1.3.1 Structure, activation and regulation of CaMKII

CaMKII is a key molecule to the establishment of synaptic plasticity. As one of the most abundant proteins in the brain (1-2% of total protein contents) (Soderling et al., 2001), it is distributed throughout the soma, dendrites, at presynaptic as well as postsynaptic sites. CaMKII can regulate both glutamergic and GABAergic transmission. Its unique properties enable it to serve as a 'memory molecule' implicated in vast array of synaptic plasticities (Lisman et al., 2002; Soderling et al., 2001).

The CaMKII family comprises of four genes (α, β, γ and δ), giving rise to 28 isoforms. The dodecameric holoenzymes usually consist of either the α or β subunit, or an α/β heteromer, which is the most predominant form in the brain (Hudmon and Schulman, 2002). Each isoform consists of: a catalytic domain, with binding sites for ATP, substrates and other anchoring proteins; an auto-inhibitory domain (AID), with a region analogous to the protein substrate (pseudosubtrate region), which binds the substrate-binding site (S site) on the catalytic domain to terminate enzymatic activity (Fig 1.5). Ca^{2+}/CaM binding to the Ca^{2+}/CaM binding domain, disrupts the AID interaction with catalytic domain, thereby opens the enzyme to protein substrate and reveals an autophosphorylation site, Thr 286 (on α isoform, 287 on β isoform) on the AID. Phosphorylation of this residue by the neighbouring subunits prolongs the gate opening, and switches the kinase to Ca^{2+} independent, autonomous activity. The other regulatory site, the T sites on the catalytic domain, binds and masks the unphosphorylated Thr 286

residue on the AID, meanwhile strengthening the binding of pseudosubtrate region with the S site (Lisman et al., 2002). The remaining part of the enzyme subunit consists of a variable region and a self-association domain. The latter is responsible for the assembly of the 12 subunits at the carboxy-terminal, forming two hexameric rings. The variable region contains between 9-127 amino acids by alternative splicing, and links the association domain to the catalytic domain and AID. This variability determines the Ca^{2+}/CaM sensitivity and the intracellular location of different CaMKII isoforms (Lisman et al., 2002).

Fig 1.5 Schematic of inactivation and activation of a single subunit of CaMKII, including the persistent activation by autophosphorylation. The autoinhibitory domain binds and inhibits the catalytic domain at S and T sites. Ca^{2+}/CaM binding opens the gate and frees the catalytic domain for autophosphorylation and persistent activity (Modified from Lisman 2002).

The extent of CaMKII activation depends on the strength of the Ca^{2+} signal. Auto-phosphorylation can only commence with sufficient Ca^{2+} load, allowing Ca^{2+}/CaM binding to two or more of the neighbouring CaMKII subunits. Subsequently, only one further Ca^{2+}/CaM is required to propagate autophosphorylation around the ring of 12 subunit-holoenzyme (Fig 1.6). Autophosphorylation results in delayed dissociation of Ca^{2+}/CaM, 'trapping' Ca^{2+}/CaM. After the dissociation of Ca^{2+}/CaM, the kinase activity is partially retained until dephosphorylated by phosphatases PP1 and PP2A (Hashimoto et al., 1987; Strack et al., 1997). This extends kinase activity beyond the initial Ca^{2+} signal in a graded fashion, as the persistent activity is a function of the number of subunits in the auto-phosphorylated state. This enables CaMKII to detect multiple Ca^{2+} waves over time, effectively acting as a Ca^{2+} frequency sensor (Lisman 2002). A second autophosphorylation site, Thr305/6, after covalent modification, could dissolve the Ca^{2+}/CaM binding to the enzyme. Auto-phosphorylation of these residues serves as an inhibitory site and locks the enzyme in an inactive state (Hanson and Schulman, 1992).

The autophosphorylation at Thr286 in αCaMKII is of particular importance in synaptic plasticity, as LTP at excitatory hippocampal CA1 synapses was abolished after the mutation of this residue (Giese et al., 1998).

Fig 1.6. Schematic representation of the cycle of activation and deactivation of CaMK-II holoenzyme. CaMKII is activated upon the binding of Ca^{2+}/CaM. Autophosphorylation occurs at Thr286 between adjacent subunits both occupied by Ca^{2+}/CaM and traps Ca^{2+}/CaM to the kinase. The autophosphorylation can be propagated around the ring of 12 subunits of the holoenzyme, by the binding of one further Ca^{2+}/CaM. The kinase activity is partially retained until the dephosphorylation of Thr286 by a protein phosphatase. The bottom insert is the three functional domains of CaMKII, a catalytic domain, an autoinhibitory domain and an association domain. Adapted from Molecular Biology of the Cell (1994), Garland Publishing.

1.3.2 Ca^{2+} signaling in PCs

The extent of CaMKII activity is largely dependent on the level of Ca^{2+} concentration. Multiple mechanisms exist to shape Ca^{2+} dynamics in PCs. AMPARs contribute to only 0.6% of the total Ca^{2+} influx into PCs, due to

the high expression level of Ca^{2+} impermeable GluR2 subunits. They indirectly contribute to the Ca^{2+} transient via generation of complex spikes and depolarization induced activation of VGCCs (Hartmann and Konnerth, 2005). Recent studies discovered functional NMDARs, formed of NR2A and 2B, subunits in mature PCs. Whether these NMDARs could participate in the Ca^{2+} surge during synaptic plasticity awaits experimental verification (Piochon et al., 2007; Renzi et al., 2007).

The first major source of Ca^{2+} entry comes from the VGCCs. $Ca_v2.1$, otherwise known as the P/Q-type Ca^{2+} channels, supply 90% of the voltage-dependent Ca^{2+} transient. The subunit α_{1A} is highly expressed on PC axons, soma and dendrites, especially in spines with high-voltage activation range. L-type, R and N –type, as well as T-type Ca^{2+} channels are also expressed and deliver the residual 10% Ca^{2+} entry (Llinas et al., 1992). The trigger for these VGCCs is the complex spike orchestrated by the CFs. Sodium action potentials initiate from the axon hillock and spread to the soma, forming the peak of the complex spike, and gradually diminishing along the extensive dendritic arborization. Potent somatic depolarization and the non-propagating, passive spread of Na^+ action potentials results in the opening of dendritic Ca^{2+} channels giving the appearance of Ca^{2+} dependent plateau and Ca^{2+} spikelets (Schmolesky et al., 2002; Stuart and Hausser, 1994). The large Ca^{2+} transient preceding the Ca^{2+} action potential is predominantly carried by P/Q-type Ca^{2+} channels. This transient is global but the dendritic Ca^{2+} elevation is more intense with faster onset in spines. Action potential independent PF mediated Ca^{2+} signals are small and locally confined to the PF synaptic inputs. However, high frequency PF firing can result in over 100μM increase in dendritic Ca^{2+}. This replies solely on AMPAR induced

depolarization activating P-type Ca^{2+} channels (Hartmann and Konnerth 2005).

The coincidental arrival of PF and CF inputs in PCs induces a large Ca^{2+} transient (> 10 μM) in the dendritic tree, pivotal to the induction of cerebellar plasticities (Wang et al., 2000b). The supralinearity of Ca^{2+} is a result of two potential pathways synergizing to amplify the Ca^{2+} transient: glutamate released from PF terminals activating mGluR1 and the sequential production of IP_3; and CF complex spikes triggered depolarization activating postsynaptic VGCCs located at PF spines, allowing Ca^{2+} and IP_3 co-activation of the intracellular Ca^{2+} stores. Two classes of intracellular Ca^{2+} stores have been classified, according to IP_3 receptor (IP_3R) distribution: one directly beneath the plasma membrane, namely the junctional stores; the other is a central cisternae and tubuli like non-junctional Ca^{2+} store, mainly found in the cytosol (Lisman et al., 2002).

The ryanodine-sensitive Ca^{2+} stores located in the ER are the sources of the Ca^{2+} dependent Ca^{2+} release (CICR). PCs are the only neurons known to express all three types of neuronal ryanodine receptors, RyR1-3. RyRs possess Homer binding motifs and colocalise with Homer 1b/c in PC soma and dendrites, but not in the spines where only IP_3Rs reside. However IP_3Rs and RyRs are known to co-express in the ER, and share a common Ca^{2+} pool, which may trigger synergy to release the Ca^{2+} in response to PC depolarization (Hartmann and Konnerth, 2005).

Additional Ca^{2+} influx may be evoked by the mGluR1 mediated slow depolarizating potential, inducing $G_{\alpha q}$- and $G_{\alpha 11}$ protein-dependent Ca^{2+}

elevation through the function of TRPC1 channels (Batchelor et al., 1994). Meanwhile precisely timed mGluR1 activation can also suppress the conductance of P/Q type VGCCs in PC dendrites, allowing bidirectional control of the Ca^{2+} transient (Hartmann and Konnerth, 2005).

The abundance of intrinsic Ca^{2+} buffering protein in PCs may also influence the shape of Ca^{2+} transients. Repetitive depolarizations triggered sigmoidal Ca^{2+} influx with a slow onset followed by marked acceleration after reaching an apparent threshold of ~1 μM. The decay of the Ca^{2+} transient appeared bi-exponential, with decay time constants of 2~3s and 30~40s for regions with lower (> 1 μM) and higher (< 1 μM) Ca^{2+}, respectively (Maeda et al, 1999).

Ca^{2+} binding proteins expressed in PCs have high Ca^{2+} binding ratio k_s, defined as [Ca^{2+} bound] : [Ca^{2+} free]. *ks* is developmentally upregulated from 900 to 2000 between P6-15 (Fierro and Llano, 1996). This creates a large capacity for Ca^{2+} management in PCs, owing mainly to two buffering proteins, $calbindin_{D28K}$ (15% of total soluble proteins in PC) and parvalbumin. Calbindin is designated as the 'fast (and medium) buffer', and parvalbumin is the slow onset buffer. Parvalbumin is freely diffusible between dendrites and spines in PCs, with a concentration of < 1 mM in axons and 50~100 μM in soma and dendrites. $Calbindin_{D28K}$ concentration was estimated to be either 210μM or 360μM (Lisman et al., 2002). Both proteins participate in the shaping of the double exponential decay of dendritic shaft Ca^{2+} transients. In parvalbumin (PV) knockout mice, the bi-phasic Ca^{2+} kinetics was reduced, without affecting peak amplitudes, emphasizing the susceptibility of the slow component to PV deletion.

Double knockout of PV and Calbindin$_{D28K}$ resulted in two-fold increase in the peak Ca^{2+} amplitude and nearly monophasic kinetics, indicative of fast Ca^{2+} sequestration by calbindin$_{D28K}$ (Schmidt et al., 2003).

The extrusion of Ca^{2+} is mostly mediated by sarco-endoplasmic reticulum Ca^{2+}–ATPase (SERCA pumps), followed by Na^{+}–Ca^{2+} –exchanger for higher $[Ca^{2+}]_i$ levels (μM range), and plasma membrane Ca^{2+}–ATPase (PMCA pump) for moderate concentrations (~500nM).

The Ca^{2+} transient mediated by the CF evoked complex spike is under further modulation by inhibitory transmission onto PCs. Simultaneous activation of inhibitory transmission, largely reduced CF induced the Ca^{2+} transient, with the most susceptible regions in the distal dendrites under stellate cell influences. Though this does not affect the immediate output of the PC, the reduction of Ca^{2+} by inhibitory transmission may prompt metaplasticity in PCs and control the onset of subsequent plasticities (Callaway et al., 1995).

1.3.3 Cerebellar plasticities

Lesion experiments first linked the cerebellum to coordinated movements in early 19th century. The motor disequilibrium caused by lesions, recovered over different periods, depending on the size of the lesions. Creation of two partial lesions in the neighbouring areas (one after the recovery of the other) led to more drastic disequilibrium than either lesion alone. This implied that recovery from the first lesion relied on the plasticity of the neighbouring region. This was the first demonstration of the cerebellar plasticity (Ito, 2001)

There are various forms of cerebellar plasticity associated with excitatory and inhibitory synapses (Gaiarsa et al., 2002; Hansel et al., 2001).

Parallel fibre LTD

This form of activity dependent, long-lasting depression of excitatory transmission occurs at the point of convergence of two separate stimuli. One of these occurs at PF inputs, and is known as the conditioned stimulation (CS), and the second occurs at CF inputs, which is referred to as the unconditioned stimulation (US). Repetitive and associative co-stimulation of CF and PF inputs within a certain temporal window, at a low frequency, induces a supralinear Ca^{2+} wave and results in the attenuation AMPAR mediated excitatory responses between PFs and PCs (Wang et al., 2000a). CF inputs initiate complex spikes to depolarize the PC and induce Ca^{2+} activation of PKC, while PFs release glutamate to activate AMPARs and mGluR1s. mGluR1 activation recruits the phospholipase C (PLC) pathway and leads to the production of both diacylglycerol (DAG) and inositol 1,4,5-trisphosphate (IP_3). DAG also activates PKC to phosphorylate and prime AMPARs for internalisation, while IP_3 binds intracellular IP_3R on the ER enabling the release of further Ca^{2+} contributing to the super-linear CICR wave (Crepel and Krupa, 1988).

In addition, nitric oxide (NO), produced from stimulated PFs after K^+ efflux causing presynaptic depolarization, may cross the synaptic cleft and anterogradely activate guanylate cyclase and protein kinase G (PKG) in the postsynaptic PC (Crepel et al., 1994). PKG and PKC are pre- and postsynaptically modulated respectively (LevRam et al., 1997), to achieve a

postulated postsynaptic modulation of AMPARs, which may involve clathrin-mediated endocytosis and a change in AMPAR kinetics, desensitization, unitary conductance, or glutamate affinity (Wang and Linden, 2000).

Parallel fiber LTP- pre and postsynaptic

Pre- and postsynaptically expressed PF LTPs have been described. Both are non-associatively induced by different frequency stimulations of PF alone. The presynaptic LTP requires low frequency (2-8Hz) repetitive PF stimulation, promoting Ca^{2+}/CaM-sensitive adenylyl cyclase to produce cAMP, subsequently activating PKA. Postsynaptic LTP requires a longer period of PF stimulation (< 300s) at a lower frequency of 1Hz. Ca^{2+} influx is not crucial for this form of LTP, nor is the activation of glutamate receptors (Salin et al., 1996). Nitrous oxide (NO) however, is utilized as an upstream anterograde signal, similar to PF LTD (Lev-Ram et al., 2002). Postsynaptic LTP is ideal to reverse the postsynaptically expressed associative PF LTD, resetting the synaptic threshold, attenuating learnt associations and refining the temporal precision of the learnt response.

Climbing fiber LTD

At birth, the innervation of PCs by climbing fibres is numerous. Developmental pruning takes place during the first 3 postnatal weeks. Activity-dependent elimination of excess CF sculpts the ultimate configuration of a single CF innervation of a single PC in the mature cerebellum (Strata and Rossi, 1998).

A saturable postsynaptically expressed LTD of CF evoked EPSCs occurs upon CF tetanization (Shen et al., 2002). The molecular constituents of CF LTD are akin to those of PF LTD. Inhibition of PKC and mGluR1, or Ca^{2+} buffering blocked this form of LTD (Shen et al., 2002).

1.3.4 Cerebellar Plasticity-inhibitory

Inhibitory transmission determines the excitability of PCs and influences the Ca^{2+} transient evoked by CF and PF activation. Over the last two decades, it is evident that inhibitory synaptic plasticity has a profound effect on PC functions.

Depolarization induced suppression of inhibition (DSI)

DSI is a transient depression of GABAergic transmission at the IN-PC synapses, induced by depolarization triggered Ca^{2+} entry. The duration of DSI lasts up to one min after induction (Llano et al., 1991; Vincent et al., 1992). During DSI, an increase in the probability of failures, and a sharp reduction in mIPSC frequency were observed, proposing a presynaptic location of modulation. DSI was also observed in hippocampal CA1 neurons and believed to have a pure presynaptic locus by monitoring the coefficient of variation for IPSC amplitudes (Alger et al., 1996).

This presynaptic plasticity entails the release of retrograde messengers from PCs in response to the Ca^{2+} waves, and subsequently reduced vesicular GABA release from presynaptic terminals. The retrograde messenger was identified as endocannabinoids (Yoshida et al., 2002). The *de novo* synthesis of 2-arachidonoylglycerol (2-AG) by sn-1-diacylglycerol lipase in the

postsynaptic PC, is believed to be the mechanism downstream of the Ca^{2+} signal responsible for the induction of DSI (Szabo et al., 2006). The release of endocannabinoids from PCs can be focal or global. Local endocannabinoid release mediated by synaptic activation can be achieved by strong activation of the mGluR1-PLCβ4 pathway at the CF-PC synapses, without the need for Ca^{2+} elevation (Maejima et al., 2005). DSI, however, may require global endocannabinoids release from the entire dendritic arbor, following strong PC depolarization and a Ca^{2+} transient of 0.4-1 μM (Brenowitz et al., 2006).

Furthermore, the Ca^{2+} transient induced by mild PC depolarization, can synergise with weak activation of mGluR1-PLCβ to induce the release of 2-AG (Maejima et al., 2005). The glutamate required for this can be released from PCs as an autocrine messenger, to participate in the production of endocannabinoids, or it can act as a retrograde messenger itself, crossing the synaptic cleft to induce depolarization induced potentiation of inhibition (Duguid et al., 2007).

Depolarization induced potentiation of inhibition (DPI)

After the cessation of DSI, a separate form of presynaptically controlled plasticity, known as DPI, takes place and increases synaptic gain by facilitating the presynaptic release of GABA. DPI utilises postsynaptically-released glutamate as a retrograde messenger to act on NMDAR at presynaptic axon terminals of stellate and basket cells. The release of glutamate is reliant on SNARE-protein and is thought to be release from depolarized PCs following CF stimulation (Duguid et al., 2007). Sequential

activation of presynaptic NMDAR enhances the release of Ca^{2+} from ryanodine-sensitive stores, causing a sustained increase in GABA release onto the PC lasting up to 15 min (Duguid and Smart, 2004). Prior to crossing the synaptic cleft to initiate DPI, glutamate released by prolonged depolarization of PCs could also lead to the cooperative release of endocannabinoids. Synergizing with the Ca^{2+} transient, the glutamate activation of the mGluR1-$G_{q/11}$ complex, could evoke PLCβ4 dependent synthesis and release of the endocannabinoid, 2-AG, which is required for the induction of DSI (Duguid et al., 2007).

1.4 Rebound potentiation

Rebound potentiation (RP) is a postsynaptically controlled inhibitory plasticity, occurring at IN-PC synapses. RP occurs in conjunction with DSI and DPI, providing simultaneous activity dependent pre- and postsynaptic regulation of GABAergic transmission.

1.4.1 RP- a postsynaptic, Ca^{2+} dependent long term potentiation of inhibitory transmission at IN-PC synapses

Kano and colleagues were the first to encounter this hetero-synaptic enhancement of inhibitory transmission at IN-PC synapses in response to repetitive CF firing (Kano et al., 1992). The amplitudes of synaptic, as well as exogenously-applied GABA currents were potentiated, indicative of a postsynaptic locus of modulation. This was further verified by the lack of change in mIPSC frequency. The potentiation time course has a fast onset and slow decay, reaching a maximum potentiation of 180% of control within

3~15 min after stimulation, and lasting up to 75 min. Internal application of the Ca^{2+} chelator, BAPTA, completely abolished the potentiation, suggesting RP is also reliant on Ca^{2+} influx, similar to other cerebellar plasticities (Kano et al., 1992). Simultaneous fluorometric Ca^{2+} measurements showed a steep transient increase of Ca^{2+} from ~30nM to ~900nM in the dendritic area of PCs and a smaller increase of ~200nM in the soma, both fell back to basal level within 40s, after RP induction (Kano and Konnerth, 1992). The brevity of the Ca^{2+} influx implies Ca^{2+} is a prerequisite for the initiation of rebound potentiation, but not for its maintenance. The source of this Ca^{2+} transient comes from both the opening of VGCCs and Ca^{2+} dependent Ca^{2+} release from IP_3-sensitive and ryanodine-sensitive (partially) Ca^{2+} stores (Hashimoto et al., 1996; Konnerth and Eilers, 1994). The latter was proven by the complete elimination of RP, following co-application of heparin and Ruthenium Red, blockers for IP_3 and ryanodine-sensitive Ca^{2+} stores, respectively. Depleting Ca^{2+} using ATP-dependent Ca^{2+} uptake blocker, thapsigargin, also had a similar effect (Hashimoto et al., 1996).

1.4.2 Induction of RP

Essentially, RP requires the stimulation of a CF to elicit a profound depolarization, via AMPA receptors (Fig 1.7), which activates VGCCs, in turn evoking supralinear Ca^{2+} transients in the PC dendrites. The CF stimulation required for RP can therefore be mimicked by the application of repetitive depolarizing pulses directly to the PCs.

1.4.3 Intracellular signaling pathways in RP

Though RP commences straight after the stimulus cessation, the 3-15 min delay to reach the maximum potentiation implies a second messenger system may be recruited to modulate the strength of GABAergic synapses. During RP, $GABA_A$Rs may be subjected to phosphorylation by multiple Ca^{2+} dependent protein kinases (see section 1.2). Application of 8-bromo-cAMP and the cAMP activator forskolin, induced PKA activity and caused a robust and long lasting potentiation of both bath-applied and action potential independent mIPSC amplitudes, akin to synaptically-evoked RP (Kano and Konnerth, 1992).

Indeed, PKA has been implicated in the induction of RP, along with CaMKII (Kano et al., 1996). Both kinases have the ability to phosphorylate the numerous phosphorylation sites within the major ICL of $GABA_A$ β and $\gamma 2$ subunits, although the role of PKA was thought to be indirect, via the disinhibition of CaMKII by suppressing PP1 activity (Kawaguchi and Hirano, 2002). CaMKII is abundantly expressed in PCs (Kano et al., 1996). Both α and β isoforms of CaMKII are expressed in the cerebellum at a ratio of 1:4 (Sola et al., 1999), though the expression of αCaMKII in PC greatly exceeds the β isoform (Hansel et al., 2006). Disruption of Ca^{2+}/CaM binding to CaMKII with calmodulin binding domain peptide (CBD), or application of CaMKII inhibitors, KN62 and calmidazolium (CMZ), abolished long term RP. However, the inhibitors were only effective when applied prior to, or during the stimulation.

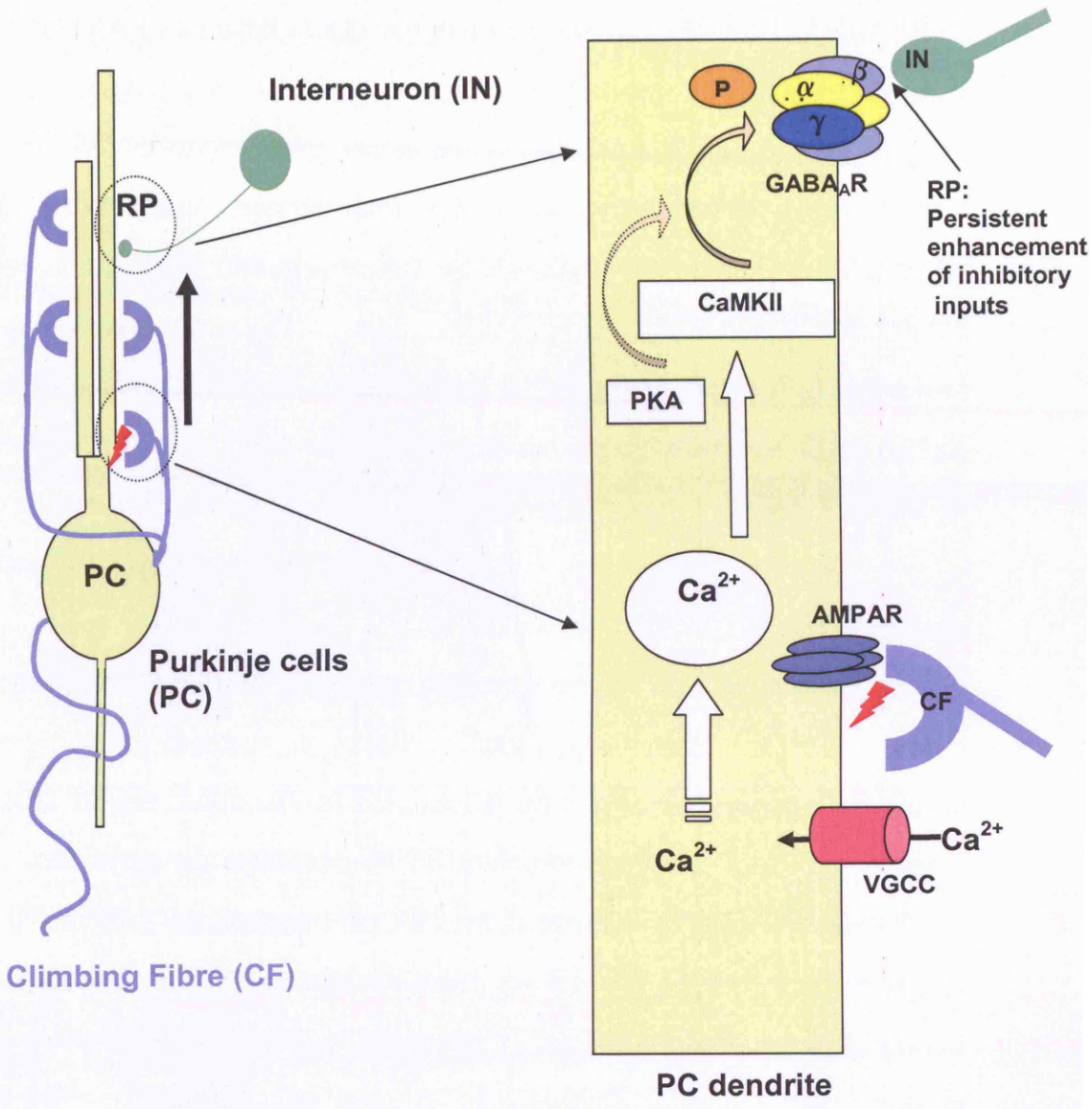

Fig 1.7 The physiological signal transduction leading to the induction of rebound potentiation.

Application after a 5 min delay failed to suppress RP (Kano et al., 1996), although the inhibitors are only affective against the Ca^{2+}/CaM binding and activation of the enzyme, not the autonomous activity, and KN62 is also known to inhibit CaMK-IV and voltage-dependent potassium

channels at high concentrations (Enslen and Soderling, 1994; LeDoux et al., 1999). This implies Ca^{2+}/CaM binding and activation of CaMKII may only initiate the induction of RP, while the maintenance phase may require separate intracellular mechanisms. A similar approach showed that activation of CaMKII directly, either by injecting activated CaMKII, or by inhibiting phosphatase PP1 and PP2A with calyculin, potentiated GABAergic currents in similar manner to RP (Kano et al., 1996). Injection of activated αCaMKII also caused a similar potentiation of GABAergic currents in cerebellar granule cells, suggesting granule cells are capable of undergoing RP (Houston and Smart, 2006).

A detailed intracellular signaling pathway for RP has been proposed by Kawaguchi and Hirano in 2002. They postulated CaMKII works downstream in the induction of RP, acting as a complex molecular switch network involving phosphatase PP2B calcineurin, PP1 and the adaptor protein, DARPP32, an endogenous PP1 inhibitor (for schematic diagram see Fig 4.1 in chapter 4). Upon depolarization, the Ca^{2+}/CaM complex binds and activates both CaMKII and calcineurin. The latter acts as a negative feedback and counteracts the activity of CaMKII. The balance between calcineurin and PKA determines the phosphorylation state of DARPP32, and its availability to inhibit PP1. Once PP1 is released, it inactivates CaMKII by dephosphorylation of Thr286, attenuating the autonomous activity of the kinase, thus preventing the induction of RP (Kawaguchi and Hirano, 2002).

A secondary site for the regulation of RP comes from the presynaptic release of GABA by interneurons and the subsequent activation of metabotropic $GABA_B$ receptors on postsynaptic PCs, concurrent with the

induction phase of RP. $GABA_B$ receptors couple to G_i/G_o proteins to downregulate the activity of adenylyl cyclase, and reduce the production of cAMP. This in turn decreases the activity of PKA, which allows liberated PP1 to suppress the induction of rebound potentiation. This suppressive function of $GABA_BR$ could be reversed by mGluR1 activation to remove PKA inhibition (Sugiyama et al., 2008). $GABA_B$ receptors also directly suppress Ca^{2+} influx through P type-Ca^{2+} channels, to curtail the Ca^{2+} surge required for RP. This self-regulation by GABA provides yet another negative feedback control, to maintain the stability of inhibitory synapses and shape the synaptic output of PCs. The involvement of mGluR1 provides additional bi-modal modulation of RP induction by both excitatory and inhibitory presynaptic activity.

Depolarization applied in conjunction with exogenous GABA or activation of the presynaptic interneurons, caused long-term sustained suppression of RP for up to 4 days (Kawaguchi and Hirano, 2000). This mechanism may utilize the activation of a MAPK signal cascade and *de novo* mRNA synthesis of the cell adhesion molecule, integrin $\alpha 3$ protein, which in turn exerts its effect on the downstream Src-PTK family. Activation of intergrin $\alpha 3\beta 1$ by Mn^{2+}, or overexpression of integrin $\alpha 3$ subunit, suppressed RP when applied during the RP induction phase and this suppression was reversed by addition of anti-integrin $\alpha 3$ or $\beta 1$ antibody, and the selective Src kinase inhibitor, pyrazolopyrimidine PP2. Conversely, the extent of RP was augmented further by pyrazolopyrimidine PP2, whilst injection of activated c-Src ablated RP. This suggests constitutive Src activity limits the basal level of RP that is achievable (Kawaguchi and

Hirano, 2006). In another study, basal mIPSC amplitude was enhanced by co-activation of Src kinase and receptor tyrosine kinase TrkB, by mGluR1 and BDNF agonists, respectively. BDNF was shown to recruit the TrkB-PLC pathway and induced Ca^{2+}-CaMKII activity, to enhance GABAergic currents in PCs, bypassing Src kinase. BDNF modulation was facilitated by PKA, though the outcome of mIPSC modulation in PCs was opposite to that in granule cells (Boxall, 2000; Cheng and Yeh, 2005). A PTK-CaMKII cross-regulation was demonstrated in neuroblastoma cell NG108 transfected with $\alpha 1\beta 3\gamma 2$ of $GABA_AR$. The potentiation of whole-cell inhibitory currents by CaMKII phosphorylation of Ser383 on $\beta 3$ subunits elicited downstream PTK phosphorylation of Tyr365, Tyr367 on the $\gamma 2$ subunits to further increase the amplitude of GABAergic currents (Houston et al., 2007).

A multitude of unanswered questions remain concerning the intermediary events downstream of RP induction. Based on evidence of direct CaMKII phosphorylation of the β and γ subunits of recombinant $GABA_ARs$, it is postulated CaMKII may directly phosphorylate native $GABA_AR$ subunits to increase either the number of surface $GABA_ARs$ or ion channel function in PCs. A recent study unveiled a potential alternative CaMKII pathway in RP, which involved a precise $\gamma 2$ subunit-GABARAP-tubulin association. It was discovered that GABARAP was sequestered to inhibitory synapses by RP induction and underwent CaMKII induced structural alteration to aid RP induction and maintenance. Interfering with either the $\gamma 2$-GABARAP, GABARAP-tubulin interactions, or tubulin polymerization, abolished RP. This implies that CaMKII may facilitate intracellular trafficking and the insertion of $GABA_ARs$ by stimulating the intermediate scaffolding protein GABARAP (Kawaguchi and Hirano, 2007).

1.5 Overview

The output of cerebellum is configured by complex integration of a vast range of plasticities. Our study is focused on the particular aspect of rebound potentiation, elucidating the intracellular mechanisms behind its appearance. In this study, we explored the phosphorylation signaling pathway in RP, provided direct evidence supporting a role for PTK phosphorylation to promote the induction of RP. We also obtained proof that postsynaptic receptor insertion was the downstream mechanism underlying the appearance of RP, and that subunit composition of $GABA_A$Rs in PCs is also a key determinant in RP.

Chapter 2

Material and methods

2.1 Slice preparation

P11-14 mice were sacrificed in a CO_2 gas chamber. The brain was placed in artificial cerebrospinal fluids (aCSF) for slicing at 2-4°C; meninges were carefully removed with forceps. The two cortical hemispheres were sliced off with a Wilkinsons razor blade, leaving the cerebellar vermis to be mounted on a Leica Vibratome VT1000s slicer and superfused in ice-cold (2-4°C) artificial cerebrospinal fluid (aCSF) bubbled with 95% O_2 , 5%CO_2. The vermis was sliced into 250 μm thick parasagittal slices. Slicing media was exchanged every two min to ensure a sufficient supply of O_2. The slices were carefully transferred to a holding chamber, containing oxygenated aCSF, and incubated at 35°C, using a water bath, for 45 min with slow aCSF solution exchange via a peristaltic pump. The slices were thereafter kept in oxygenated aCSF at room temperature (22-24°C) during selection for electrophysiological recording.

2.2 Composition of media

2.2.1 Slicing media

Most of the slicing was performed in aCSF with the following composition:

125mM NaCl, 2.5mM KCl, 1.25mM NaH_2PO_4,, 25mM $NaHCO_3$, 10mM glucose, 2mM $MgCl_2$, 1mM $CaCl_2$.

Later we adopted a high sucrose concentration solution, to obtain healthier slices, minimizing osmotic changes during slicing. The composition of the sucrose rich solution was:

85 mM NaCl, 2.5 mM KCl, 0.5 mM $CaCl_2$, 4 mM $MgCl_2$, 25 mM $NaHCO_3$, 1.25 mM NaH_2PO_4, 75 mM sucrose, 25 mM glucose, pH 7.4 at room temperature, bubbled with 95% O_2 and 5% CO_2. The exchange of this solution with an aCSF solution for recording (see below) required the slow peristaltic pump to minimize the osmotic shock to the slices. This exchange was carried out simultaneously with the heat incubation.

2.2.2 Bath superfusion media

Sucrose-based slicing media was replaced by the standard perfusion solution during and after heat incubation with low Mg^{2+}, and high Ca^{2+} concentrations to enable synaptic transmission. This solution contained:

125 mM NaCl, 2.5 mM KCl, 2 mM $CaCl_2$, 1 mM $MgCl_2$, 25 mM $NaHCO_3$, 1.25 mM NaH_2PO_4 and 25 mM (or 10mM) glucose. During recording, the perfusion solution was supplemented with 50μM D-(–)2-amino-5-phosphonopentanoic acid (D-AP5), to block N-methyl-D-aspartic acid receptor (NMDAR), and 10μM 2,3-dihydroxy-6-nitro-7-sulfamoyl-benzo[f]quinoxaline-2,3-dione (NBQX), an inhibitor of α-amino-3-hydroxy-5-methyl-4-isoxazolepropionic acid receptors (AMPAR). 500nM of tetrodotoxin (TTX), a Na^+ channel blocker, was also added to ablate action potential generation.

2.2.3 Composition of patch pipette solution

A Cs^+ based Cl^- internal solution was used containing: 150mM $CsCl_2$, 1.5mM $MgCl_2$, 0.5mM EGTA, 10mM HEPES, 2mM Na-ATP, 0.4mM

Na-GTP, 5mM N-(2,6-Dimethylphenylcarbamoylmethyl) triethylammonium bromide (QX-314), to block postsynaptic sodium-based action potentials. The pH of the internal solution was adjusted to 7.3 by CsOH at room temperature, and osmolarity was adjusted to 295 mOsm using an Osmometer. For experiments involving reconstruction of PCs, biocytin was dissolved in the internal solution at a concentration of 5mg/ml.

2.3 Electrophysiological techniques

2.3.1 Equipment

A Nikon Eclipse E600FN upright microscope was used to identify PCs (Fig 2.1). Broad viewing of the slices was achieved with a plan fluor 10x differential interference contrast objective. For more detailed visualisation, x40 or x63 immersion objectives were used for patching. Mechanical coarse manipulators Narishige (MP-285) and water-based micromanipulators (MWO-3) were used to position the patch electrodes. The PC slices were fixed in the recording bath with a slice-holder made of a platinum wire 'harp' with crossing nylon fibres. The bath was constantly perfused with circulating oxygenated perfusion media with an approximate exchange rate of 1ml/min. For experiments at physiological temperature, a heating block was used to maintain the aCSF at 31~32°C.

Patch pipette electrodes were pulled from borosilicate thin-walled glass capillaries (Havard apparatus), using a Narishige PC-10 vertical automated electrode puller. Subsequent heat polishing produced electrodes with resistances of 2~3 MΩ. After part-filling the patch pipettes with

internal solution, a coated AgCl wire was inserted into the pipette until the internal solution just covered the tip of the wire, to provide optimal electrical contact with minimal noise and capacitance. The electrode was fitted into the Axon instrument head-stage CV-7B which connected to the main multiclamp 700B amplifier. The bath was earthed to the head-stage.

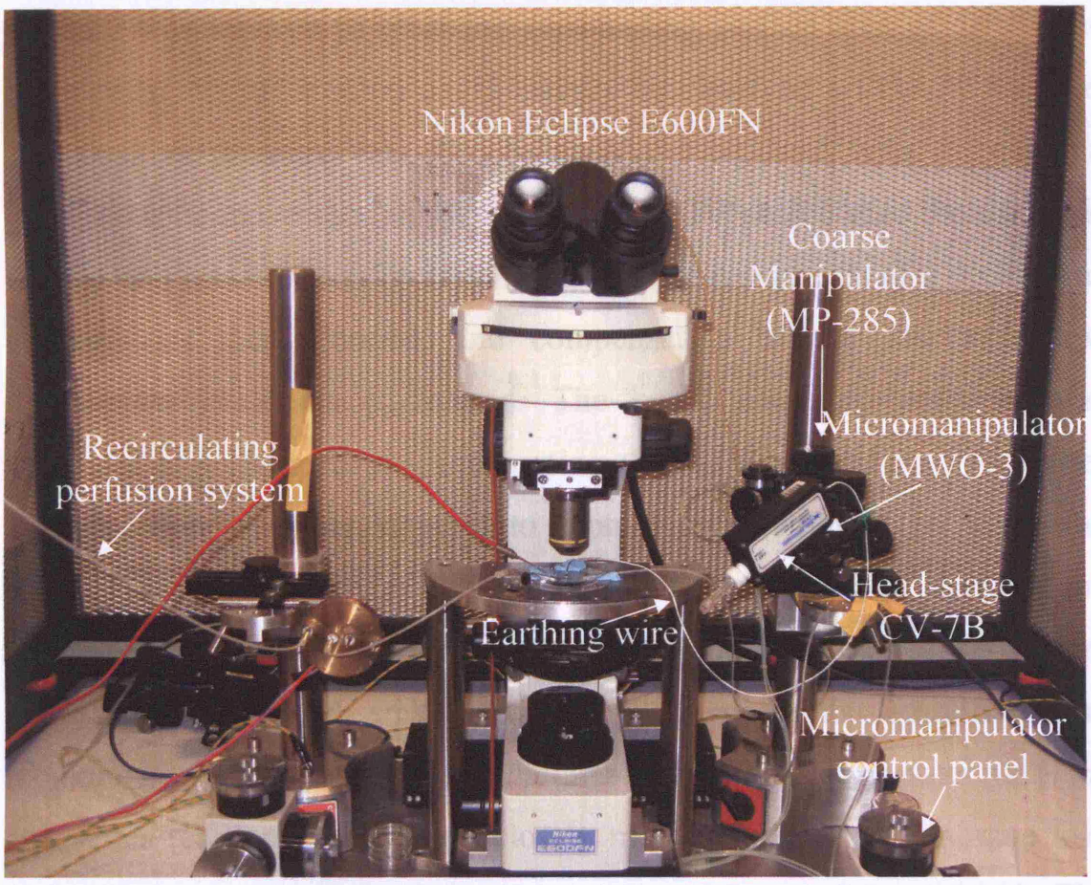

Fig 2.1 Microscope and experimental setup used for whole-cell patch clamp recording.

2.3.2 Whole-cell recordings

Prior to entering the bath solution with the electrode, slight positive pressure was applied to the patch pipettes. Clampex 9.2 software provided a seal-test, used to calculate the electrode resistance and monitor the fidelity of the cell-electrode seal resistances, by repetitively injecting small

voltage-steps of -5mV (50Hz, 10ms duration) to initiate a current response. The amplifier provided the option of electrode capacitance compensation by the injection of the small current to optimally reduce the fast and slow transient.

As the electrodes came into close contact with the PCs, the positive pressure was kept on to clear the surrounding surface area of debris and other cells. An indentation could usually be observed on the PC surface. The positive pressure was then relieved and replaced with a small but continuous negative suction by month. As the PC sealed onto the electrode tip, the cell-attached configuration formed with resistances of 1-5 GΩ. The suction was then stopped, and compensation of the fast and slow capacitance transients performed. The patch electrode potential was increased and clamped to -70mV using the 700B multiclamp. A further sharp suction was then applied to rupture the membrane to allow the equilibration of electrolytes between the electrode and the PC forming the whole-cell configuration. Whole-cell capacitance and series resistance, were compensated by small current injections by the amplifier. The membrane property parameters, including resting membrane potential (*Vm*) and series resistance (*Rs*), were closely monitored by the membrane test. *Vm* was on average -52.3 ± 2.3 mV (n = 10) and *Rs* was 8.9 ± 1.9 MΩ. The data were carefully filtered and selected for analysis so that recordings with *Vm* more depolarised than -50mV, or *Rs* fluctuation over 15%, were discarded to ensure a consistent quality of recordings. Recordings with holding currents over -500pA were also immediately rejected as a sign of cell leakage or damage.

2.4 Data acquisition and electrical stimulation

2.4.1 Gap free recording

Miniature IPSC currents were sampled at 20kHz, filtered via an 8-pole Bessel filter at 3KHz and digitised via a Digidata 1322A (Axon instruments) before viewing on Dell Pentium IV computer. All continuous control recordings were performed using a gap-free protocol in the main analysis/recording window of Clampex 9.2 (Fig 2.2). A three min period was allowed after whole-cell formation for the completion of Cl^- equilibration before starting recording. Gap free recordings were stopped, and switch to the episodic stimulation protocol (see below) to induce RP.

Fig 2.2 Gap-free recording of mIPSCs in the Clampex 9.2 scope window.

2.4.2 Electrical stimulation

An episodic stimulation protocol was used to apply repetitive depolarising voltage steps to the PC to evoke RP. A typical stimulation train consisted of eight 100ms pulses depolarising the membrane potential of PCs from -70mV to 0mV at a frequency of 0.5Hz, a total duration of the train of 16s. The *Rs* was monitored immediately after the stimulation to ensure the repetitive depolarising steps did not alter the electrical properties of the PC. Different stimulation latencies were investigated, with the depolarisation protocol being applied at 5', 8', 12', 15, and 20' after the formation of the whole-cell configuration.

2.4.3 Drug application

With the exception of CaMKIINtide, most drugs were dissolved in the pipette solution by vortexing or ultrasonicating for internal dialysis into the cell. Due to the limited diffusion rate of certain large molecular weight drugs (e.g. botulinum toxin and kinase peptide inhibitors), the stimulation latency, i.e. time between whole-cell formation and stimulation, was prolonged to accommodate this and allow sufficient time for the drugs to reach their putative sites of action. CaMKIINtide was dissolved in the aCSF superfusion media and bath-applied.

2.5 Immunohistochemical staining

2.5.1 Double-staining of parasagittal cerebellar slices

Wild-type or β2 knockout (β2-/-) mouse was dissected in ice cold slicing media, and the cerebellum was detached with the meninges

removed, then fixed in 0.4% w/v paraformaldehyde (PFA) solution for an hour at room temperature. After fixation, the cerebellum was mounted on the Leica Vibratome VT1000s in ice-cold (2-4°C) PFA solution and sliced into 100 μm parasagittal slices. The slices were then washed 3x with blocking buffer (10% w/v Bovine serum albumin BSA in phosphate buffer solution PBS), followed by thorough rinsing with PBS, 3 times. The slices were then placed in 0.04% w/v Triton-X, dissolved in blocking buffer, for another hour. The effect of Triton-X was to permeabilise the cell membrane and allow the access of antibodies to intracellular epitodes on the receptors. Triton-X was carefully removed by washing (3x) with blocking buffer followed by washing (3x) with PBS, before incubating the slices in primary antibody solution overnight at 4°C. Primary antibody solutions were made up in washing buffer and diluted according to different antibody concentrations and relative ability to stain tissues (see table 2.1). Identification of Purkinje cells was achieved with anti-Calbindin$_{D28K}$, recognizing an epitope on the endogenous calcium binding protein, calbindin. They were co-stained with different $GABA_AR$ subunit antibodies. Individual subunit antibodies were selected carefully to avoid cross-reactivity and the optimal concentration was determined by titration to maximize the signal-to-noise ratio. Secondary antibodies, donkey anti-mouse TRITC and donkey anti-rabbit FITC, were diluted at 1/200 to visualize calbindin$_{D28K}$ and $GABA_A$ subunits respectively. All antibody solutions were vortexed. Approximately 24 hours later, the primary antibody solutions were washed with blocking buffer and PBS, 3 times each, before secondary antibody incubation at room temperature for 3 hours under dark conditions, to minimize any loss of the fluorescence signal. The slices were then transferred onto microscope slides, and

mounted in 30μl of vector shield, covered with a cover-slip and sealed with nail varnish ready for viewing under the microscope.

Primary antibody	Dilution	Source	Secondary Conjugate	Dilution
Anti-cabindin$_{D28K}$ (mouse)	1:1750	Sigma	Donkey anti-mouse TRITC	1:200
Anti-GABA$_A$R α1 subunit (Rabbit)	1:200	Alomone	Donkey anti-rabbit FITC	1:200
Anti-GABA$_A$R α3 subunit (Rabbit)	1:250	Alomone	Donkey anti-rabbit FITC	1:200
Anti-GABA$_A$R α5 subunit (Rabbit)	1:150	Prof. W. Sieghart	Donkey anti-rabbit FITC	1:200
Anti-GABA$_A$R β1 subunit (Rabbit)	1:325	Santa Cruz Biotech.	Donkey anti-rabbit FITC	1:200
Anti-GABA$_A$R β2 subunit (Rabbit)	1:150	Abcam	Donkey anti-rabbit FITC	1:200
Anti-GABA$_A$R β3 subunit (Rabbit)	1:100	Abcam	Donkey anti-rabbit FITC	1:200

Table 2.1 Primary and secondary antibodies with their dilution factors. Donkey anti-mouse TRITC and donkey anti-rabbit FITC was purchased from Stratech Scientific Ltd, U.K.

2.5.2 Biocytin reconstruction of PC

To visualize the morphology of individual PCs in detail and study the differences across the genotypes, biocytin was dissolved in the patch pipette solution at 5 mg/ml, and applied intracellularly to PCs of wt, β2-/- and $\gamma2^{Y365,367F}$+/- animals for 30 min during current recording. After

recording ceased, the patch electrodes were carefully retracted. The slices with injected PCs were then transferred into 0.4% w/v PFA solution and kept at 4°C.

The slices were processed by removing the PFA solution and placing them in a 24-well plate, and followed by washing in PBS (3x, 20 min per wash). They were then immersed in 0.4% w/v Triton-X (in blocking buffer) for one hour on a shaker table. Triton-X was then washed off with PBS (3x) for maximal removal. Strep-Alexa-Fluor 488 was diluted to a concentration of 0.5-1 mg/ml in the blocking buffer to react with biocytin. Slices were incubated in this solution on the shaker table for two hours. Afterwards, slices underwent two short PBS washes of 5 min each and two long 30 min washes. Finally, the slices were mounted with Vectashield and sealed with nail varnish ready for viewing, as described before.

2.6 Confocal Microscopy

The mounted slices were viewed with a Zeiss laser-scanning confocal microscope (LSM 510 Meta). Confocal images were acquired using an argon laser (emission wavelength 488 nM) to visualize rhodamine/FITC fluorescence, and krypton (568 nM) to visualize tetramethylrhodamine isothiocyanate (TRITC), fluorsecence. An oil-immersion objective lens, x40 Plan-Neofluor, was used to visualize the cross-sections of the cerebellum for double-staining or for individual Purkinje cells injected with biocytin.

Double immunofluorescent co-staining of PCs and individual $GABA_AR$ subunits, required both lasers. Detector gain and amplifier offset was altered to achieve maximal signal-to-noise ratio.

The visualization of a single Purkinje cell only required excitation of Alexa 488 FITC by the argon laser channel. To construct a 3-Dimensional image of the PC, optical sections (Z stacks) of 0.45 μm intervals (pinhole size was set to 1 Airy unit) were transversely taken through the cell. These images were stacked together and combined to project the 3-D image of a single cell, using a panoramic projection program (from 64 projections) by LSM 510 META.

2.7 Data analysis of electrophysiological signals

2.7.1 Synaptic current analysis by MiniAnalysis

Synaptic currents were exported from Clampex 9.2 to MiniAnalysis (Synaptosoft) as Axon binary files.

Individual detection parameters were set to a threshold, for the batch analysis of the entire recording, (for example see table 2.2). The data was reviewed to manually delete distorted events, or repetitive detections of the same event. MiniAnaylsis detected the peak of the mIPSCs. The program then subtracted this peak from the baseline noise level (typically around 5 pA) to give the true value of mIPSC amplitude. The events were grouped by time into consecutive one min epochs. The mean amplitude and frequency within each epoch was calculated by the program to create a time profile for the mIPSCs.

Fig 2.3 Synaptic current analysis by MiniAnalysis program.

X – indicates the maximal current and the corresponding time

X – indicates the amplitude of half-point of average baseline

■ – indicates the starting time point of the event

■ – time where the current decays to e^{-1} of its maximum amplitude.

Parameter	Value
Amplitude threshold	10pA
Period to reach a local maximum	30000 μs
Time before a peak for baseline	15000 μs
Period to search for a decay time	100000 μs
Fraction of peak to find a decay time	0.37
Period to average a baseline	2000 μs
Area threshold	30 units
Direction of peak	Negative

Table 2.2 Synaptic current parameter detection criteria for optimal batch analysis.

Rise-times and decay time constants were fitted to groups of mIPSCs and analysed by the MiniAnalysis curve fitting program (Fig 2.7). 50 consecutive single events (with no deflections in rising or decaying phases) were chosen and filtered. These events were grouped and aligned by their 50% rise time, from which the maximal amplitude and mean rise-time can be calculated. This subsequently allowed regression analysis to determine the best fit for a single exponential decay time constant τ, defined as the time taken for the current to decay to e^{-1} (37%) of the maximal peak amplitude.

Fig 2.4 The group analysis and curve-fitting window for the calculation of rise times and decay time constants.

2.7.2 Peak-scaled Non-Stationary Noise Analysis (PS-NSNA)

MiniAnalysis provides peak-scaled NSNA, to estimate the single channel properties and the average number of functional channels in the synapse. One hundred single events were chosen randomly within a similar

time period during all recordings. PS-NSNA utilises a least squares scaling method, estimating γ and N_p circumventing the statistical errors of the ensemble variance. Assuming a maximum channel opening probability, *Po*, the lowest current variance occurs at the peak of the mIPSC. PS-NSNA was performed on a fixed length of mIPSC decay, starting from the peak current to the end of the mIPSC decay. The average current was scaled to the peak of the individual mIPSC amplitudes, and the amplitude was divided into equal size bins. The fluctuations due to channel opening and shutting during the decay, were found by subtracting the mean current variance from the mean mIPSC current decay. The amplitude variance within each scaled average bins was then calculated and plotted against the average bin current (De Koninck and Mody, 1994). The variance against mean amplitude relationship was fitted by:

Equation 2.1. $\sigma^2 = (iI_m - I^2_m/N_p) + Var_b$

where σ^2 is the current variance, i is the unitary current, I_m is mean current and N_p is the average number of receptor channels open in response to a single vesicle release in the synapse. Var_b is the baseline variance. Hence this function should adopt the shape of a symmetrical parabola (Fig 2.5).

Fig 2.5 PS-NSNA of 100 single mIPSCs using the peak-scaled method in MiniAnalysis

This plot estimated single channel current (pA) by the initial gradient of the parabola, which was converted to unitary conductance by

Equation 2.2: $$\gamma = i/(V_m - E_{Cl})$$

where γ is the unitary conductance, V_m is the holding potential of the cell, E_{Cl} is the Cl^- reversal potential and i represents the single channel current. The reversal potential of Cl^- for PCs was calculated by the Nernst equation (equation 2.3) to be +0.69 mV, as a result of the equimolar extracellular and intracellular Cl^- concentrations.

Equation 2.3: $$V_{Cl} = \frac{RT}{zF} \ln ([Cl^-]_{in}/[Cl^-]_{out})$$

The MiniAnalysis program used a peak-scaled method for IPSC amplitudes such that *Po* values were assumed to be close to 1, to minimize the intrinsic variance caused by the stochastic behaviour of channel

opening and closing at the peak. This distorted the estimation of the total number of receptors, N, allowing only a true estimate of N_p, the average number of receptors open at the peak of the mIPSC.

2.7.3 Data presentation

Data extracted from MiniAnalysis was transferred to Origin Ver6.0 as a normal text or ascii file. All time profiles and histograms were plotted in Origin 6.0. In addition, Gaussian distributions were used to fit the amplitude distributions. In most PCs, multiple (usually 3) Gaussian compoments could be identified and fitted separating individual mIPSC populations.

2.7.4 Statistical analysis

All statistical tests were performed using GraphPad Instat program 3.01 (GraphPad, USA). Mean values of amplitude and frequency at equivalent time points from two different conditions were compared using unpaired Student's t-test to calculate their statistical significance. When multiple means were involved, ANOVA tests were used with a Bonferroni post-test. 2 way ANOVA were performed on selected time profile of mIPSC amplitudes and frequencies. Two means were considered significantly different if $P < 0.05$.

2.8 Drugs preparation and application

2.8.1 Drug preparation

With the exception of CaMKIINtide, NBQX, AP5 and TTX, all drugs were applied internally. The reagent stock solutions were made up in

internal solution or 1M Dimethyl sulfoxide (DMSO). The stock solutions were kept at 4°C, -18 °C or -70 °C according to guidelines and diluted in 1ml of internal patch pipette solution on the day of recording. CaMKIINtide, NBQX, AP5 and TTX were dissolved in the perfusion solution during recording.

- **Okadaic acid sodium salt** (Sigma), inhibitor of protein phosphatase, was made up in stock concentration of 100 μM, applied internally at a final concentration of 150 nM.
- **Sodium Orthovanadate** (Sigma), tyrosine phosphatase inhibitor, was heat-dissolved in distilled water, and adjusted to pH 10. Stock solutions of 20 mM concentration were diluted to 200 μM in the internal solution before usage.
- **CaMKIINtide** (Calbiochem) peptide inhibitor of CaMKII, was dispensed in distilled water at stock concentrations of 500 μM, then diluted at 1:1000 to achieve a final concentration of 500 nM.
- **Genistein** (Sigma) inhibitor of protein tyrosine kinase, was dissolved in DMSO to make up stock solution of 80 mM concentration. The final concentration in the internal pipette solution was 100 μM.
- **β3 peptide intracellular loop 303-312**, a GST fusion peptide of protein sequence, VNYIFFGRGP, from residues 303-312 of the major intracellular loop of $GABA_AR$ β3 subunit, was synthesized by Mr. M. Lumb to inhibit the putative binding of CaMKII to β3 subunits. This peptide was dissolved in pipette solution via sonication at a concentration of 170 μg/ml.
- **Scrambled peptide FRNIGPFGYV*** was used at the same concentration as the β3 intracellular loop 303-312.

- **Staurosporine** (Sigma) non-specific inhibitor of protein kinases. Stock solution of 10 mM was made up in DMSO, final concentration applied internally was 10 μM.

- **Botulinum Toxin light chain B** (Listlabs) BoNT light chain B was dissolved in distilled water to 500 nM concentration. This solution was then filled at the tip of the pipette electrode by back suction while the rest of the pipette was filled with normal internal solution. The volume of the tip solution was sufficient for inhibition of vesicle fusion after 20 min diffusion.

- **Guanosine 5′-[β-thio]diphosphate trilithium salt GDP-β-S** (Sigma), inhibitor of G proteins, was dissolved in internal solutions to make up the final concentration of 1 mM.

- **N-ethylmaleimide (NEM)** (Sigma) stock solution of 250 mM was made up in DMSO, then diluted 1:1000 to achieve a final internal concentration of 250 μM.

- **Monensin sodium salt** (Sigma), DMSO stock solution was made of 75 mM, final internal concentration was 75 μM.

- **Brefeldin A** (Sigma) was dissolved in DMSO at stock concentration of 200 μM, with a further 1:1000 dilution to achieve the final internal concentration of 200 nM.

- **2,3-dihydroxy-6-nitro-7-sulfamoyl-benzo[f]quinoxaline 2,3dione (NBQX)** (Tocris) was dissolved in distilled water at 10 mM, aliquots of solution were dissolved in aCSF to achieve final concentration of 10 μM.

- **D-(–)2-amino-5-phosphonopentanoic acid (D-AP5)** (Tocris), was dissolved in distilled water for stock concentration of 50 mM, then 1:1000 diluted in aCSF to achieve 50μM.

- **Tetrodotoxin TTX citrate salt** (Tocris) is water soluble, stock solution was made of 500 μM, final bath concentration of 500 nM.
- **N-(2,6-Dimethylphenylcarbamoylmethyl) triethylammonium bromide QX-314** (Tocris) was dissolved in internal solution at concentration of 5 mM and kept in at -18°C.
- **Biocytin** (sigma) was dissolved in the internal solution at 5 mg/ml via vortexing.
- **Strepto-avidin Alexa fluor 488** was provided by Dr I. Duguid, T-octylphenoxypolyethoxyethanol (Triton-X), PFA, PBS and BSA were all obtained from Sigma.

2.8.2 Pre-activation of recombinant α-CaMKII (New England Biolabs).

In experiments using the direct internal perfusion of αCaMKII, truncated 33 kDa monomer of rat α-CaMKII (1-325 amino acids) with specific activity of ~5,000,000 units/mg was used at 500 units/μl. The CaMKII stock solution was supplemented with 100 mM NaCl, 50 mM Tris-HCL (pH 7.5 at 25°C), 0.1 mM Na_2EDTA, 1mM dithiothreitol (DTT), 0.02% v/v Tween-20 and 50% v/v glycerol and kept at -70°C to preserve the kinase activity. Prior to usage, glycerol content was removed, with Slide-A-Lyzer MINI Dialysis kit. The Dialysis kits were soaked in de-ionised water for 15 min, and placed in microtubes filled with 1.3 ml of dialysate units containing 100 mM NaCl, 50 mM Tris-HCl (pH 7.5 at 25°C), 0.1 mM EDTA and 1 mM DTT. Without penetrating the membrane, the αCaMKII mix solution was placed over the membrane just immersed in

the dialysate. The dialysate unit was then capped and kept at 4°C for 1 - 2 hours to allow the glycerol to be removed. Afterwards the purified αCaMKII was extracted from above the membrane, and aliquoted into 20 μl volumes, to be frozen at -70°C.

On the day of recording, the defrosted 20 μl of αCaMKII aliquot was pre-activated on the bench in the presence of 5 μl CaMKII buffer (supplied with a composition of 50 mM Tris-HCl, 10 mM $MgCl_2$, 2 mM DTT, 0.1 mM Na_2EDTA, pH 7.5 at 25°C), 5 μl of 1.2 μM calmodulin (CaM), 5 μl of 1.5 mM $CaCl_2$, 5μl of 0.4 mM ATP, at 25°C for 15 min. This made up of a total of 40 μl of αCaMKII solution, which was then mixed with 190 μl of internal solution to achieve a 1:12 dilution hence an effective concentration of 100 nM αCaMKII in the patch pipette solution.

For control experiments, the activated αCaMKII solution was heat-inactivated at 65°C, using a water bath to denature the kinase.

2.9 Knockout mice

The α1 knockout mouse strain was constructed by the disruption of exon 4 of the α1 subunit gene. The β2 knockout mouse was generated by the deletion of exons 6 and 7 of the β2 subunit gene by homologous recombination (Sur et al., 2001) (both obtained from Merck Sharp and Dohme, UK). Homozygous generation of > F10 were breed to produce α1-/- and β2-/- strains.

The $\gamma 2^{Y365,367F}$ +/- mouse strain (obtained from by Dr. V.Tretter, UCL) had exon 10 of the $\gamma 2$ gene disrupted. Heterozygous < F5 generation mice were cross-bred to produce $\gamma 2^{Y365,367F}$ +/- and littermate wild-type animals.

All mice strains were taken at the age between P11-14 for slice preparation and recording. The mouse tails were retained and kept for genotyping to identify the genotypes of the mice. DNA was extracted from the mouse tails of interest, and run through a PCR reaction using primers for each subunit ($\beta 2$ and $\gamma 2$) gene and a primer complimentary to the neomycin cassette as a positive control for homologous recombination. Most of the genotyping was carried out by Mr. M. Lumb.

Chapter 3

Characterisation of rebound potentiation

3.1 Introduction

The cerebellum is of fundamental importance to motor learning and for regulating the coordinated movement of vertebrates (Fuentes and Bastian, 2007; Glickstein, 2007; Mccormick and Thompson, 1984; Robinson, 1976). This requires long-term learning and memory acquisition as well as the ability to rapidly adapt to external and internal stimuli by activity dependent changes to synaptic transmission. The principal neuron of the cerebellum, the PC, receives direct excitatory inputs from granule cell-derived PFs, and inputs from CFs that originate from the inferior olive. In the mature brain, CF inputs innervate PCs in a 1:1 ratio with multiple synapses throughout the PC dendritic tree, creating ~1500 release sites, thought to be the strongest excitatory connection in the CNS (Strata and Rossi, 1998). CF stimulation of PCs triggers a powerful depolarisation via the activation of AMPARs, resulting in complex spikes with a fast Na^+ component and slower multiple Ca^{2+} and Na^+ currents (Daniel et al., 1998; Maeda et al., 1999). This subsequently activates VGCCs. The majority of the VGCCs involved in the depolarising complex are of P/Q-type (~90%), with smaller contributions (10%) from L-, N- and R-types in PCs (Llinas et al., 1992).

The activation of VGCCs causes a large elevation of cytosolic (particularly dendritic) Ca^{2+} level, with further release of Ca^{2+} from

intracellular Ca^{2+} stores, facilitating expression of multiple long-term as well as transient synaptic plasticities within the cerebellum (Hartmann and Konnerth, 2005; Hashimoto et al., 1996; Konnerth and Eilers, 1994). Of interest, coincident stimulation from PF and CF strengthens the Ca^{2+} transient and creates a supralinear Ca^{2+} wave. This promotes AMPAR internalisation leading to long-term depression (LTD) of excitatory transmission at PF-PC synapses (Weber et al., 2003). This PF-LTD could be reversed by postsynaptically expressed LTP, thereby resetting synaptic strength (Lev-Ram et al., 2002).

DSI is an example of short term plasticity triggered by CF stimulation, with duration of 30-40s (Vincent et al., 1992). This is mediated by Ca^{2+} induced release of endocannabinoids from PCs that act as retrograde messengers by binding to the presynaptic CB1 receptors to reduce the presynaptic release of GABA (Yoshida et al., 2002). The outcome is a transient reduction in mIPSC frequency with little effect on mIPSC amplitude, reflecting a presynaptic locus of modification. A similar retrograde signalling system has also been implicated to underlie DPI, after the cessation of DSI. DPI utilises glutamate as the retrograde messenger and requires the activation of presynaptic NMDA receptors to achieve a long-term enhancement of presynaptic GABA release (Duguid and Smart, 2004). The putative somatodendritic release of glutamate can also act in an autocrine manner to activate mGluR1 receptors on the PCs, through coupling to G_{q11} proteins and PLCβ4, to induce endocannabinoid production and release, facilitating DSI expression (Duguid et al., 2007).

Rebound potentiation is defined as the long-term potentiation of inhibitory transmission between cerebellar interneurons and PCs, triggered by repetitive CF stimulation. The superlinear Ca^{2+} influx from the VGCCs and subsequent Ca^{2+} dependent Ca^{2+} release from intracellular Ca^{2+} stores activates multiple Ca^{2+} dependent kinase pathways leading to the enhancement of inhibitory currents (Kano et al., 1992; Kano et al., 1996). This potentiation had a relatively fast onset, peaking between 3-15 min, with mIPSC amplitudes reaching a peak of 180% of control. The mIPSC potentiation slowly decayed with time, but sustained during the 75 min recording. Simultaneous fluorometric Ca^{2+} measurements showed a transient, steep increase in Ca^{2+} from ~30nM to ~900nM in the dendritic area of Purkinje cells and a smaller increase to ~200nM in the soma. These increments fell back to basal levels ~40s after the stimulation. The critical importance of cytosolic Ca^{2+} was confirmed by the inhibition of RP by intracellularly dialysing the Ca^{2+} chelator, BAPTA (Kano et al., 1992), intracellular IP_3 and ryanodine-sensitive Ca^{2+} store inhibitors, heparin and Ruthenium Red respectively, and also by using the Ca^{2+} store uptake blocker, thapsigargin (Hashimoto et al., 1996).

The modulation of mIPSC amplitude but not frequency, implies RP has a postsynaptic loci of expression. In accord with this observation, responses to exogenously-applied GABA exhibited a similar profile of augmentation to synaptic events after depolarisation of PCs, exposing an increase in postsynaptic $GABA_AR$ responsiveness.

In this chapter, the mIPSCs recordings were taking from P11-14 PCs, an age near the final maturation of PCs and rapid dendritic growth (McKay

and Turner, 2005), and studied before and after RP induction for amplitude, frequency and kinetics analysis. Different latency protocols were used to achieve a basic understanding of the physiological profiles of RP.

3.2 Results

Whole-cell voltage clamp recordings of PCs were performed in 250 μm parasagittal cerebellar slices taken from P11-P14 mice (see Methods). PCs were identified by their alignment in the Purkinje cell layer of the cerebellum. The reconstructed image of a PC (Fig 3.1 A) after 30 min dialysis of biocytin-conjugated to streptoavidin alexa fluor 488 (concomitant with recording) showed that the dendritic tree and soma of the PC was undamaged during slicing and recording. PCs were voltage clamped at -70mV, mIPSCs were recorded in the presence of AMPAR and NMDAR blockers, NBQX (10 μM) and AP5 (20 μM) respectively, and the sodium channel blocker, TTX (500 nM), to inhibit action potential dependent release of transmitter. This ensures that we monitored only miniature inhibitory postsynaptic currents (mIPSCs), resulting from spontaneous GABA release. Unlike the single quantal unitary mIPSCs at other inhibitory synapses, mIPSCs recorded in PCs may also arise from spontaneous (action potential-independent) multivescular releases, owing to the presence of ryanodine-sensitive Ca^{2+} stores in the presynaptic terminals of interneurons. This unique feature gives rise to the appearance of lamIPSCs in PCs (Llano et al., 2000).

3.2.1 Basic electrophysiological profile of mIPSC in PCs

A typical recording of mIPSCs is shown in Fig 3.1B. The mIPSC amplitudes were highly variable, with the lamIPSCs from multivesicular release defined as having amplitudes > 200pA (Llano et al., 2000). Application of 20 μM bicuculline completely abolished all synaptic currents, confirming that they were wholly mediated

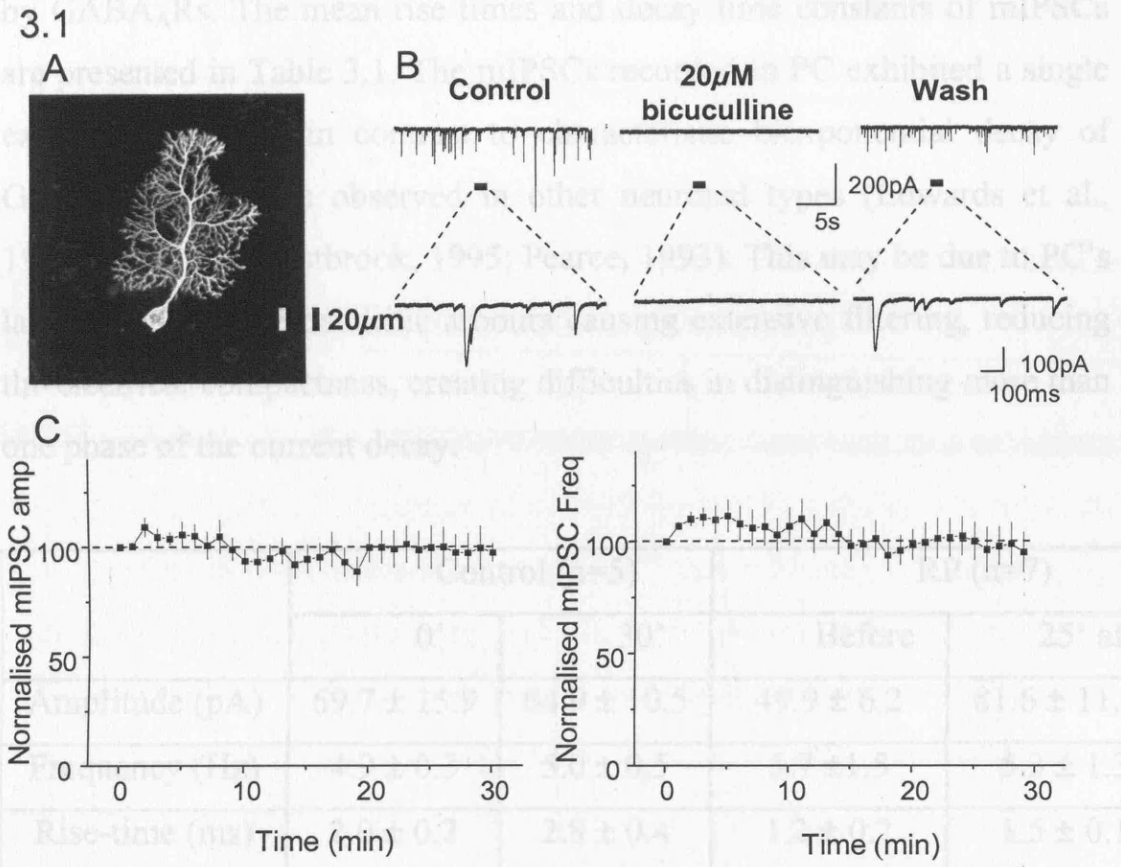

Fig. 3.1 The morphology and baseline mIPSC recordings in a cerebellar Purkinje cell.

A) Morphology of a single P11 Purkinje cell in a parasagittal slice. The image was reconstructed after dialysis of biocytin, conjugated to strepto-avidin alexa fluor 488. The cell was processed after a 30 min period of recording. The image was obtained using x63 oil immersion objective on a Zeiss LSM confocal microscope.

B) Basal mIPSC recording: before, during and after 20μM bicuculline application. Expanded epochs are shown below.

C) Time profiles for both amplitude and frequency of mIPSCs over a period of 30 min. No discernible fluctuations occur for either, indicating the stability of recording. Amplitude and frequency of mIPSCs were normalised to the first min epoch recording. All points are means ± s.e. (n=12)

by $GABA_A$Rs. The mean rise times and decay time constants of mIPSCs are presented in Table 3.1. The mIPSCs recorded in PC exhibited a single exponential decay, in contrast to characteristic biexponential decay of GABAergic currents observed in other neuronal types (Edwards et al., 1990; Jones and Westbrook, 1995; Pearce, 1993). This may be due to PC's large soma and the dendritic arbours causing extensive filtering, reducing the electrical compactness, creating difficulties in distinguishing more than one phase of the current decay.

	Control (n=5)		RP (n=7)	
	0'	30'	Before	25' after
Amplitude (pA)	69.7 ± 15.9	64.9 ± 10.5	49.9 ± 6.2	81.6 ± 11.9*
Frequency (Hz)	4.9 ± 0.3	5.0 ± 0.5	5.7 ±1.5	5.3 ± 1.3
Rise-time (ms)	2.0 ± 0.2	2.8 ± 0.4	1.2 ± 0.2	1.5 ± 0.1
Decay time constant τ (ms)	10.3 ± 0.8	16.1 ± 1.8*	10.9 ± 0.5	12.3 ± 0.8

Table 3.1 Amplitude, frequency and kinetics of mIPSCs.

Rise time (ms) and decay time constants (τ) were compared for mIPSCs recorded in control PCs and those induced for RP. Values of rise time and τ were taken from an average of 50 consecutive single events (see Methods) at the beginning and end in a subset of control recordings (n=5); for RP measurement, values were taking just before and 25 min after the induction for RP. Values are mean ± s.e. (mIPSC amplitudes following RP, and decay time constants in control recordings exhibited significant difference, * $P < 0.05$)

Prior to the induction of RP, it was established that the PCs in slices were stable to maintain whole-cell recordings of up to half an hour, as there were no discernable changes in mIPSC amplitude or frequency over this period of recording (Fig 3.1C).

3.2.2 Properties of mIPSCs before and after RP induction

To mimic the stimulation from a CF, a 0.5 Hz depolarising train of 8 voltage steps from -70mV to 0mV were applied with each one of 100ms duration (Fig 3.2A), 5 min after whole-cell formation initially. During each voltage-step, a large transient inward Ca^{2+} current was perceptible (Fig 3.2B). After the stimulation protocol, the average peak mIPSC amplitudes were normalised to the mean amplitudes measured during the control recording periods. The mIPSC amplitudes increased gradually after stimulation and attained a plateau within 10-15 min (Fig 3.3 A, 3.4 A). The extent of the amplitude potentiation at 25 min reached 162.8 ± 9.4% (mean ± s.e, n = 7) of control (=100%) and was sustained over the period of recording (Fig 3.4A, 3.5A).

In the mean time, a transient reduction in mIPSC frequency was observed, attributed to the presynaptically expressed DSI. mIPSC frequency was reduced to 75.1 ± 6.5% (20s after the depolarisation, n=7 $P < 0.05$) of control (=100%), and recovered shortly (Fig 3.3B and 3.4B). DPI was blocked in all experiments by the inclusion of NMDA receptor antagonist, AP5 (Duguid and Smart, 2004). The frequency fluctuated during the period of recording (at 10' after stimulation the frequency exhibited significant difference from control as indicated by asterisk Fig

3.4B), but there was no general trends in frequency change over the period of 25 min recording after stimulation (Fig 3.5B).

These data confirmed that a depolarisation-induced postsynaptic enhancement of inhibitory synaptic current occurs in PCs, in accordance with the development of RP. Overall, there was no significant difference between the decay kinetics of mIPSCs before and 25 min after the induction of RP (Table 3.1).

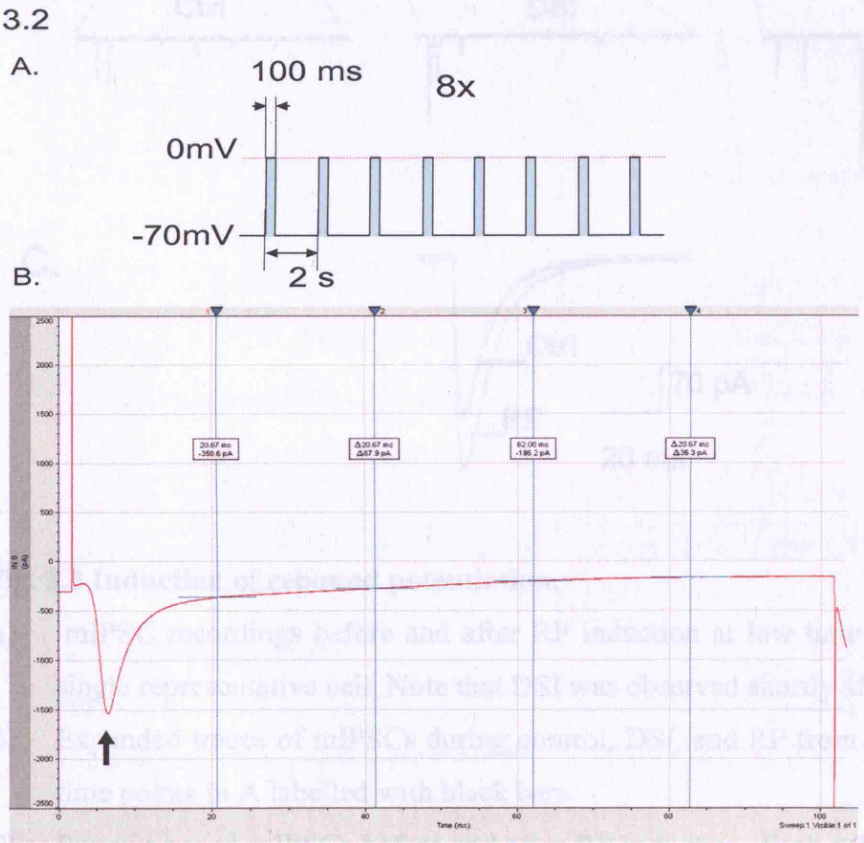

Fig 3.2 Stimulation protocol for PCs

A. Stimulus train of 8 depolarising voltage steps from -70mV to 0mV of 100ms duration at a frequency of 0.5 Hz. B. The corresponding current trace triggered by each voltage step. Note the transient inward current carried by Ca^{2+} (arrow).

3.3

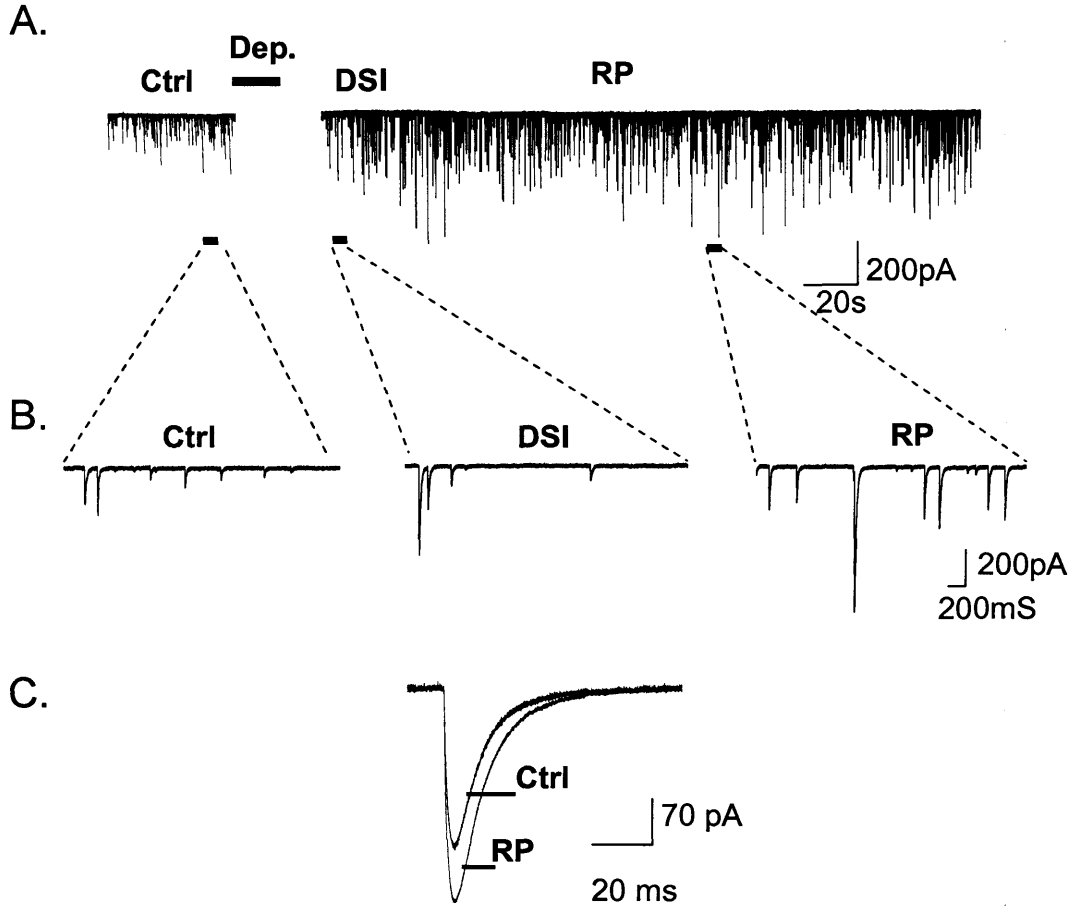

Fig. 3.3 Induction of rebound potentiation.

A) mIPSC recordings before and after RP induction at low time resolution from a single representative cell. Note that DSI was observed shortly after the stimulus.

B) Expanded traces of mIPSCs during control, DSI, and RP from the corresponding time points in A labelled with black bars.

C) Superimposed mIPSCs before and after RP induction. Each mIPSC was a scaled average from 50 single mIPSC events (**Dep** Short for depolarisation in following text).

3.4

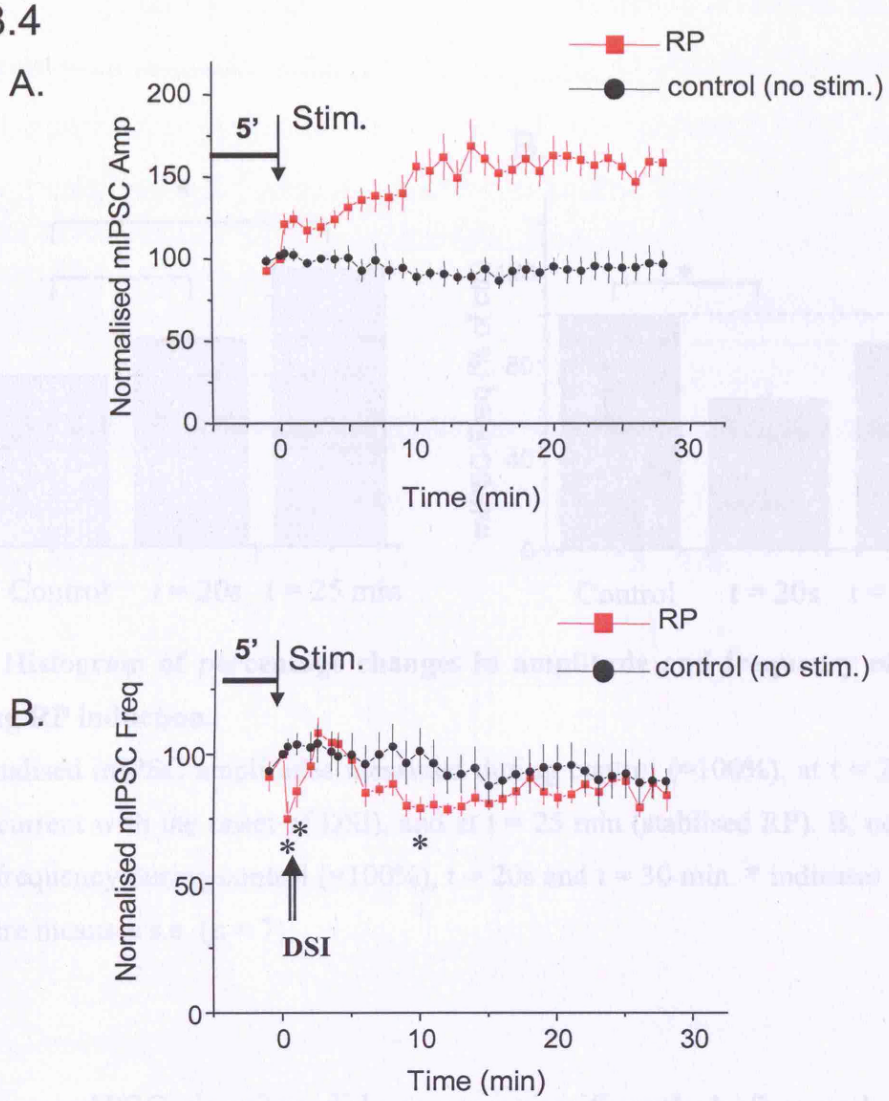

Fig 3.4 Time profiles of RP.

A) Normalised mIPSC amplitudes in control and after induction of RP. All events were normalised to a mean amplitude calculated from mIPSCs recorded one min before applying the stimulus and corresponding time in control (t= 0', RP mIPSC amplitudes were significantly different from control, from t = 20s to t = 28 min with $P < 0.05$).

B) Time profile of normalised mIPSC frequency for control and after induction of RP. The double arrow indicates the transient DSI (frequency did not differ significantly between control and RP unless indicate with asterisks at t = 20s, 1 min and 10 min. Single arrows indicate the time point of stimulation (t=0', n=7).

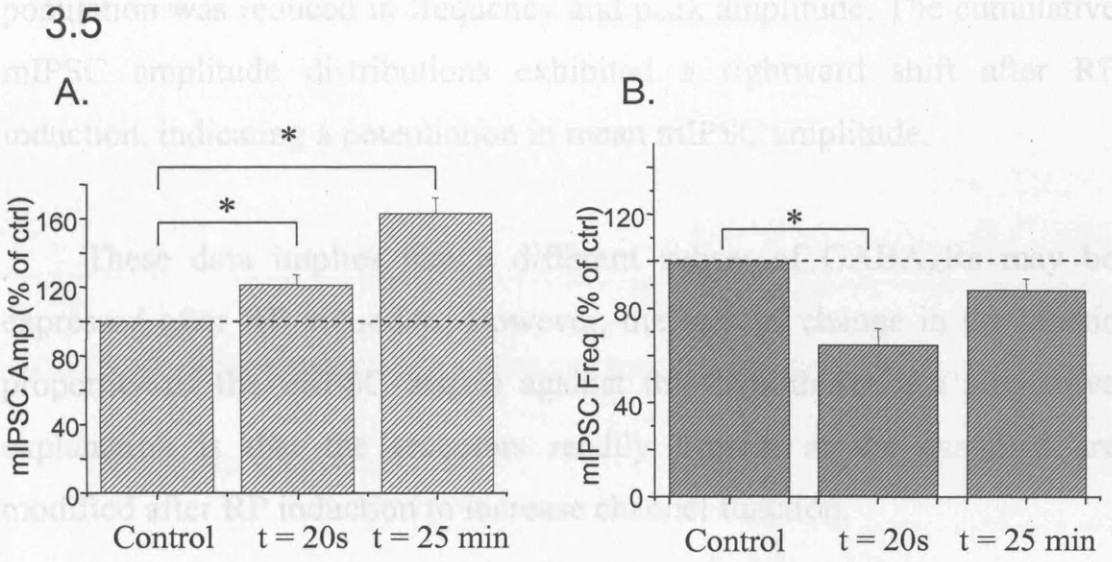

Fig 3.5 Histogram of percentage changes in amplitude and frequency of mIPSC following RP induction.

A. Normalised mIPSC amplitudes measured during control (=100%), at t = 20s (early RP, concurrent with the onset of DSI), and at t = 25 min (stablised RP). B, normalised mIPSC frequency during control (=100%), t = 20s and t = 30 min. * indicates $P < 0.05$. Values are means ± s.e. (n = 7).

Mean mIPSC rise time did not vary significantly before and after RP induction (Table 3.1). However, a scatter-plot of mIPSC amplitude *vs* rise time reflected a preferential potentiation of mIPSC events with fast rise times after RP induction. This population has a peak rise time of approximately 2 ms (Fig 3.6A), which may be resultant of more somatic inputs, most likely innervated by basket cells. This population-selective enhancement of mIPSCs suggests RP could be an input specific form of synaptic plasticity. In Fig 3.6 B, mIPSC distributions revealed a visible increase in peak amplitude (to over 250pA) and frequency of the large

amplitude population after RP induction, whilst the lower amplitude population was reduced in frequency and peak amplitude. The cumulative mIPSC amplitude distributions exhibited a rightward shift after RP induction, indicating a potentiation in mean mIPSC amplitude.

These data implies that a different subset of $GABA_A$Rs may be expressed after RP induction. However, the lack of change in the kinetic properties of the mIPSC argues against this hypothesis. An alternative explanation is that the receptors readily present at the synapses are modified after RP induction to increase channel function.

3.6

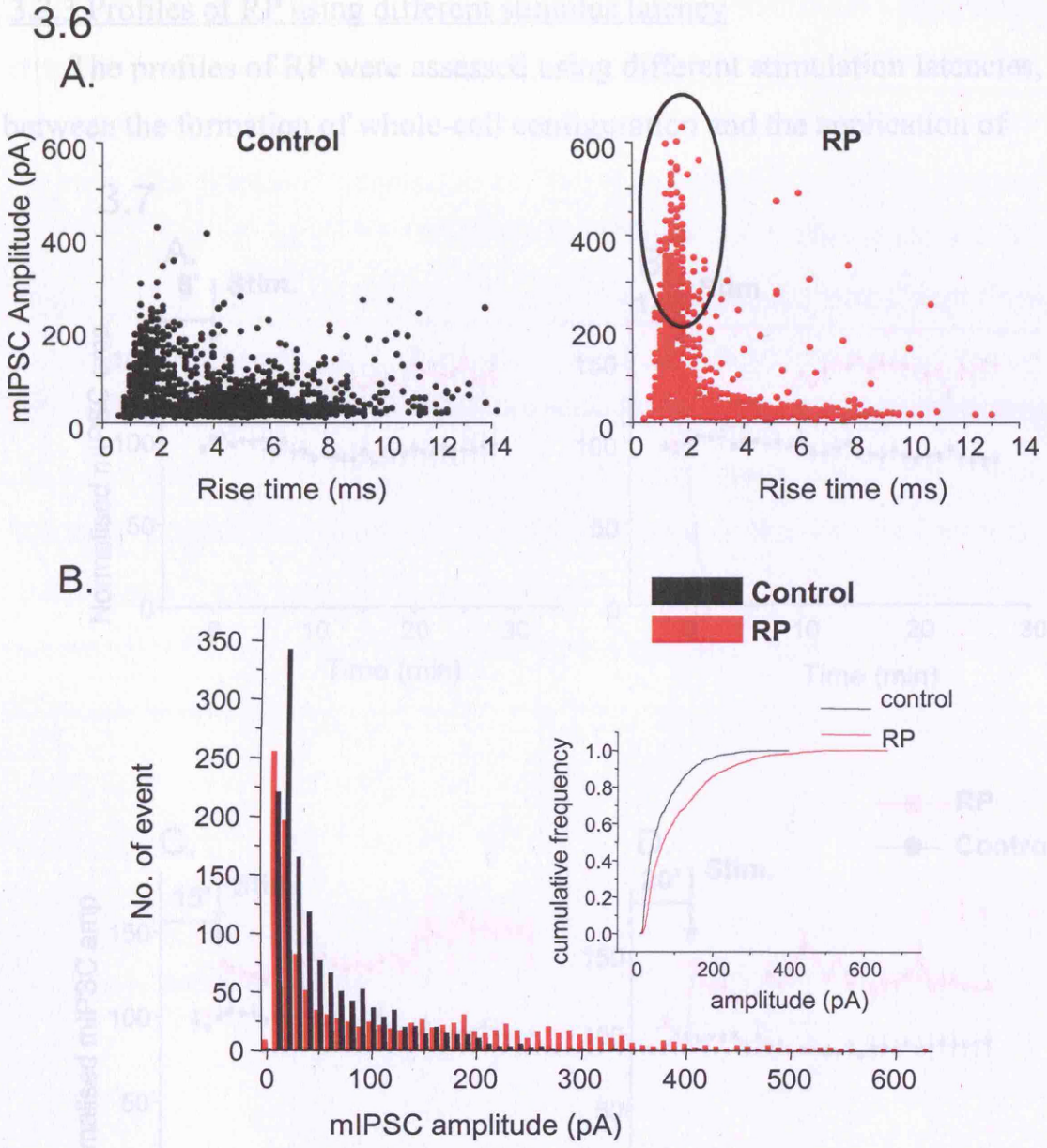

Fig 3.6 Amplitude distributions for mIPSC during RP.

A). Scatter plots of mIPSC amplitude *vs* rise time for under control condition (black, left) and after the induction of RP (red, right). The black circle on the right highlights the prominent preferential potentiation of fast rise-time events after RP.

B). Amplitude distributions for mIPSCs before (black) and after RP (red). Insert shows the cumulative mIPSC amplitude for control and after RP distribution ($P < 0.05$).

3.2.3 Profiles of RP using different stimulus latency

The profiles of RP were assessed using different stimulation latencies, between the formation of whole-cell configuration and the application of

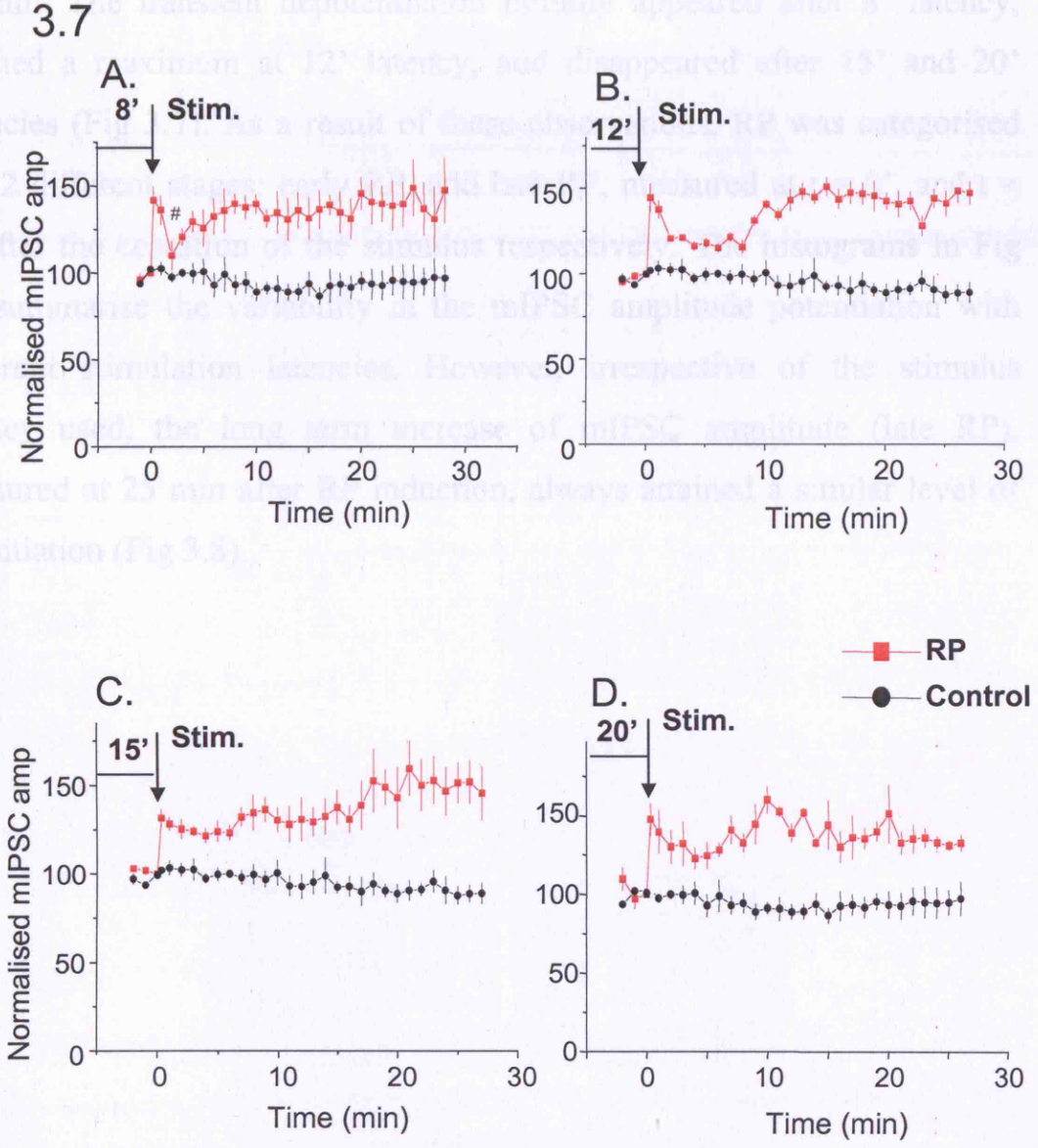

Fig. 3.7 mIPSC amplitude time profiles using different stimulation latencies.

A, latency = 8 min (n=5). B, latency = 12 min (n=20). C, latency = 15 min (n=5). D, latency = 20 min (n=5), before induction of RP (all points are significantly different between control and RP from t = 20s $P < 0.05$, with the exception of t = 2 min in the 8' profile marked by #).

the depolarising stimulus. As the latency increased, the initial potentiation in mIPSC amplitude became faster followed by a transient depotentiation in amplitude, which recovered to the initial level of potentiation within 10-15 min. The transient depotentiation initially appeared after 8' latency, reached a maximum at 12' latency, and disappeared after 15' and 20' latencies (Fig 3.7). As a result of these observations, RP was categorised into 2 different stages: early RP, and late RP, measured at t = 0', and t = 25'after the cessation of the stimulus respectively. The histograms in Fig 3.8 summarise the variability in the mIPSC amplitude potentiation with different stimulation latencies. However, irrespective of the stimulus latency used, the long term increase of mIPSC amplitude (late RP), measured at 25 min after RP induction, always attained a similar level of potentiation (Fig 3.8).

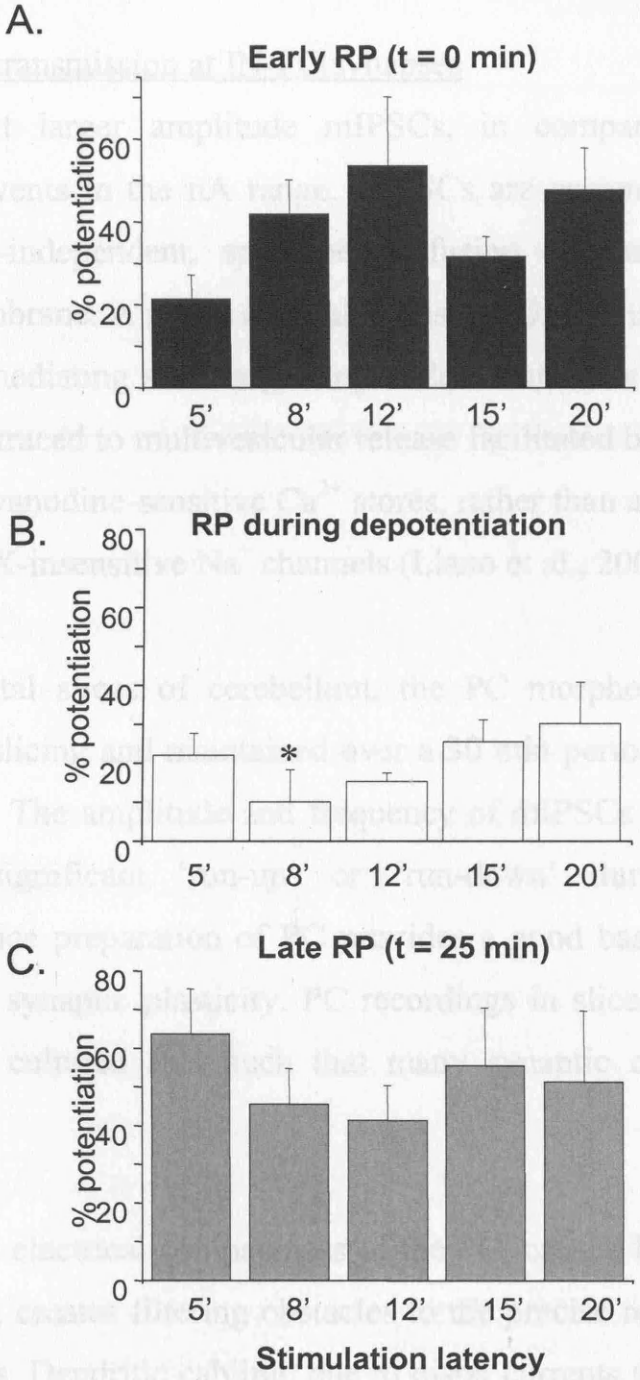

Fig 3.8 RP at different time points after induction following different latency stimuli. A, Early RP, measured immediately after stimulus cessation (t = 0min). B, RP measured at the lowest level of enhancement between early and late RP. C. Late RP measured at the end of recording (all points are significantly different from control, $P < 0.05$ with the exception of 8' profile in panel B marked by *).

3.3 Discussion

3.3.1 Inhibitory transmission at IN-PC synapses

PCs exhibit larger amplitude mIPSCs, in comparison to many neurons, with events in the nA range. mIPSCs are currents mediated by action potential-independent, spontaneous fusion of vesicles with the presynaptic membrane. A single quantal release of GABA is believed to be inadequate for mediating such large amplitude events. The origin of these events could be traced to multivesicular release facilitated by the activation of presynaptic ryanodine-sensitive Ca^{2+} stores, rather than action potentials triggered by TTX-insensitive Na^{+} channels (Llano et al., 2000).

In parasagital slices of cerebellum, the PC morphology was well preserved after slicing and maintained over a 30 min period of whole-cell patch recording. The amplitude and frequency of mIPSCs was stable and exhibited no significant 'run-up' or 'run-down' during recording. Therefore the slice preparation of PC provides a good basis on which to study inhibitory synaptic plasticity. PC recordings in slices also have the advantage over cultured PCs such that many synaptic connections are intact.

The limited electrical compactness of the PC, caused by its extensive dendritic arbour, creates filtering obstacles to the precise resolution of PC synaptic currents. Dendritic cabling, due to distal currents travelling to the somatic recording site from remote dendrites, could lead to distortion of measurements, with prolonged rise-times and underestimated amplitudes. To improve the quality of data, recordings were chosen for analysis with membrane resistance of approximately 100MΩ and access resistance of

approximately 10 MΩ. Under these conditions, the rise times of mIPSCs had a broad distribution from less than 1 ms to over tens of ms. The PC mIPSCs were described by a single exponential decay, τ_{decay} exhibited a slight run up over 30 min of recording. After RP induction, this variation was no longer evident. The decay time constant may be affected by the loss of intracellular proteins, as ligand unbinding and desensitization rate can be determined, in part, by the phosphorylation state of neurons. Inhibition of dephosphorylation by calcineurin (PP2B) inhibitors, shortened the rapid GABA current profiles (that mimic IPSCs) in outside-out patches of hippocampal neurons, by increasing the microscopic ligand unbinding rate and the gating kinetics (Jones and Westbrook, 1997). Given that RP is a phosphorylation-dependent phenomenon (see chapter 4), depolarization is likely to activate multiple protein kinases to enhance receptor phosphorylation. This may have the same effect as inhibition of phosphatases, which could account for the lack of increase in τ_{decay} after RP.

3.3.2 Ca^{2+} dependent synaptic plasticity at IN-PC synapses: DSI

The CF-PC synaptic connection is believed to be one of the strongest excitatory synapse within the CNS. Stimulation from CF generates profound Ca^{2+} transients in the postsynaptic PC to levels as high as 15 μM (Hartmann and Konnerth, 2005). Ca^{2+} entry is the crucial precursor for all cerebellar synaptic plasticity. Here, we encountered two forms (DPI was blocked by AP5) of plasticities induced simultaneously by depolarisation-induced activation of Ca^{2+} transients, namely DSI and RP.

DSI originates from a presynaptic locus, entails the postsynaptic release of endocannabinoids, which act as a retrograde messenger to activate the presynaptic CB1 receptor. The reduction in frequency due to depressed GABA release reached 75.1 ± 6.5% of control, in accordance with previously published values of 65-70% (Glitsch et al., 2000). The lowered mIPSC frequency recovered shortly (< 1 min) after the stimulus, concurrent with the expression of RP. Though the two forms of plasticity are independently regulated, it has been proposed that DSI, is required to reduce the presynaptic release of GABA during the onset of RP, thereby eradicating the suppressive effect of postsynaptic $GABA_BR$ on RP, via inhibition of cAMP-PKA pathway, and increasing the activity of the phosphatase PP1 to reduce CaMKII activity (Kawaguchi and Hirano, 2000).

3.3.3 Rebound potentiation: assessing mIPSC amplitude, frequency and kinetics

Rebound potentiation occurred instantaneously after the cessation of the induction stimulus. The mIPSC amplitude was augmented after a standard 5 min latency protocol, gradually reached a maximum and sustained throughout the period of recording, in accord with published results (Kano et al., 1992). With the inclusion of AP5, presynaptic NMDARs were blocked, preventing the occurrence of DPI (Duguid and Smart, 2004). The mIPSC frequency exhibited little long-term change, supporting the postsynaptic origin of RP.

The kinetics of mIPSCs also showed no discernible differences between RP and control conditions. However, the amplitude rise-time

scatter-plots unveiled a prominent separation of two populations of events after RP induction. The amplitude potentiation of fast rise-time events (mean < 2ms) was greater than that for slower rise-time mIPSCs (mean >5ms). The amplitude distribution also revealed an increment in the peak of the larger amplitude population of mIPSCs. Owing to dendritic cabling, currents initiated from distal dendritic areas may appear to have slower rise-times and lower amplitudes. However, fluorometric measurements suggested the Ca^{2+} transients in the dendrites were larger compared to that in the soma (Kano et al., 1992). It is therefore unlikely that a discrepancy in the Ca^{2+} transient caused RP to be less inducible in distal dendritic regions.

The differential potentiation of mIPSC populations may be governed by their distinct presynaptic inputs. The proximal dendritic region of the PC is known to be innervated by basket cells which form a dense network with numerous PCs (Ghez et al., 1985). Basket cell terminals are particularly enriched with ryanodine sensitive Ca^{2+} stores, eliciting large amplitude fast rise time somatic mIPSCs (Conti et al., 2004). The distal end of the PC dendritic tree, on the other hand, receives inputs from stellate cells, which only influences local synaptic activities (Ghez, et al., 1985). The data presented here suggests that basket cell inputs are preferentially targeted in RP over the stellate cell inputs. The occurrence of input specific synaptic plasticity has been reported previously in cerebellar stellate cells and hippocampal neurons (Losonczy et al., 2008; Soler-Llavina and Sabatini, 2006).

An alternative explanation may be the distinct localisation of different $GABA_AR$ subunits on PCs. Somatic receptors on PCs, composed mainly of $\alpha1\beta2\gamma2$, may have higher sensitivity toward phosphorylation than the postulated $\alpha3$ and/or $\beta3$ subunits containing receptors on the dendrites (see chapter 6) (Brandon et al., 2002; Brandon et al., 2000; Gutierrez et al., 1994; Kittler and Moss, 2003; McDonald et al., 1998), as the outcome of phosphorylation is subunit- and cell type specific.

The increment in mIPSC amplitudes may concern the possibility of receptor insertion (see chapter 5). Although to date, no direct evidence has been provided to explain the precise mechanism by which kinases, such as CaMKII, induces RP.

3.3.4 Different latency stimulations affect the RP profiles

Whole-cell patch recording allows intracellular proteins to diffuse out through the patch pipette, potentially disrupting the innate physiological state of the cell. Indeed, a 'wash-out' effect on RP has been report in PCs (Boxall et., al 1997). In the study, optimal RP expression occurred when the stimulus was applied 3 min after forming the whole-cell configuration. As the latency period increased, the extent of rebound potentiation declined from the maximum.

We also revealed a correlation between the degree of rebound potentiation and the stimulus latency. Interestingly, late RP, remained at 160% regardless of the latency period. As the latency increased, a depotentiation appeared following the early RP. This peak and trough

phenomenon was most obvious at 12', and gradually disappeared as the latency period increased further.

A simple 'wash-out' of intracellular protein kinases seems inadequate to fully account for this complex profile of RP, as the potentiation did recover following the transient depotentiation. These observations favour the hypothesis of two phases of RP, short-term (early) and long-term (late) RP. Whether early and late RP are regulated through common or independent pathways were explored further in later chapters (see chapter 4 and 5).

One possible explanation for the two phases is that, providing receptor insertion contributes to the expression of RP (see chapter 5), the early RP might be instigated by insertion of a readily-accessible recycling receptor vesicle pool located close to the membrane. Indeed, the existence of a subsynaptic reservoir of $GABA_ARs$, aggregated close to the postsynaptic density, has been identified in hippocampal neurons (van Rijnsoever et al., 2005). Postsynaptic (intracellular receptor containing cargo) vesicles may undergo a direct Ca^{2+} induced exocytosis to trigger early RP, prior to late RP which may involve separate intracellular receptor pools, such as the newly-synthesed receptors from the ER, delivered via the route of trans-Golgi-network (TGN) to membrane surface. Increasing the stimulus latency may disrupt the transition of these two phases, giving the appearance of a trough between early and late RP.

Increasing the latency period before RP induction may also disturb the subtle balance between kinases and phosphatases. Previous work on RP

provided a general hypothesis that kinases promote the induction of RP (Kano et al., 1996), whlist phosphatases counteract kinase activities by dephosphorylation, suppressing RP induction (Kawaguchi and Hirano, 2002). However, this hypothesis is not absolute, as inhibition of protein tyrosine kinase Src PP2 enhanced the extent of RP (Kawaguchi and Hirano, 2006). Differences in the wash-out rate of kinases and phosphatises, due to their intracellular mobility (e.g. βCaMKII is known to bind F-actin, hence may be less mobile; receptor activated PTKs such as TrkB, are tethered at the membrane, unlike soluble PTK such as Src, may have a slower washout rate; PP1 is thought to be more confined to synaptic region, while PP2A is free to move in the cytosome), increasing the latency change the ratio of kinase/phosphatase, hence resulting in depotentiation between early and late RP.

The role of direct $GABA_AR$ phosphorylation and insertion is investigated in chapters 4 and 5 respectively.

3.4 Conclusion

In this chapter, the basic properties of RP were explored. RP manifests simultaneously with presynatically expressed DSI, as a long term increase in the responsiveness of postsynaptic $GABA_AR$. We have also found, by increasing the latency between the formation of whole-cell configuration and application of stimulus, RP could be separated into an early and a late component. Intriguingly, the biased potentiation of the fast rise-time, large amplitude population of events, raised the prospect of an input specific plasticity.

Chapter 4

Phosphorylation signalling pathways for rebound potentiation

4.1 Introduction

Extensive internal Ca^{2+} elevation from both VGCCs and Ca^{2+} dependent Ca^{2+} release (CICR) following CF stimulation is the trigger for RP (Hashimoto et al., 1996; Kano et al., 1992). The 3~ 15 min delay between this Ca^{2+} transient and peak RP implicates the recruitment of Ca^{2+} activated second messenger systems (Kano et al., 1992). Previous work focused on the role of CaMKII and cAMP-dependent protein kinase A (PKA) (Kano et al., 1996). Both kinases are known to phosphorylate $GABA_AR\beta$ and $\gamma2$ subunits on residues in their major ICLs (Brandon et al., 2002; McDonald and Moss, 1994; McDonald and Moss, 1997). The application of 8-bromo-cAMP and the adenylate cyclase activator forskolin, caused a robust and long lasting potentiation of mIPSC amplitude similar to RP (Kano and Konnerth, 1992). A similar approach showed that enhancing CaMKII, either by injecting activated αCaMKII, or inhibiting phosphatases PP1 and PP2A with calyculin, also created RP-like potentiation of GABAergic currents in PCs (Kano et al., 1996).

Pharmacological inhibition of CaMKII with the calmodulin (CaM) binding domain (CBD), antagonist, KN62 (1-[N,O-Bis(5-isoquinolinesulfonyl)-N-methyl-L-tyrosyl]-4-phenylpiperazine), and calmidazolium (CMZ), a CaM antagonist, abolished long-term RP. However the suppression of RP only occurred if the inhibitors were applied prior to or during the stimulation. Delayed application (5 min

after the stimulation), proved ineffective against RP (Kano et al., 1996). This suggests that Ca^{2+}/CaM binding and activation of CaMKII is only involved in the induction of RP, whilst the maintenance of RP, may require Ca^{2+} independent autonomous activity of CaMKII by autophosphorylation, or a separate intracellular signaling mechanism.

A signaling model to account for RP was proposed by Kawaguchi in 2002 (Fig 4.1). Here, a Ca^{2+} /CaM complex formation activates Ca^{2+}/CaM-dependent proteins, CaMKII and calcineurin (PP2B). The latter acts as a negative control to antagonize the activity of CaMKII. Meanwhile, simultaneous $GABA_BR$ activation of Gi/Go protein, suppresses the activity of adenylate cyclase (AC), thereby inhibits the cAMP-PKA pathway. PKA is thought to act upstream of CaMKII and counteract calcineurin to determine the phosphorylation state of the adaptor protein DARPP32 (D-32). Dephosphorylated D-32 loses the ability to inhibit PP1, which is then free to deactivate CaMKII by dephosphorylating the Thr 286 autophosphorylation site, hence preventing the induction of RP. $GABA_BR$ activation also suppresses RP induction by reducing the Ca^{2+} influx via P type-Ca^{2+} channels. This provide GABA-mediated negative feedback controls of the efficacy of inhibitory synaptic transmission. Depolarization, applied in conjunction with exogenous GABA or activation of the presynaptic interneuron, caused a long-term sustained suppression of RP (LSRP) for up to 4 days (Kawaguchi and Hirano, 2000; Kawaguchi and Hirano, 2006). mGluR1 activation on the other hand, counteracts the suppression of RP induction by $GABA_BR$ via coupling to Gs and enhancing signaling via AC-PKA (Sugiyama et al., 2008).

Fig 4.1. A model for the signaling cascades regulating RP induction and suppression. CaM, Calmodulin; D-32, DARPP-32; P, phosphate; AC, adenylate cyclase. All these pathways converge on the level of CaMKII activity. (Modified from Kawaguchi and Hirano 2002 and Sugiyama 2008).

Ca^{2+}/CaM dependent kinase II (CaMKII) is one of the most abundant proteins in the brain accounting for 1-2% of total protein, existing in several different isoforms (Lisman et al., 2002). It has been proposed to serve as a 'memory molecule', and is widely implicated in the expression of synaptic plasticity, at both excitatory and inhibitory synapses, hence contribute to the formation of learning and memory (Lisman et al., 2002). While some studies observed concomitant long-lasting activity of CaMKII (including Ca^{2+} independent activity and the autophosphorylation of the enzyme) with the expression of LTP in hippocampal CA1 neurons (Fukunaga, 1993), others detected only a

transient increase of the autonomous activity of CaMKII during hippocampal LTP (Lengyel et al., 2004). Studies on RP supported that CaMKII and other kinases are only required for the induction and not the maintenance of RP (Kano et al., 1996).

The CaMKII dodecameric holoenzyme consists of either α, β or both subunits. αCaMKII is the predominant isoform in PCs, although the total α/β CaMKII ratio in the cerebellum 1:4 (Hansel et al., 2006; Sola et al., 1999). Each isoform is made up of a catalytic domain, sitting on the N-terminal, a regulatory auto-inhibitory domain (AID) overlapping with the Ca^{2+}/CaM binding domain, a variable region and a self association domain on the C-terminal. Ca^{2+}/CaM binding to the CaM binding domain disrupts AID association with the catalytic domain, and exposes the catalytic domain to protein substrates, revealing the autophosphorylation site, Thr 286 (on α isoform, 287 on β isoform) on the AID. Phosphorylation of this residue by a neighbouring subunit prevents further AID association with the catalytic domain, thereby enabling the Ca^{2+} independent activity. The enzyme hence becomes constitutively-active (autonomous state, see Chapter 1). This extends kinase activity beyond the initial Ca^{2+} signal in a graded fashion, as the persistent activity depends on the number of subunits autophosphorylated (Lisman et al., 2002).

The $GABA_AR$ β and $\gamma 2$ subunits contain several phosphorylation sites for CaMKII, located in their major ICL (McDonald and Moss, 1994; McDonald and Moss, 1997). Ser 409 in $\beta 1$, 408/409 in $\beta 3$, and Ser 410 in

β2 subunits are substrates, as well as S384 and S383 in β1- and β3 subunit respectively.

$GABA_AR$ modulation by CaMKII has multiple consequences. In synaptosomal membranes, CaMKII increased the binding of the agonist muscimol to $GABA_ARs$, indicative of an increased availability of functional receptors (Churn and DeLorenzo, 1998). Direct enhancement of GABA mediated Cl^- current was also observed by either injection of thiophosphorylated, pre-activated CaMKII in acutely-isolated spinal cord neurons (Wang et al., 1995), or by increasing Ca^{2+} influx in cortical neurons (Aguayo et al., 1998). αCaMKII potentiated GABAergic currents in cultured rat cerebellar granule cells and in recombinant receptors expressed in neuroblastoma NG108-15 cells, of subunit composition, α1β3γ2, but not α1/β2γ2. The phosphorylation mediated potentiation was partially reduced by the mutation of the CaMKII substrate S383 in the β3 subunit, and completely eliminated by further mutation of tyrosine phosphorylation sites Y365 and Y367 in the γ2 subunit, exposing the possibility of cross-talk between protein tyrosine kinase (PTK) and CaMKII (Houston and Smart, 2006; Houston et al., 2007).

PTK phosphorylation of $GABA_ARs$ also bears functional implications. The γ2 subunit is known to be phosphorylated by Src on Y365 and Y367 (in γ2S, Y373 and Y375 in γ2L) in cultured cortical neurons (Brandon et al., 2001; Moss et al., 1995), and resulted in augmentation of the $GABA_A$ channel opening probability. Src phosphorylation is dynamically regulated in neurons and enhances

$GABA_AR$ function, via specific interactions with the β and $\gamma 2$ subunits (Brandon et al., 2001). $\beta 1$ subunit phosphorylation by vSrc, on Y384 and Y386 appeared functionless (Moss et al., 1995). In spinal dorsal horn and medulla neurons, $\beta 2/\beta 3$ phosphorylation by PTK ^{pp60}c-Src enhanced GABA activated currents. Using the HEK293 heterologous expression system, the $\beta 2$ subunit was identified as the sole target for PTK mediated augmentation of GABAergic currents (Wan et al., 1997a).

Both Src family kinase and receptor tyrosine kinase, TrkB are abundantly expressed in the cerebellum. TrkB is activated by neurotrophin BDNF, to facilitate the differentiation of PC primary dendrites and cerebellar synaptogenesis. Mice with a deletion of the TrkB gene exhibited reduced volumes of the molecular- and granule cell layer, as well as reduced levels of GABA biosynthetic enzyme GAD 65, and the GABA transporter, GAT-1 in the PC terminals, thereby having a profound effect on inhibitory synapses in the cerebellum (Rico et al., 2002). On a molecular level, co-activation of TrkB by BDNF, and Src via mGluR1, potentiated mIPSC amplitudes in PCs (Boxall, 2000). On the contrary, the direct injection of c-Src reduced the extent of RP induced in PCs, whereas PP2, an inhibitor of Src, amplified RP in PCs (Kawaguchi and Hirano, 2006). The exact roles of PTKs in RP remain to be clarified.

Initiated by the results of these previous studies, the role of CaMKII, PTK, and phosphatases was investigated to understand the signalling cascade underlying RP.

4.2 Results

4.2.1 Endogenous CaMKII in the induction of RP

The role of CaMKII has been well established in the induction, but not the maintenance of RP (Kano et al., 1996). Previous work used CaMKII inhibitors, KN93 (2 -[N- (2-hydroxyethyl) – N - (4-methoxybenzenesulfonyl) Jamino – N - (4- chlorocinnamyl) –N-methylbenzylamine), or KN62, by interfering with Ca^{2+}/CaM binding to CaMKII, preventing the Ca^{2+} dependent activity of CaMKII, but these inhibitors are ineffective once CaMKII is activated and autophosphorylation commences (Sumi et al., 1991; Tokumitsu et al., 1990). Recently, a novel 28 amino acid peptide inhibitor, CaMKIINtide, corresponding to the inhibitory region of the endogenous inhibitor CaMKIINα, was discovered. Substrate phosphorylation (by interaction with the catalytic S site), was potently inhibited non-competitively. This peptide interacted with the T site, and competitively inhibited the binding of the T site to Thr 286. Although autophosphorylation on Thr 286 was only mildly affected, while autophosphorylation on the inhibitory Thr 305 was inhibited to strengthen the CaM binding, CaMKIINtide was postulated to inhibitory the enzyme activity by blocking the substrate entrance into the neighbouring catalytic S site (Vest et al., 2007). CaMKIINtide has the advantage of blocking the catalytic activity of the kinase after its activation by autophosphorylation thereby attenuating the autonomous activity of CaMKII (Chang et al., 1998).

We chose to use a myristoylated form of CaMKIINtide with improved cell permeability. Myristoylated CaMKIINtide, bath applied at a

concentration of 500nM, reduced RP (Fig 4.2 A-C). Using 5' stimulation latency, early and late RP (t=25' after induction) was reduced to 95.6 ± 1.4% and 87.9 ± 7.9% respectively (n=5, $P < 0.05$). Both DSI and long term mIPSC frequency were unaffected by CaMKIINtide (frequency = 4.81 ± 0.91 Hz, DSI = 62.3 ± 5.7%, $P > 0.05$, data not shown). The ablation of RP was reflected by the lack of change in mIPSC amplitude, rise-time or decay time constant (Fig 4.2 C, Table 4.1) of the scaled average mIPSCs, taken before and 25 min after RP stimulation in the absence and presence of CaMKIINtide. However, using a 12' stimulation latency, early RP persisted at 125.6 ± 6.5 % ($P > 0.05$ compared to control early RP 144.7 ± 8.2%, n = 5), the inhibition was only significant at t = 2 after stimulation, thereafter sustained throughout the period of recording (late RP at t = 25 min, was blocked to 96.0 ± 3.0%, $P < 0.05$ n = 5), The inability of CaMKIINtide to block the early RP using 12' latency matched the KN93/62 inhibition profile of RP (Kano et al., 1996; Kawaguchi and Hirano, 2000). CaMKIINtide did not appear to affect the basal mIPSC amplitudes or frequency (n = 5), compared to a group of control (no drug, n = 12) recordings (Table 4.1), although the lack of interleaved controls may overlook the possibility that basal inhibitory transmission may change over the period of months, or be affected by the slicing and recording condition on the particular experimental day. DSI remained at 72.1 ± 9.4%.

4.2

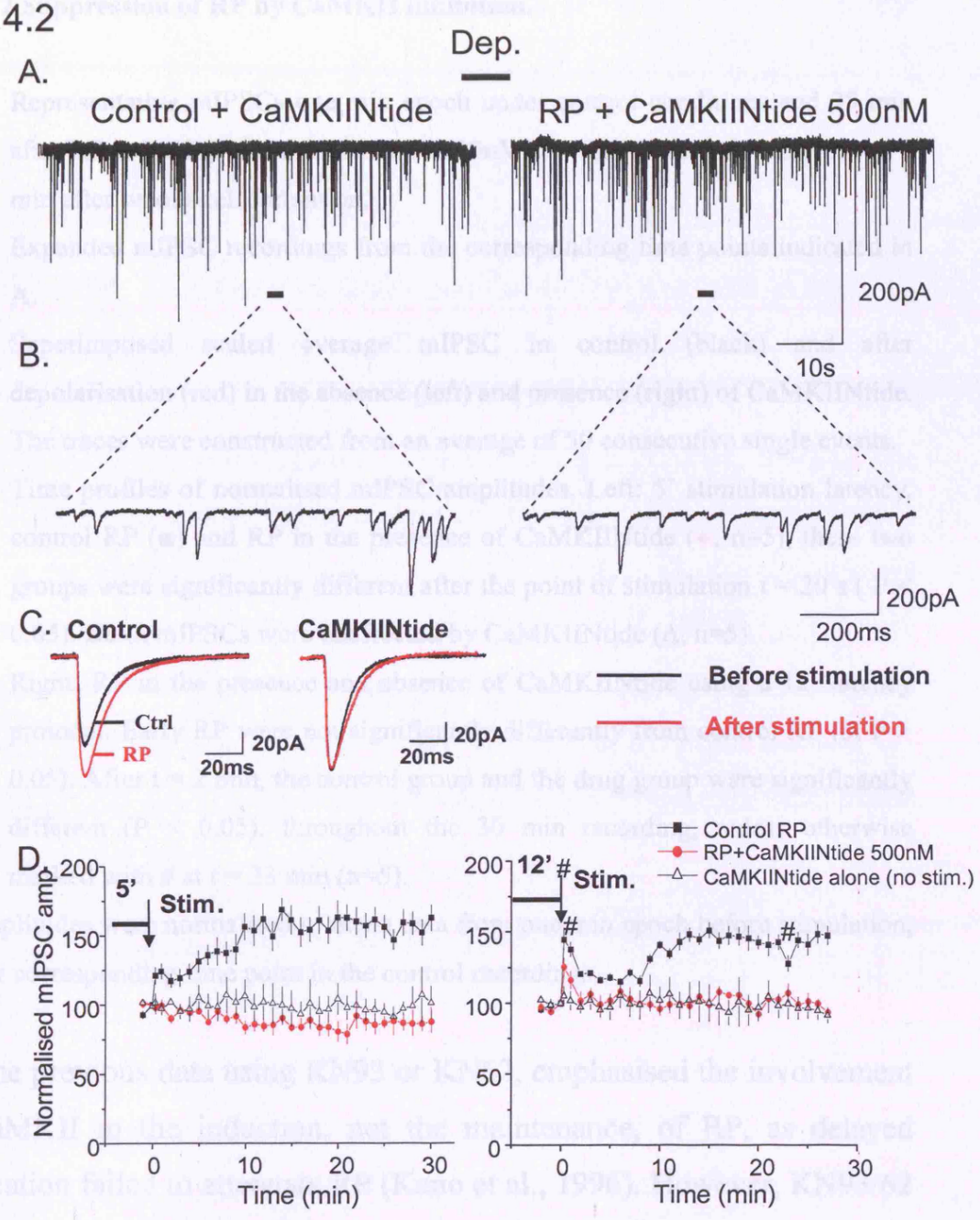
A.
Dep.
Control + CaMKIINtide
RP + CaMKIINtide 500nM
200pA
10s
B.
200pA
200ms
C.
Control
CaMKIINtide
Ctrl
RP
20pA
20ms
20pA
20ms
Before stimulation
After stimulation
D.
Control RP
RP+CaMKIINtide 500nM
CaMKIINtide alone (no stim.)
Normalised mIPSC amp.
5'
Stim.
12'
Stim.
Time (min)
Time (min)

Fig 4. 2 Suppression of RP by CaMKII inhibition.

A) Representative mIPSCs one min epoch under control conditions and 25 min after RP induction in the presence of 500nM CaMKIINtide. RP was induced 5 min after whole-cell formation.

B) Expanded mIPSC recordings from the corresponding time points indicated in A.

C) Superimposed scaled average mIPSC in control (black) and after depolarisation (red) in the absence (left) and presence (right) of CaMKIINtide. The traces were constructed from an average of 50 consecutive single events.

D) Time profiles of normalised mIPSC amplitudes. Left: 5' stimulation latency, control RP (■) and RP in the presence of CaMKIINtide (●, n=5), these two groups were significantly different after the point of stimulation t = 20 s ($P < 0.05$). Basal mIPSCs were unaffected by CaMKIINtide (Δ, n=5).
Right: RP in the presence and absence of CaMKIINtide using a 12' latency protocol. Early RP were not significantly differently from control RP (#, $P > 0.05$). After t = 2 min, the control group and the drug group were significantly different ($P < 0.05$), throughout the 30 min recording, unless otherwise marked with # at t = 23 min (n=5).

All amplitudes were normalised to mean data from one min epoch before stimulation, and the corresponding time point in the control recordings.

The previous data using KN93 or KN62, emphasised the involvement of CaMKII in the induction, not the maintenance, of RP, as delayed application failed to attenuate RP (Kano et al., 1996). However, KN93/62 is unable to inhibit the Ca^{2+} independent autonomous activity of CaMKII once the enzyme is activated (Tokumitsu et al., 1990).

To ascertain whether sustained RP is maintained by persistent CaMKII activity, we applied CaMKIINtide 5 min after RP induction (Fig

4.3). After half-maximal RP was established at 130.3 ± 7.1% (t = 5'), bath application of CaMKIINtide reduced the potentiation to 102.7 ± 0.42% (n = 6, $P < 0.05$, t =25' after stimulus Fig 4.3 A-C). The time profile for RP revealed, even after induction, CaMKIINtide was sufficient to block RP and reset the strength of inhibitory transmission (Fig 4.3 C, D). This result indicates that CaMKII is involved in both the induction and the maintenance of RP.

Previous biochemical studies have identified a CaMKII binding site on the β2/3 subunits to be upstream of the presumed phosphorylation sites in the major ICL of β3 subunits (McAnish et al., 2002). A short peptide (10 amino acids) was created to mimic this region, which should act as a dominant-negative, to inhibit CaMKII binding to $GABA_AR$ β subunits (the binding sequences are conserved between β2 and β3 subunits). This GST linked peptide (GST-VNYIFFGRGP) reproduced the intracellular loop

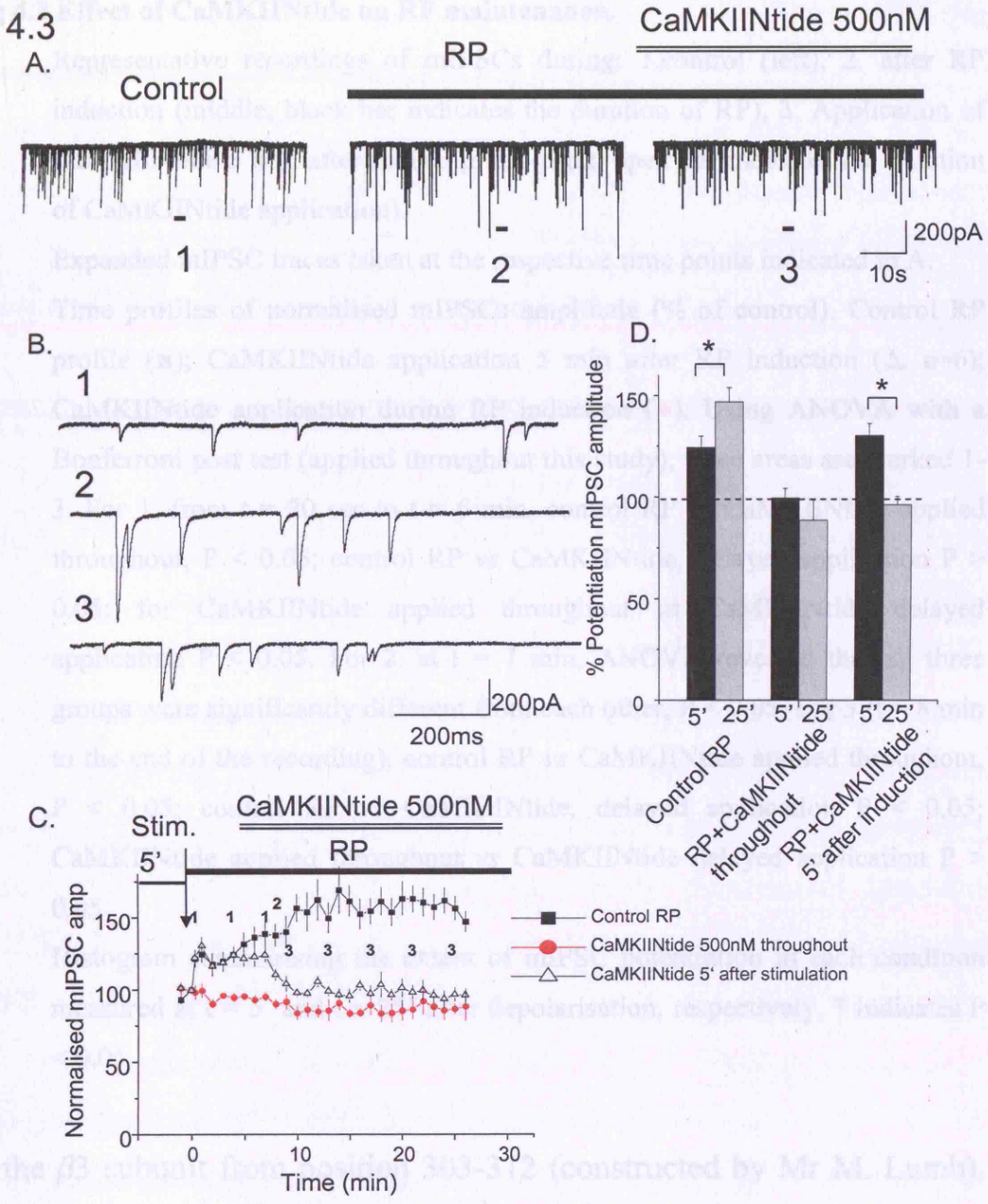
4.3
A.
Control
RP
CaMKIINtide 500nM
1
2
3
200pA
10s
B.
1
2
3
200pA
200ms
D.
% Potentiation mIPSC amplitude
150
100
50
0
5' 25' 5' 25' 5' 25'
Control RP
RP+CaMKIINtide throughout
RP+CaMKIINtide 5' after induction
C.
Stim.
5'
CaMKIINtide 500nM
RP
Normalised mIPSC amp
150
100
50
0
0 10 20 30
Time (min)
Control RP
CaMKIINtide 500nM throughout
CaMKIINtide 5' after stimulation

Fig 4.3 Effect of CaMKIINtide on RP maintenance.

A) Representative recordings of mIPSCs during: 1.control (left), 2. after RP induction (middle, black bar indicates the duration of RP), 3. Application of CaMKIINtide 5 min after inducing RP (right, open bar indicates the duration of CaMKIINtide application).

B) Expanded mIPSC traces taken at the respective time points indicated in A.

C) Time profiles of normalised mIPSCs amplitude (% of control). Control RP profile (■); CaMKIINtide application 5 min after RP induction (Δ, n=6); CaMKIINtide application during RP induction (●). Using ANOVA with a Bonferroni post test (applied throughout this study), three areas are marked 1-3. For 1, from t = 20 sec to t = 6 min, control RP *vs* CaMKIINtide applied throughout, $P < 0.05$; control RP *vs* CaMKIINtide, delayed application $P > 0.05$; for CaMKIINtide applied throughout *vs* CaMKIINtide delayed application $P < 0.05$. For 2, at t = 7 min, ANOVA revealed that all three groups were significantly different from each other, $P < 0.05$. For 3 (t = 8 min to the end of the recording), control RP *vs* CaMKIINtide applied throughout, $P < 0.05$; control RP *vs* CaMKIINtide, delayed application $P < 0.05$; CaMKIINtide applied throughout *vs* CaMKIINtide delayed application $P > 0.05$.

D) Histogram summarising the extent of mIPSC potentiation in each condition measured at t = 5' and t = 25' after depolarisation, respectively. * indicates $P < 0.05$.

of the β3 subunit from position 303-312 (constructed by Mr M. Lumb). The peptide was dialysed at 170μg/ml into PCs and allowed to diffuse for 20 min after whole-cell formation, prior to the induction of RP. Late RP was abolished by the β3 loop peptide (98.5 ± 3.4%, n = 7 compared to 132.5 ± 5.1% in control, measured at t = 25' after RP induction, $P < 0.05$; Fig 4.4 A-C), but unaffected by the scrambled peptide sequence, FRNIGPFGYV, used at same concentration (potentiation reached

144.7±7.5%, n = 5). The time profile of RP (Fig 4.4 C) verified the elimination of late RP and partial block of early RP (119.3 ± 4.7% at t = 20 sec after RP, $P < 0.05$). Fig 4.4D summarises the extent of mIPSC potentiation under these conditions. Thus, RP may require interaction between CaMKII and $GABA_A$Rs, which supports direct receptor phosphorylation as the underlying mechanism of RP.

4.2.2 Role of PTK in RP

To date, the role of PTK in RP has not been studied in detail, even though PTKs, including TrkB, TrkC, and the Src family, are extensively expressed in mature PCs (Boxall, 2000; Kawaguchi and Hirano, 2006; Rico et al., 2002). By using a PTK inhibitor, genistein (Akiyama et al., 1987) at an effective concentration of 100μM, applied internally to PCs, mIPSC recordings indicated RP was abolished (Fig 4.5 A-D). Using the 5' latency protocol, a small residual potentiation was still seen between t = 20 sec and t = 4 min after stimulation in the presence of genistein (107.3 ± 4.8 % at t = 20 sec $P > 0.05$), late RP was completely blocked to 101.5 ± 11.9% ($P < 0.05$ at t = 25', n = 5, Fig 4.5C). Similarly, using a 12' stimulus latency, early RP was unaffected at 126.9 ± 17.8% ($P > 0.05$), whilst late RP was suppressed to 96.9 ± 1.1% (n = 5, $P < 0.05$). Genistein did not affect the baseline mIPSC amplitude in general, but with fluctuations during the recordings, in particular at t = 11' and t = 12'. These soon returned to baseline. Genistein was applied internally, hence it is difficult to determine the mIPSC amplitude before and after genistein application. We relied on comparing the mean amplitude of mIPSC during a 30 min control recording, with a 30 min recording in the presence of genistein, which did not show any significant difference

4.4

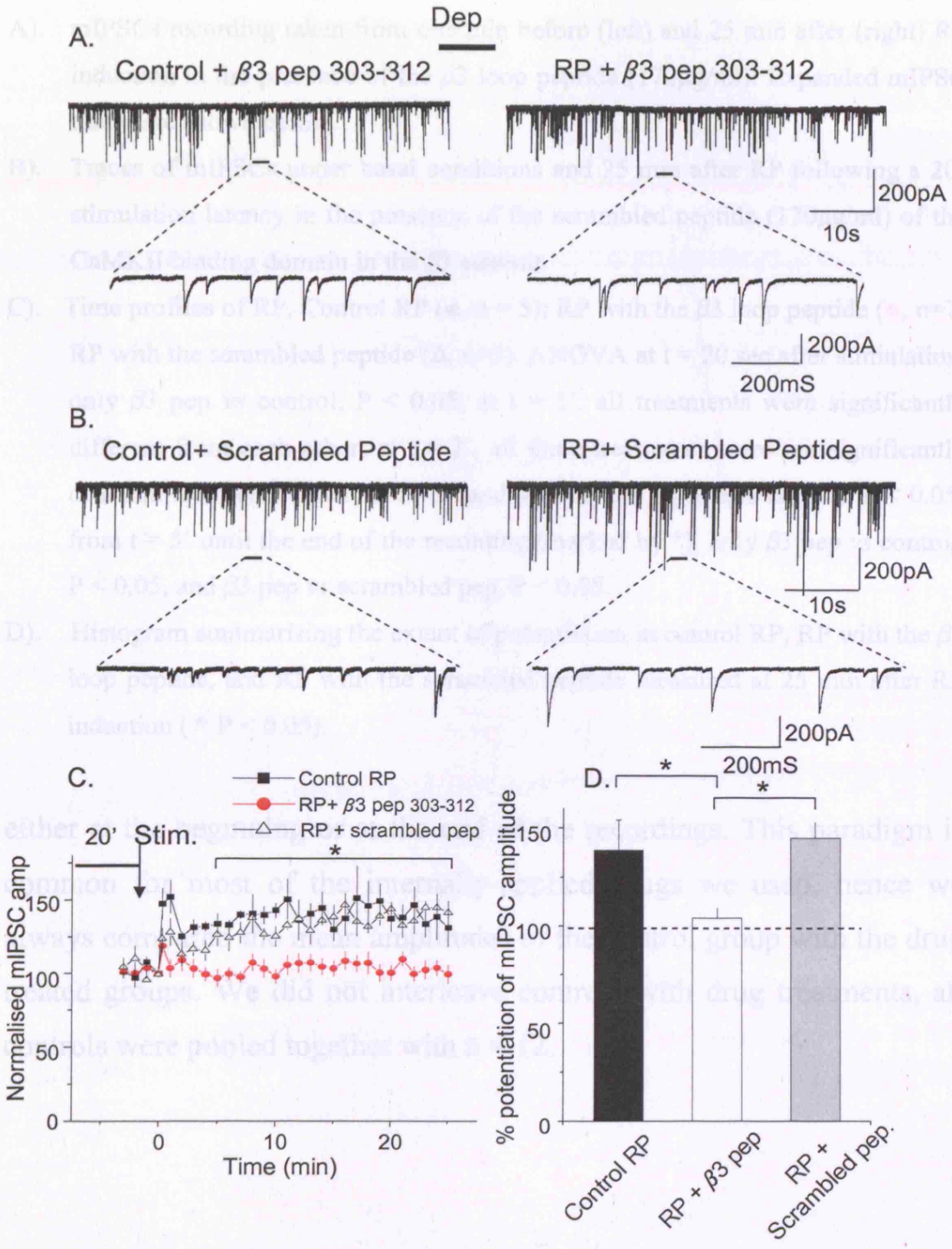
A.
Dep
Control + β3 pep 303-312
RP + β3 pep 303-312
200pA
10s
200pA
200mS
B.
Control+ Scrambled Peptide
RP+ Scrambled Peptide
200pA
10s
200pA
C.
Control RP
RP+ β3 pep 303-312
RP + scrambled pep
20' Stim.
*
Normalised mIPSC amp
150
100
50
0
0
10
20
Time (min)
D.
*
200mS
*
% potentiation of mIPSC amplitude
150
100
50
0
Control RP
RP + β3 pep
RP + Scrambled pep.

Fig 4.4 Inhibition of RP by a peptide resembling the CaMKII binding site in the β3 subunit.

A). mIPSCs recording taken from one min before (left) and 25 min after (right) RP induction in the presence of the β3 loop peptide (170μg/ml). Expanded mIPSC traces are shown below.

B). Traces of mIPSCs under basal conditions and 25 min after RP following a 20' stimulation latency in the presence of the scrambled peptide (170μg/ml) of the CaMKII binding domain in the β3 subunit.

C). Time profiles of RP. Control RP (■, n = 5); RP with the β3 loop peptide (●, n=7); RP with the scrambled peptide (Δ, n=5). ANOVA at t = 20 sec after stimulation, only β3 pep *vs* control, $P < 0.05$; at t = 1', all treatments were significantly different from each other; at t = 2', all three treatments were not significantly different from each other; at t = 3' and 4', only β3 peptide *vs* control, $P < 0.05$; from t = 5' until the end of the recording (marked by *), only β3 pep *vs* control, $P < 0.05$, and β3 pep *vs* scrambled pep, $P < 0.05$.

D). Histogram summarising the extent of potentiation in control RP, RP with the β3 loop peptide, and RP with the scrambled peptide measured at 25 min after RP induction (* $P < 0.05$).

either at the beginning or at the end of the recordings. This paradigm is common for most of the internally-applied drugs we used, hence we always compared the mean amplitudes of the control group with the drug treated groups. We did not interleave controls with drug treatments, all controls were pooled together with n = 12.

4.5

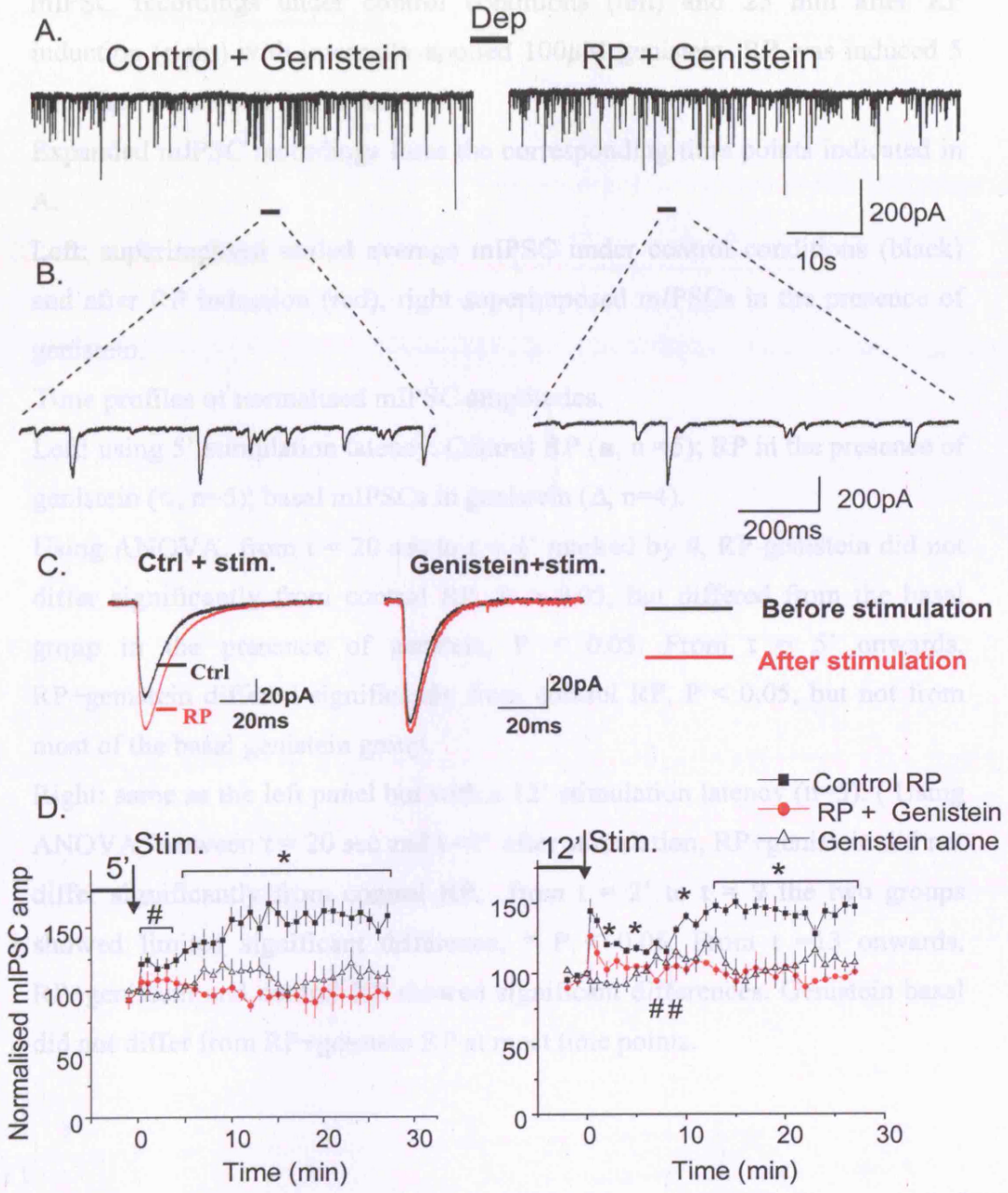
A.
Dep
Control + Genistein
RP + Genistein
200pA
10s
B.
200pA
200ms
C.
Ctrl + stim.
Genistein+stim.
Ctrl
RP
20pA
20ms
20pA
20ms
Before stimulation
After stimulation
D.
Control RP
RP + Genistein
Genistein alone
Stim.
5'
12'
Normalised mIPSC amp
Time (min)
Time (min)

Fig 4. 5 Suppression of RP by PTK inhibition.

A). mIPSC recordings under control conditions (left) and 25 min after RP induction (right) with internally-applied 100μM genistein. RP was induced 5 min after whole-cell formation.

B). Expanded mIPSC recordings from the corresponding time points indicated in A.

C). Left: superimposed scaled average mIPSC under control conditions (black) and after RP induction (red), right superimposed mIPSCs in the presence of genistein.

D). Time profiles of normalised mIPSC amplitudes.

Left: using 5' stimulation latency. Control RP (■, n =5); RP in the presence of genistein (○, n=5); basal mIPSCs in genistein (Δ, n=4).

Using ANOVA, from t = 20 sec to t = 4' marked by #, RP-genistein did not differ significantly from control RP, $P > 0.05$, but differed from the basal group in the presence of genstein, $P < 0.05$. From t = 5' onwards, RP+genistein differed significantly from control RP, $P < 0.05$, but not from most of the basal genistein group.

Right: same as the left panel but with a 12' stimulation latency (n=5). (Using ANOVA, between t = 20 sec and t =1' after stimulation, RP+genistein did not differ significantly from control RP, from t = 2' to t = 9 the two groups showed limited significant difference, * $P < 0.05$. From t =13 onwards, RP+genistein and control RP showed significant differences. Genistein basal did not differ from RP+genstein RP at most time points.

The similarity in the actions of CaMKIINtide and genistein suggested CaMKII and PTK might work through similar signalling pathways.

Subsequently, we tested whether residue early RP was dependent on the combined effects of CaMKII and PTK by co-application of

CaMKIINtide and genistein. Early RP persisted at 130.3±11.1% (n = 5, P > 0.05; Fig 4.6 A). To test whether early RP is phosphorylation dependent, we applied a non-specific protein kinase inhibitor, staurosporine, internally via the patch electrolyte (Kano et al., 1996) at concentration of 10 μM, sufficient to inhibit a broad spectrum of protein kinases. Under this condition, early RP still remained at 119.9±4.0% (n = 5 P > 0.05; Fig 4.6B-D). Fig 4.6 D summarises the relative blockage of early and late RP by various kinase inhibitors.

4.6

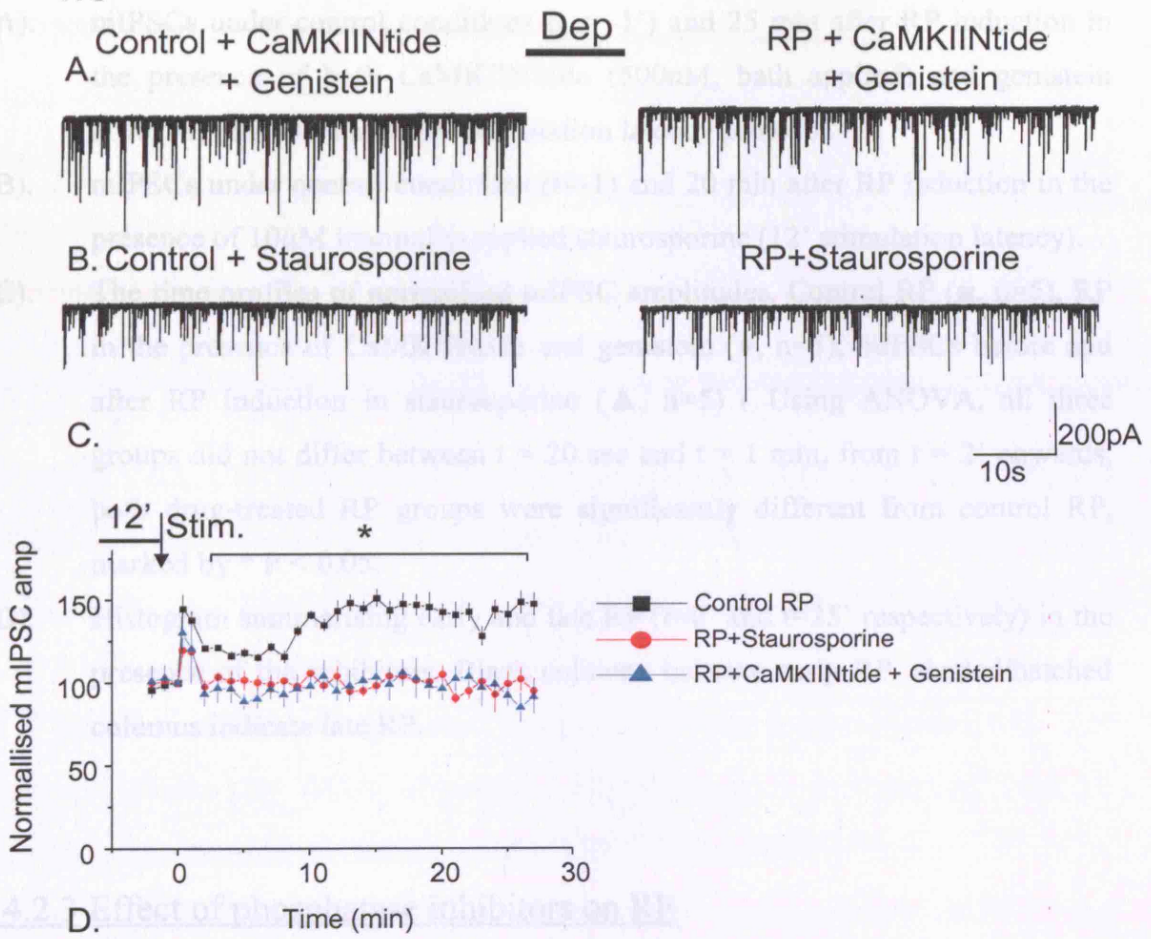

black columns indicate early RP,
shaded columns indicate late RP

Fig 4.6 Effect of total inhibition of kinases on early RP.

A). mIPSCs under control conditions (t = -1') and 25 min after RP induction in the presence of both CaMKIINitide (500nM, bath applied) and genistein (100μM, internal) under 12' stimulation latency protocol.

B). mIPSCs under control conditions (t=-1) and 20 min after RP induction in the presence of 10μM internally-applied staurosporine (12' stimulation latency).

C). The time profiles of normalised mIPSC amplitudes. Control RP (■, n=5), RP in the presence of CaMKIINtide and genistein (●, n=5), mIPSCs before and after RP induction in staurosporine (▲, n=5) (Using ANOVA, all three groups did not differ between t = 20 sec and t = 1 min, from t = 2' onwards, both drug-treated RP groups were significantly different from control RP, marked by * $P < 0.05$.

D). Histogram summarising early and late RP (t=0' and t=25' respectively) in the presence of the inhibitors. Black columns indicate early RP, shaded/hatched columns indicate late RP.

4.2.3 Effect of phosphatase inhibitors on RP

In Chapter 3, we observed two phases to RP which emerged as the stimulation latency increased. We postulated the transient depotentiation of mIPSCs was due to the activity of phosphatases, to inactivate kinases or directly dephosphorylate the potentiated receptors. To investigate this further, phosphatase inhibitors were used to study the induction and maintenance of RP.

Okadaic acid (ODA,), is able to inhibit most protein phosphatases PP1, 2A 2B (calcineurin) and 2C, with an IC_{50} of 1nM against PP2A, and an IC_{50} of 100-500nM against PP1. PP2B was inhibited to lesser extent (IC_{50}=4-5μM) (Bialojan and Takai, 1988). PP1 and 2A both

dephosphorylate T286 on CaMKII, inhibiting its autophosphorylation at Thr286, and blocking autonomous activity. We applied 150nM okadaic acid internally to PCs, sufficient to block both PP1 and PP2A, used previously to remove the suppressive effect of PP1 on RP (Kawaguchi and Hirano, 2002). By using the 12' latency protocol with the most profound separation between early and late RP, okadaic acid affected neither late RP (141.0 ± 12.5%, n = 5, $P > 0.05$; Fig 4.7), nor early RP (126.3 ± 7.0% compared to control RP 153.6 ± 16.6%, $P > 0.05$; Fig 4.7). Despite this, the addition of ODA changed the appearance of RP, the induction and plateau of RP appeared less definitive; instead the mIPSC amplitude increase was gradual, continuing until the end of recording. ODA-RP showed significant difference from control RP at 1, 10 and 13-15 minutes after stimulation. Basal inhibitory transmission was not greatly affected by ODA, although a slight run up was observed from 10 to 20 min, before returning to baseline. Internal application of ODA make it difficult to compare pre-treatment to post-treatment mIPSC, but mIPSC amplitude did not show significant difference in control mIPSC and ODA treated mIPSC (Table 4.1).

4.7

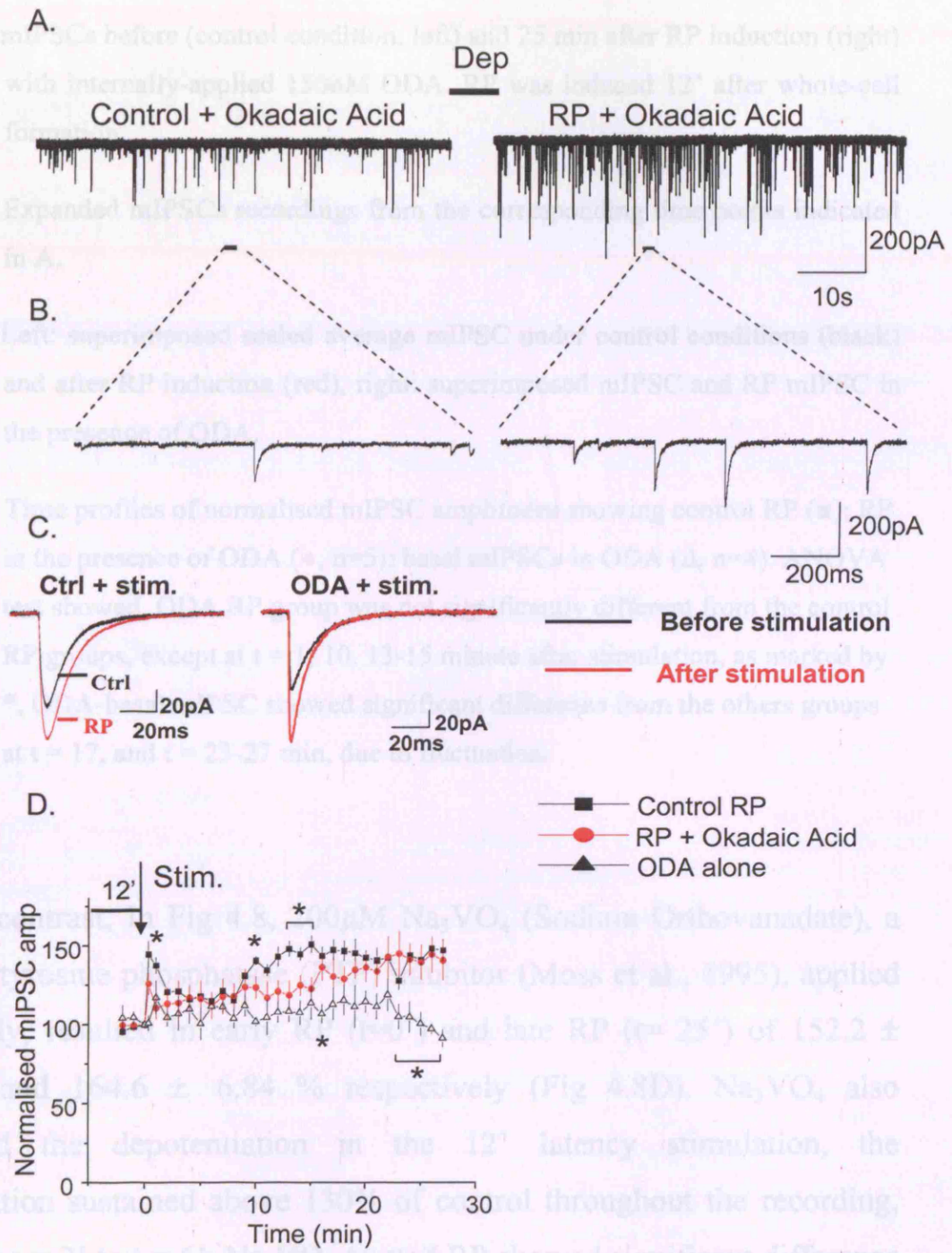
A.
Dep
Control + Okadaic Acid
RP + Okadaic Acid
200pA
10s
B.
C.
200pA
200ms
Ctrl + stim.
ODA + stim.
Before stimulation
After stimulation
Ctrl
RP
20pA
20ms
20pA
20ms
D.
Control RP
RP + Okadaic Acid
ODA alone
12'
Stim.
Normalised mIPSC amp
150
100
50
0
0
10
20
30
Time (min)

Fig 4.7 RP and protein phosphatase inhibitor okadaic acid.

A). mIPSCs before (control condition, left) and 25 min after RP induction (right) with internally-applied 150nM ODA. RP was induced 12' after whole-cell formation.

B). Expanded mIPSCs recordings from the corresponding time points indicated in A.

C). Left: superimposed scaled average mIPSC under control conditions (black) and after RP induction (red), right: superimposed mIPSC and RP mIPSC in the presence of ODA.

D). Time profiles of normalised mIPSC amplitudes showing control RP (■); RP in the presence of ODA (●, n=5); basal mIPSCs in ODA (Δ, n=4). ANOVA test showed, ODA RP group was not significantly different from the control RP groups, except at t = 1, 10, 13-15 minute after stimulation, as marked by *. ODA-basal mIPSC showed significant difference from the others groups at t = 17, and t = 23-27 min, due to fluctuation.

By contrast, In Fig 4.8, 200μM Na_3VO_4 (Sodium Orthovanadate), a protein tyrosine phosphatase (PTP) inhibitor (Moss et al., 1995), applied internally, resulted in early RP (t=0') and late RP (t= 25') of 152.2 ± 11.5% and 164.6 ± 6.84 % respectively (Fig 4.8D). Na_3VO_4 also removed the depotentiation in the 12' latency stimulation, the potentiation sustained above 130% of control throughout the recording, between t = 2' to t = 6', Na_3VO_4-treated RP showed significant difference to control RP (n = 5, $P < 0.05$). The removal of depotentiation by the addition of PTP inhibitor implies the loss of PTK, or activity of PTP may cause the depotentiation.

4.8

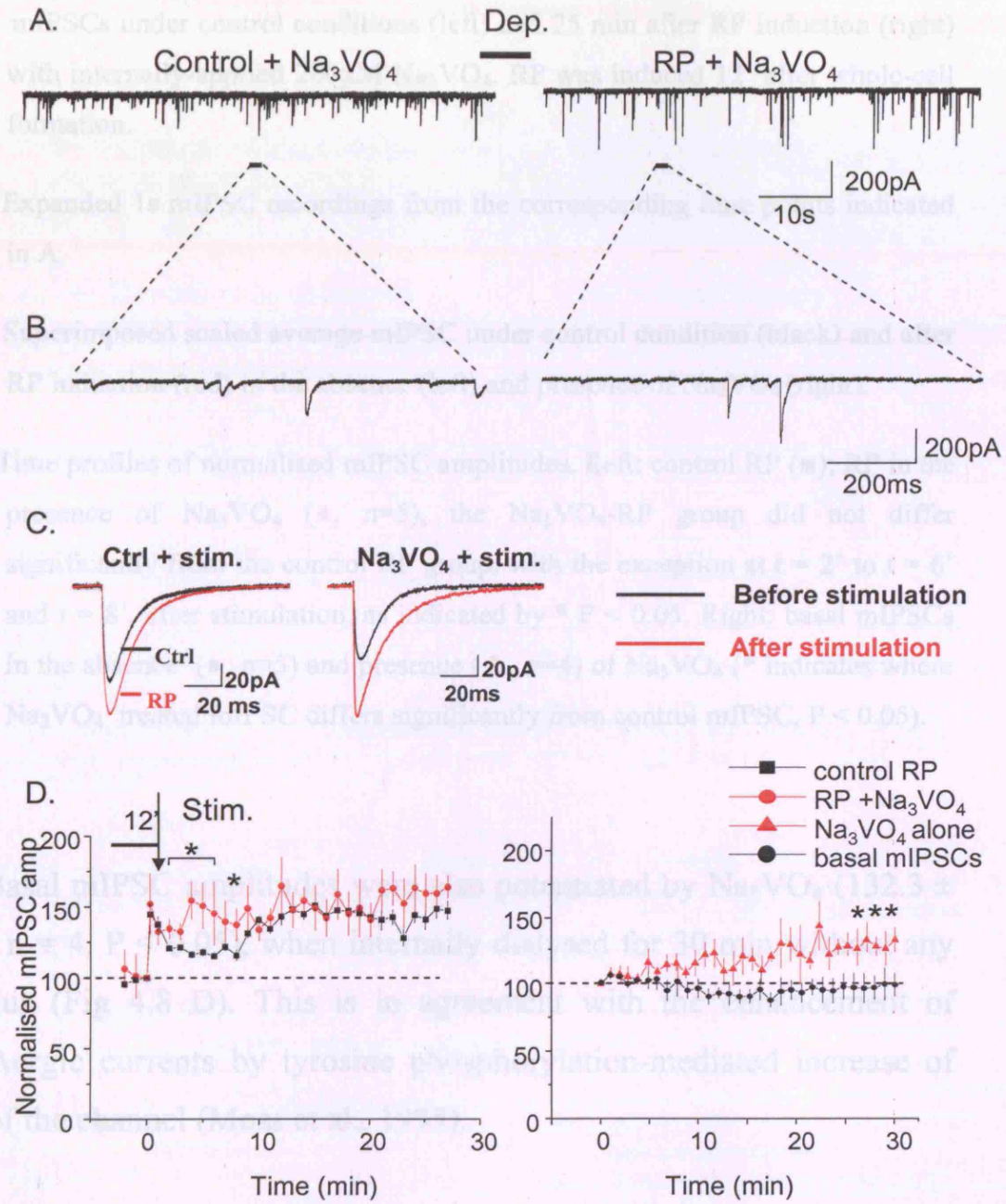
A.
Dep.
Control + Na_3VO_4
RP + Na_3VO_4
200pA
10s
B.
200pA
200ms
C.
Ctrl + stim.
Na_3VO_4 + stim.
Ctrl
RP
20pA
20 ms
20pA
20ms
Before stimulation
After stimulation
D.
12'
Stim.
Normalised mIPSC amp
control RP
RP +Na_3VO_4
Na_3VO_4 alone
basal mIPSCs
Time (min)
Time (min)

Fig 4. 8 RP and protein tyrosine phosphatase inhibitor sodium orthovanadate.

A). mIPSCs under control conditions (left) and 25 min after RP induction (right) with internally-applied 200μM Na_3VO_4. RP was induced 12' after whole-cell formation.

B). Expanded 1s mIPSC recordings from the corresponding time points indicated in A.

C). Superimposed scaled average mIPSC under control condition (black) and after RP induction (red) in the absence (left) and presence of Na_3VO_4 (right).

D). Time profiles of normalised mIPSC amplitudes. Left: control RP (■); RP in the presence of Na_3VO_4 (●, n=5), the Na_3VO_4-RP group did not differ significantly from the control RP group, with the exception at t = 2' to t = 6' and t = 8', after stimulation, as indicated by * $P < 0.05$. Right: basal mIPSCs in the absence (●, n=5) and presence (▲, n=4) of Na_3VO_4 (* indicates where Na_3VO_4 treated mIPSC differs significantly from control mIPSC, $P < 0.05$).

Basal mIPSC amplitudes were also potentiated by Na_3VO_4 (132.3 ± 9.0%, n = 4, $P < 0.05$), when internally dialysed for 30 min without any stimulus (Fig 4.8 D). This is in agreement with the enhancement of GABAergic currents by tyrosine phosphorylation-mediated increase of P_{open} of the channel (Moss et al., 1995).

4.2.4 Dual kinase regulation of RP

A connection between CaMKII and PTK activity has been established to modulate $GABA_AR$ function in cerebellar granule cells (Houston et al., 2007). This possibility in the expression of RP was

explored by simultaneously inhibiting one kinase while promoting the activity of the other, using specific phosphatase inhibitors.

4.9

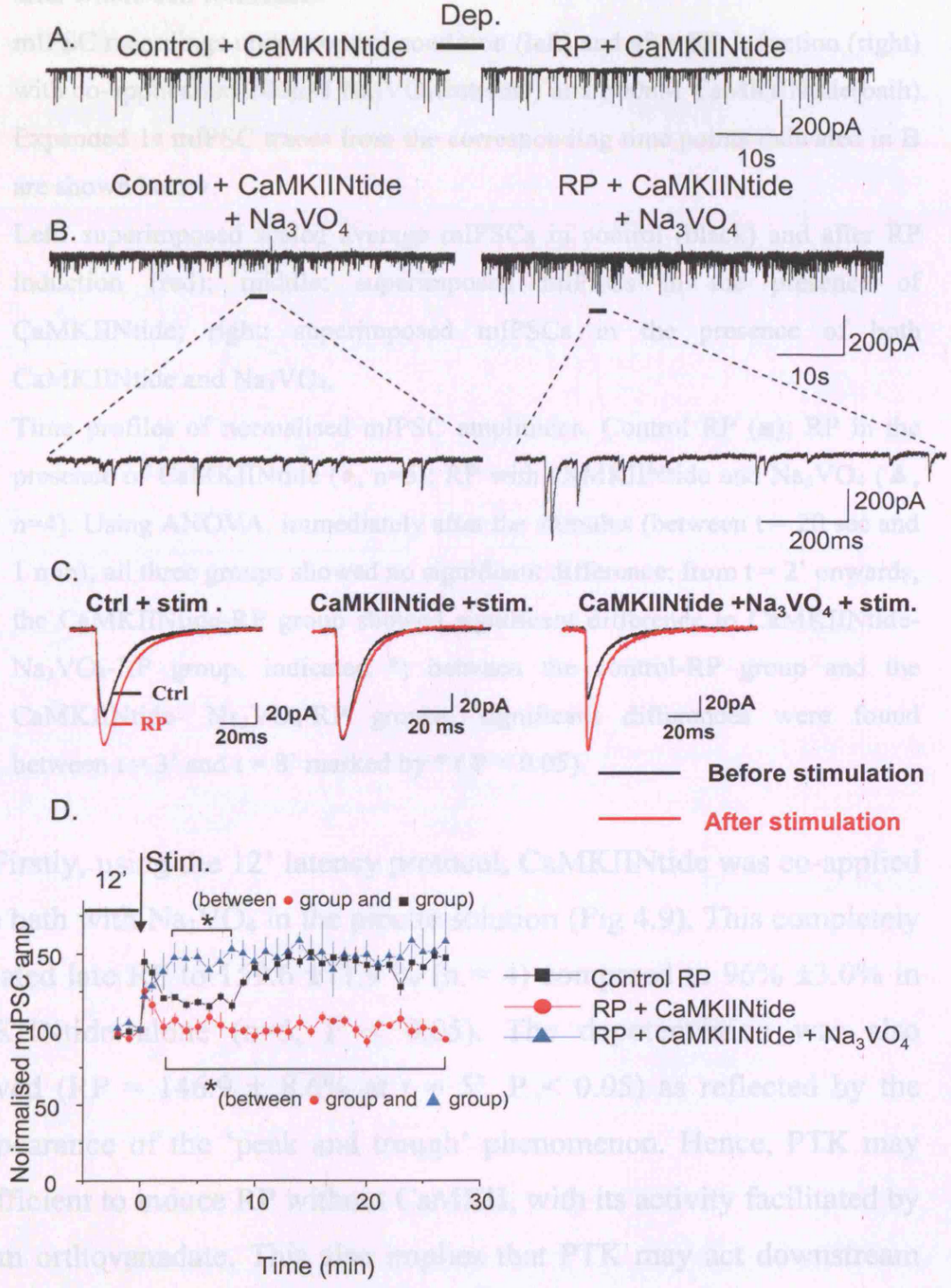

Fig 4.9 Rescuing suppression of RP by CaMKIINtide by enhancing PTK activity.

A). mIPSC recordings under control conditions (left) and 25 min after RP induction (right) with 500nM bath-applied CaMKIINtide. RP was induced 12' after whole-cell formation.

B). mIPSC recordings under control condition (left) and after RP induction (right) with co-application 200μM Na_3VO_4(internal) and 500nM CaMKIINtide(bath). Expanded 1s mIPSC traces from the corresponding time points indicated in B are shown below.

C). Left: superimposed scaled average mIPSCs in control (black) and after RP induction (red); middle: superimposed mIPSCs in the presence of CaMKIINtide; right: superimposed mIPSCs in the presence of both CaMKIINtide and Na_3VO_4.

D). Time profiles of normalised mIPSC amplitudes. Control RP (■); RP in the presence of CaMKIINtide (●, n=5); RP with CaMKIINtide and Na_3VO_4 (▲, n=4). Using ANOVA, immediately after the stimulus (between t = 20 sec and 1 min), all three groups showed no significant difference; from t = 2' onwards, the CaMKIINtide-RP group showed significant difference to CaMKIINtide-Na_3VO_4-RP group, indicated *; between the control-RP group and the CaMKIINtide- Na_3VO_4-RP groups, significant differences were found between t = 3' and t = 8' marked by * ($P < 0.05$).

Firstly, using the 12' latency protocol, CaMKIINtide was co-applied in the bath with Na_3VO_4 in the pipette solution (Fig 4.9). This completely reinstated late RP to 159.6 ±11.9 % (n = 4) compared to 96% ±3.0% in CaMKIINtide alone (n=5, $P < 0.05$). The depotentiation was also removed (RP = 146.9 ± 8.6% at t = 5', $P < 0.05$) as reflected by the disappearance of the 'peak and trough' phenomenon. Hence, PTK may be sufficient to induce RP without CaMKII, with its activity facilitated by sodium orthovanadate. This also implies that PTK may act downstream of CaMKII in the induction of RP.

Similarly, inhibiting PTK while enhancing CaMKII with ODA (150nM) also restored late RP.

4.10

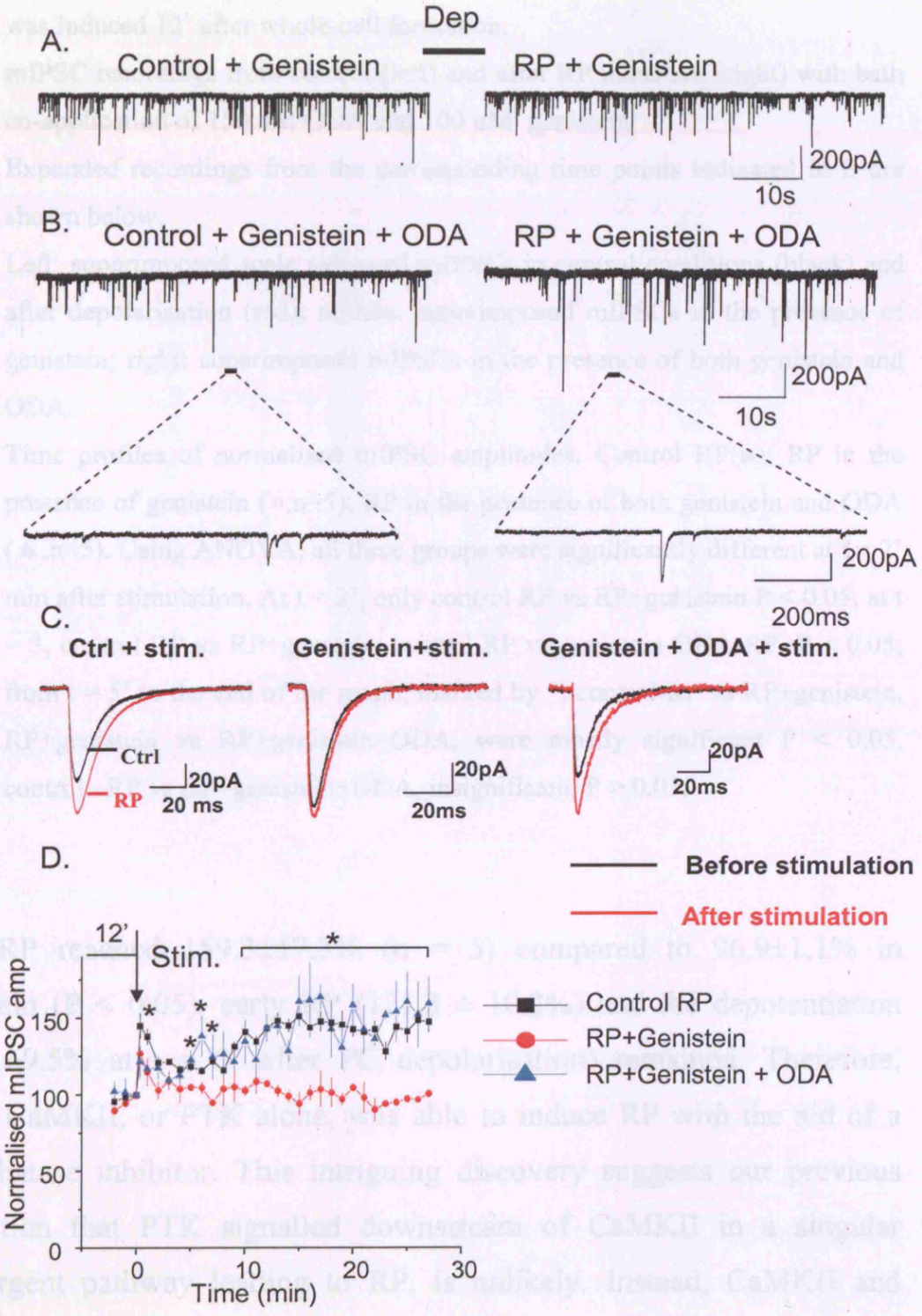

Fig 4.10 Rescuing suppression of RP by genistein with enhanced CaMKII activity.

A). mIPSC recordings under control conditions (left) and 25 min after depolarisation (right) with 100 μM genistein applied internally. Depolarisation was induced 12' after whole-cell formation.

B). mIPSC recordings from control (left) and after RP induction (right) with bath co-application of 150 nM ODA and 100 μM genistein.
Expanded recordings from the corresponding time points indicated in B are shown below.

C). Left: superimposed scale averaged mIPSCs in control conditions (black) and after depolarisation (red); middle: superimposed mIPSCs in the presence of genistein; right: superimposed mIPSCs in the presence of both genistein and ODA.

D). Time profiles of normalised mIPSC amplitudes. Control RP(■); RP in the presence of genistein (●,n=5); RP in the presence of both genistein and ODA (▲,n=5). Using ANOVA, all three groups were significantly different at t = 2' min after stimulation. At t = 2', only control RP vs RP+genistein $P < 0.05$; at t = 3, control RP vs RP+genstein, control RP vs genistein-ODA-RP, $P < 0.05$; from t = 5' to the end of the graph, marked by *, control-RP vs RP+genistein, RP+genistein vs RP+genistein+ODA, were mostly significant $P < 0.05$, control –RP vs RP+genistein+ODA, insignificant, $P > 0.05$.

Late RP reached 159.3±17.3% (n = 5) compared to 96.9±1.1% in genistein ($P < 0.05$), early RP (121.3 ± 10.2%) and the depotentiation (111.1±9.5% at t = 5' after PC depolarisation) remained. Therefore, either CaMKII, or PTK alone, was able to induce RP with the aid of a phosphatase inhibitor. This intriguing discovery suggests our previous prediction that PTK signalled downstream of CaMKII in a singular convergent pathway leading to RP, is unlikely. Instead, CaMKII and

PTK may act through independent parallel pathways. Histogram in Fig 4.11 summarises the extent of mIPSC potentiation under each drug treated conditions.

4.11

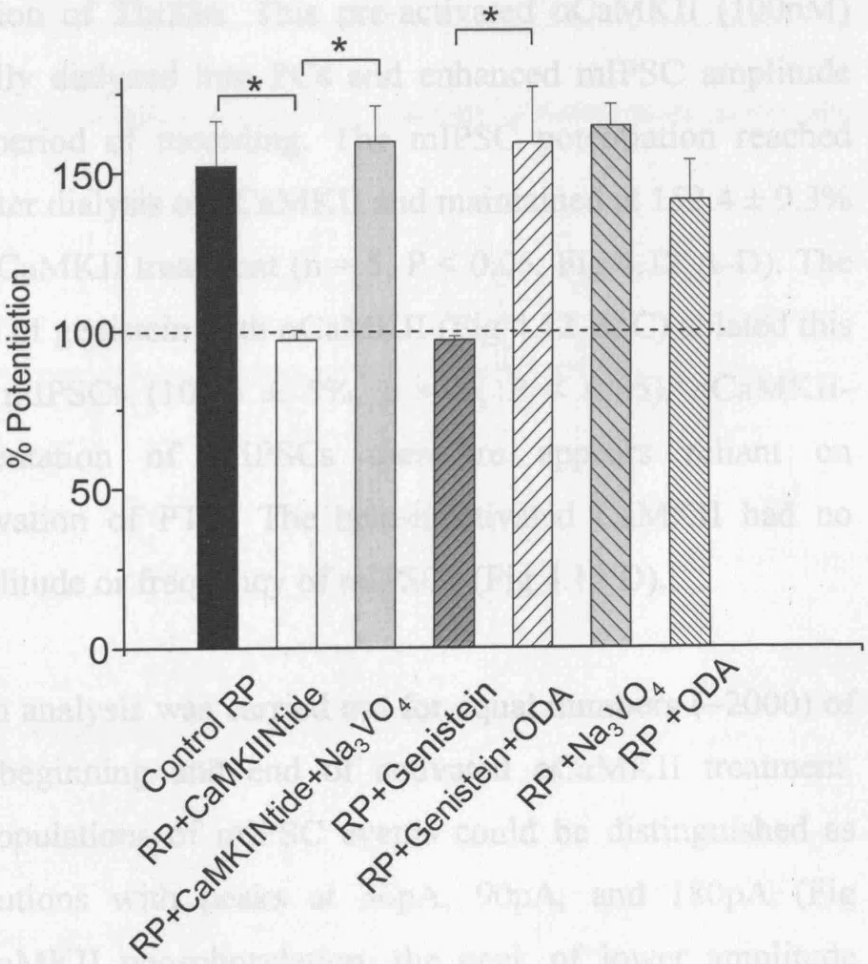

Fig 4.11 Histogram summarising the extent of RP measured in the presence of various kinases or phosphatase inhibitors. (Measured 25 min after RP induction * $P < 0.05$).

4.2.5 Modulation of mIPSCs by exogenous αCaMKII and genistein

To clarify the connection between CaMKII and PTK, PTK was inhibited to ascertain whether it affected αCaMKII mediated enhancement of mIPSCs in PCs. αCaMKII was incubated in the presence of Ca^{2+}, CaM, and ATP for 15 min to promote Ca^{2+}/CaM binding and autophosphorylation of Thr286. This pre-activated αCaMKII (100nM) was then internally dialyzed into PCs and enhanced mIPSC amplitude over a 50 min period of recording. The mIPSC potentiation reached plateau 10 min after dialysis of αCaMKII and maintained at 152.4 ± 9.3% after 40 min of αCaMKII treatment ($n = 5$, $P < 0.05$, Fig 4.12 A-D). The co-administration of genistein with αCaMKII (Fig 4.12 B, C) ablated this enhancement of mIPSCs (105.6 ± 5%, $n = 6$, $P < 0.05$). αCaMKII-mediated augmentation of mIPSCs therefore appears reliant on downstream activation of PTK. The heat-inactivated CaMKII had no effect on the amplitude or frequency of mIPSCs (Fig 4.12 D).

A population analysis was carried out for equal numbers (~2000) of mIPSCs at the beginning and end of activated αCaMKII treatment. Initially, three populations of mIPSC events could be distinguished as Gaussian distributions with peaks at 36pA, 90pA, and 180pA (Fig 4.13A). After CaMKII phosphorylation, the peak of lower amplitude subpopulation remained the same, while the peaks of medium and large amplitude subpopulations were shifted towards larger peaks at 120pA and 220pA respectively (Fig 4.13 A). Furthermore, the frequency of the lower peak amplitude subpopulation was reduced (reflected by the percentage area) whilst that of the higher peak populations increased. This revealed a general shift in the distribution towards higher amplitude

4.12

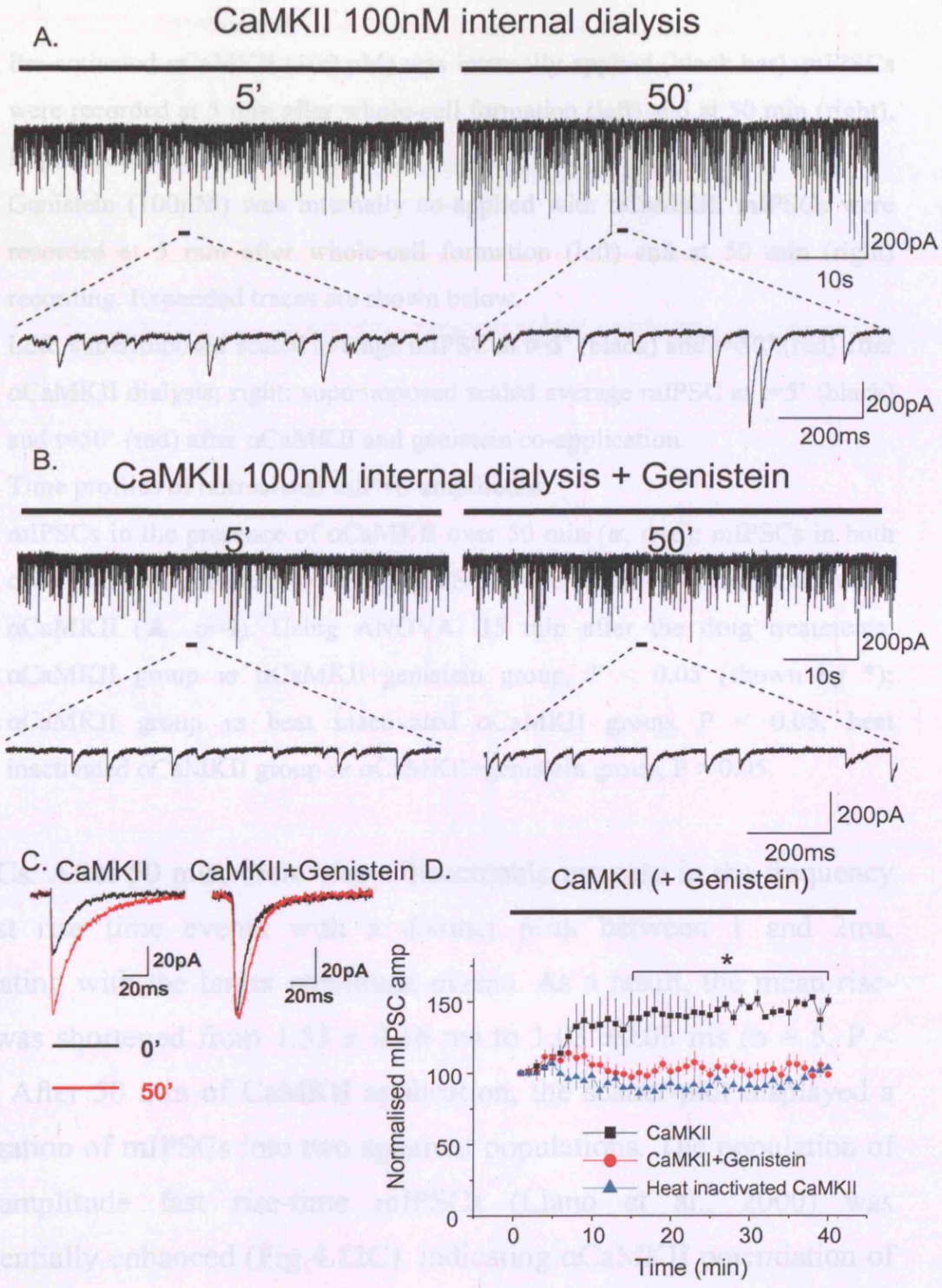
A.
CaMKII 100nM internal dialysis
5'
50'
200pA
10s
200pA
200ms
B.
CaMKII 100nM internal dialysis + Genistein
5'
50'
200pA
10s
200pA
200ms
C.
CaMKII
CaMKII+Genistein
20pA
20ms
20pA
20ms
0'
50'
D.
CaMKII (+ Genistein)
*
Normalised mIPSC amp
150
100
50
0
0
10
20
30
40
Time (min)
CaMKII
CaMKII+Genistein
Heat inactivated CaMKII

Fig 4.12 Direct modulation of mIPSCs by activated αCaMKII and regulation by PTK.

A). Pre-activated αCaMKII (100 nM) was internally-applied (black bar). mIPSCs were recorded at 5 min after whole-cell formation (left) and at 50 min (right). Expanded traces are shown below.

B). Genistein (100μM) was internally co-applied with αCaMKII. mIPSCs were recorded at 5 min after whole-cell formation (left) and at 50 min (right) recording. Expanded traces are shown below.

C). Left: superimposed scaled average mIPSC at t=5' (black) and t=50' (red) after αCaMKII dialysis; right: superimposed scaled average mIPSC at t=5' (black) and t=50' (red) after αCaMKII and genistein co-application.

D). Time profiles of normalised mIPSC amplitudes.
mIPSCs in the presence of αCaMKII over 50 min (■, n=6); mIPSCs in both αCaMKII and genistein (●, n=6); mIPSC in the presence of heat-inactivated αCaMKII (▲, n=4). Using ANOVA, 15 min after the drug treatments: αCaMKII group *vs* αCaMKII+genistein group, $P < 0.05$ (shown by *); αCaMKII group *vs* heat inactivated αCaMKII group, $P < 0.05$; heat inactivated αCaMKII group *vs* αCaMKII+genistein group, $P > 0.05$.

mIPSCs. After 50 min, there was a discernable increase in the frequency of fast rise time events with a distinct peak between 1 and 2ms, correlating with the larger amplitude events. As a result, the mean rise-time was shortened from 1.53 ± 0.18 ms to 1.03 ±0.03 ms ($n = 5$, $P < 0.05$). After 50 min of CaMKII application, the scatter-plot displayed a segregation of mIPSCs into two apparent populations. The population of large-amplitude fast rise-time mIPSCs (Llano et al., 2000) was preferentially enhanced (Fig 4.12C), indicating αCaMKII potentiation of synaptic currents originated close to the soma. The shortening in rise-

time might be indicative of a migration of receptors towards the soma, or increased receptor insertion around this region.

4.13 αCaMKII in the patch pipette

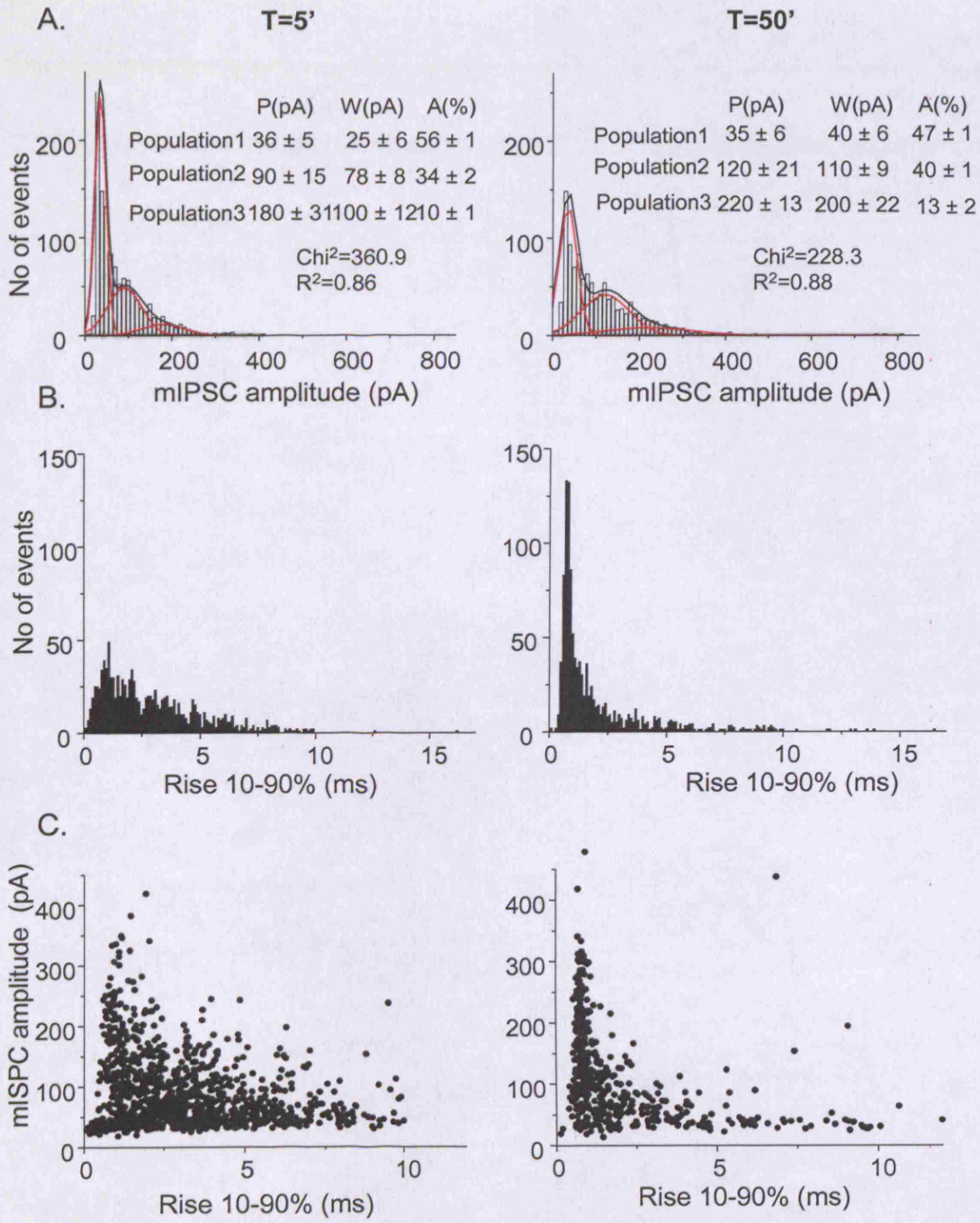

Fig 4.13 Population analyses of mIPSCs during αCaMKII modulation.

A). Amplitude distributions of mIPSCs at the beginning (t=5' left) and end (t=50') of αCaMKII modulation. Gaussian distributions were fitted. Peak (P), Width (W), Area (A), of the subpopulations are shown. Values are mean ± s.e. Chi^2 and R^2 values are indicated.

B). Distribution of rise times (10-90%) initially (left) and at the end (right) of αCaMKII modulation.

C). Scatter-plots of amplitude *vs* rise time of mIPSCs initially (left) and at the end (right) of αCaMKII modulation.

2000 events were selected at each time point to construct the analyses. Above analyses were from a single representative cell.

	mIPSC Amplitude(pA)		mIPSC Frequency(Hz)		Rise time (ms)		Decay time constant τ (ms)	
	t=0'	t=30'	t=0'	t=30'	t= 0'	t= 30'	t= 0'	t= 30'
Control n=12	69.7±15.9	64.9±10.5	4.9±0.3	5.0±0.5	2.0±0.2	2.8±0.4	9.8±0.7	11.6±0.9
RP n=5	49.9±5.2	81.6±12*	5.7±1.5	5.3±1.3	1.2±0.2	1.5±0.1	11.8±0.6	13.5±0.7
CaMKIIN n=4	77.2±7.2	74.2±6.1	4.0±0.6	4.3±1.0	1.3±0.3	1.4±0.6	7.8±0.5	12.9±2.5
RP + CaMKIIN n=5	81.5±14.3	71.7±12.4	8.7±2.0	7.4±1.3	1.1±0.1	1.1±0.2	14.5±0.5	15.9±0.6
Genistein n=4	41.0±10.6	46.0±11.6	2.4±0.7	2.1±0.4	1.3±0.4	1.2±0.3	9.2±1.0	12.5±1.2
RP + Genistein n=5	96.4±4.6	98.7±13.3	6.9±2.7	7.0±1.9	2.0±0.2	2.2±0.2	9.0±0.5*	15.3±1.5 *
Na_3VO_4 n=4	65.7±7.3	71.1±10.4	2.5±0.5	2.3±0.4	2.3±0.1	2.2±0.2	10.4±1.1	15.2±2.2
RP +Na_3VO_4 n=5	93.3±14.7	129.7±31	3.9±0.7	3.5±0.8	2.3±0.4	1.3±0.2	14.5±2.3	16.5±4.6
ODA n=4	77.7±6.8	76.0±8.6	2.4±0.3	2.1±0.1	2.3±0.7	3.1±0.5	9.4±0.3*	14.3±1.9 *
RP+ODA n=5	87.0±12.0	119.9±11	4.5±1.5	4.3±1.2	1.5±0.3	1.1±0.1	12.1±0.7	10.3±0.3
CaMKII n=6	63.6±9.4	99.1±8.1*	3.4±0.7	3.3±0.7	1.5±0.2	1.0±0.0	10.5±1.0	13.6±2.3

Table 4.1 Rise times and decay time constants for mIPSCs in kinase and phosphatase inhibitors: in control condition (t=0' and t=25'); 1 min before and 25 min after RP induction; basal values in reagent at t=0' and t=25'; before and after RP values in the presence of drugs. Values are mean ± s.e. *P<0.05 between the values at t = 0' and t = 25'.

4.3 Discussion

4.3.1 Regulation of RP by kinase-induced phosphorylation – CaMKII

CaMKII has long been recognized as the mediator of synaptic plasticity (Soderling and Derkach, 2000; Lisman, 2002). At glutamergic synapses, CaMKII is known to translocate to the PSD (postsynaptic density) where it binds to substrates such as the NR2B subunit and other PSD proteins after a Ca^{2+} signal. Autophosphorylation of Thr286 enhances further Ca^{2+}/CaM binding to the holoenzyme, prolonging sequestration of CaMKII at the PSD, potentially serving as a short term biochemical 'memory' (Shen and Meyer, 1999). Hence, autophosphorylation lengthens the activation period of CaMKII, and converts the enzyme into a Ca^{2+}/CaM independent state of autonomous activity. The classical antagonists, KN-93 and KN-62 competitively block the binding of Ca^{2+}/CaM to the enzyme, to prevent only the activation of CaMKII, but have no effect on readily activated enzyme in the autonomous state. Another disadvantage is their lack of specificity at high concentrations, inhibiting CaMK-IV and voltage-dependent potassium channels (Enslen and Soderling, 1994; LeDoux et al., 1999). Recent identification of an endogenous protein, CaMKIIN, that binds specifically to the AID of both α and βCaMKII (Chang et al., 2001), suggests it interacts with activated CaMKII, and may terminate synaptic plasticity endogenously. Truncated CaMKIIN of 28 amino acids peptide (KRPPKLGQIGRSKRVVIEDDRIDDVLK) retained all its inhibitory potency. This peptide, CaMKIINtide, specifically inhibits activated CaMKII, with no specificity for other Ca^{2+}/CaM-dependent kinases such as CaMKI, CaMKIV, CaMKK. CaMKIINtide has been utilised to

specifically block AMPAR phosphorylation mediated by CaMKII (Chang et al., 1998).

CaMKIINtide completely inhibited both early and late RP using the 5' latency protocol, and the late RP with the 12' stimulation latency protocol. This verified the phosphorylation-dependent nature of RP as previously proposed (Kano et al., 1996). The early RP noted in the 12' latency protocol appeared to be largely phosphorylation-independent, and may rely on separate mechanisms, such as direct Ca^{2+} induced exocytosis of $GABA_AR$-containing vesicles. Evidence in support of this hypothesis comes from the completely ablation of RP (both early and late) by internal dialysis of Ca^{2+} chelator BAPTA (Kano et al., 1992).

Over the past two decades, there has been considerable debate over the necessity of continuous CaMKII activity in the maintenance of RP. The evidence so far suggests that CaMKII does not contribute to RP maintenance, as a 5 min delay in applying KN62 renders RP insensitive to inhibition (Kano et al., 1996). However, using the novel inhibitor, CaMKIINtide, inhibiting the autophosphorylation of CaMKII (Sanhueza, et al 2007), reversed established half maximum RP back to control levels (baseline). This proves for the first time, that persistent activity of CaMKII is indeed required to preserve inhibitory synaptic strength during RP. A lack of effect of CaMKIINtide on basal mIPSC amplitudes indicates that the constitutive level of CaMKII phosphorylation must be low in PCs, leaving GABAergic transmission unaffected.

The elimination of RP with a β3-loop peptide emphasized the importance of CaMKII binding to the receptors for the induction of RP.

This peptide, comprising the first quarter of the intracellular loop from TM3 in the β3 subunit has been demonstrated to interact with autophosphorylated CaMKII in COS7 cells (McAnish et al., 2003). This region is upstream of the actual phosphorylation sites S383, S408 and S409 in the β3 subunit, which are known to be phosphorylated by CaMKII in cortical neurons. Subsequent work led to the shortening of this sequence to a condensed 10 amino acids peptide corresponding to sequence 303 to 312 in the β3 subunit. This sequence is conserved in both β2 and β3 subunits, and differs from the β1 subunit by only one residue (K310 in β1 and R310 in β2/3). Hence this peptide is likely to eradicate all CaMKII binding to the β subunits. The suppression of RP by this peptide strongly supports a direct CaMKII mediated phosphorylation of β2/3 subunit-containing $GABA_A$Rs during the onset of RP.

CaMKII can modulate GABAergic transmission through multiple mechanisms. At the IN-PC synapses, CaMKII-dependent conformational changes in $GABA_A$ receptor-associated protein (GABARAP), which links $GABA_A$R γ2 subunits to tubulins, has been reported during RP (Kawaguchi and Hirano, 2007). Translocation of GABARAP to the plasma membrane upon stimulation, followed by lasting interactions with both the γ2 subunit and tubulins, seems imperative for the induction of RP. This requires CaMKII-induced sustained conformational changes in GABARAP (Kawaguchi and Hirano, 2007). Furthermore, inhibition of microtubule polymerization with vincristine also selectively inhibited sustained RP, but not the early RP (Kawaguchi and Hirano, 2007).

These data are in accordance with a previous finding of IP_3R mediated CaMKII enhancement of GABAergic current in CA1 neurons,

by increasing or stabilizing actin and microtubule polymerization (Wei et al., 2004). Microtubules serve as decks for $GABA_AR$ anchoring in postsynaptic membranes and facilitate the clustering of receptors in the synapses. GABARAP and gephyrin are also known to be phosphorylated by kinases (Johnson et al., 1998; Kirsch et al., 1991) Phosphorylation of GABARAP by CaMKII may initiate cytoskeleton-mediated receptor trafficking, to increase the number of surface receptors, thus enhancing GABAergic currents. The role of receptor trafficking in the expression RP is examined in chapter 5.

Alternatively, GABARAP may alter the channel function of $GABA_AR$ such as increase in single channel conductance and P_{open}, as demonstrated in L929 cells expressed with $\alpha 1\beta 2/3\gamma 2$ (Everitt et al., 2004; Luu et al., 2006).

4.3.2 Regulation of RP by kinase phosphorylation – PTK

To date, the direct role of PTK in RP has received little attention, though $GABA_BR$ activation was shown to negatively regulate RP induction via integrin and downstream Src kinase activity (Kawaguchi and Hirano, 2006). On the other hand, GABAergic currents was potentiated by synergized TrkB and Src kinase activation in PCs (Boxall, 2000). An interaction between CaMKII and PTK activity in regulating $GABA_ARs$ in cerebellar granule cells (Houston and Smart, 2006) raised the prospect of a potential role for PTK in RP. PTK mediated phosphorylation of $\gamma 2$ subunit may influence its association with GABARAP (Chen et al., 2005).

Genistein inhibition of sustained RP, revealed for the first time the direct requirement of PTK in the induction of RP. The inhibition profile of RP resembled CaMKIINtide inhibition of RP. This implies these kinases may utilize a common pathway in regulating RP. Notably, CaMKII phosphorylation of $GABA_AR$ of $\alpha1\beta3\gamma2$ receptors in NG-108 cells, elicited both phosphorylation of Ser383 on the $\beta3$ subunit, and tyrosine phosphorylation of Y365, Y367 on the $\gamma2$ subunit (Houston and Smart, 2006). It is plausible that the extent of constitutive phosphorylation of Y365, Y367 by PTK (Brandon et al., 2001) under basal conditions (unveiled upon inhibition of phosphatases) may be sufficient to induce RP in conjunction with CaMKII phosphorylation. Upon removal of PTK activity by genistein, CaMKII may become less effective at phosphorylating $GABA_ARs$ or initiating subsequent events that lead to RP. CaMKII-dependent structural alteration of GABARAP, and $\gamma2$ subunits phosphorylation by PTK, may both be important in order for their interaction and RP to take place.

Genistein did not reduce basal mIPSC amplitude, reflecting a lack of basal PTK phosphorylation in PCs. Intriguingly, the PTP inhibitor sodium orthovanadate substantially enhanced basal mIPSC amplitudes, which suggests high endogenous activity of protein tyrosine phosphatases, restricting the basal activity of PTK. Additional tyrosine phosphorylation residues are found on the β subunits (Moss et al., 1995). The $\beta2$ subunit in particular, can account for the insulin induced tyrosine phosphorylation-dependent recruitment of $GABA_AR$ into postsynaptic domains, to enhanced whole-cell inhibitory currents in HEK 293 cells and mIPSCs amplitudes in neurons (Wan et al., 1997a; Wan et al.,

1997b). Therefore, tyrosine phosphorylation of β subunits, have a separate effect to that of $\gamma 2$ tyrosine phosphorylation (Moss et al., 1995). $\gamma 2$ subunit-mediated change in channel function and $\beta 2$ subunit-mediated increase in receptor number, by PTK phosphorylation may synergize to upregulate inhibitory currents in RP. PTK phosphorylation of $\gamma 2$ subunit could also downregulate endocytosis by inhibiting interaction with AP2, effective stabilizing and increase the cell surface number of $GABA_A$Rs (Kittler et al., 2008).

BDNF was found to enhance mIPSC amplitudes in PCs via TrkB receptors, which required co-activation of Src kinase by mGluR1 (Boxall, 2000). BDNF is known to affect GABAergic transmission in a cell-type specific manner (Mizoguchi et al., 2003a; Mizoguchi et al., 2003b; Tanaka et al., 1997). In the rat visual cortex, a BDNF-TrkB-PLCγ pathway enhanced GABAergic transmission by rapidly increasing the number of receptors in the synapse, with an increase in somatic area, number and length of primary dendrites, dendritic branching points to accommodate receptor insertion (Mizoguchi et al., 2003a; Palizvan et al., 2004). On the other hand, downregulation of GABAergic transmission via receptor internalization was detected by BDNF-TrkB activation in both cerebellar granule cells and hippocampal pyramidal cells (Brunig et al., 2001; Cheng and Yeh, 2003). Unfortunately, the classical TrkB inhibitor, K252a, also has affinity for CaMKII, further experiments with specific antibody against TrkB receptor, TrkB-Fc, may be beneficial to elucidate any role of BDNF and TrkB in RP (Cheng and Yeh, 2003).

The reliance of early RP (of the 12' latency profile) on phosphorylation was addressed using a combination of CaMKIINtide and genistein, and also the non–specific protein kinase inhibitor, staurosporine. Early RP displayed complete resistance to kinase inhibition, indicating it was not a result of an additive effect of CaMKII and PTK, nor did it involve other protein kinases such as, PKA, PKC or PKG. The initial peak in early RP is most likely phosphorylation-independent.

4.3.3 Modulation of RP by phosphatases

Protein phosphatases 1 and 2A, 2C can dephosphorylate activated CaMKII at Thr286 and switch off kinase activity, hence have the ability to reduce RP (Millward et al., 1999). A previous study demonstrated the suppression of RP induction only required PP1, which implied RP might be mediated by CaMKII anchored at synapses (Kawaguchi and Hirano, 2002). Furthermore, PP1 and PP2A could, in theory, directly dephosphorylate the potentiated $GABA_AR$ subunits. In this study, inhibition of PP1 and PP2A had no effect on basal mIPSC amplitude, nor did it increase the extent of RP, suggesting direct dephosphorylation of $GABA_AR$ subunits in PCs was low. On the contrary, addition of sodium orthovanadate increased basal mIPSC amplitudes, implicating high level of endogenous PTK activity, in agreement with previous work (Moss et al., 1995).

4.3.4 CaMKII and PTK cross-regulation of RP

The notion of a common signaling pathway was tested. Increasing PTK activity with sodium orthovanadate restored the suppression RP by CaMKIINtide. Thus PTK activity seemed sufficient to induce RP in the absence of CaMKII. However, RP inducing PTK activity may be curtailed by the high expression of intrinsic PTP under basal condition, as inhibition of PTP caused considerable increases in mIPSC amplitude in PCs.

Curiously, enhancing CaMKII with ODA also reinstated the late RP in the presence of genistein, contradicting the hypothesis that CaMKII and PTK converged into a common pathway. As a result, we predicted two possible scenarios in Fig 4.14.

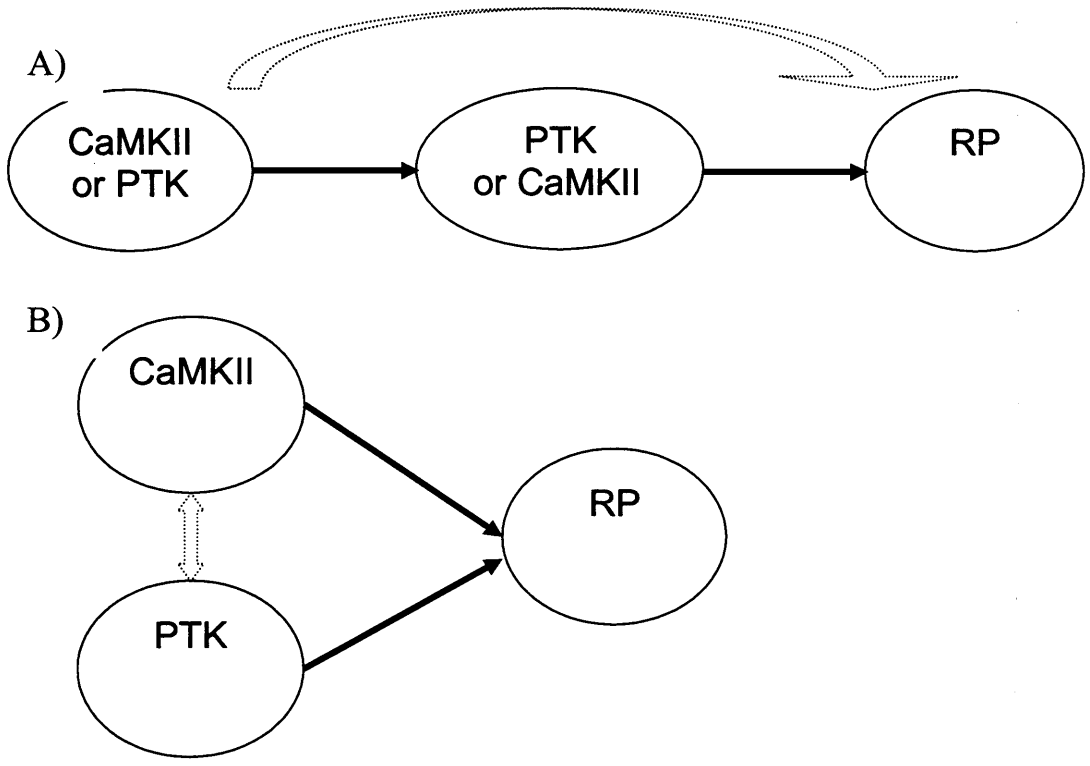

Fig 4.14. The predicted pathways of CaMKII and PTK signaling in the induction of RP. A. A common dominating pathway of CaMKII and PTK, acting in series, to ensure the expression of RP, with a secondary dormant pathway, elicited upon inhibition by phosphatases. B. Two inter-connected pathways of CaMKII and PTK activity, leading to the induction of RP.

In Fig 4.14 A), RP is presumed to be induced by a direct (dominating) and an indirect (dormant) pathway. When the dominating pathway is inhibited, the dormant pathway may be recruited (after the removal of counteracting phosphatase activity), to bypass the downstream kinases and induce RP. In Fig 4.14 b), CaMKII and PTK may act through two separate pathways, which are inter-regulated. Both kinases may be activated at sub-threshold levels by the RP stimulus and synergise to potentiate inhibitory currents in PCs.

Finally, we addressed the extent of PTK dependent CaMKII activity in PCs. Direct injection of activated αCaMKII resulted in a RP-like potentiation of mIPSCs in PCs. Furthermore, this potentiation preferentially increased the frequency of fast rise time large amplitude mIPSC events, accompanied with a reduction in frequency of small amplitude mIPSCs. This profile resembles that of synaptically evoked RP. Hence, the synapses from proximal inputs of basket cells, are more likely to be potentiated by αCaMKII, whereas the distal inputs seemed to be suppressed. This supports the notion that CaMKII affects inhibitory transmission the same way as RP. The αCaMKII mediated potentiation was completely suppressed by genistein, which strongly implied that PTK was downstream effector of CaMKII activity to enhance the inhibitory currents in PCs. Similar results were reported when 100μM

genistein partially inhibited αCaMKII-mediated enhancement of GABAergic responses to exogenous application of GABA in NG108 cells transfected with $\alpha 1\beta 3\gamma 2S$ (Houston et al., 2007).

4.4 Conclusion

In this chapter, the phosphorylation cascade of RP was studied in detail. The requirement of PTK activity was identified, for the first time, which may interact with CaMKII activity to ensure the expression of RP. Furthermore, we postulated either a direct augmentation of $GABA_AR$ channel function, or an increase in surface receptor number could be achieved by kinase activation, in order to increase inhibitory synaptic transmission in RP. These possibilities are investigated in chapter 5.

Chapter 5

$GABA_AR$ trafficking and its role in RP

5.1 Introduction

At synapses where postsynaptic receptor channels have a high opening probability (e.g. between interneurons and PCs in the cerebellum), caused by large synchronous presynaptic neurotransmitters release increasing the likelihood of receptor saturation, the most effective means of augmenting postsynaptic responses is to increase the number of postsynaptic receptors. Indeed, receptor insertion and internalisation has long been recognized to alter synaptic strength during plasticity.

In the prototypic LTP of hippocampal CA1 neurons, transient NMDAR activation instigates CaMKII/PKA/PKC phosphorylation mediated AMPAR insertion (Hayashi et al., 2000; Lu et al., 2001; Pickard et al., 2001). Conversely, hippocampal LTD requires the removal of AMPARs, by dephosphorylation of PKA and CaMKII phosphorylation sites (Heynen et al., 2000; Lee et al., 2000; Lissin et al., 1999). Similarly in the cerebellum, clathrin-mediated internalization of AMPARs has also been implicated in parallel fibre (PF) LTD. This was initiated by PKC-phosphorylation mediated dissociation of GluR2 subunits, from the postsynaptic anchoring protein, GRIP (Wang and Linden, 2000). Interestingly, cerebellar PF plasticities operate inversely from the hippocampal plasticities, such that an increase in synaptic gain is promoted by dephosphorylation, and vice-versa. This was thought to be attributed to the relative expression ratio of GluR1 and GluR2 subunits in the

hippocampus and cerebellum, of which phosphorylation of each subunit favoured receptor insertion and removal, respectively (Hansel, 2005; Isaac et al., 2007; Jiang et al., 2006; Shepherd and Huganirl, 2007).

At inhibitory synapses, an increase in $GABA_AR$ density has been found in the granule cells of adult dentate gyrus, for an experimental model of temporal-lobe epilepsy. Increased immunostaining of the $GABA_AR$ $\alpha 1$, $\alpha 2$, $\beta 2/3$ and $\gamma 2$ subunits, combined with a doubling of receptor numbers, estimated by non-stationary noise analysis, suggested that recruitment of receptors to the synapses underlay the increase in the quantal size of the inhibitory synaptic current in this model of plasticity (Nusser et al., 1998; Otis et al., 1994). Increased surface expression of $GABA_ARs$ was also implicated in the insulin-mediated potentiation of GABAergic currents, through the phosphorylation of $\beta 2$ subunits (Wan et al., 1997). A different mechanism, involving the alteration of synaptic $GABA_AR$ subunit composition, was found in the synaptic plasticity of oxytocin neurons. This was achieved by switching between the $GABA_AR$ $\alpha 1$ and $\alpha 2$ subunits, thus establishing subunit redistribution as a basis for inhibitory plasticity (Brussaard et al., 1997).

The high concentration of GABA within a single presynaptic vesicle, against the low number of $GABA_AR$ channels required to elicit mIPSCs, indicates that the number of channels, *N*, not the transmitter content of vesicles, is the limiting factor for determining the amplitude of mIPSCs (Otis et al., 1994). In the case of hippocampal dentate gyrus granule cells, pharmacological saturation of postsynaptic $GABA_ARs$ by GABA release from a single vesicle led to the opening of all channels at the peak of the

mIPSC, as confirmed by the lack of effect of pentobarbital and benzodiazepine on the peak mIPSC amplitude, although the decay time constant was prolonged, as expected (De Koninck and Mody, 1994).

Multiple lines of evidences have affirmed the purely postsynaptic origin of RP: the lack of change in mIPSC frequency during RP; the increase in response to exogenously-applied GABA (Kano et al., 1992); and the ablation of late RP by the internal application of kinase inhibitors. Postsynaptic modulation can be achieved by upregulating postsynaptic receptor number (N), or enhancing channel function, by increasing channel open probability (Po), and/or the single (unitary) channel conductance (γ). In this chapter, peak-scaled non-stationary noise analysis (PS-NSNA) was utilised to estimate the above parameters during RP (Sigworth, 1980). This revealed a predominant increase in N_p, the mean number of activated channels at the peak of the mIPSC. Hence the role of $GABA_AR$ trafficking was assessed using numerous exocytosis inhibitors and blockers of endoreticulum(ER)-Golgi trafficking.

5.2 Results

The mIPSCs recorded in PCs exhibited a highly skewed amplitude histogram, biased toward smaller amplitudes (Fig 5.3), and best fitted by triple Gaussian distributions, possibly attributed to the variable size of receptor aggregates opposite presynaptic boutons on the PC membrane (De Koninck and Mody, 1994). The extensive electronic filtering in PCs may cause difficulty in distinguishing different conductance levels of $GABA_AR$ subtypes, as single channel conductance of slower rise time events might be underestimated. This limits the accuracy of NSNA, hence the PS-NSNA was used cautiously and validated by corroborating experimental evidence.

5.2.1 Non-stationary noise analysis (NSNA)

Neher and Stevens pioneered the method of stationary fluctuation noise analysis in 1977, which was later adapted and used extensively to extract the kinetics and conductance properties of single ligand-gated channels, inaccessible to direct measurement (Neher and Stevens, 1977). Further modification resulted in the non-stationary fluctuation method, which introduced this analysis for channels in dynamic states, e.g. sodium channels (Sigworth, 1980). Nowadays, the high resolution analysis of action potential independent synaptic events from tight-seal whole-cell patch clamp recordings from neurons can be achieved (Otis et al., 1994).

PS-NSNA assumes the highest *Po*, hence lowest current variance, occurs at the peak of the response. The analysis is performed on a fixed length of mIPSC decay, starting from the peak current to near the end of the decay. The amplitudes are divided into equal size time bins, and the average mIPSC current of each bin is scaled to the peak amplitude of the

given mIPSC. Peak-scaling helped to negate the variable release patterns risen from multiple innervations of a PC. The mIPSC amplitude variance within each scaled average bin are calculated and plotted against the average bin currents (De Koninck and Mody, 1994). The variance against mean amplitude relationship can be fitted by the equation 5.1:

Equation 5.1: $\sigma^2 = i\bar{I}_m - \bar{I}^2{}_m/N_p + \sigma^2{}_b$

where σ^2 is the current variance, i is the single channel current, $\bar{I}_m$ is the mean current and N_p is the average number of receptor channels open in the synapse at the peak of the mIPSC. $\sigma^2{}_b$ represents the background current variance.

In this study, we used the PS-NSNA method adapted from Traynelis's method of estimating the conductance of non NMDA receptors (Traynelis et al., 1993). Using this approach, single channel parameters for the $GABA_A$Rs underlying mIPSCs in PCs were extracted. Variance-current plots of mIPSCs, in both control and RP conditions (Fig 5.1A), displayed parabolic relationships, in accord with the assumption that most channels activated by the neurotransmitters are open at the peak of the mIPSC amplitude, and close randomly during its decay. This also reflected the low intrinsic variance at the peak of the current, indicative of longer mean channel opening times compared to the rise-times of the mIPSCs (De Koninck and Mody, 1994). As the mean amplitudes were scaled to the peak mIPSC amplitude, this analysis did not determine the absolute number of receptors in the synapse (N), nor the opening probability (P_o), but instead reported the average number of open channels (N_p).

The variance-current plot estimated single channel current (pA) from the initial gradient of the parabola, which was converted to single channel conductance by the equation 5.2:

Equation 5.2: $\gamma = i/(V_m - E_{Cl})$,

where γ is the single channel conductance, V_m is the holding membrane potential of the cell, E_{Cl} is the Cl^- reversal potential and i represents the single channel current. The reversal potential for Cl^- in PCs was calculated by the Nernst equation (equation 5.3) to be + 0.69 mV using equimolar extracellular and intracellular Cl^- concentrations.

Equation 5.3: $V_{Cl} = \frac{RT}{zF} \ln([Cl]_i/[Cl]_o)$

Taking into account the junction potential, the single channel conductance of $GABA_A$Rs in PCs was calculated to be 23.7 ± 5.3 pS (grey bar in Fig 5.1C) before RP induction, at room temperature of 24°C (n=5). This is similar to reported values of 28pS at a physiological temperature of 35°C, and 20pS at 22 °C in hippocampal dentate gyrus neurons, with a temperature dependence Q_{10} of 1.2 (De Koninck and Mody, 1994). After RP induction, γ remained at 24.5 ± 4.5 pS (Fig 5.1C n = 5, P>0.05). The parabola was shifted upwards and rightwards but the initial gradient appeared unaffected (Fig 5.1 A). The consistency of single channel conductance was observed in various non-stationary analyses of $GABA_A$Rs, in agreement with the theory that the channel conductance is resistant to modulation (De Koninck and Mody, 1994). This also supports the hypothesis that a variable receptor population at the synapses probably

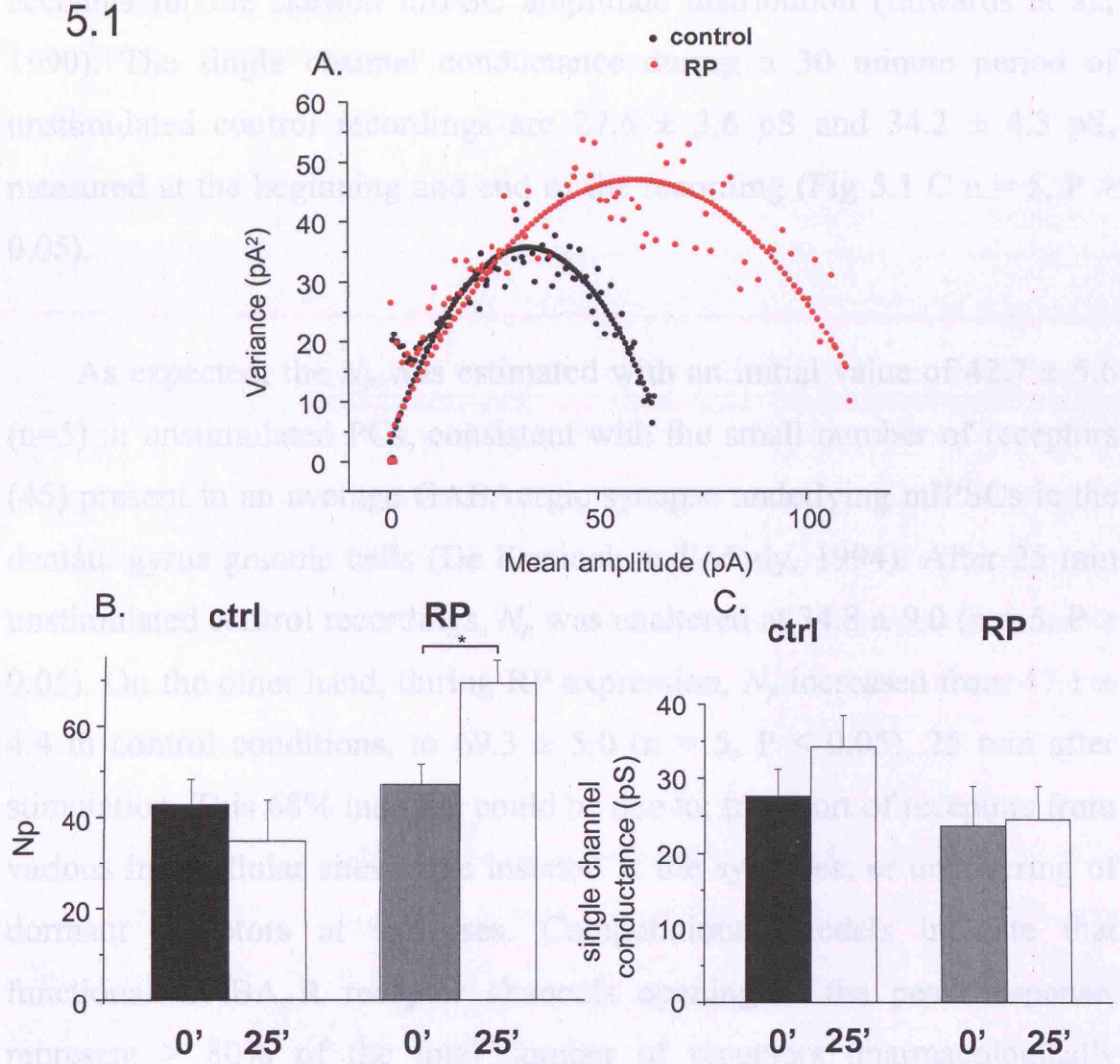

Fig 5.1 PS-NSNA of mIPSCs during RP.

A. Plot of mIPSC variance against mean current amplitude within each bin of 10pA in size during the decay of mIPSC. 100 consecutive single events were selected before (t = 0') and t = 25' after RP induction, filtered and fitted to construct the plot. B. Histogram of N_p estimated at the t = 0' and t = 25' of unstimulated control recordings (n=5), before and 25 min after RP induction (*P < 0.05). C. Single channel conductance histogram under the same conditions as in B.

accounts for the skewed mIPSC amplitude distribution (Edwards et al., 1990). The single channel conductance during a 30 minute period of unstimulated control recordings are 27.6 ± 3.6 pS and 34.2 ± 4.3 pS, measured at the beginning and end of the recording (Fig 5.1 C n = 5, P > 0.05).

As expected, the N_p was estimated with an initial value of 42.7 ± 5.6 (n=5) in unstimulated PCs, consistent with the small number of receptors (45) present in an average GABAergic synapse underlying mIPSCs in the dentate gyrus granule cells (De Koninck and Mody, 1994). After 25 min unstimulated control recordings, N_p was unaltered at 34.8 ± 9.0 (n = 5, P > 0.05). On the other hand, during RP expression, N_p increased from 47.1 ± 4.4 in control conditions, to 69.3 ± 5.0 (n = 5, P < 0.05), 25 min after stimulation. This 68% increase could be due to: transport of receptors from various intracellular sites to be inserted at the synapses; or uncovering of dormant receptors at synapses. Computational models indicate that functional $GABA_AR$ receptor channels opening at the peak response, represent > 80% of the total number of receptors pharmacologically saturated by the cleft GABA concentration, allowing room for the awakening of silent receptors (Faber et al., 1992). Lateral movement of $GABA_AR$ receptors within the membrane lipid bilayer, from extrasynaptic to synaptic sites, may also account for this (Thomas et al., 2005). We also cannot disregard the possibility of an increase in *Po*.

To distinguish which of these potential sources may underlie the increase in N_p during RP, we utilized numerous inhibitors of exocytosis to study the function of receptor trafficking in rebound potentiation.

5.2.2 Effect of exocytosis inhibitors on RP

Irrespective of the origin of the transporter vesicles, the secretory pathways converge on the definitive step of vesicle fusion with the plasma membrane. N-ethylmaleimide (NEM,), a widely used inhibitor of exocytosis, was used first to study synaptic receptor delivery during RP (Lledo et al., 1998; Luscher et al., 1999; Thomas et al., 2005). Inhibition of vesicular transport by NEM occurred by blocking NEM-sensitive factor (NSF), a cytosolic adenosine triphosphate binding protein, which hydrolyses ATP and generates energy for regenerative SNARE protein recycling. NSF interacts with both SNAPs (soluble NSF attachment proteins) and GABARAP, thus may underlie fusion between the plasma membrane and $GABA_AR$ containing transporter vesicles (Chen and Olsen, 2007; Luscher and Keller, 2004).

NEM was internally applied at concentration of 250 μM, for 12 min following the establishment of whole-cell configuration, to allow sufficient diffusion into the distal dendrites of the PCs (Thomas et al., 2005). With the inclusion of NEM, early (t = 0') and were suppressed to 111.5 ± 2.9 % (Fig 5.2A-C and 5.17, n = 5, $P < 0.05$ compared to control RP). The fluctuation in control-RP amplitude revealed an overlap between control-RP and NEM-RP (between t=4' and t=8', the two groups were not significantly different), but in long term, late RP (t = 25') were suppressed to 112.3 ± 11.9% ($P < 0.05$). During NEM treatment, the scaled average mIPSC showed no change in the amplitude before and after

5.2

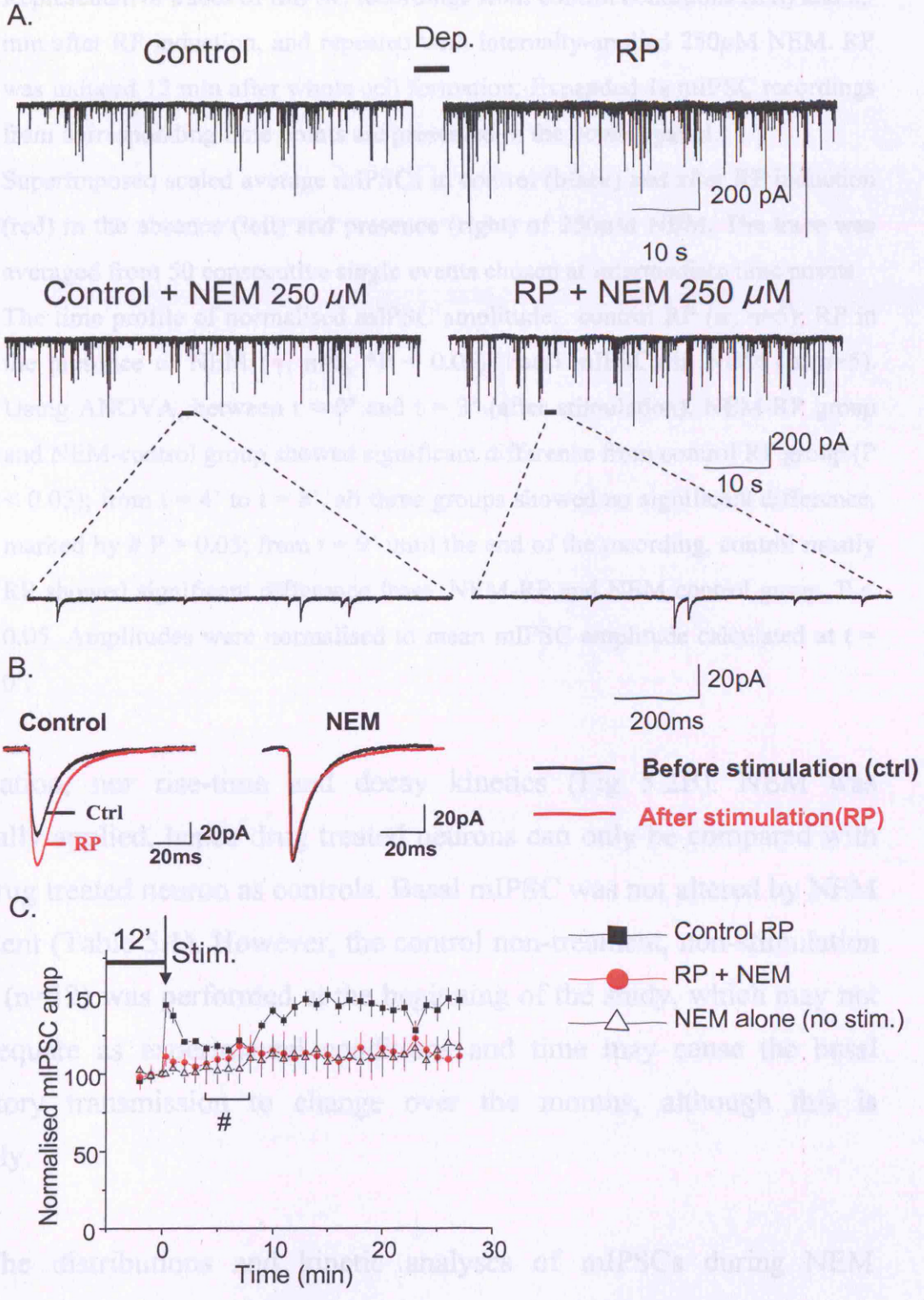
A.
Control
Dep.
RP
200 pA
10 s
Control + NEM 250 μM
RP + NEM 250 μM
200 pA
10 s
B.
20pA
200ms
Control
NEM
Ctrl
RP
20pA
20ms
20pA
20ms
Before stimulation (ctrl)
After stimulation(RP)
C.
12'
Stim.
Normalised mIPSC amp
150
100
50
0
#
0
10
20
30
Time (min)
Control RP
RP + NEM
NEM alone (no stim.)

Fig 5.2 Suppression of RP by NEM.

A. Representative traces of mIPSC recordings from control conditions (left) and 25 min after RP induction, and repeated with internally-applied 250μM NEM. RP was induced 12 min after whole cell formation. Expanded 1s mIPSC recordings from corresponding time points are presented in the bottom panel.

B. Superimposed scaled average mIPSCs in control (black) and after RP induction (red) in the absence (left) and presence (right) of 250μM NEM. The trace was averaged from 50 consecutive single events chosen at intermediate time points.

C. The time profile of normalised mIPSC amplitude: control RP (■, n=5); RP in the presence of NEM (●, n=5, *P < 0.05); basal mIPSCs in NEM (Δ, n=5). Using ANOVA, between t = 0' and t = 3' (after stimulation), NEM-RP group and NEM-control group showed significant difference from control RP group (P < 0.05); from t = 4' to t = 8', all three groups showed no significant difference, marked by # P > 0.05; from t = 9' until the end of the recording, control mostly RP showed significant difference from NEM-RP and NEM control group, P < 0.05. Amplitudes were normalised to mean mIPSC amplitude calculated at t = 0'.

stimulation, nor rise-time and decay kinetics (Fig 5.2B). NEM was internally applied, hence drug treated neurons can only be compared with non-drug treated neuron as controls. Basal mIPSC was not altered by NEM treatment (Table 5.1). However, the control non-treament, non-stimulation group (n=12) was performed at the beginning of the study, which may not be adequate as experimental conditions and time may cause the basal inhibitory transmission to change over the months, although this is unlikely.

The distributions and kinetic analyses of mIPSCs during NEM treatment of RP are shown in Fig 5.3. The amplitude distribution exhibited

triple Gaussian populations, contributing to the overall leftward skewed distribution (Fig 5.3A). The Gaussian distributions were repetitively fitted by iteration until the best Chi^2 and R^2 values were obtained. The peaks of all three populations were unaltered after RP depolarization in the presence of NEM, although the frequency of small amplitude population appeared reduced (by eye measurement).

5.3

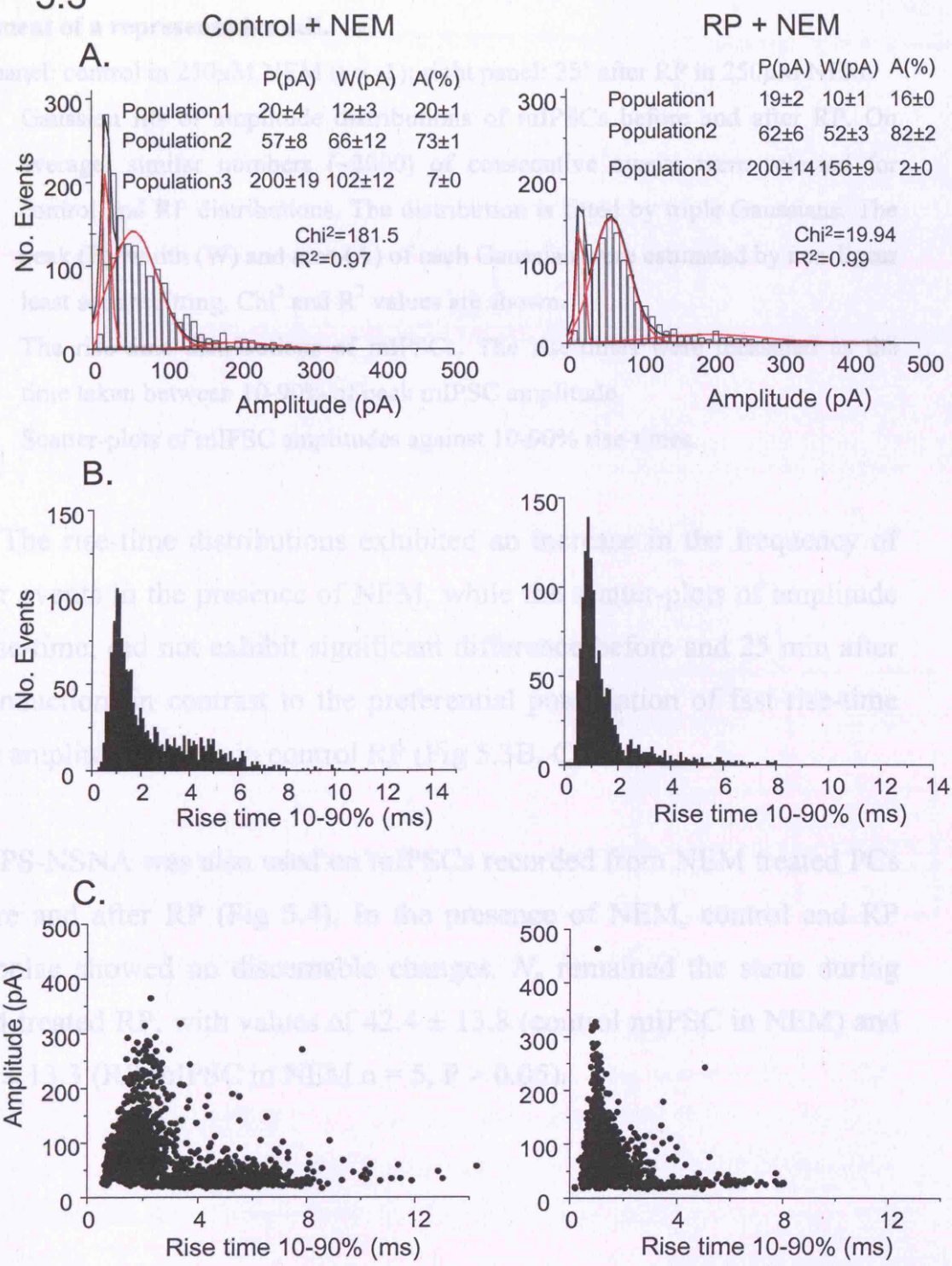
Control + NEM
RP + NEM
A.
P(pA) W(pA) A(%)
Population1 20±4 12±3 20±1
Population2 57±8 66±12 73±1
Population3 200±19 102±12 7±0
Chi²=181.5
R²=0.97
P(pA) W(pA) A(%)
Population1 19±2 10±1 16±0
Population2 62±6 52±3 82±2
Population3 200±14 156±9 2±0
Chi²=19.94
R²=0.99
No. Events
Amplitude (pA)
B.
No. Events
Rise time 10-90% (ms)
C.
Amplitude (pA)
Rise time 10-90% (ms)

Fig 5.3 Distribution analyses of mIPSCs before and after RP during NEM treatment of a representative cell.

Left panel: control in 250μM NEM (t = -1); right panel: 25' after RP in 250μM NEM.

A) Gaussian fits of amplitude distributions of mIPSCs before and after RP. On average, similar numbers (~2000) of consecutive events were selected for control and RP distributions. The distribution is fitted by triple Gaussians. The peak (P), width (W) and area (A) of each Gaussian were estimated by non-linear least square fitting. Chi^2 and R^2 values are shown.

B) The rise-time distributions of mIPSCs. The rise-times were measured as the time taken between 10-90% of peak mIPSC amplitude.

C) Scatter-plots of mIPSC amplitudes against 10-90% rise-times.

The rise-time distributions exhibited an increase in the frequency of faster events in the presence of NEM, while the scatter-plots of amplitude *vs* rise-time, did not exhibit significant difference before and 25 min after RP induction, in contrast to the preferential potentiation of fast rise-time large amplitude events in control RP (Fig 5.3B, C).

PS-NSNA was also used on mIPSCs recorded from NEM treated PCs before and after RP (Fig 5.4). In the presence of NEM, control and RP parabolae showed no discernable changes. N_p remained the same during NEM treated RP, with values of 42.4 ± 13.8 (control mIPSC in NEM) and 44.8 ± 13.3 (RP mIPSC in NEM n = 5, P > 0.05).

5.4

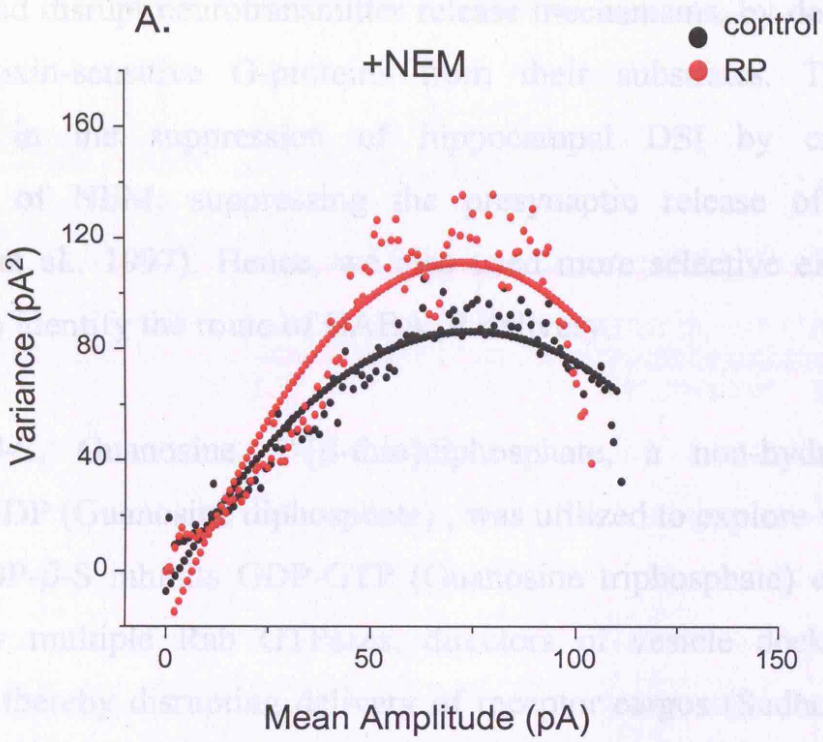

B.

	Control + NEM	RP + NEM
N_p	42.7 ± 13.8	44.8 ± 13.3
Single channel conductance γ (pS)	33.6 ± 5.3	36.1 ± 4.3

Fig 5.4 PS-NSNA of mIPSCs from NEM treated control and RP.

A) mIPSC current variance against mean mIPSC current plot, 100 consecutive single events were selected, filtered and fitted using the peak-scaled method. NEM-control mIPSCs (●), NEM-RP (●, 25 min after induction). B) Single channel parameters N_p (average number of open channels) and γ (single channel conductance) extracted from the curve fits (see methods). Values are mean ± s.e.

Although NEM is a classic tool in studying membrane fusion machinery, it also has multiple actions including inactivating NMDA

receptors (Lledo et al., 1998;). NEM may also leak into the presynaptic terminals and disrupt neurotransmitter release mechanisms, by decoupling pertussis toxin-sensitive G-proteins from their substrates. This was implicated in the suppression of hippocampal DSI by externally application of NEM, suppressing the presynaptic release of GABA (Morishita et al., 1997). Hence, we also used more selective exocytosis inhibitors to identify the route of $GABA_AR$ delivery.

GDP-β-S, Guanosine 5′-[β-thio]diphosphate, a non-hydrolysable analog of GDP (Guanosine diphosphate) , was utilized to explore vesicular release. GDP-β-S inhibits GDP-GTP (Guanosine triphosphate) exchange required by multiple Rab GTPases, directors of vesicle docking and trafficking, thereby disrupting delivery of receptor cargos (Sudhof, 1995; Sudhof, 1997).

Intracellular application of 1 mM GDP-β-S for 12 min inhibited RP, in similar fashion to NEM (Fig 5.5 A-C). Both early and late RP were completely blocked (105.7± 8.0 % and 101.6 ± 6.7 %, at t = 0' and t = 25' after RP induction, respectively, n = 6, $P < 0.05$ compared to control RP Fig 5.17). The rise-times and decay kinetics were not affected by GDP-β-S (Fig 5.5 B, Table 5.1), neither were the basal amplitude, or frequency of mIPSCs, although again, these are compared with the same set of controls (n=12) performed at the start of the study. DSI appeared normal in the presence of GDP-β-S, reflecting a different locus of regulation from RP (Data not shown).

The analyses of amplitude distributions and kinetics of mIPSCs, before and after RP, under the influence of GDP-β-S are shown in Fig 5.6. Similar to NEM treatment, the mean peak amplitude of each Gaussian-fitted population did not vary significantly before and after RP-inducing stimulus in the presence of GDP-β-S, (22pA, 42pA, 125 pA, before and 23pA, 51 pA, 119pA after; Fig 5.6 A). By eye measurement, a reduction in frequency of both small and large amplitude events can be seen in GDP-β-S treated RP, compensated by an increase in the medium amplitude population events; hence the overall mean amplitude did not alter. In Fig 5.6B, the rise-times distribution patterns of mIPSCs were similar, before and after RP induction, in the presence of GDP-β-S, with a slight reduction in the fast rise-time events. The rise-time *vs* amplitude scatter plotter in Fig 5.6 C revealed a heavier distribution of slower, smaller amplitude events after RP in GDP-β-S.

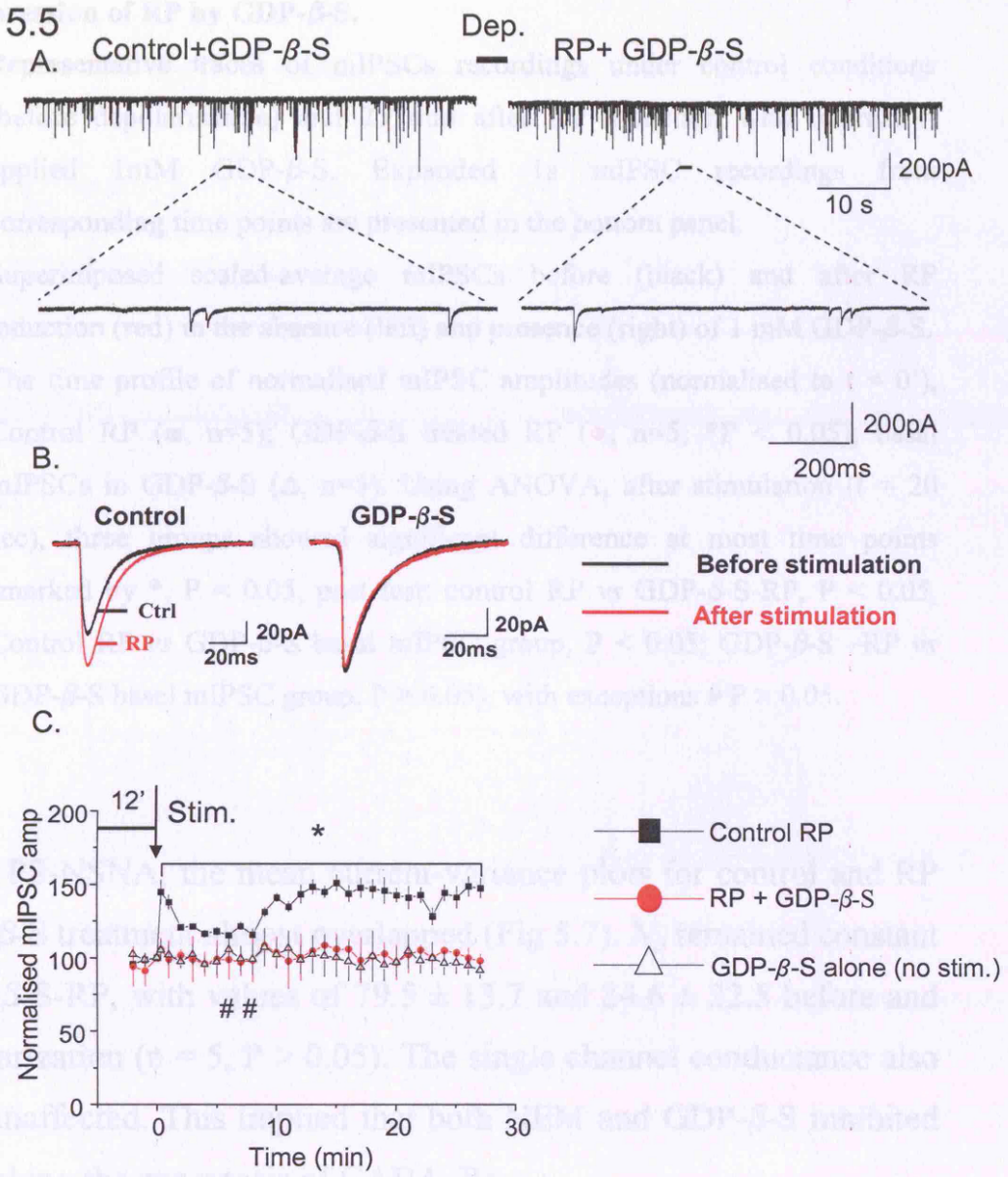
5.5
A.
Control+GDP-β-S
Dep.
RP+ GDP-β-S
200pA
10 s
200pA
200ms
B.
Control
GDP-β-S
Ctrl
RP
20pA
20ms
20pA
20ms
Before stimulation
After stimulation
C.
12'
Stim.
*
# #
Normalised mIPSC amp
200
150
100
50
0
0
10
20
30
Time (min)
Control RP
RP + GDP-β-S
GDP-β-S alone (no stim.)

Fig 5.5 Suppression of RP by GDP-β-S.

A) Representative traces of mIPSCs recordings under control conditions (before depolarisation) and 25 min after RP induction with internally-applied 1mM GDP-β-S. Expanded 1s mIPSC recordings from corresponding time points are presented in the bottom panel.

B) Superimposed scaled-average mIPSCs before (black) and after RP induction (red) in the absence (left) and presence (right) of 1 mM GDP-β-S.

C) The time profile of normalised mIPSC amplitudes (normalised to t = 0'), Control RP (■, n=5); GDP-β-S treated RP (●, n=5, *P < 0.05); basal mIPSCs in GDP-β-S (Δ, n=5). Using ANOVA, after stimulation (t = 20 sec), three groups showed significant difference at most time points (marked by *, P < 0.05, post test: control RP *vs* GDP-β-S-RP, P < 0.05, Control RP *vs* GDP-β-S basal mIPSC group, P < 0.05; GDP-β-S –RP *vs* GDP-β-S basal mIPSC group, P > 0.05), with exceptions # P > 0.05.

Using PS-NSNA, the mean current-variance plots for control and RP with GDP-β-S treatment almost overlapped (Fig 5.7). N_p remained constant after GDP-β-S-RP, with values of 79.5 ± 13.7 and 84.6 ± 22.5 before and after depolarization (n = 5, P > 0.05). The single channel conductance also remained unaffected. This implied that both NEM and GDP-β-S inhibited RP, by blocking the exocytosis of $GABA_A$Rs.

5.6

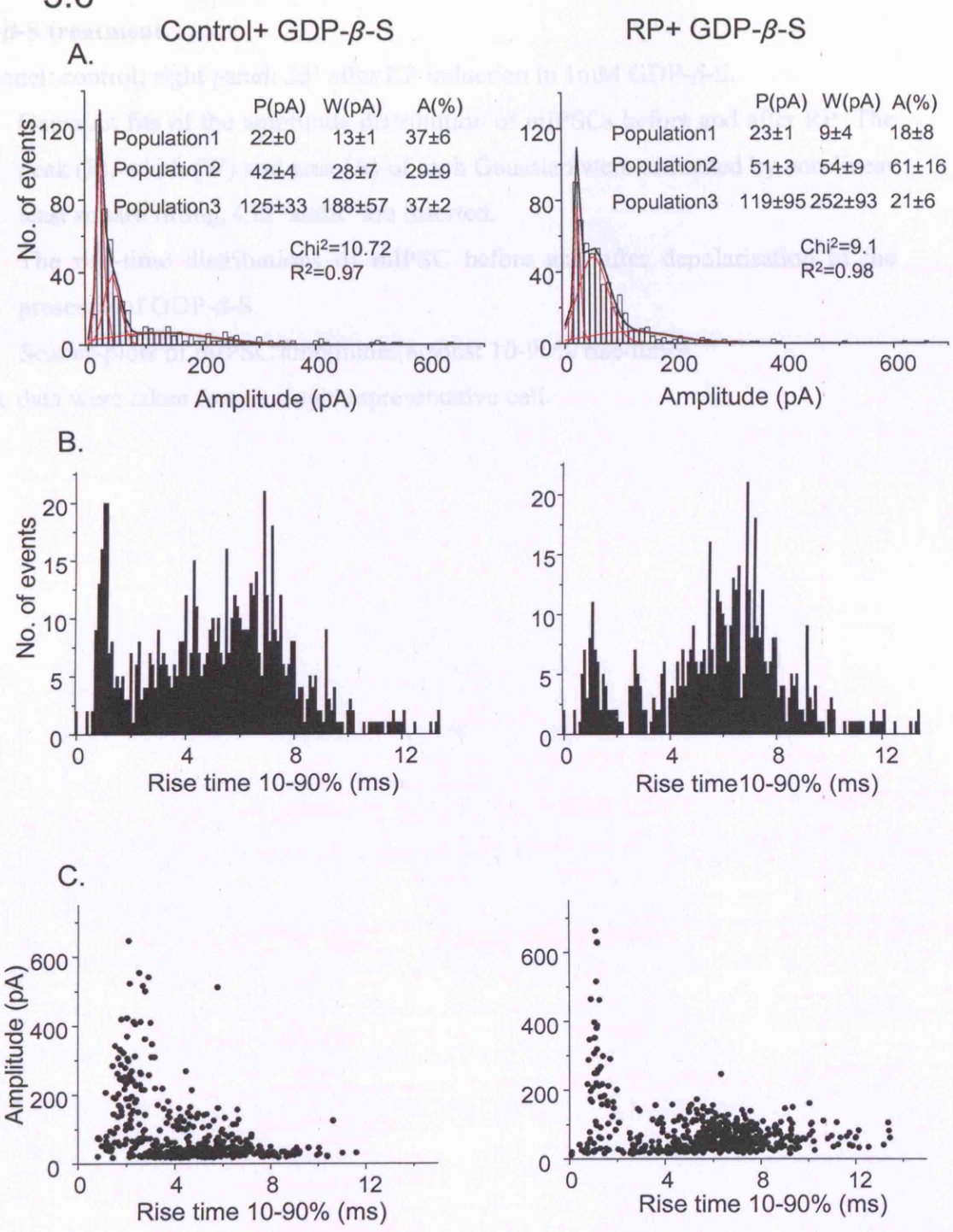
Control+ GDP-β-S
RP+ GDP-β-S
A.
P(pA) W(pA) A(%)
Population1 22±0 13±1 37±6
Population2 42±4 28±7 29±9
Population3 125±33 188±57 37±2
Chi²=10.72
R²=0.97
P(pA) W(pA) A(%)
Population1 23±1 9±4 18±8
Population2 51±3 54±9 61±16
Population3 119±95 252±93 21±6
Chi²=9.1
R²=0.98
No. of events
Amplitude (pA)
B.
No. of events
Rise time 10-90% (ms)
Rise time10-90% (ms)
C.
Amplitude (pA)
Rise time 10-90% (ms)
Rise time 10-90% (ms)

Fig 5.6 Distribution analyses of mIPSCs before and after RP induction during GDP-β-S treatment.

Left panel: control; right panel: 25' after RP induction in 1mM GDP-β-S.

A) Gaussian fits of the amplitude distribution of mIPSCs before and after RP. The peak (P), width (W) and area (A) of each Gaussian were estimated by non-linear least square fitting, Chi^2 andR^2 are inserted.

B) The rise-time distributions of mIPSC before and after depolarisation in the presence of GDP-β-S.

C) Scatter-plots of mIPSC amplitudes against 10-90% rise-times.

Above data were taken from a single representative cell.

5.7

A.

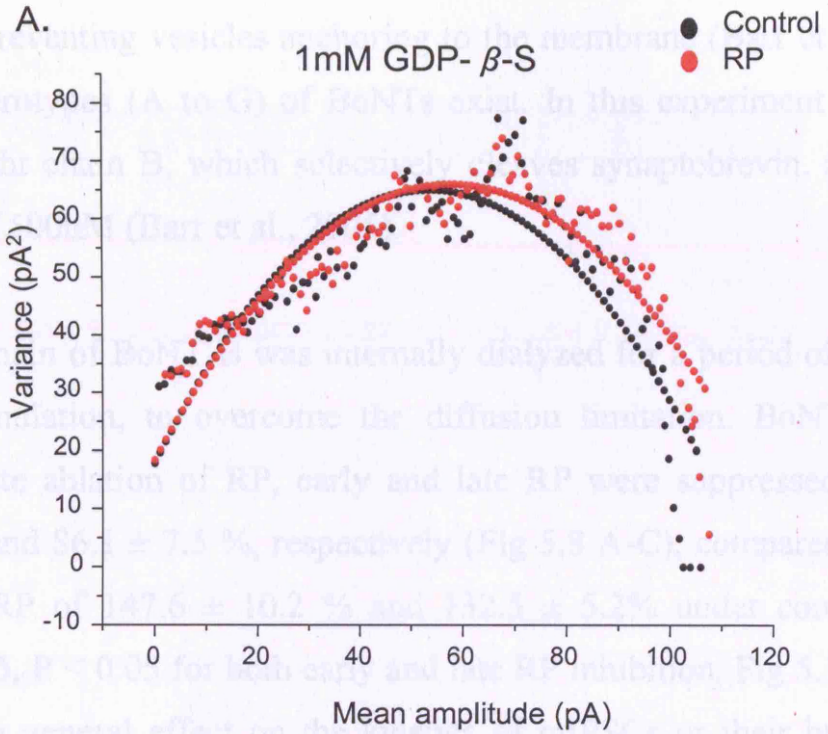

B.

	Control	RP
N_p	79.5 ± 13.7	84.6 ± 22.5
Single channel conductance γ (pS)	19.8 ± 3.0	20.1 ± 3.2

Fig 5.7 PS-NSNA of GDP-β-S treated mIPSCs in control and after RP.

A). mIPSC current variance against mean mIPSC amplitude plot. GDP-β-S (1 mM) control mIPSCs (●), GDP-β-S treated RP (●, 25 min after RP induction)

B). Tabulated values of single channel parameters N_p and γ extracted from the curve fits.

The botulinum neurotoxins (BoNT) from *Clostridium botulinum* are also potent, yet selective, inhibitors of exocytosis used to study receptor trafficking (Kakegawa and Yuzaki, 2005; Schiavo et al., 2000). The 50kDa

light chain is an endopeptidase which cleaves the fusion proteins SNAP-25, syntaxin or synaptobrevin before the formation of the SNARE complex, thus preventing vesicles anchoring to the membrane (Barr et al., 2005). Seven serotypes (A to G) of BoNTs exist. In this experiment we chose BoNT light chain B, which selectively cleaves synaptobrevin, at a concentration of 500nM (Barr et al., 2005).

The light chain of BoNT-B was internally dialyzed for a period of 20 min before stimulation, to overcome the diffusion limitation. BoNT-B induced complete ablation of RP, early and late RP were suppressed to 103.7 ± 4.2 % and 86.1 ± 7.5 %, respectively (Fig 5.8 A-C), compared to early and late RP of 147.6 ± 10.2 % and 132.5 ± 5.2% under control conditions ($n = 5$, $P < 0.05$ for both early and late RP inhibition, Fig 5.17). BoNT-B had no general effect on the kinetics of mIPSCs or their basal amplitudes (Table 5.1), although the time profile of basal BoNT-treated mIPSC exhibited fluctuation, and at certain time points did not show significant difference from the potentiated mIPSCs in control RP group (marked by # $P > 0.05$, Fig 5.8 B-C). The effect of BoNT-B on basal inhibitory transmission was determined by comparing BoNT-B-treat mIPSC with control mIPSC as BoNT-B was internally applied, but the control experiments were not interleaved with BoNT-B experiments, enhance may limit the accuracy of these results. This further verified the strong dependence of RP on receptor trafficking.

5.8

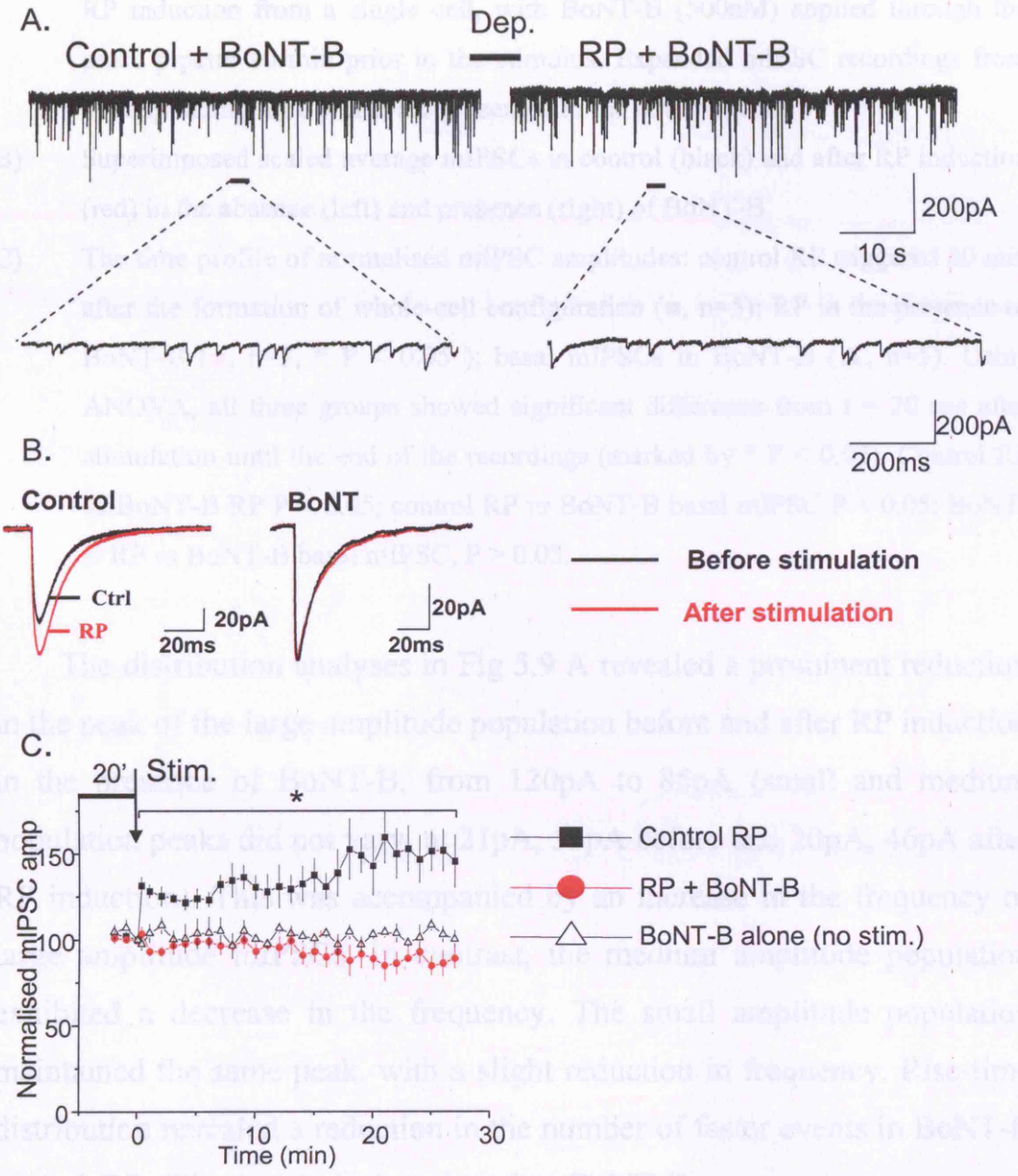
A.
Control + BoNT-B
Dep.
RP + BoNT-B
200pA
10 s
200pA
200ms
B.
Control
BoNT
Ctrl
RP
20pA
20ms
20pA
20ms
Before stimulation
After stimulation
C.
20'
Stim.
*
Normalised mIPSC amp
150
100
50
0
0
10
20
30
Time (min)
Control RP
RP + BoNT-B
BoNT-B alone (no stim.)

Fig 5.8 Suppression of RP by BoNT- B.

A) Representative recordings of mIPSCs under control conditions and 25 min after RP induction from a single cell, with BoNT-B (500nM) applied through the patch pipette 20 min prior to the stimulus. Expanded mIPSC recordings from corresponding time points are presented in the bottom panel.

B) Superimposed scaled average mIPSCs in control (black) and after RP induction (red) in the absence (left) and presence (right) of BoNT-B.

C) The time profile of normalised mIPSC amplitudes: control RP triggered 20 min after the formation of whole-cell configuration (■, n=5); RP in the presence of BoNT-B (●, n=5, * $P < 0.05$); basal mIPSCs in BoNT-B (▲, n=5). Using ANOVA, all three groups showed significant difference from t = 20 sec after stimulation until the end of the recordings (marked by * $P < 0.05$). Control RP *vs* BoNT-B RP $P < 0.05$; control RP *vs* BoNT-B basal mIPSC $P < 0.05$; BoNT-B RP *vs* BoNT-B basal mIPSC, $P > 0.05$.

The distribution analyses in Fig 5.9 A revealed a prominent reduction in the peak of the large amplitude population before and after RP induction in the presence of BoNT-B, from 120pA to 85pA (small and medium population peaks did not vary, at 21pA, 53pA before and 20pA, 46pA after RP induction). This was accompanied by an increase in the frequency of large amplitude mIPSCs. In contrast, the medium amplitude population exhibited a decrease in the frequency. The small amplitude population maintained the same peak, with a slight reduction in frequency. Rise-time distribution revealed a reduction in the number of faster events in BoNT-B treated RP (Fig 5.9B), insinuating that BoNT-B suppression were more effective against the somatodendritic events, although this could be a result of limited diffusion of BoNT-B to the distal dendrites. These minor alterations in each population did not influence the general shape of the mIPSC distributions, as the amplitude *vs* rise time plot in Fig 5.9C

revealed no discernable difference in scatter pattern before and after stimulus in the presence of BoNT-B.

5.9

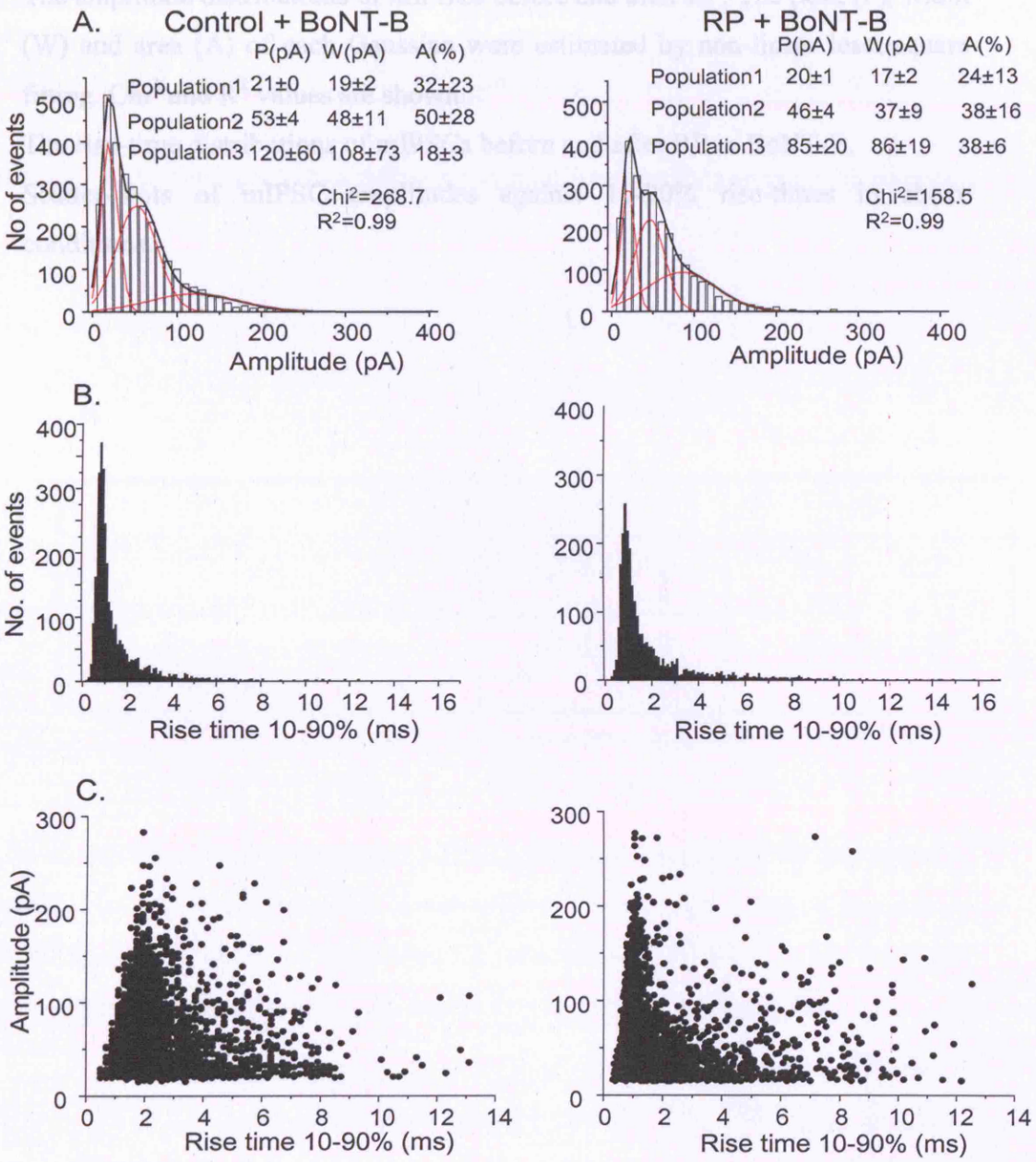

Fig 5.9 Distribution analyses of mIPSCs before and after RP induction during BoNT-B treatment.

Left panel: control mIPSCs in 500nM BoNT; right panel: 25' after RP induction in 500nM BoNT-B.

A) The amplitude distributions of mIPSCs before and after RP. The peak (P), width (W) and area (A) of each Gaussian were estimated by non-linear least square fitting. Chi^2 and R^2 values are shown.

B) The rise-time distributions of mIPSCs before and after RP in BoNT-B.

C) Scatter-plots of mIPSC amplitudes against 10-90% rise-times in above conditions.

5.10

A.

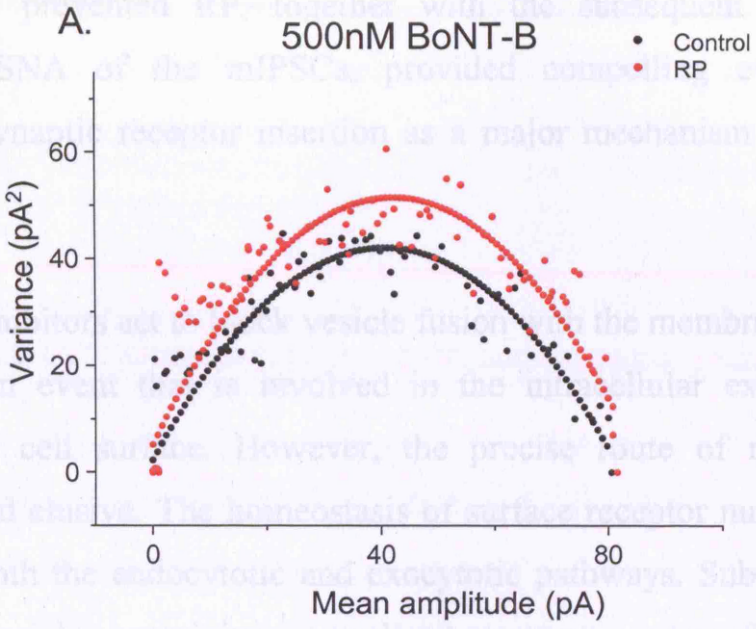

B.

	Control	RP
N_p	32.6 ± 7.2	28.5 ± 4.2
Single channel conductance, γ (pS)	28.6 ± 2.2	32.3 ± 2.6

Fig 5.10 PS-NSNA of BoNT-B treated mIPSCs in control and after RP induction. A). mIPSC current variance against mean mIPSC current plot. Control mIPSCs in 500nM BoNT-B (●), mIPSCs 25 min after RP induction in BoNT-B (●). B). Tabulated values of single channel parameters, N_p and γ, extracted from the curve fits.

Using PS-NSNA, the BoNT-B treated control and RP mean current-variance plots were comparable (Fig 5.10), N_p was calculated to be 32.6 ± 7.2 and 28.5 ± 4.2 before and after RP (n = 5, P > 0.05), single channel conductance also remain unaffected.

To conclude, inhibition of exocytosis with NEM, GDP-β-S, and BoNT-B largely prevented RP, together with the subsequent kinetic analysis and NSNA of the mIPSCs, provided compelling evidence supporting postsynaptic receptor insertion as a major mechanism behind RP.

All three inhibitors act to block vesicle fusion with the membrane, the most downstream event that is involved in the intracellular export of receptors to the cell surface. However, the precise route of receptor delivery remained elusive. The homeostasis of surface receptor number is maintained by both the endocytotic and exocytotic pathways. Subsequent to endocytosis, vesicles containing internalized receptors are transferred to early endosomes, sorted into recycling endosomes and reinserted, or sorted into late endosomes, where they are destined to be degraded in the lysosomal complex (Grosshans et al., 2006). To study the specific origin of the intracellular stores supplying these additional synaptic receptors, we used more specific inhibitors of intracellular trafficking pathways.

5.2.3 Inhibition of intracellular trafficking and RP

Monensin, a naturally occurring polyether, and selective-monovalent ionophore antibiotic, extracted from *Streptomyces cinnamonensis*, was used as it facilitates transmembrane exchange of Na^+ for protons (H^+), leading to the neutralization of acidic intracellular organelles, such as the trans Golgi apparatus cisternae, lysosomes and acidic endosomes, thereby disrupting their normal function in intracellular trafficking. Monensin has potent inhibitory effects on late Golgi processing events, such as terminal

glycosylation and proteolytic cleavages, by causing the swelling of Golgi and cisternae. However, many unprocessed molecules are not susceptible to monensin inhibition via non Golgi transport. Monensin also prevents the degradation of internalized molecules with no direct effect on internalization (Mollenhauer et al., 1990).

Monensin (75μM) was internally applied for 20 min before stimulation, and attenuated both early and late RP to 101.3 ± 4.0% and 91.7 ± 4.2% ($n = 5$, $P < 0.05$ for both early and late; Fig 5.11A-C Fig 5.17), despite fluctuations in a few intermediate points (in particular during depotentiation, where control-RP and monensin-RP showed no significant differences). There was no change in baseline mIPSC amplitude with monensin treatment, as during 30 min control recording, mIPSCs in the absence and presence of monensin attended similar amplitudes (Table 5.1). Although one drawback was that the controls were perform prior to the monensin experiment (not intercalated), hence they might not be adequate.

5.11

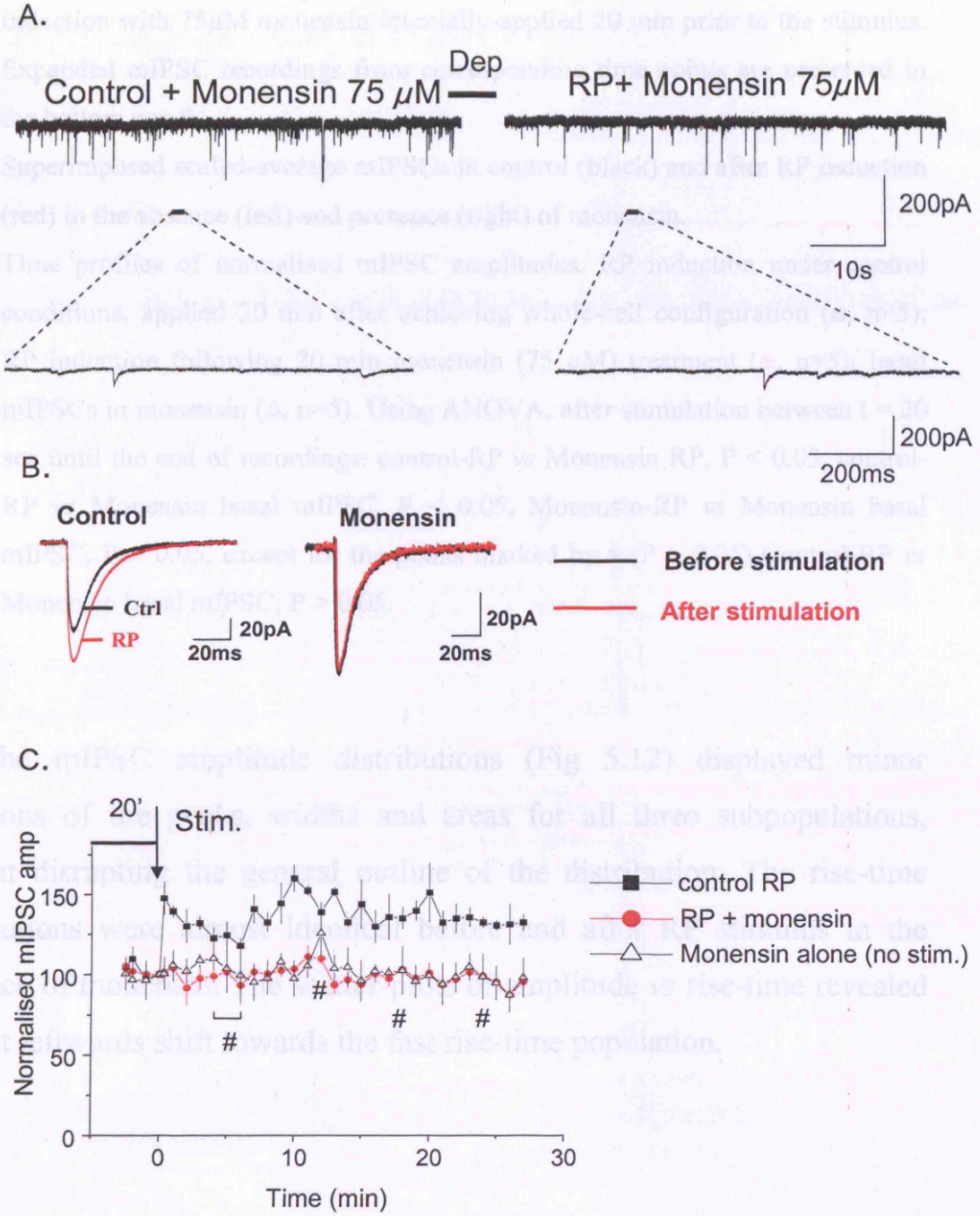
A.
Control + Monensin 75 μM
Dep
RP+ Monensin 75μM
200pA
10s
200pA
200ms
B.
Control
Monensin
Ctrl
RP
20pA
20ms
20pA
20ms
Before stimulation
After stimulation
C.
20'
Stim.
Normalised mIPSC amp
150
100
50
0
0
10
20
30
Time (min)
#
#
#
#
control RP
RP + monensin
Monensin alone (no stim.)

Fig 5.11 Suppression of RP by monensin.

A) Representative recordings under control conditions and 25 min after RP induction with 75μM monensin internally-applied 20 min prior to the stimulus. Expanded mIPSC recordings from corresponding time points are presented in the bottom panel.

B) Superimposed scaled-average mIPSCs in control (black) and after RP induction (red) in the absence (left) and presence (right) of monensin.

C) Time profiles of normalised mIPSC amplitudes. RP induction under control conditions, applied 20 min after achieving whole-cell configuration (■, n=5); RP induction following 20 min monensin (75 μM) treatment (●, n=5); basal mIPSCs in monensin (Δ, n=5). Using ANOVA, after stimulation between t = 20 sec until the end of recordings: control-RP *vs* Monensin RP, $P < 0.05$, control-RP *vs* Monensin basal mIPSC, $P < 0.05$, Monensin-RP *vs* Monensin basal mIPSC, $P > 0.05$, except for the points marked by # ($P > 0.05$) Control-RP *vs* Monensin basal mIPSC, $P > 0.05$.

The mIPSC amplitude distributions (Fig 5.12) displayed minor variations of the peaks, widths and areas for all three subpopulations, without disrupting the general outline of the distribution. The rise-time distributions were almost identical before and after RP stimulus in the presence of monensin. The scatter-plots of amplitude *vs* rise-time revealed a slight leftwards shift towards the fast rise-time population.

5.12

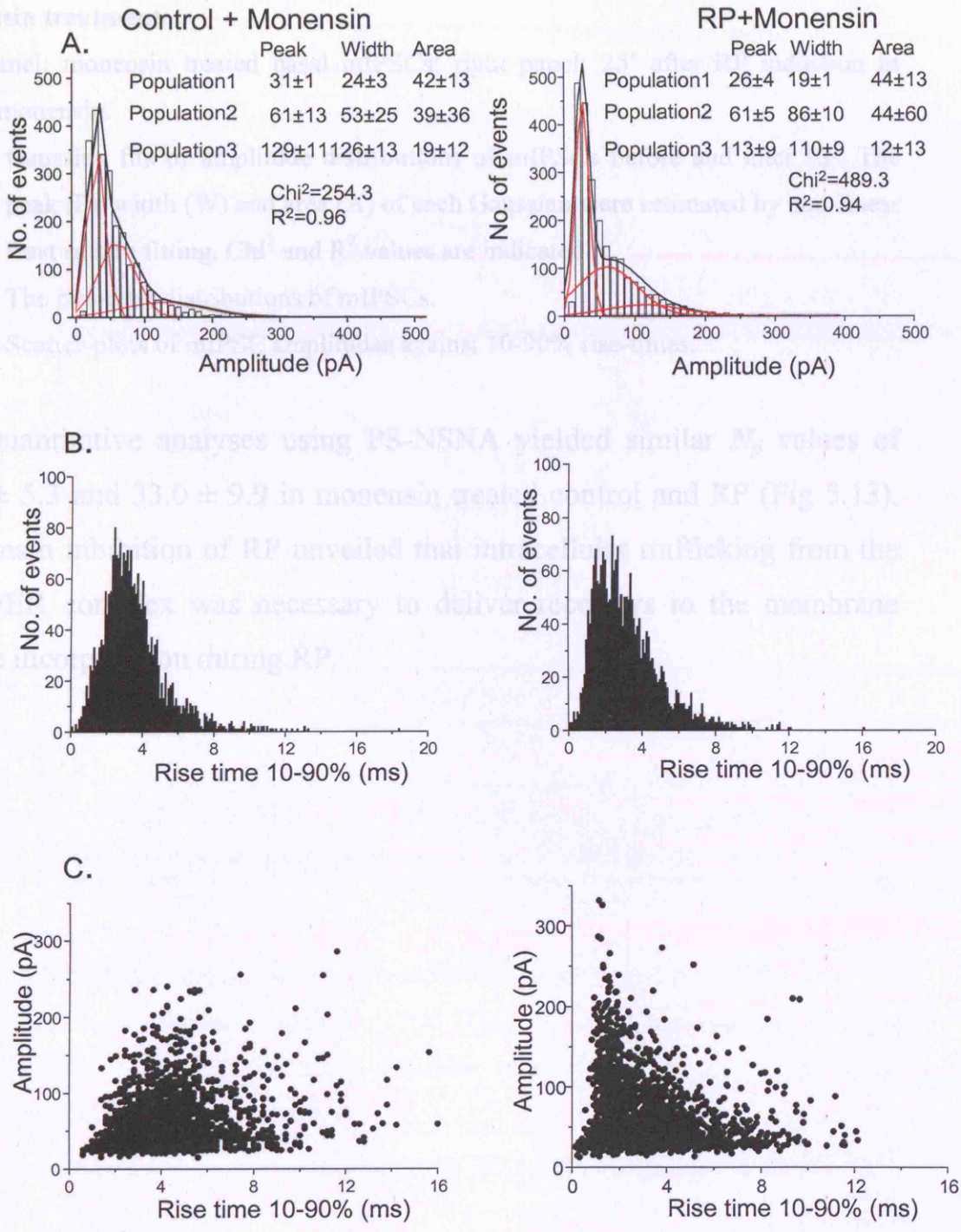
Control + Monensin
A.
Peak Width Area
Population1 31±1 24±3 42±13
Population2 61±13 53±25 39±36
Population3 129±11 126±13 19±12
Chi²=254.3
R²=0.96
No. of events
Amplitude (pA)
RP+Monensin
Peak Width Area
Population1 26±4 19±1 44±13
Population2 61±5 86±10 44±60
Population3 113±9 110±9 12±13
Chi²=489.3
R²=0.94
No. of events
Amplitude (pA)
B.
No. of events
Rise time 10-90% (ms)
No. of events
Rise time 10-90% (ms)
C.
Amplitude (pA)
Rise time 10-90% (ms)
Amplitude (pA)
Rise time 10-90% (ms)

Fig 5.12 Distribution analyses of mIPSCs before and after RP induction during monensin treatment.

Left panel: monensin treated basal mIPSCs; right panel: 25' after RP induction in 75μM monensin.

A) Gaussian fits of amplitude distributions of mIPSCs before and after RP. The peak (P), width (W) and area (A) of each Gaussian were estimated by non-linear least square fitting. Chi^2 and R^2 values are indicated.

B) The rise-time distributions of mIPSCs.

C) Scatter-plots of mIPSC amplitudes against 10-90% rise-times.

Quantitative analyses using PS-NSNA yielded similar N_p values of 32.8 ± 5.3 and 33.0 ± 9.9 in monensin treated control and RP (Fig 5.13). Monensin inhibition of RP unveiled that intracellular trafficking from the Golgi/ER complex was necessary to deliver receptors to the membrane before incorporation during RP.

5.13

A.

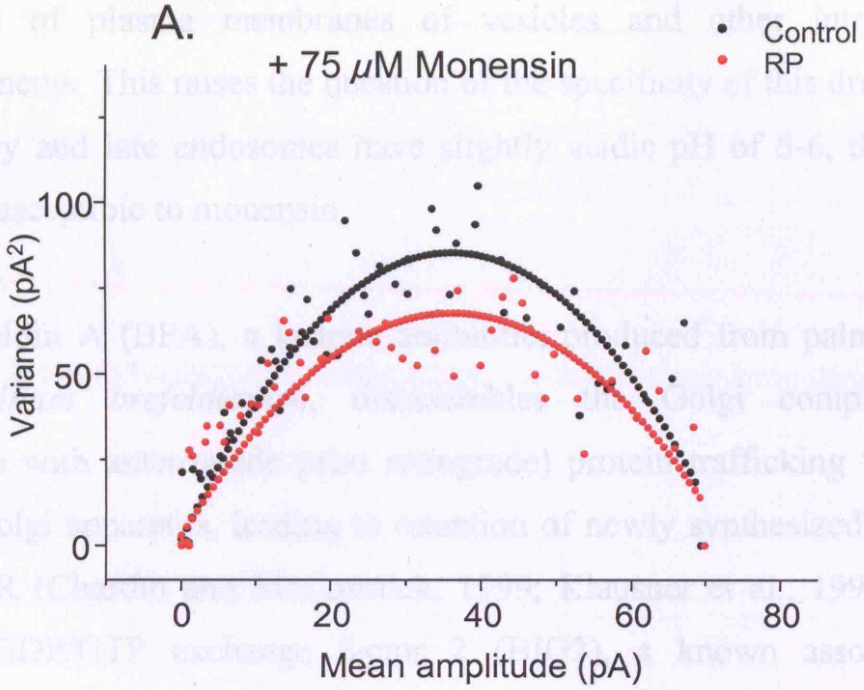

B.

	Control	RP
Np	32.8 ± 5.3	33.0 ± 9.9
Single channel conductance (pS)	30.4 ± 6.2	29.6 ± 8.7

Fig 5.13 PS-NSNA of monensin treated mIPSCs in control and after RP.

A). mIPSC current variance against mIPSC mean current plot. Control mIPSCs in monensin (●); mIPSC after RP induction in monensin (●, 25 min after RP induction).

B). Tabulated value of single channel parameters, N_p and γ, extracted from the curve fits.

Essentially, the mode of action of monensin is to collapse the pH gradients of plasma membranes of vesicles and other intracellular compartments. This raises the question of the specificity of this drug, since both early and late endosomes have slightly acidic pH of 5-6, they may also be susceptible to monensin.

Brefeldin A (BFA), a lactone antibiotic, produced from palmitate by *Eupenicillium brefeldianum*, disassembles the Golgi complex and interferes with anterograde (also retrograde) protein trafficking from the ER to Golgi apparatus, leading to retention of newly synthesized proteins in the ER (Chardin and McCormick, 1999; Klausner et al., 1992). BFA targets GDP/GTP exchange factor 2 (BIG2), a known associate of $GABA_AR$ β subunits (Charych et al., 2004). BIG2 activates GTPase ARF1 and 3, constituents in the formation of transport vesicles by recruiting coat proteins to intracellular membrane and aids vesicle budding from the ER. In HEK293 cells, BIG2 was found to direct the intracellular trafficking of $GABA_AR$ by promoting their departure from the ER (Charych et al., 2004). Therefore, BFA disrupts intracellular trafficking of $GABA_AR$ by selectively targeting BIG2 function, which is highly specific to the early secretory pathway (in pre-Golgi compartment) of $GABA_ARs$ containing vesicles. Golgi independent recycling pathway of vesicles is not known to be susceptible to BFA inhibition.

5.14

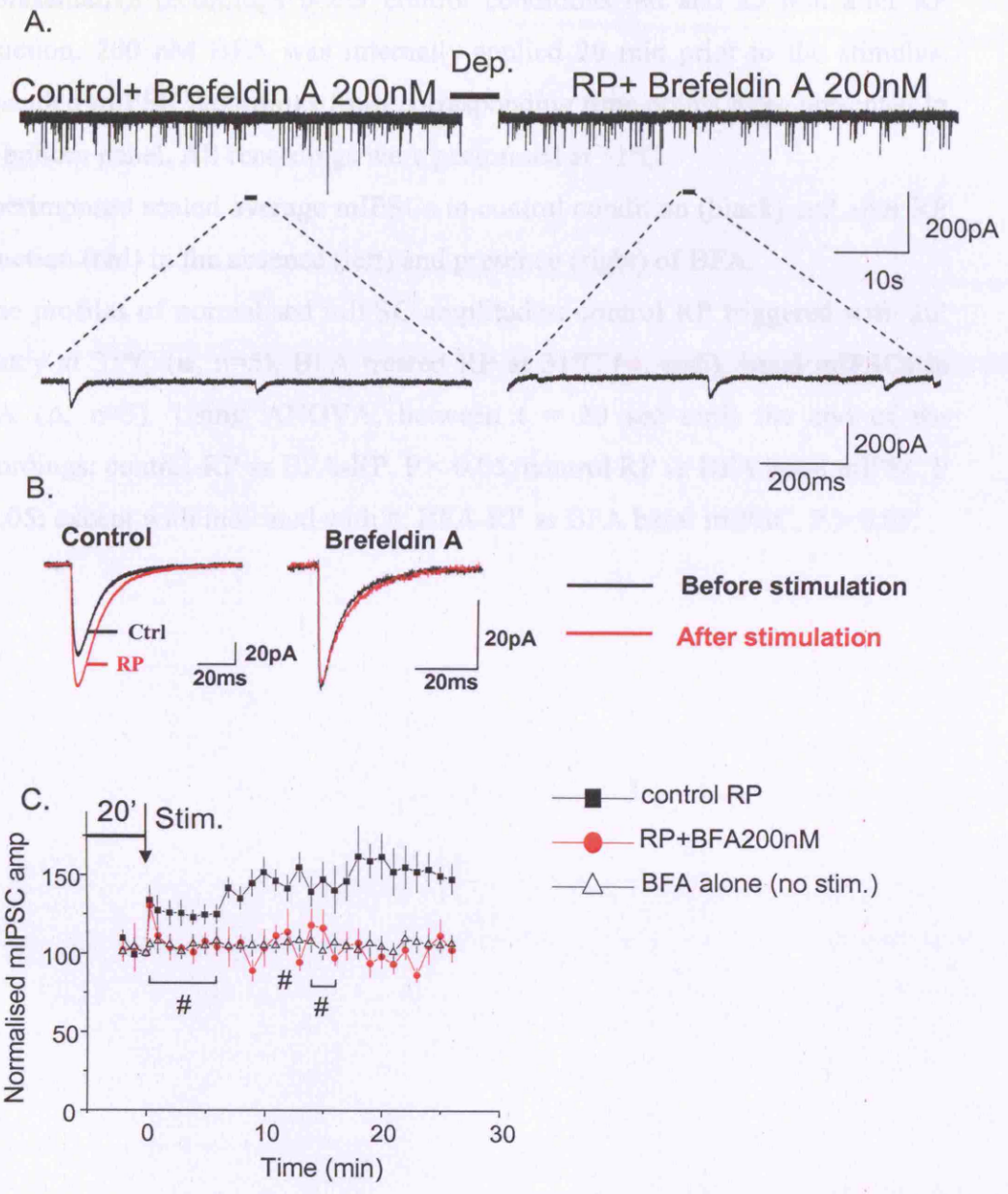
A.
Control+ Brefeldin A 200nM
Dep.
RP+ Brefeldin A 200nM
200pA
10s
200pA
200ms
B.
Control
Brefeldin A
Ctrl
RP
20pA
20ms
20pA
20ms
Before stimulation
After stimulation
C.
20'
Stim.
Normalised mIPSC amp
150
100
50
0
#
#
#
0
10
20
30
Time (min)
control RP
RP+BFA200nM
BFA alone (no stim.)

Fig 5.14 Suppression of RP by BFA.

A) Representative recordings under control conditions left and 25 min after RP induction. 200 nM BFA was internally-applied 20 min prior to the stimulus. Expanded mIPSC recordings from corresponding time points were presented in the bottom panel. All recordings were performed at 31°C.

B) Superimposed scaled average mIPSCs in control condition (black) and after RP induction (red) in the absence (left) and presence (right) of BFA.

C) Time profiles of normalised mIPSC amplitudes: control RP triggered with 20' latency at 31°C (■, n=5), BFA treated RP at 31°C (●, n=5), basal mIPSCs in BFA (Δ, n=5). Using ANOVA, between t = 20 sec until the end of the recordings: control-RP *vs* BFA-RP, $P < 0.05$; control RP *vs* BFA basal mIPSC $P < 0.05$; except with indicated with #; BFA-RP *vs* BFA basal mIPSC, $P > 0.05$.

5.15

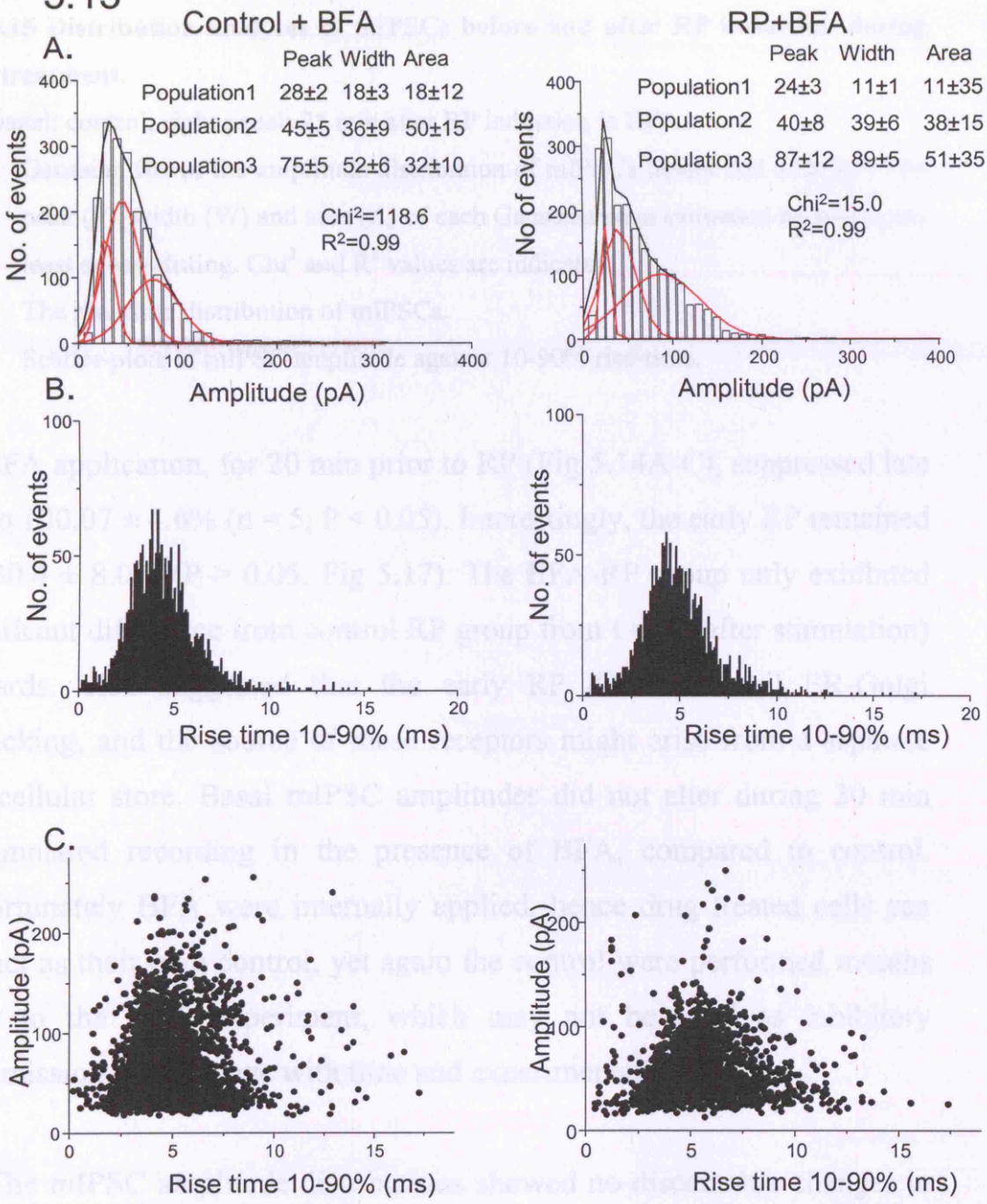
Control + BFA
RP+BFA
A.
Peak Width Area
Population1 28±2 18±3 18±12
Population2 45±5 36±9 50±15
Population3 75±5 52±6 32±10
Chi²=118.6
R²=0.99
Peak Width Area
Population1 24±3 11±1 11±35
Population2 40±8 39±6 38±15
Population3 87±12 89±5 51±35
Chi²=15.0
R²=0.99
No. of events
Amplitude (pA)
B.
Rise time 10-90% (ms)
C.
Amplitude (pA)

Fig 5.15 Distribution analyses of mIPSCs before and after RP induction during BFA treatment.

Left panel: control; right panel: 25 min after RP induction in BFA.

A) Gaussian fits of the amplitude distribution of mIPSCs before and after RP. The peak (P), width (W) and area (A) of each Gaussian were estimated by non-linear least square fitting. Chi^2 and R^2 values are indicated.

B) The rise-time distribution of mIPSCs.

C) Scatter-plots of mIPSC amplitude against 10-90% rise-time.

BFA application, for 20 min prior to RP (Fig 5.14A-C), suppressed late RP to 100.07 ± 4.6% (n = 5, P < 0.05). Interestingly, the early RP remained at 130.4 ± 8.0% (P > 0.05, Fig 5.17). The BFA-RP group only exhibited significant difference from control RP group from t = 7' (after stimulation) onwards. This suggested that the early RP did not entail ER-Golgi trafficking, and the source of these receptors might arise from a separate intracellular store. Basal mIPSC amplitudes did not alter during 30 min unstimulated recording in the presence of BFA, compared to control. Unfortunately BFA were internally applied, hence drug treated cells can not act as their own control, yet again the control were performed months prior to the BFA experiment, which may not be ideal as inhibitory transmission may change with time and experimental conditions.

The mIPSC amplitude distributions showed no discernable changes in the three populations of events (Fig 5.15). Likewise, the rise-time distributions, and amplitude *vs* rise-time scatter-plots also displayed similar appearances in BFA treated control and RP mIPSCs. Using PS-NSNA, the estimated N_p for events during control and after RP induction, in the

presence of BFA were 37.4 ± 12.1 and 32.6 ± 7.6, respectively (n = 5, P > 0.05).

5.16

A.

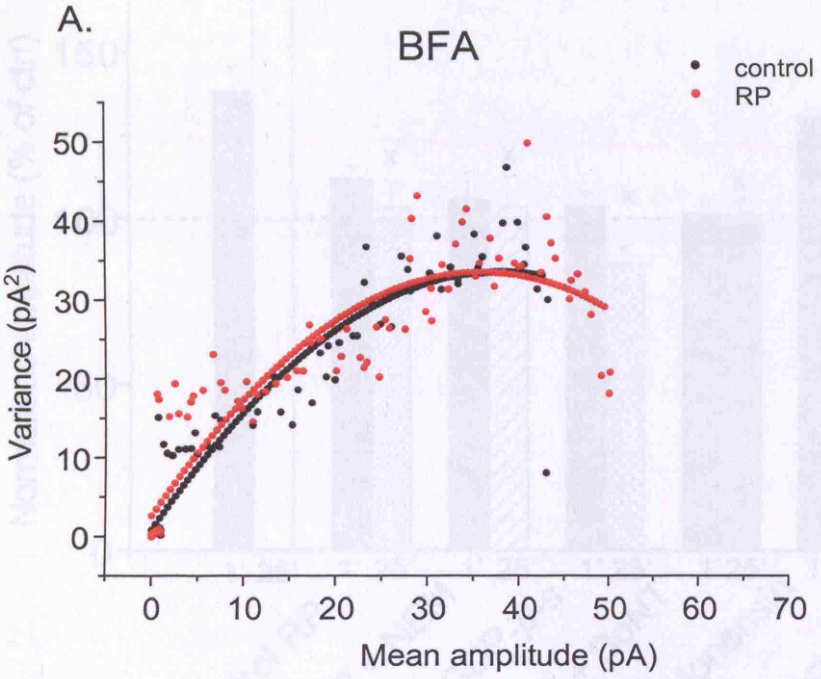

B.

	Control	RP
Np	37.4 ± 12.1	32.6 ± 7.6
Single channel conductance (pS)	29.3 ± 4.7	29.4 ± 3.8

Fig 5.16 PS-NSNA of BFA (200 nM) treated mIPSCs in control and after RP.

A). mIPSC current variance against mean mIPSC current plot. Control mIPSCs in BFA (●); mIPSCs 25 min after RP induction in 200nM BFA (●).

B). Tabulated values of single channel parameters, N_p and γ extracted from the PS-NSNA curves.

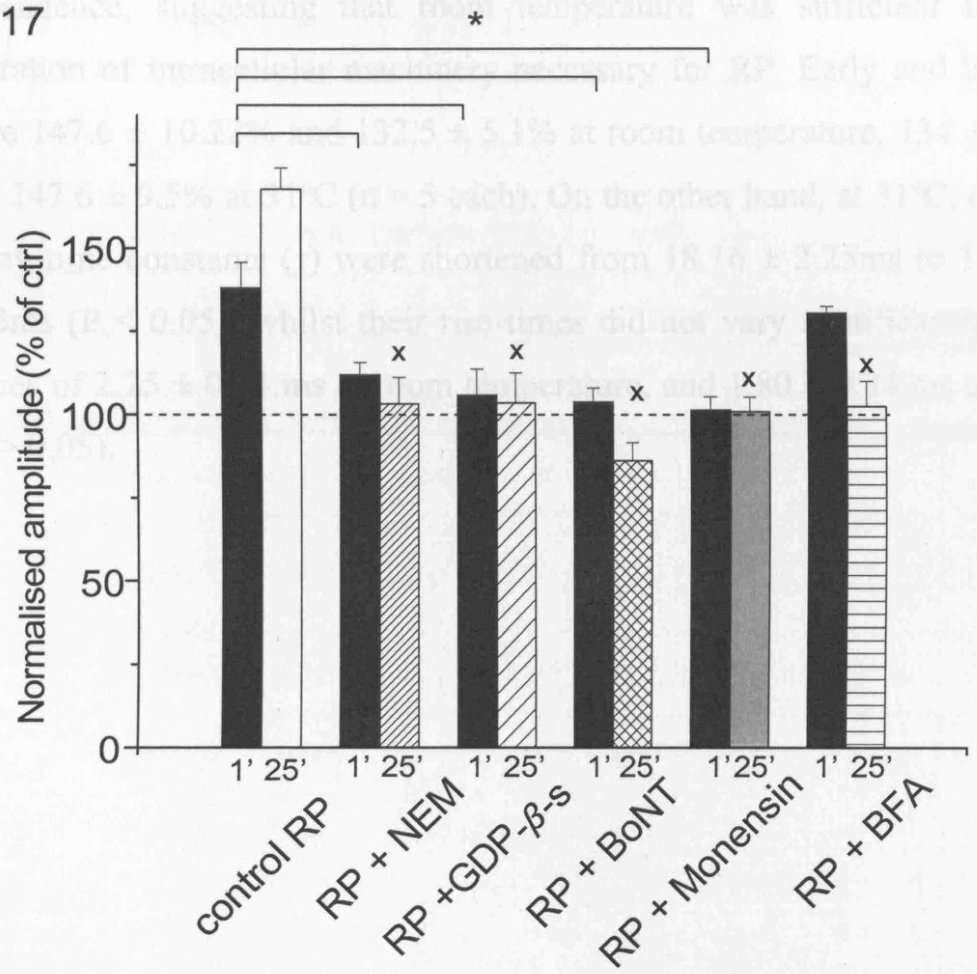

Fig 5.17 Histogram of early (t = 1') RP and late (t = 25') RP in the presence of exocytosis inhibitors. Black bars indicates early RP, open shaded bars indicate late RP. (^{x} $P < 0.05$, between control late RP and late RP in the presence of all inhibitors; * $P < 0.05$, between control early RP and early RP in NEM, GDP-β-S, BoNT-B, Monensin, but not BFA)

As physiological temperature is vital for normal functioning of intracellular processes, such as budding and ER-Golgi trafficking. By performing electrophysiological recordings at 31°C, the profiles of RP triggered at 20 min after whole-cell formation did not exhibit temperature

dependence, suggesting that room temperature was sufficient for the operation of intracellular machinery necessary for RP. Early and late RP were 147.6 ± 10.22% and 132.5 ± 5.1% at room temperature, 134 ± 9.2% and 147.6 ± 9.5% at 31°C (n = 5 each). On the other hand, at 31°C, mIPSC decay time constants (τ) were shortened from 18.16 ± 2.25ms to 11.73 ± 0.83ms ($P < 0.05$), whilst their rise-times did not vary significantly, with values of 2.25 ± 0.64 ms at room temperature, and 1.80 ± 0.34 ms at 31°C ($P > 0.05$).

	Amplitude (pA)		Frequency (Hz)		Rise time (ms)		Decay time constant τ (ms)	
	t= 0'	t= 30'	t= 0'	t= 30'	t= 0'	t= 30'	t= 0'	t= 30'
Control n=12	69.7±16	64.9±11	4.9±0.3	5.0±0.5	2.3±0.8	1.6±0.4	18.2±2.3	18.9±2.4
RP n=7	49.9±5.2	81.6±12*	5.7±1.5	5.3±1.3	1.2±0.2	1.5±0.1	11.8±0.6	13.5±0.7
NEM N=5	67.3±0.5	76.0±11	3.3±1.1	3.1±0.7	1.5±0.4	2.7±0.8	11.7±0.5*	20.8±1.9*
RP + NEM N=5	89.4±16	92.4±14	6.4±2.6	5.1±1.3	1.0±0.3	0.8±0.2	10.9±1.4	11.1±1.6
GDP-β-S N=5	69.3±8.3	62.6±10	5.3±0.9	4.7±1.1	2.4±0.4	2.5±0.3	12.7±2.7	14.4±3.4
RP+ GDP-β-S N=5	72.6±11	76.4±16	3.2±1.7	3.3±0.9	1.5±0.7	1.3±0.9	15.9±0.8	17.8±4.0
BoNT n=5	74.3±8.1	83.9±11	3.8±0.4	3.1±0.2	1.7±0.2	1.2±0.2	13.3±0.2*	16.1±0.8*
RP+BoNT n=5	85.6±18	73.8±20	5.9±1.4	3.7±0.9	2.0±0.4	2.1±0.3	16.3±2.6	22.9±4.5
Monsensin n=5	77.5±18	72.7±18	1.1±0.3	1.2±0.2	2.2±0.5	2.1±0.4	10.3±1.7	11.7±1.6
RP+ Monsensin n=5	60.1±6.3	54.3±0.6	3.3±0.9	3.1±0.9	1.0±0.2	0.9±0.1	12.5±0.8	15.4±1.6
31°C RP n=5	85.1±19	109±12	4.0±0.9	3.0±0.8	0.6±0.1	0.8±0.4	11.7±0.8	9.9±2.3
BFA n=5	75.26±12	75.0±11	2.6±0.3	2.3±0.2	1.7±0.4	1.0±0.2	8.2±0.9	10.9±1.7
RP+BFA n=5	66.2±8.5	59.5±10	1.7±0.4	1.3±0.3	1.8±0.3	1.7±0.5	11.8±1.5	11.3±1.6

Table 5.1 Rise time and decay time constants (τ) of mIPSCs in exocytosis and intracellular trafficking inhibitors. Under control conditions, measurements were at taken at t = 0' and t = 25'; for RP values were measured 1 min before and 25 min after induction in the presence of inhibitors; basal values in the inhibitors are taken at t = 0' and t = 25'. Values are mean ± s.e. (*P < 0.05 between the values in the neighbouring cells).

5.3 Discussion

5.3.1 Increase in postsynaptic receptor numbers after RP induction

The PS-NSNA estimation of single channel parameters revealed an almost two fold increase in the N_p after RP induction. The single channel conductance ranged between 20~30pS, consistent with published data, and remained unaltered after RP induction (Bier et al., 1996; De Koninck and Mody, 1994). Both postsynaptic receptor insertion and increased probability of channel opening can be expected to account for the enhancement of mIPSC amplitudes in RP. Nevertheless, the peak-scaled method assumes equal opening probability for all channels at the peak of the mIPSC (Traynelis et al., 1993), which means that determining *Po* was not possible. Furthermore, we can only estimate N_p, the average number of channels opening at the peak of the mIPSC. As discussed in the introduction, increase in postsynaptic receptor number is arguably the most effective mean of augmenting synaptic strength. With this in mind, we applied inhibitors of different stages of intracellular trafficking to study their roles in RP.

5.3.2 Suppression of RP by inhibition of exocytosis

The most downstream step in the cascade of synaptic $GABA_AR$ cell surface insertion is the fusion of vesicles with the inner lumen of the plasma membrane, thereby presenting the receptors opposite the presynaptic boutons.

To clarify the role of receptor insertion in RP, we chose three well known inhibitors of exocytosis: NEM, GDP-β-S, and BoNT-B, which all

interfere with membrane fusion. All three inhibitors completely suppressed RP in a similar manner, suggesting that RP was predominantly instigated by postsynaptic receptor insertion. Intriguingly, the phosphorylation-independent early RP, which persisted during kinase inhibition (see chapter 3), was completely abolished by all three exocytosis inhibitors. This implied that early RP was reliant on receptor insertion, without the need for phosphorylation, unlike the late RP. The only previous instance of complete suppression of RP, was achieved by intracellular sequestration of Ca^{2+} (Kano et al., 1992). It was thought that the main function of the climbing fiber evoked Ca^{2+} surge was to activate Ca^{2+} dependent kinases (Kano et al., 1996). However, these observations here may suggest the likelihood of direct Ca^{2+} mediated vesicle fusion with the cell membrane, or other Ca^{2+} related, phosphorylation independent mechanisms, to shape the sharp peak of early RP.

The use of these inhibitors allowed us to draw the conclusion that an increase in postsynaptic receptor number, rather than an enhancement of channel opening probability, is the prime candidate for augmenting inhibitory synaptic strength.

5.3.3 Inhibition of intracellular trafficking

Monensin inhibited both early and late RP. It disrupts intracellular trafficking by neutralising the pH of intracellular compartments such as Golgi apparatus cisternae, and lysosomes. Acidic endosomes are also susceptible to the action of monensin, causing difficulty in distinguishing between the recycling endosomes and ER as the major supply of receptors

during RP. Monensin inhibited both early and late RP, without disturbing the distribution of mIPSC events before and after RP induction.

To overcome this disadvantage of monensin, the Golgi-specific inhibitor BFA was used. Prior to BFA treatment, control RP recordings were performed at 31°C, better suited for physiological intracellular ER-Golgi trafficking. The higher temperature increased the rate of mIPSC decay. The physiological temperature RP profile showed late RP may be more reliant on ER-Golgi trafficking, as late, but not early RP was slightly facilitated at higher, more physiological temperature. The inclusion of BFA eliminated late RP by functionally disassembling the Golgi complex and causing the Golgi to retract into the ER. Hence, the Golgi-dependent transport was vitally important in the maintenance of late RP, indicating that the ER maybe the source of those receptors that are inserted during the late stage of RP. However, unlike the other exocytosis inhibitors, BFA failed to inhibit early RP. Therefore, although early RP requires postsynaptic receptor insertion, it is not originated from the ER or via the TGN transport.

5.3.4 Sources of mobilized receptors during RP

Dynamic trafficking of receptors is important in maintaining normal transmission and synaptic plasticity. The source of mobilized receptors during RP can arise from multiple intracellular compartments. One potential route of delivery may entail *de novo* synthesis and assembly of receptors in ER, and anterograde ER-Golgi transport, via the trans-Golgi-Network (TGN) prior to secretion into the membrane. This time

consuming process may constitute the late RP. Alternatively, resident surface $GABA_AR$s undergo clathrin-dependent internalization upon the binding of AP2 with β or $\gamma 2$ subunits (Kittler et al., 2005; Kittler et al., 2008). Once entering the cytoplasm, endocytotic vesicles lose their clathrin coat and fuse with other vesicles. This function is primed by NSF-SNAP untangling of v- and t-SNARE proteins on the vesicles. Early endosomes have a lowered pH (5.9 - 6) which enables the release of receptors to be presented to the plasma membrane. Internalised receptors can be sorted into early recycling endosomes for reinsertion into plasma membrane (Fig 5.18), or alternatively, they can be sorted to late endosomes, sometimes via

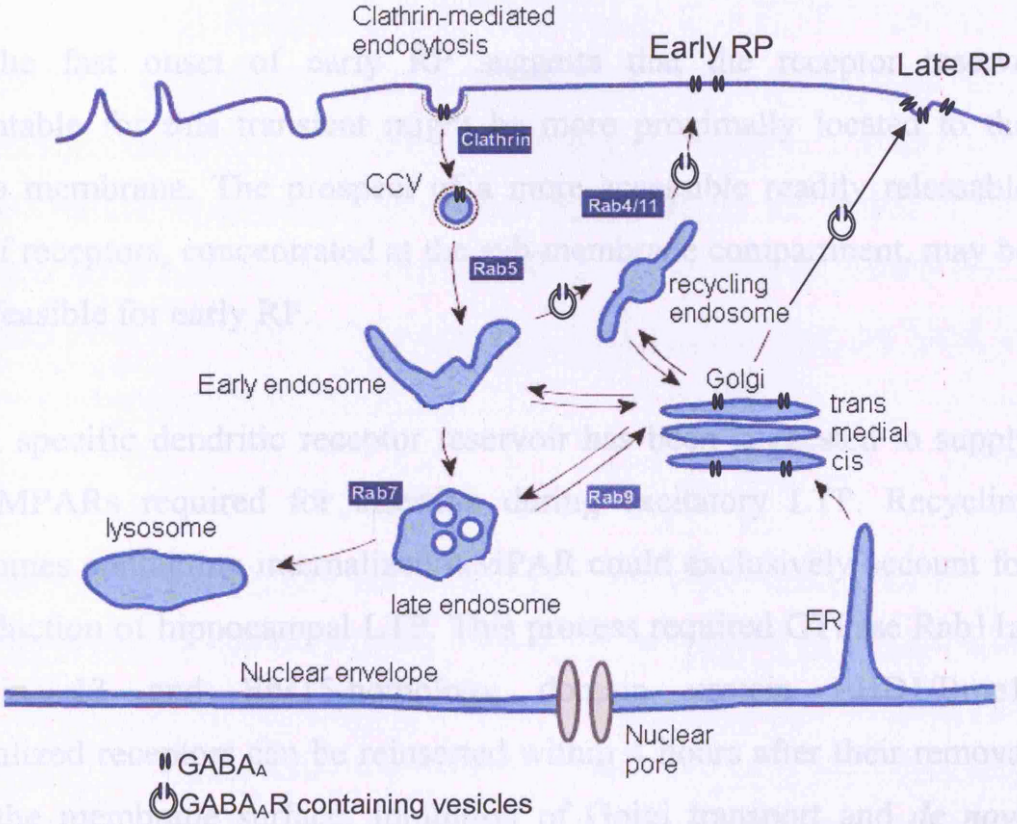

Fig 5.18 Route for intracellular trafficking: surface $GABA_ARs$ are internalised via clathrin-dependent mechanisms, by the function of Rab GTPase 5. The internalised vesicles fuse to form the early endosome, which is sorted into recycling endosomes. They can also fuse with the Golgi complex, or became late endosomes, destined for degradation in lysosomes. Late RP required the function of ER-Golgi transport, for delivery of newly synthesised receptors, whilst early RP is independent of this function. Hence early RP may entail the recycling endosome, via the function of Rab4/11 only. (Modified from Sieczkarski and Whittaker, 2002).

Golgi complex, destined to be degraded in lysosomes. Early endosomes mediated receptor reinsertion, bypassing the Golgi complex, may occur on a faster time scale.

The fast onset of early RP suggests that the receptor reserve accountable for this transient might be more proximally located to the plasma membrane. The prospect of a more accessible readily releasable pool of receptors, concentrated at the sub-membrane compartment, may be more feasible for early RP.

A specific dendritic receptor reservoir has been suggested to supply the AMPARs required for insertion during excitatory LTP. Recycling endosomes containing internalized AMPAR could exclusively account for the induction of hippocampal LTP. This process required GTPase Rab11a, syntaxin 13 and Eps15-homology domain protein EHD1/Rme1. Internalized receptors can be reinserted within 4 hours after their removal from the membrane surface. Inhibition of Golgi transport and *de novo* synthesis of new receptors had no influence on the induction of LTP (Park et al., 2004).

Compartmentalized endosomal trafficking was thought to be engaged in the synaptic delivery of AMPAR constitutively and during hippocampal LTP in two sequential steps. Translocation of AMPARs from dendrites to spines by Rab11, occurred prior to Rab-8 endosomal driven insertion of AMPARs into the synaptic membranes. Expression of dominant negative mutants of either Rab-8 or Rab-11 completely abolished LTP. Rab4-dependent trafficking was responsible for constitutive recycling and maintaining the spine size (Brown et al., 2007).

The role of early endosomes or more readily releasable pools of $GABA_ARs$ has not been studied in RP, though it is highly feasible to consider them as the reservoir for early RP. Existence of subsynaptic pools of $GABA_ARs$ in hippocampal cell cultures was identified to associate with gephyrin on the postsynaptic sites (van Rijnsoever et al., 2005). These pools contain the majority of internalized $GABA_ARs$. They participate in rapid and short term control of receptor trafficking, and thus are ideal for supplying receptors for early RP.

5.3.5 Mechanism of receptor release from intracellular receptor stores

Intracellular receptors are assumed to be embedded in the transport vesicle membrane with their major intracellular loop facing the cytoplasmic side. Therefore, the phosphorylation residues within the loop are accessible to kinases upon RP stimulation. It is possible that the kinases (CaMKII and PTK) may directly phosphorylate these residues on intracellular receptors, triggering a signal for fusion of the vesicles with the

plasma membrane and sequential exposure of the receptors on the cell surface during late RP. Phosphorylation-dependent recruitment of $GABA_ARs$ to the surface has been noted after insulin treatment (Vetiska et al., 2007; Wan et al., 1997). Phosphorylation might also occur on trafficking machinery or scaffolding proteins, which subsequently lead to the insertion of receptors. For instance, synaptic vesicle proteins synapsins I (a,b) contain substrates for CaMKII on their C-terminus. Phosphorylation by CaMKII regulates the binding of synapsin I to actin filaments and neurofilaments, promoting release of vesicles (Sudhof, 1995). A previous study revealed the prerequisite of CaMKII-evoked GABARAP conformational change for the sustained phase of RP (Kawaguchi and Hirano, 2007), though a direct CaMKII phosphorylation site(s) on GABARAP is unknown. Combined with the results presented here, this strongly supports receptor insertion, presumably followed by CaMKII mediated conformation change of GABARAP, as the trafficking signal, instigates the expression of RP. GABARAP, together with the clustering protein gephyrin, are thought to orchestrate protein interactions in the postsynaptic domains of $GABA_AR$ (see chapter 1). They bind microtubules, PRIP, GRIP, and NSF, to coordinate the $GABA_AR$ trafficking (Chen and Olsen, 2007). In addition, $GABA_AR$ β subunit interacting protein, BIG2, homologous to vesicle trafficking proteins, may initiate the exocytosis of $GABA_AR$ to the surface, as supported by the extinction of RP by BFA inhibition. Plic-1 protein stabilises intracellular $GABA_AR$ by preventing degradation by ubiquitination (Bedford et al., 2001). These proteins described above may potentially participate in the trafficking of $GABA_ARs$ during RP.

Early RP relies on Ca^{2+} induced rapid trafficking of receptors from reserves, other than the ER, most likely involving early or recycling endosomes. What is the mechanism for this release? The direct action of Ca^{2+} may involve increased vesiculation of the endosomes, translocation to plasma membrane or fusion (Knight, 2002). In transfected PC12 cells, direct Ca^{2+} triggered exocytosis has been reported and was subject to inhibition by functional GTP dependent Rab11b, a brain enriched isoform of Rab11 (Khvotchev et al., 2003). Hence, it is likely the sharp rise and fall of intracellular Ca^{2+} transients could directly modulate the release of the more locally positioned vesicles, synergising with phosphorylation to ensure the appearance of early RP.

5.4 Conclusion

In this chapter, we identified receptor insertion as the principle mechanism for the manifestation of RP. Inhibition of receptor exocytosis attenuated both early and late RP, however inhibition of ER-Golgi trafficking only impaired late RP. Combined with evidences from kinase inhibitors in chapter 4, we conclude that late RP is maintained by phosphorylation-dependent recruitment of receptors into the synaptic membrane. Early RP may require rapid receptor trafficking from more proximal endosomes or receptor reserves.

Chapter 6

$GABA_AR$ subunits responsible for rebound potentiation

6.1 Introduction

The subunit composition of $GABA_ARs$ in various brain regions have been extensively studied, leading to the notion that subunit expression varies depending on the neuronal cell types (Fritschy et al., 1992; Laurie et al., 1992a; McKernan and Whiting, 1996). The subunit compositions of $GABA_ARs$ determine the functional outcomes of modulation by intracellular signalling molecules such as kinases and phosphatases (McDonald et al., 1998). Hence, the $GABA_AR$ subunit composition in Purkinje cells is fundamental to the understanding of rebound potentiation.

The expression of $GABA_AR$ subunits is developmentally regulated. The first subunits to be expressed in foetal brain are $\alpha 2$, $\alpha 3$ and $\beta 3$, with later substitution by $\alpha 1$ and $\beta 2$ subunits in adulthood (Laurie et al., 1992b; Zhang et al., 1991). Prior immunohistochemistry and *in situ* hybridisation studies in Purkinje cells has partially clarified the $GABA_AR$ subunit expression patterns. mRNAs for $\alpha 1$, $\beta 2/3$ and $\gamma 2$ subunits were detected in PCs, although certain studies detected the immunofluorescence of other subunits ($\alpha 2$, $\alpha 3$, $\alpha 5$, $\beta 1$) (Laurie et al., 1992a; Pirker et al., 2000). The $\alpha 1$ subunit is heavily expressed in rat PCs at both synaptic and extrasynaptic sites, with most intense punctate staining on the soma and diffuse staining in the molecular layer (ML) (Fritschy et al., 1992). Double and triple immunofluorescence revealed colocalisation of $\alpha 1$ and $\alpha 3$ subunits on the

PC soma, speculating co-assembly at these sites, although the synaptic marker, gephyrin, was absent. In contrast, this association was absent from PC dendrites, where gephyrin appeared to be co-stained with α1 subunits only (Fritschy et al., 1992; Pirker et al., 2000; Sassoe-Pognetto et al., 2000). The α1 subunit staining first appeared at P7 on the soma, before undergoing developmental upregulation and migration towards the cell processes during adulthood. A parallel increase was observed in α1 mRNA levels. The α3 subunit expression pattern was inversely correlated with that of α1 subunits, displaying more intense staining on the dendrites than soma. It has been argued that α3 subunit expression was transient and disappeared after one week, postnatally, together with α2 subunits (Takayama and Inoue, 2004).

The β2 subunit is the predominant β isoform found in PCs, with heavy mRNA labelling in excess of that for the β3 subunit. Most data suggests β2 subunits are expressed mainly in the dendrites and infrequently on the PC soma. *In situ* hybridisation and [^{3}H] muscimol labelling studies failed to detect β2 subunits on the soma (Gutierrez et al., 1994; Laurie et al., 1992a; Pirker et al., 2000), raising the question of whether the β2 subunits can co-assemble with somatic α1 and γ2 subunits. Secondly, despite the detection of β3 subunit mRNA, little β3 subunit immunoreactivity was found in PCs; whilst β1 subunit immunoreactivity was sparingly detected on multiple processes, mostly in the molecular layer (Laurie et al., 1992a; Pirker et al., 2000).

The γ2 subunit is the most abundant subunit in PCs and is strongly associated with gephyrin (Sassoe-Pognetto et al., 2000). Its mRNA level

increases dramatically over the first postnatal week (Laurie et al., 1992b). Various reports illustrated coexistence of splice variants γ2L and γ2S in PCs, though somatic immunoreactivity of γ2L exceeds that of γ2S (Gutierrez et al., 1994; Khan et al., 1996b). Using dual immunogold labelling, γ2 subunit was found to be co-localised with α1, β2/3 subunits at both distal and proximal dendritic synapses innervated by stellate and basket cells, respectively (Somogyi et al., 1996). The importance of γ2 subunits to CNS function was emphasised by the lack of sensitivity towards diazepam and prenatal fatality in a global knockout of the γ2 subunit (Chandra et al., 2005; Gunther et al., 1995). The presence of γ2 subunits increases $GABA_AR$ channel conductance, and prolongs the mean open time. Single channel recording from hippocampal and dorsal root neurons from mice of γ2-/- revealed a lower single channel conductance and shortened mean open time compared to wild-type (wt, γ2+/+) and heterozygous (γ2+/-) mice (Lorez et al., 2000).

Immunoreactivity for γ1 and γ3 subunits was found in PCs, despite the failure to detect their mRNA levels (Laurie et al., 1992a; Pirker et al., 2000).

The limited $GABA_AR$ subunit repertoire in PCs implies most synaptic $GABA_ARs$ are comprised of α1β2/3γ2, a common composition adopted by ~43% of $GABA_ARs$ in the brain (McKernan and Whiting, 1996; Poltl et al., 2003), though the dendritic receptors in PCs may be composed of α3β2/3γ2.

Both β and γ subunits are subjected to phosphorylation on residues located in the major ICL (see chapter 3). We postulated that the phosphorylation of β2 and/or γ2 subunits, the principle subunits expressed in PCs, are required for the manifestation of RP. In particular, CaMKII targets serines S410 on the β2 subunit and S348, S350 in both γ2 splice variants. The extra 8 amino acids insert of γ2L contains an additional CaMKII phosphorylation site, S343 (McDonald and Moss, 1994; McDonald and Moss, 1997). Protein tyrosine kinase may also contribute to RP by phosphorylation of Y365 and Y367 on γ2S (equivalent to Y373, Y375 on γ2L), and β2/β3 subunits (Moss et al., 1995; Wan et al., 1997a). The functional implication of β2 subunit phosphorylation by CaMKII is unknown, though numerous reports described a β2/3 subunit phosphorylation dependent recruitment of surface receptors upon insulin stimulation (Mielke and Wang, 2005; Wan et al., 1997b; Wang et al., 2003). Phosphorylation of γ2 subunits by Src kinase increased the channel open probability (Moss et al., 1995). Furthermore, γ2 subunits govern the endocytosis of surface receptors, initiating clathrin-dependent internalisation of the receptors by the recruitment of the adaptor protein, AP2 (Connolly et al., 1999; Kittler et al., 2008). A similar function was carried by the β subunits. Both β and γ2 subunits interactions with AP2 are negatively regulated by phosphorylation, thereby dynamically altering cell surface receptor numbers. The recent discovery of a cross-talk between CaMKII and PTK activity in modulating $GABA_AR$ (Houston et al., 2007) speculates the requirement for synergetic β3 and γ2 subunit phosphorylation by CaMKII and PTK during RP onset.

To address the involvement of phosphorylation of individual $GABA_AR$ subunits in RP, this chapter utilizes knockout (KO) mice with the deletion of $\alpha 1$ and $\beta 2$ subunit genes.

$\alpha 1$ and $\beta 2$ subunit knockout mice have been characterised both behaviourally and electrophysiologically (Sur et al., 2001). Surprisingly, both mice are viable and do not exhibit major behavioural phenotypes, although the $\alpha 1$-/- strain exhibited generation dependent improvement of mortality, and juvenile $\alpha 1$-/- mice also appeared underweight. Both mice lines showed no neurological and movement deficiency, with the exception of a slight handling tremor in $\alpha 1$-/- mice and enhanced locomotor activity in $\beta 2$-/- mice.

Autoradiography binding with [^{35}S]*t*-butylbicyclophosphorothionate (TBPS) revealed ~ 67% and ~71% loss in total number of surface $GABA_ARs$ in $\alpha 1$-/- and $\beta 2$-/- respectively. Immunoprecipitation revealed a putative upregulation of $\alpha 3\beta\gamma$ receptors by [^{3}H]Ro15-1788 binding in $\alpha 1$-/- mice. Western blots also demonstrated an increase in $\alpha 2$ and $\alpha 3$ subunit expression in the cerebellum, possibly attributed to a generation dependent adaptation. Neither $\alpha 4$ nor $\alpha 5$ subunits were upregulated in the cerebellum. In contrast, $\alpha 6$ subunit expression in cerebellar granule cells was reduced, as expected from its functional overlap and coassembly with the $\alpha 1$ subunit (Khan et al., 1996a; Vicini et al., 2001). In the $\beta 2$-/- animals, all α subunits expressions were reduced accordingly. Inhibitory currents evoked by exogenously-applied GABA were significantly reduced in both knockout mice strains, almost half of the PCs appeared unresponsive in the $\alpha 1$-/-

mice, and the remaining PCs exhibited 10-fold decreases in inhibitory currents, and reduced potency of exogenous GABA (Sur et al., 2001).

A novel knock-in mouse, with mutations of Y365F, Y367F on the γ2 subunits, was also used to study the role of γ2 subunit and these tyrosine residues in RP.

6.2 Results

Prior to establishing the relationship between individual $GABA_AR$ subunits in PCs and RP, we used immunohistochemical techniques to monitor the subunit expression patterns in transgenic mice. All the double immunofluorescence images were acquired from 100 μm thick parasagittal cerebellar slices.

The α1-/- and β2-/- mice (from Merck Sharp and Dohme,UK) were of the same genetic background as wt mice (from the same supplier). Heterozygous F3 generation mice were cross-bred to produce the wt, α1-/- and β2-/- mice. Thereafter, homozygous breeding pairs of knockout mice were used for subsequent generations of offspring. It is conceivable that homozygously bred knockout animals may not be adequately controlled for by homozygously bred wt animals if they show genetic drift. However, our electrophysiology and immunohistochemistry is comparable to previously published reports with these knockout mice (Sur et al., 2001), suggesting genetic drift is minimal.

6.2.1 α subunit expression in wt, α1-/- and β2-/- mice

PCs were identified with a TRITC-conjugated secondary antibody and an anti-$calbindin_{D28K}$ primary antibody, as calbindin is exclusively expressed in PCs in cerebellum, thereby considered as a PC specific cell marker. The red staining pattern revealed the soma of PCs and their elaborate fan-shaped planar dendritic trees, extending into the molecular layer, where their processes received synaptic contacts from basket and stellate cells, which appeared as black cavities amongst the red staining (Fig 6.1). The α1 subunit expression was studied with a FITC-conjugated

secondary antibody and an anti-α1 primary antibody, emitting a green fluorescence signal (Fig 6.1). Co-expression of calbindin and α1 subunits was revealed in the overlaid images. The α1 subunit expression appeared to span all three layers of the cerebellum with intense staining on the PC soma and most regions of the dendritic tree in the ML (Fig 6.1 A top, the immunohistochemical staining was not quantified; most descriptions were based on eye measurement). The high contrast of the α1 subunit signal on the dendrites against the diffused staining in the background ML suggests this dendritic α1 subunit expression was genuine and not derived from other ML constituents. The α1 subunit staining was completely lost from the α1 -/- mice, confirming the specificity of the antibody (Fig 6.1 A). In the β2-/- mice, there were no apparent differences in the expression of α1 subunit compared to wt animals (Fig 6.1 B). The α3 subunit expression appeared similar in the wt, α1-/- and β2-/- animals, residing ambiguously on the somas and dendrites (Fig 6.1A, B). No visible upregulation of the α3 subunit was observed to compensate for the loss of the α1 subunits.

To ascertain whether other α subunits can substitute for the loss of α1 subunits, we stained for the α5 subunits. The α5 staining patterns in wt and α1-/- was diffused and inconclusive (Fig 6.1 C).

6.1

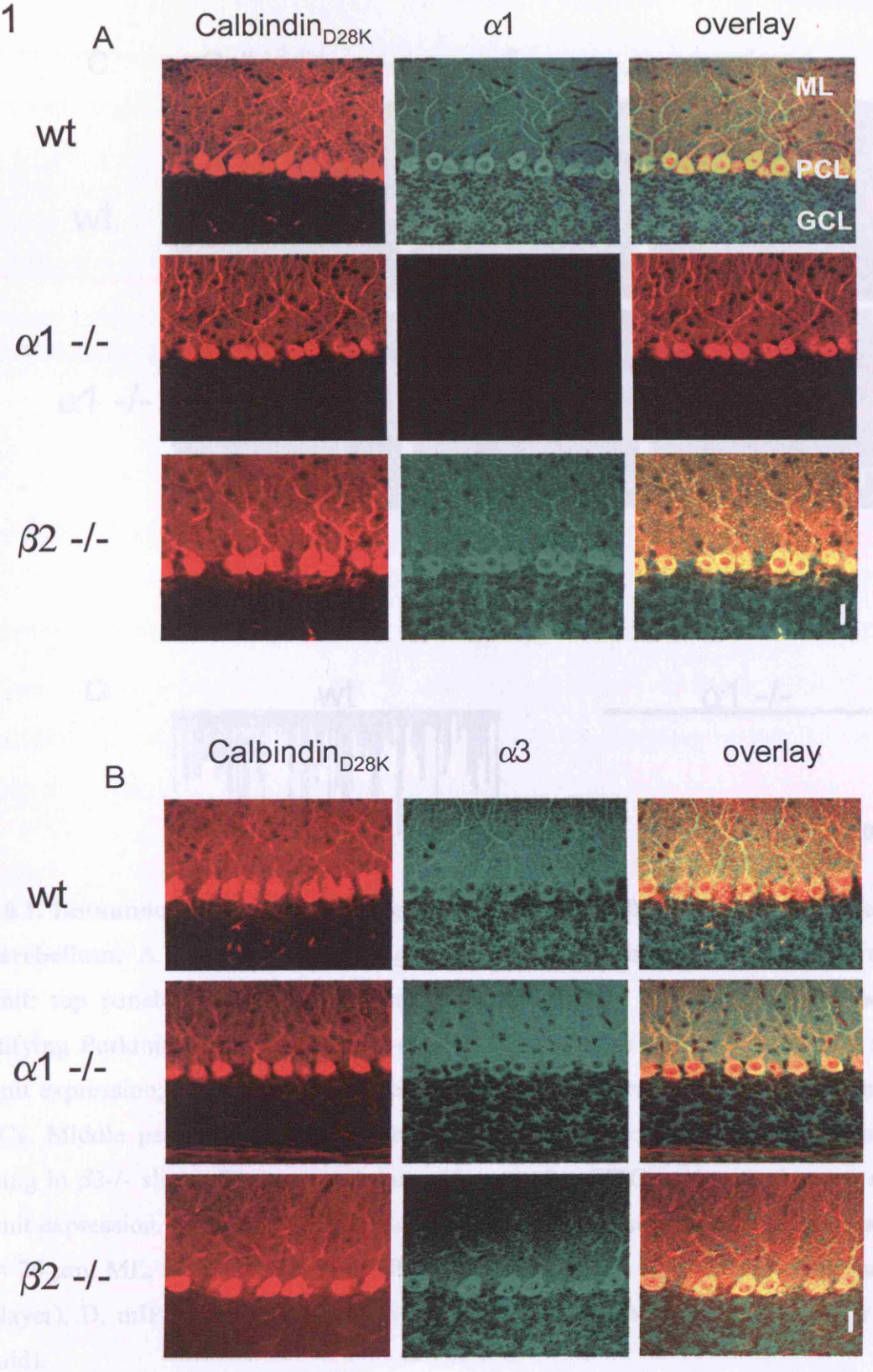
A
Calbindin$_{D28K}$
α1
overlay
wt
α1 -/-
β2 -/-
ML
PCL
GCL
I
B
Calbindin$_{D28K}$
α3
overlay
wt
α1 -/-
β2 -/-
I

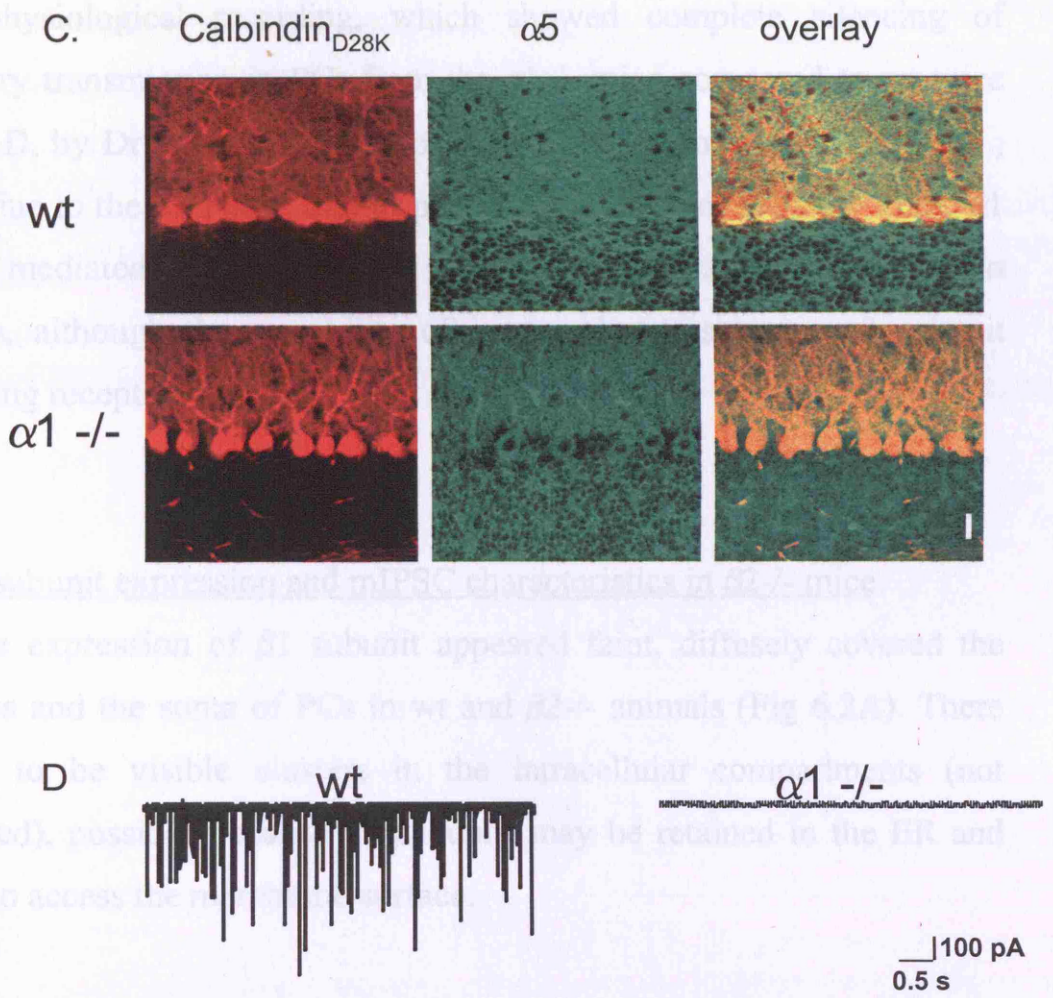

Fig 6.1. Immunocytochemical staining of α subunits in 100μm parasagittal slices of cerebellum. A. Representative images of immunocytochemical labelling of α1 subunit: top panels, wt animal; left, anti-calbindinD28K – TRITC conjugate stain identifying Purkinje Cells; middle, anti-α1 – FITC conjugate stain displaying the α1 subunit expression; right, overlaid images illustrating the expression of the α1 subunit in PCs. Middle panel, same as above but in α1-/- slices. Bottom panel, α1 subunit staining in β2-/- slices. B, same as A but with anti-α3 – FITC conjugate showing α3 subunit expression. C, anti-α5 – FITC conjugate showing α5 subunit expression (scale bar = 20 μm; ML, the molecular layer; PCL, the Purkinje cell layer; GCL, the granule cell layer). D, mIPSC recordings from wt PC and α1-/- PC held at -70mV (by Dr I. Duguid).

The consequences of ablating α1 subunit expression was revealed by electrophysiological recording, which showed complete silencing of inhibitory transmission in PCs from the α1-/- mice compared to wt mice (Fig 6.1D, by Dr I Duguid), in accordance with previous work (Sur et al., 2001), due to the extensive loss of postsynaptic receptor clusters. Thus, α1 subunit mediated phasic inhibition was not compensated for by other α subunits, although the possibility of increased extrasynaptic α3 subunit containing receptors remains.

6.2.2 β subunit expression and mIPSC characteristics in β2-/- mice

The expression of β1 subunit appeared faint, diffusely covered the dendrites and the soma of PCs in wt and β2-/- animals (Fig 6.2A). There seemed to be visible clusters in the intracellular compartments (not quantified), possibly because β1 subunits may be retained in the ER and unable to access the membrane surface.

The β2 subunit was sparsely stained on wt PC soma and dendrites, although most previous studies failed to detect β2 subunit expression on the PC soma (Gutierrez et al., 1994c; Laurie et al., 1992a; Pirker et al., 2000). The β2 staining was completely lost in the β2-/- mice.

Staining of β3 subunits was visualised mostly in the granule cell layer, with a few intracellular aggregates appearing in PCs (not quantified). The staining pattern appeared similar in the β2-/- animals (Fig 6.2C).

Though immunohistochemistry showed no obvious compensation by other β isoforms for the loss of the β2 subunits, inhibitory transmission was still detected (Fig 6.3B). The morphology of PCs in β2-/- mice displayed no abnormality (Fig 6.3A). However, the basal amplitude of mIPSCs was drastically reduced from 108.2 ± 16.2pA in wt to 41.7 ± 9.3pA in β2-/- (Fig 6.3 B-C, Table 6.1, $n = 5$, $P < 0.05$). mIPSC frequency was also decreased from 4.88 ± 0.33 Hz in wt to 2.69 ± 0.23 Hz in β2-/- ($n= 5$, $P < 0.05$). It is of importance to point out the wt recordings used to control for the β2-/- animals were the same group of controls used in previous chapters, which may be inadequate as these wt and β2-/- animals were not cross bred for littermate controls.

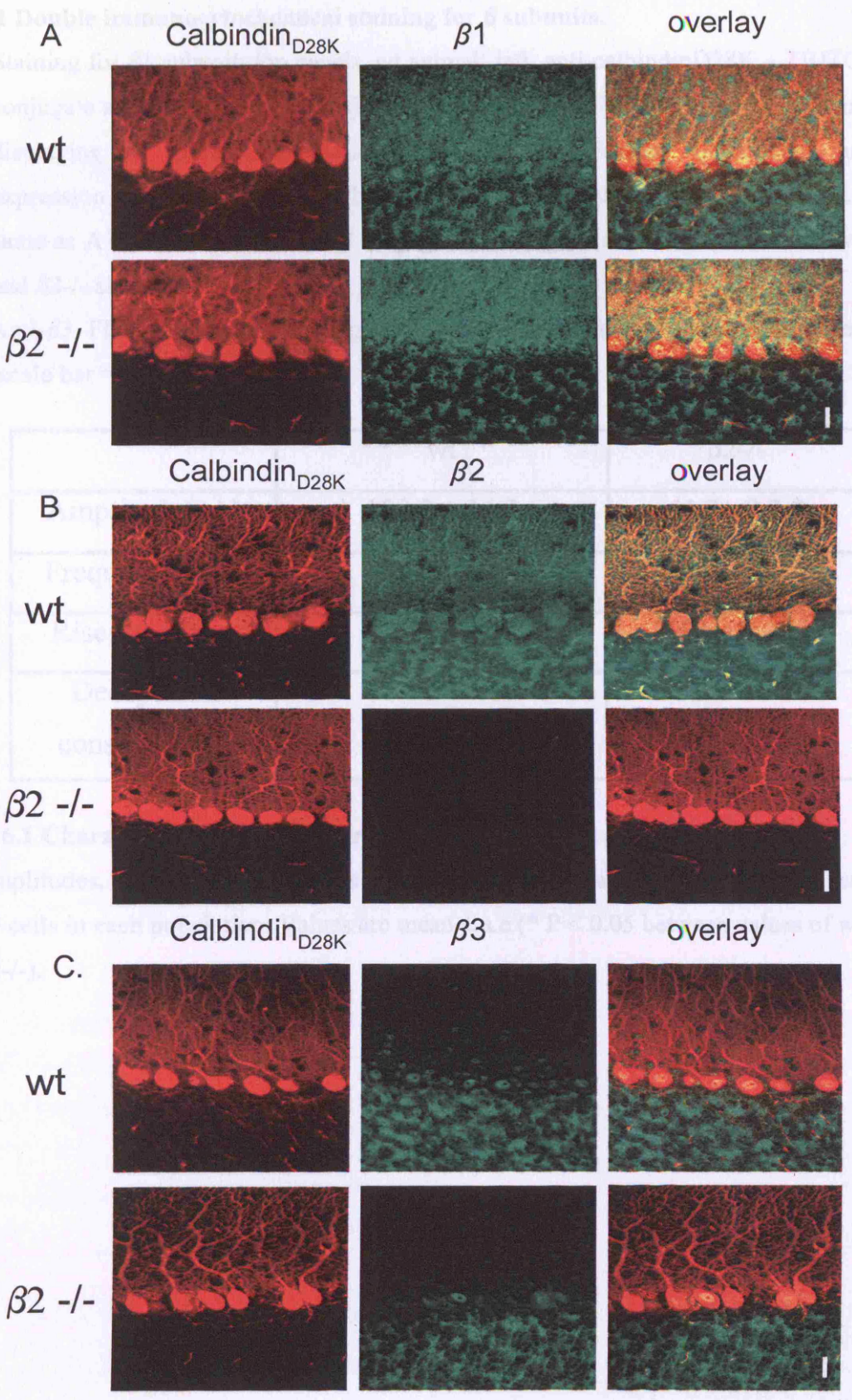
A
Calbindin$_{D28K}$
β1
overlay
wt
β2 -/-
B
Calbindin$_{D28K}$
β2
overlay
wt
β2 -/-
C.
Calbindin$_{D28K}$
β3
overlay
wt
β2 -/-

Fig 6.2 Double immunocytochemical staining for β subunits.

A. Staining for β1 subunit: top panels, wt animal; left, anti-calbindinD28K – TRITC conjugate stain identifying Purkinje cells; middle, anti- β1 – FITC conjugate stain displaying β1 subunit expression; right, overlaid images illustrating the expression of β1 subunits in PCs. bottom panel, same as above but in β2-/- slices.

B. Same as A but with anti-β2–FITC conjugate showing β2 subunit expression in wt and β2-/- slices.

C. Anti-β3–FITC conjugate showing β3 subunit expression in wt and β2-/- slices (scale bar = 20 μm).

	wt	β2-/-
Amplitude(pA)	108.2 ± 16.2	41.7± 9.3 *
Frequency (Hz)	4.88 ± 0.33	2.69 ± 0.23 *
Rise time (ms)	1.53 ± 0.21	2.59 ± 0.06 *
Decay time constant (ms)	11.82 ± 0.66	10.92 ± 0.20

Table 6.1 Characteristics of mIPSCs recorded from wt and β2-/- PCs.

The amplitudes, frequencies, rise-times and decay time constants were averages taken from 5 cells in each population. Values are mean ± s.e (* $P < 0.05$ between values of wt and β2-/-).

6.3

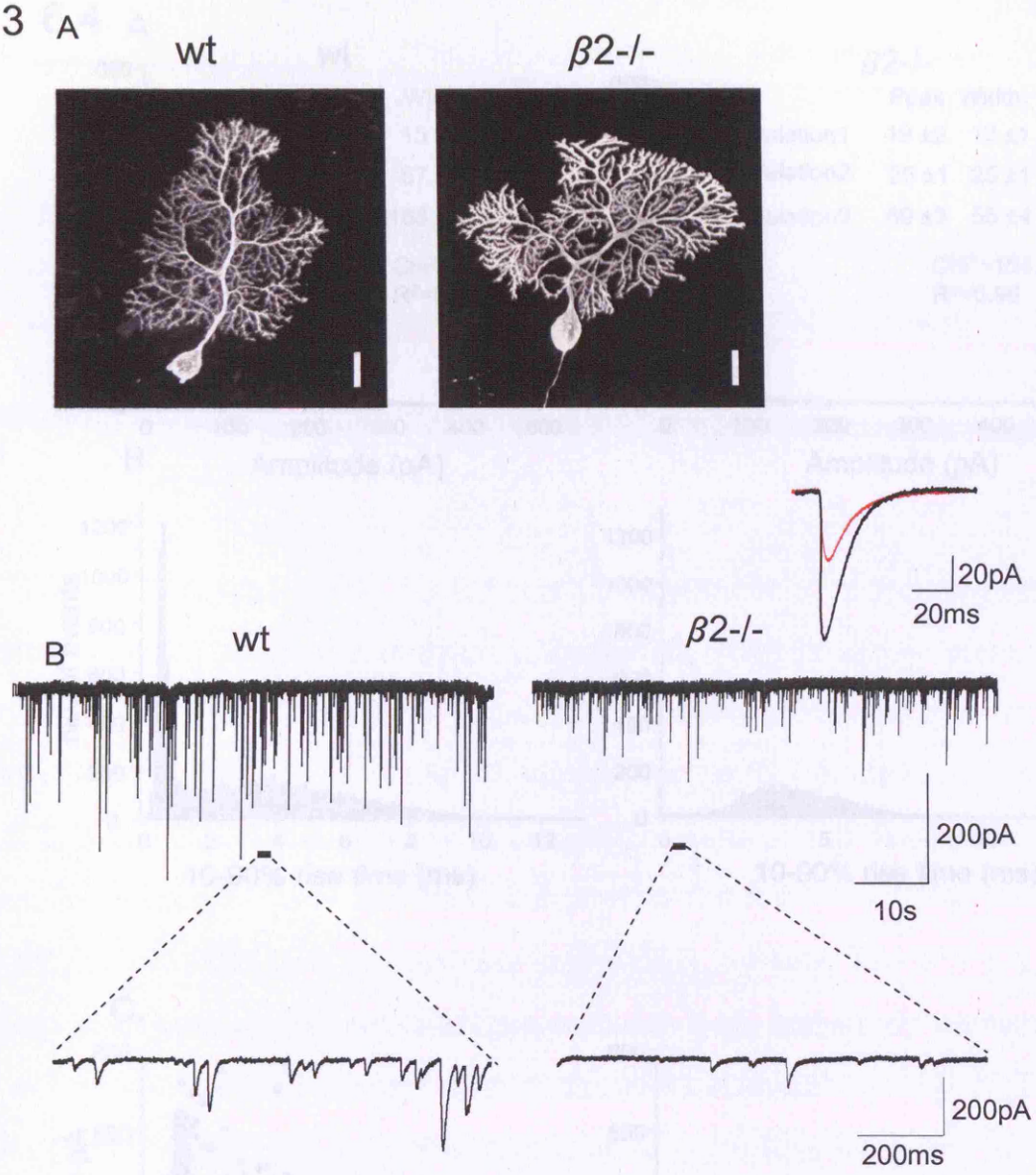

Fig 6.3 Morphology of PCs and mIPSC recordings from β2-/- PCs.

A, biocytin filled – Strep-Alexa-Fluor 488 conjugate reconstructed single PC from a wt (left, P11) and β2-/- (right, P12) animal (scale bar = 20 μm). B, mIPSC recordings from wt (left) and β2-/- PCs. Below: 1s expanded trace; insert, superimposed scaled average of 50 consecutive mIPSC events selected from wt (black) and β2-/- (red) PCs.

6.4 A

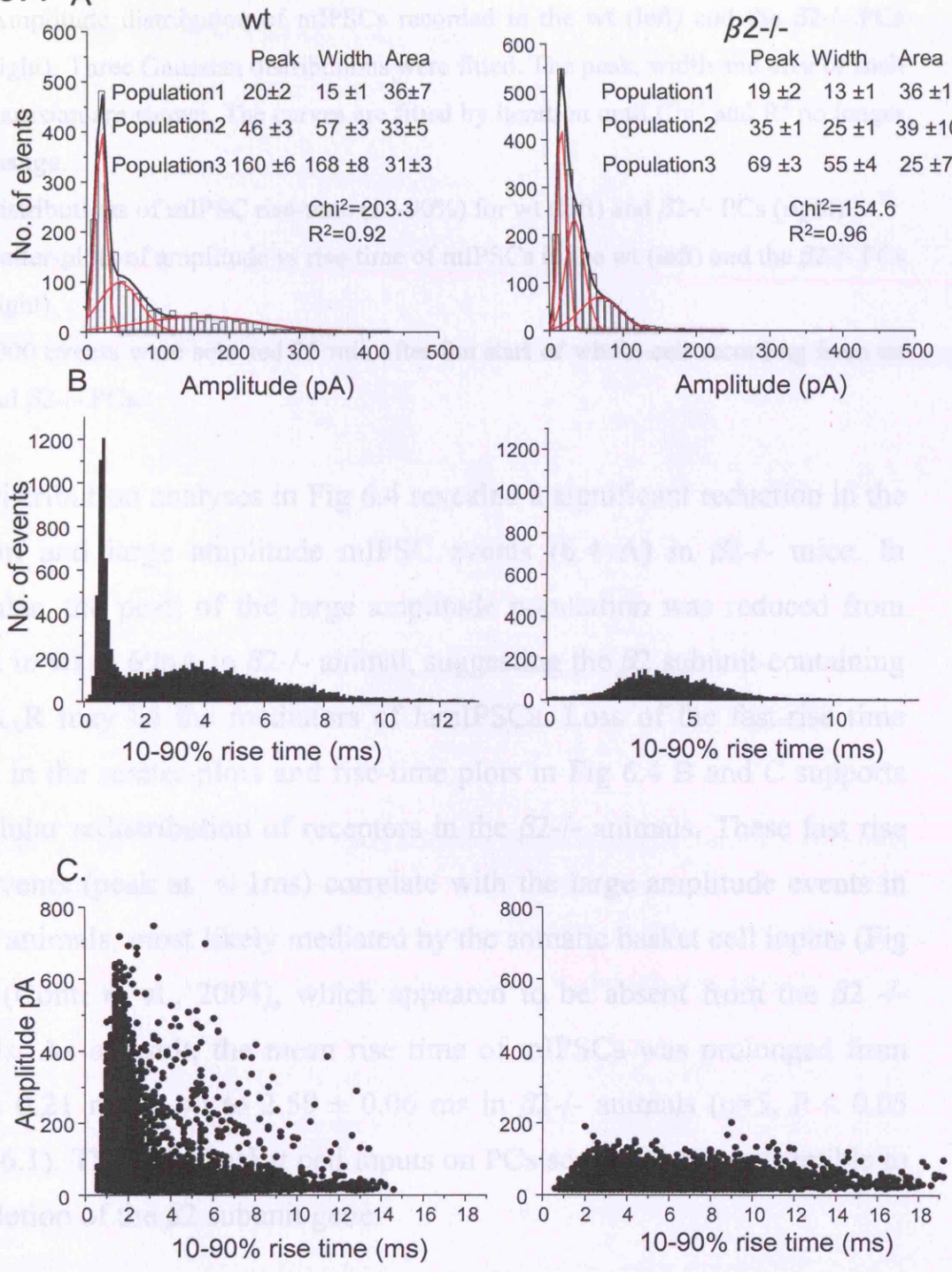
wt
Peak Width Area
Population1 20±2 15 ±1 36±7
Population2 46 ±3 57 ±3 33±5
Population3 160 ±6 168 ±8 31±3
Chi²=203.3
R²=0.92
β2-/-
Peak Width Area
Population1 19 ±2 13 ±1 36 ±15
Population2 35 ±1 25 ±1 39 ±10
Population3 69 ±3 55 ±4 25 ±7
Chi²=154.6
R²=0.96
No. of events
Amplitude (pA)
B
No. of events
10-90% rise time (ms)
C.
Amplitude pA
10-90% rise time (ms)

Fig 6.4 Population analyses of mIPSCs from wt and β2-/- PCs.

A). Amplitude distribution of mIPSCs recorded in the wt (left) and the β2-/- PCs (right). Three Gaussian distributions were fitted. The peak, width and area of each Gaussian are shown. The curves are fitted by iteration until Chi^2 and R^2 no longer change.

B). Distributions of mIPSC rise-time (10-90%) for wt (left) and β2-/- PCs (right).

C). Scatter-plots of amplitude *vs* rise-time of mIPSCs in the wt (left) and the β2-/- PCs (right).

~2000 events were selected 25 min after the start of whole-cell recording from wt and β2-/- PCs.

Distribution analyses in Fig 6.4 revealed a significant reduction in the medium and large amplitude mIPSC events (6.4 A) in β2-/- mice. In particular, the peak of the large amplitude population was reduced from 160pA in wt to 69pA in β2-/- animal, suggesting the β2 subunit-containing $GABA_AR$ may be the mediators of lamIPSCs. Loss of the fast-rise time events in the scatter-plots and rise-time plots in Fig 6.4 B and C supports subcellular redistribution of receptors in the β2-/- animals. These fast rise time events (peak at < 1ms) correlate with the large amplitude events in the wt animals, most likely mediated by the somatic basket cell inputs (Fig 6.4B) (Conti et al., 2004), which appeared to be absent from the β2 -/- animals. As a result, the mean rise time of mIPSCs was prolonged from 1.53 ± 0.21 ms in wt to 2.59 ± 0.06 ms in β2-/- animals ($n=5$, $P < 0.05$ Table 6.1). Thus, the basket cell inputs on PCs seemed more susceptible to the deletion of the β2 subunit gene.

Salicylidene salicylhydrazide (SCS), a selective inhibitor of the β1 subunit containing receptors (Thompson et al., 2004), failed to affect

mIPSCs in β2-/- mice (Fig 6.5 A, C, unpublished work by Dr I Duguid). This excludes β1 subunit as the mediators of the remaining phasic inhibitory transmission in the absence of β2 subunits.

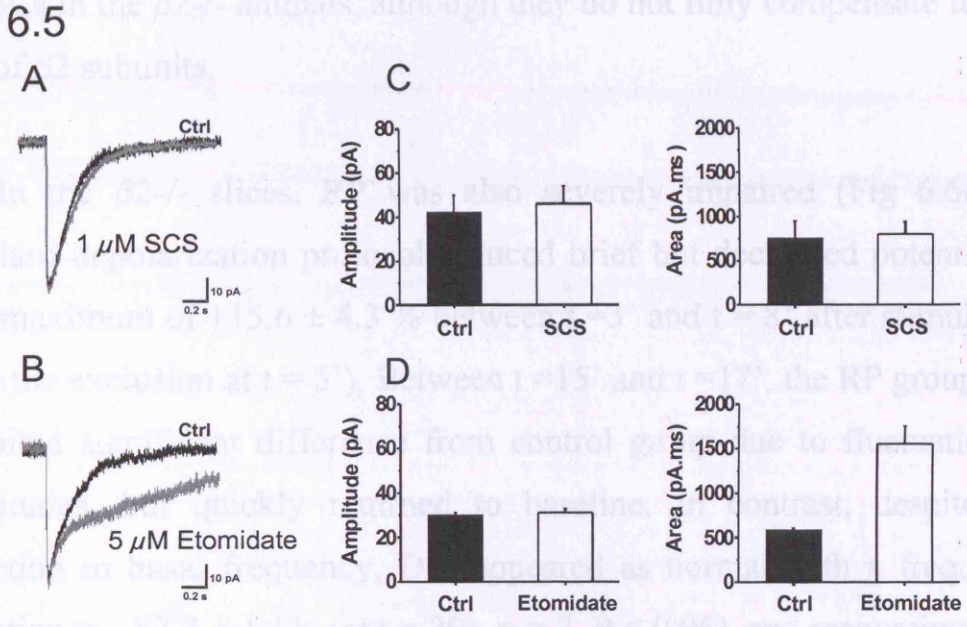

Fig 6.5 Effect of β1 and β2/3 subunit selective modulators on mIPSCs recorded from PCs in β2-/- slices.

A). Superimposed scaled average traces of control mIPSC (black) and mIPSC in the presence of the 1μM β1 subunit selective inhibitor, salicylidene salicylhydrazide (SCS) (grey) in a β2-/- PC.

B). Superimposed scaled average traces of control mIPSC (black) and mIPSC in the presence of the 5μM β2/3 subunit selective enhancer, etomidate (grey) in the β2-/- PCs.

C). Top left, histograms summarising the β2-/- PC mIPSC amplitudes in control conditions and in the presence of SCS; top right, area under the mIPSC traces in control and SCS. Bottom, same as above but for etomidate. Values are mean ± s.e. (* $P < 0.05$ work contributed by Dr I. Duguid)

On the other hand, the β2/3 selective enhancer etomidate (Drexler et al., 2005), prolonged the decay of mIPSC in β2-/- animals (6.5 B, C), unveiling the presence of β3 subunit containing receptors (I Duguid). Therefore, the β3 subunit containing receptors may mediate the majority of mIPSCs in the β2-/- animals, although they do not fully compensate for the loss of β2 subunits.

In the β2-/- slices, RP was also severely impaired (Fig 6.6A-C). Standard depolarization protocol induced brief but decreased potentiation with maximum of 115.6 ± 4.3 % between t =3' and t = 8' after stimulation (with the exclusion at t = 5'). Between t =15' and t =17', the RP group also exhibited significant difference from control group due to fluctuation in amplitudes, but quickly returned to baseline. In contrast, despite the reduction in basal frequency, DSI appeared as normal with a frequency reduction to 83.2 ± 1.1% (at t = 20s, n = 7, $P < 0.05$), and recovering soon after. The presence of AP5 blocked the induction of DPI. This emphasized the discrete nature of RP and other forms of synaptic plasticities at IN-PC synapses.

We then explored the effect of kinase inhibition on the residual RP in β2-/- slices. Bath-applying CaMKIINtide at 500nM resulted in no change of RP in β2-/- PCs (potentiation significant between t = 2' and t = 8' after stimulus, maximum potentiation of 115.3 ± 7.1 % at t = 3', n = 5, $P < 0.05$, Fig 6.7), nor did it affect baseline mIPSC amplitudes or frequencies. Intracellular application of genistein (100 μM) also failed to alter the profile of β2-/- RP (potentiation significant between t = 3' and t = 10' after stimulus, with maximum potentiation of 132.3 ± 5.6% at t = 8' n = 5, P <

0.05 Fig 6.8). Hence, CaMKIINtide and genistein, previously shown to suppress RP (see chapter 3), were ineffective against RP in the β2-/- mice, implying that their actions were manifested through the β2 subunit.

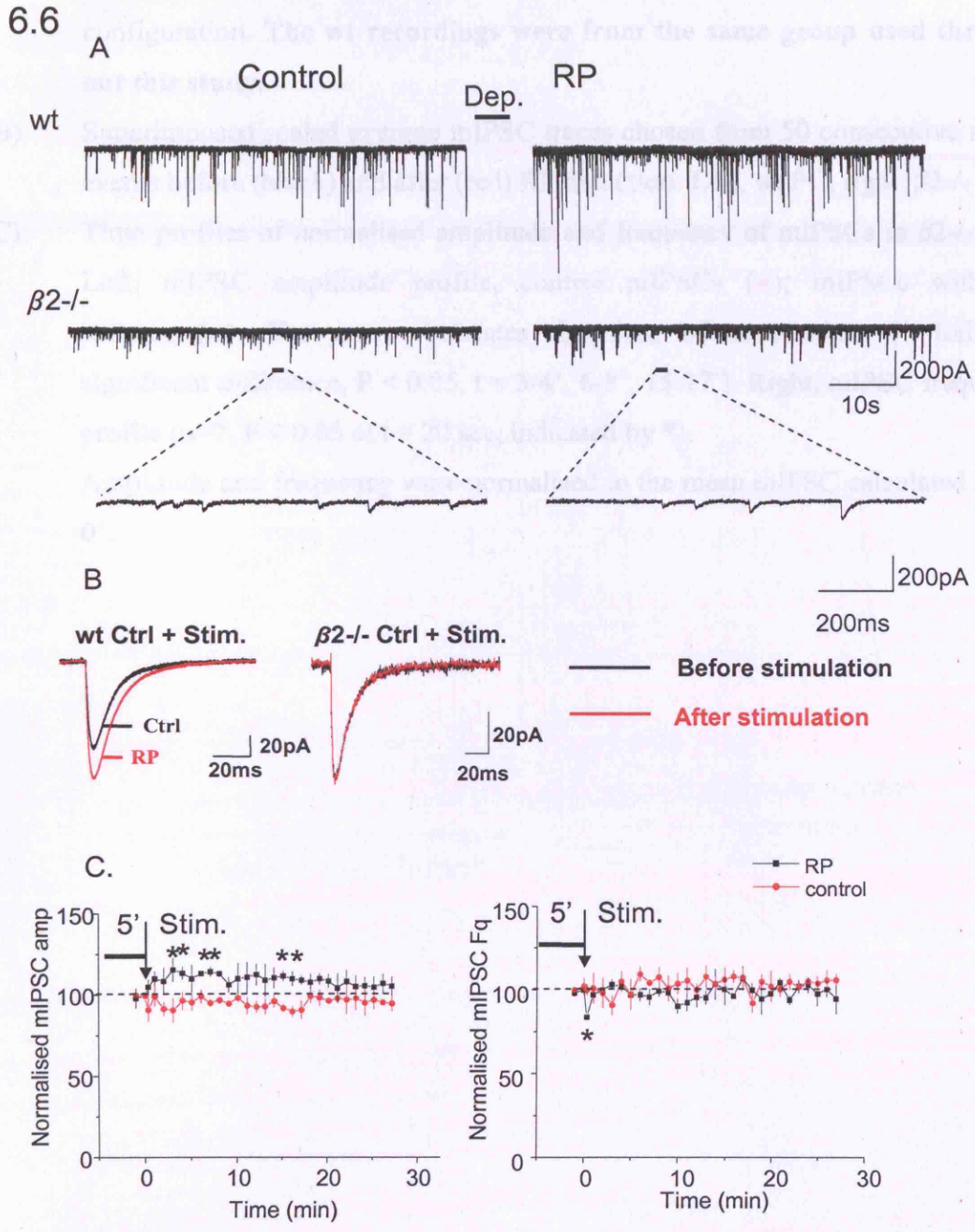

Fig 6.6 Comparison of RP in wt and β2-/- PCs.

A). mIPSCs recordings before (left) and 25 min after (right) RP induction in the wt (top) and the β2-/- (middle) PCs. Expanded traces are inserted below. In both genotypes, stimuli were applied 5 min after the formation of the whole-cell configuration. **The wt recordings were from the same group used through out this study.**

B). Superimposed scaled average mIPSC traces chosen from 50 consecutive single events before (black) and after (red) RP induction. Left, wt PC; right, β2-/- PC.

C). Time profiles of normalised amplitude and frequency of mIPSCs in β2-/- PCs. Left, mIPSC amplitude profile, control mIPSCs (●); mIPSCs with RP induction(■). The arrow indicates the time of stimulation. (* indicates significant difference, $P < 0.05$, t = 3-4', 6-8', 15-17'). Right, mIPSC frequency profile (n=7, $P < 0.05$ at t = 20 sec, indicated by *).

Amplitude and frequency were normalised to the mean mIPSC calculated at t = 0'.

6.7

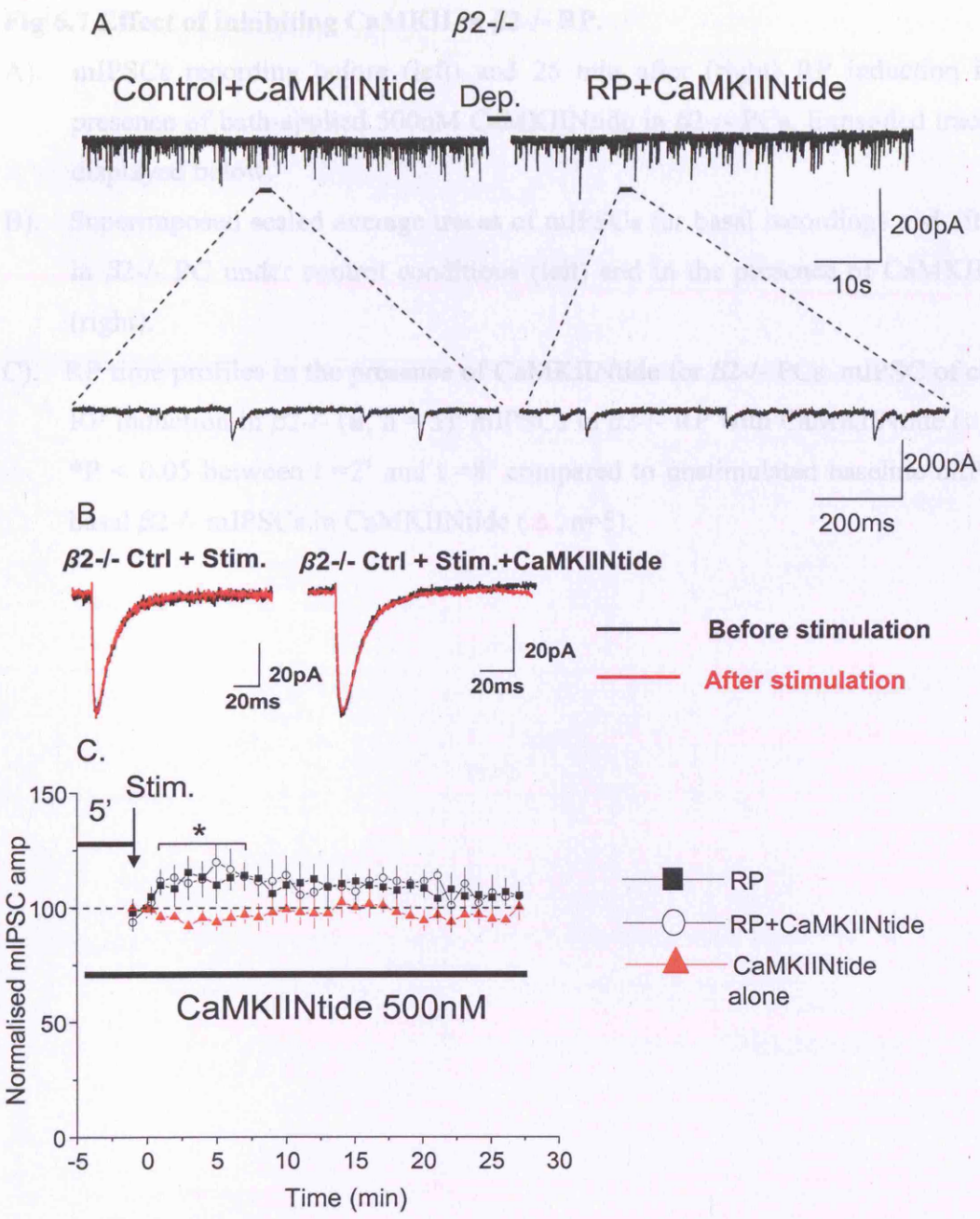
A
β2-/-
Control+CaMKIINtide
Dep.
RP+CaMKIINtide
200pA
10s
200pA
200ms
B
β2-/- Ctrl + Stim.
β2-/- Ctrl + Stim.+CaMKIINtide
20pA
20ms
20pA
20ms
Before stimulation
After stimulation
C.
Stim.
5'
*
150
100
50
0
Normalised mIPSC amp
CaMKIINtide 500nM
-5
0
5
10
15
20
25
30
Time (min)
RP
RP+CaMKIINtide
CaMKIINtide alone

Fig 6.7 Effect of inhibiting CaMKII in β2-/- RP.

A). mIPSCs recording before (left) and 25 min after (right) RP induction in the presence of bath-applied 500nM CaMKIINtide in β2-/- PCs. Expanded traces are displayed below.

B). Superimposed scaled average traces of mIPSCs for basal recordings and after RP in β2-/- PC under control conditions (left) and in the presence of CaMKIINtide (right).

C). RP time profiles in the presence of CaMKIINtide for β2-/- PCs. mIPSC of control RP induction in β2-/- (■, n = 5); mIPSCs in β2-/- RP with CaMKIINtide (○, n=5, *P < 0.05 between t =2' and t =8' compared to unstimulated baseline mIPSCs); basal β2-/- mIPSCs in CaMKIINtide (▲, n=5).

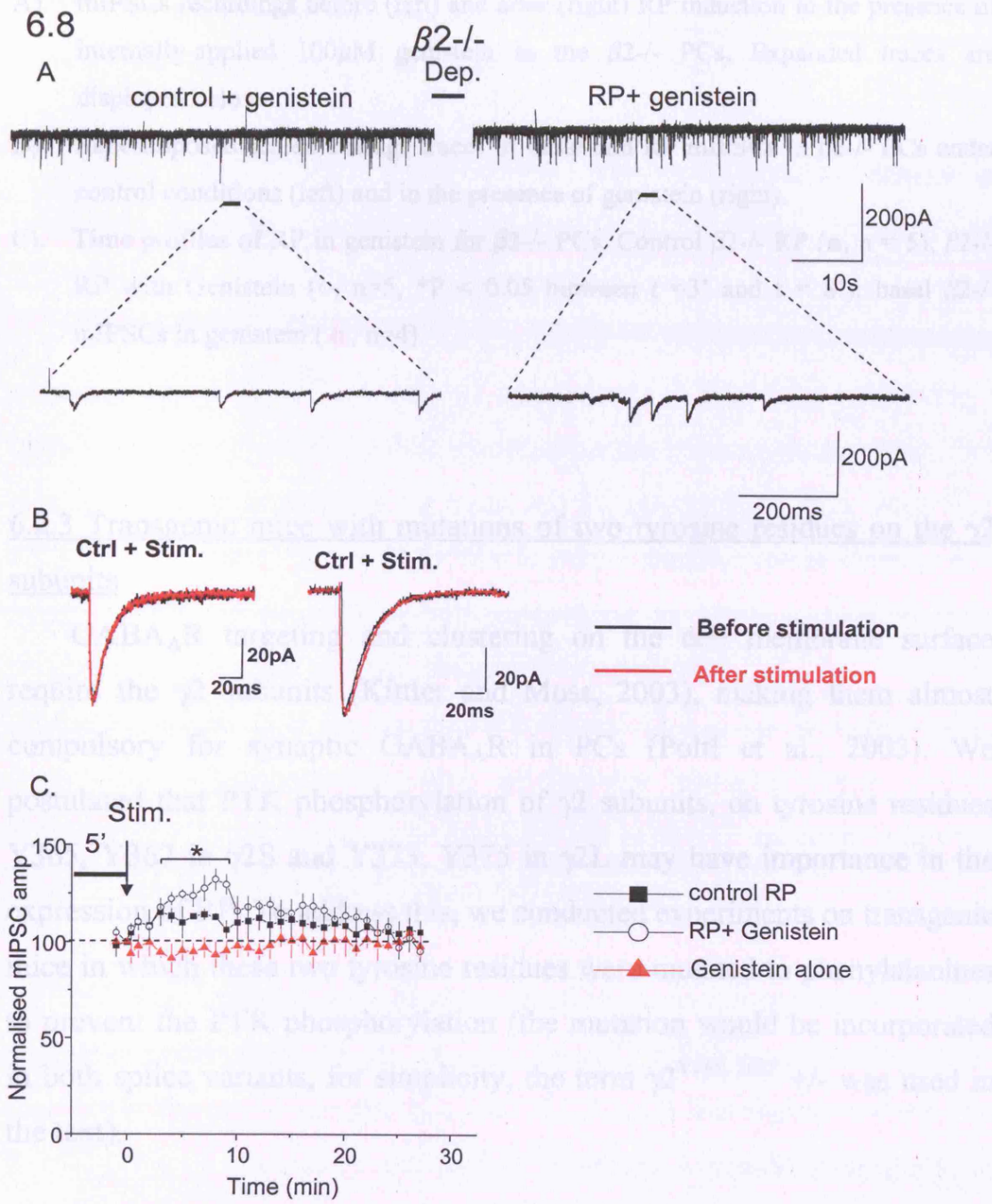
6.8
A
β2-/-
Dep.
control + genistein
RP+ genistein
200pA
10s
200pA
200ms
B
Ctrl + Stim.
Ctrl + Stim.
20pA
20ms
20pA
20ms
Before stimulation
After stimulation
C.
Stim.
5'
*
150
100
50
0
Normalised mIPSC amp
0
10
20
30
Time (min)
control RP
RP+ Genistein
Genistein alone

Fig 6.8 Effect of inhibiting PTK in β2-/- RP.

A). mIPSCs recordings before (left) and after (right) RP induction in the presence of internally-applied 100μM genistein in the β2-/- PCs. Expanded traces are displayed below.

B). Superimposed scaled average traces of basal and RP mIPSCs in β2-/- PCs under control conditions (left) and in the presence of genistein (right).

C). Time profiles of RP in genistein for β2-/- PCs. Control β2-/- RP (■, n = 5); β2-/- RP with Genistein (○, n=5, *P < 0.05 between t =3' and t = 8'); basal β2-/- mIPSCs in genistein (▲, n=4).

6.2.3 Transgenic mice with mutations of two tyrosine residues on the γ2 subunits

$GABA_AR$ targeting and clustering on the cell membrane surface require the γ2 subunits (Kittler and Moss, 2003), making them almost compulsory for synaptic $GABA_AR$ in PCs (Poltl et al., 2003). We postulated that PTK phosphorylation of γ2 subunits, on tyrosine residues Y365, Y367 in γ2S and Y373, Y375 in γ2L may have importance in the expression of RP. To address this, we conducted experiments on transgenic mice in which these two tyrosine residues were mutated to phenylalanines to prevent the PTK phosphorylation (the mutation would be incorporated in both splice variants, for simplicity, the term $\gamma2^{Y365,\ 367F}$ +/- was used in the text).

Homozygous knock-in mice did not survive postnatally, accentuating the critical importance of these two residues for neuronal development. We therefore opted to use heterozygous mice, which did not exhibit obvious

behavioural phenotypes on initial analysis (unpublished observations by Dr C. Stanford). The mutant mice were cross breed with same back ground wt mice to obtain heterozygous mice and wt littermate controls.

Immunohistochemical data revealed a cell specific 200% increase in total surface receptor number in PC (contributed by Dr V. Tetter). Using PS-NSNA, N_p of 79.9 ± 13.4 (n = 10, from groups exhibiting rebound depression, RD, only, see latter text) and 23.7 ± 4.3 (n = 4, $P < 0.05$) was obtained for $\gamma 2^{Y365,\ 367F}$ +/- and wt respectively (Table 6.2), supporting a higher density of active surface receptors in the heterozygous mouse. We also observed an increase in the mean mIPSC amplitude in PCs, from 62.1 ±5.3 pA (littermate wt, n = 4) to 99.6 ± 9.6 pA (heterozygous animals, n = 10, $P < 0.05$), in accordance with an increase in active surface receptor numbers. The mean mIPSC frequency in the $\gamma 2^{Y365,\ 367F}$ +/- PC was unaltered compared to the wt, (9.2 ± 3 Hz and 12.2 ± 2.0 Hz respectively, $P > 0.05$). Curiously, the lack of tyrosine phosphorylation in the heterozygous mice appeared to facilitate the export of receptors onto the plasma membrane and incorporation into synapses in PCs.

PC were injected with biocytin through the patch pipette, fixed and stained to obtain reconstructed images from $\gamma 2^{Y365,\ 367F}$ +/- slices (Fig 6.9A; age P13). The mutations did not alter the overall morphology of the PC. Soma, primary, secondary and tertiary dendrites appeared comparable to wt.

The mIPSC amplitude distribution (of a single representative cell) exhibited enhancement of the mean mIPSC amplitude (skewness was

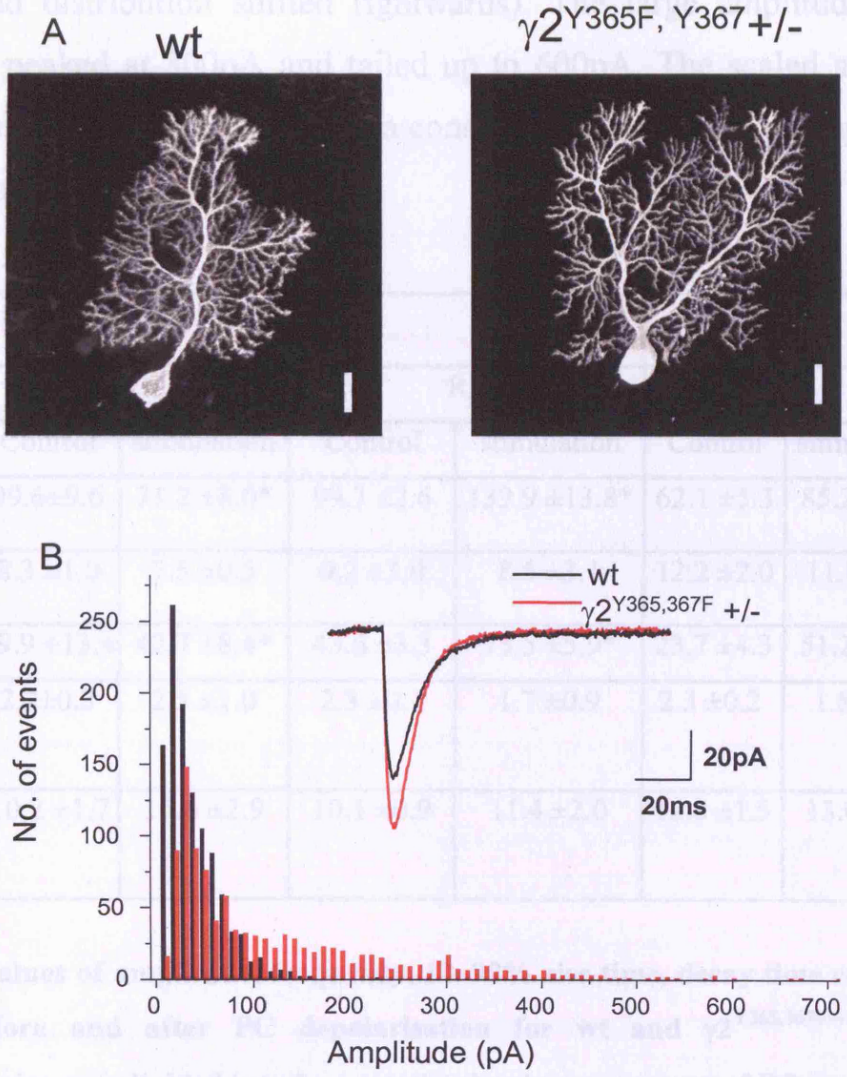

Fig 6.9 Morphology of PCs and basal mIPSC amplitude distribution in $\gamma2^{Y365,367F}$+/- PC.

A). Biocytin - strepavidin-alexa-fluor 488 conjugated reconstruction for a single P11 PC from wt slice (left) and P13 PC from a $\gamma2^{Y365,367F}$+/- slice (right; scale bar = 20 μm).

B). Amplitude distributions of mIPSCs in wt (black) and $\gamma2^{Y365,367F}$+/- (red) PCs. Insert, superimposed scaled average mIPSCs from wt and $\gamma2^{Y365,367F}$+/- mice.

reduced and distribution shifted rightwards). The large amplitude sub-population peaked at 300pA and tailed up to 600pA. The scaled average mIPSC from mutant mice displayed a considerable increment in amplitude in comparison to control (Fig 6.9 B).

	Heterozygous				wt	
	RD		RP			
	Control	stimulation	Control	stimulation	Control	stimulation
Amplitude (pA)	99.6±9.6	71.2 ±8.0*	99.3 ±2.6	139.9 ±13.8*	62.1 ±5.3	85.2 ±5.3*
Frequency (Hz)	8.3 ±1.0	7.5 ±0.5	9.2 ±3.0	8.5 ±3.1	12.2 ±2.0	11.8 ±1.7
N_p	79.9 ±13.4	42.7 ±8.4*	43.6 ±3.3	73.5 ±5.9*	23.7 ±4.3	51.2 ±8.6*
10-90% Rise time (ms)	2.2±0.3	2.5 ±1.0	2.3 ±0.1	1.7 ±0.9	2.3 ±0.2	1.8 ±0.4
Decay time constant (ms)	10.2 ±1.7	16.6 ±2.9	10.1 ±0.9	11.4 ±2.0	12.0 ±1.5	13.0 ±1.2

Table 6.2. Values of amplitude, frequency, 10~90% rise time, decay time constant and N_p before and after PC depolarisation for wt and $\gamma2^{Y365,367F+/-}$ mice. $\gamma2^{Y365,367F+/-}$ mice was divided into 2 population by the appearance of RP (n=3), and RD (n=10). Values are mean ± s.e. * $P < 0.05$ for values in neighbouring cells before and after stimulation. Using ANOVA analysis, amplitudes between wt, and the two heterozygous group are not significant ($P > 0.05$), Bonferroni post-test suggested statistical significance between amplitudes of **wt** *vs* **heterozygous RD group**, and **wt** *vs* **heterozygous RP group**. N_p between wt and both heterozygous groups exhibited statistical significance using ANOVA ($P < 0.05$).

In the attempt to elicit RP in $\gamma2^{Y365, 367F}$ +/- PCs, divergent outcomes were apparent, possibly due to the heterogeneity of these mice.

6.10

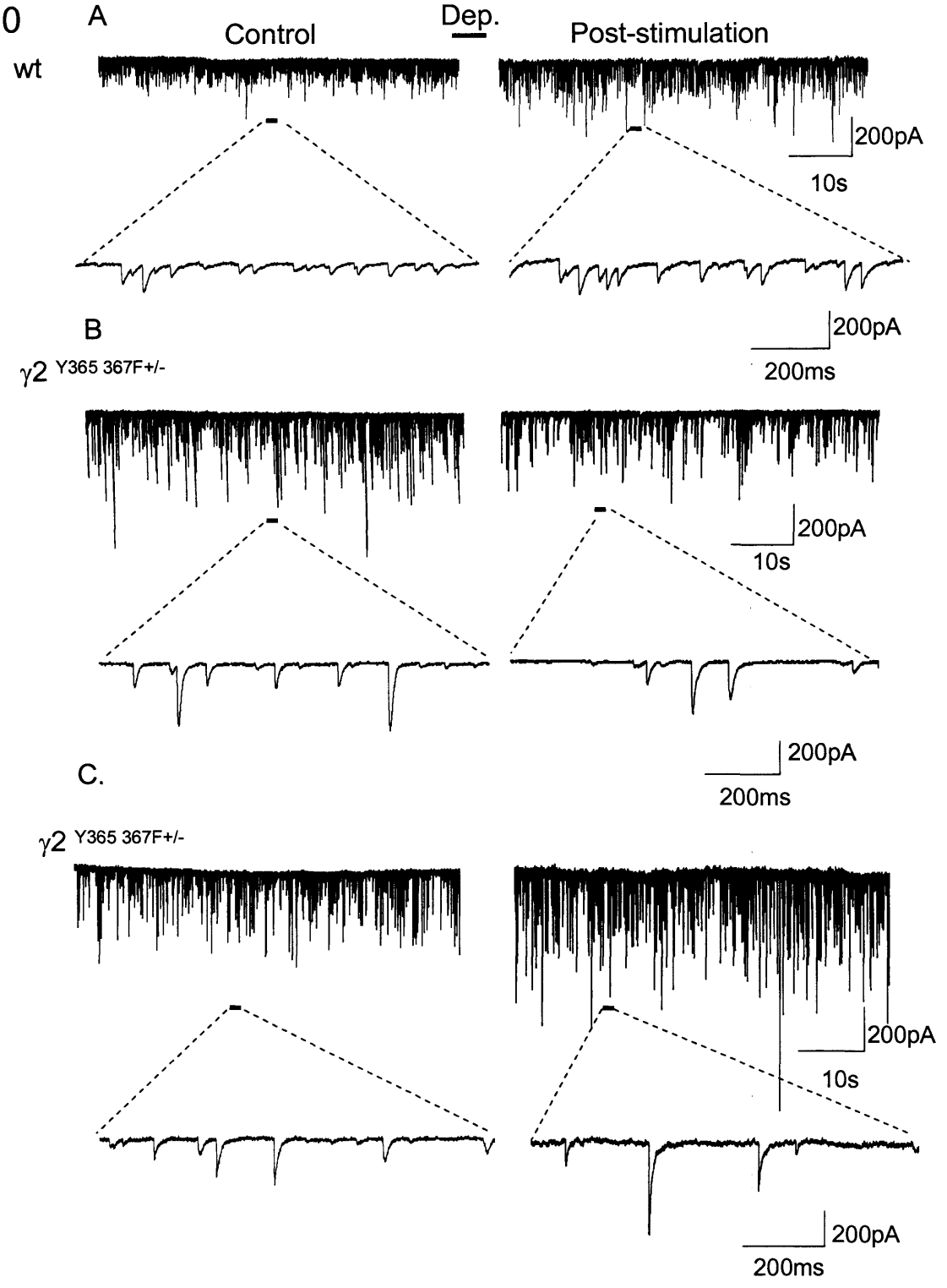
A
Control
Dep.
Post-stimulation
wt
200pA
10s
B
200pA
200ms
γ2 Y365 367F+/-
200pA
10s
200pA
200ms
C.
γ2 Y365 367F+/-
200pA
10s
200pA
200ms

Fig 6.10 mIPSCs before and after PC depolarisation for wt and $\gamma2^{Y365,367F}$+/- PCs.

A). mIPSCs recordings before (left) and after (right) RP induction for a wt PC. Expanded traces are inserted below.

B). Traces of mIPSCs before and after PC depolarisation in one PC from a $\gamma2^{Y365,367F}$+/- slice exhibiting RD.

C). Traces of mIPSCs recorded in a $\gamma2^{Y365,367F}$+/- PC exhibiting RP.

Stimuli were applied uniformly at 5 min after the whole-cell configuration was formed.

A small number of recordings (3/13) exhibited normalRP (149.6 ± 17.7 % at t = 25', n = 3), which was similar to wt (141.2 ± 5.8%, n = 4; Fig 6.10 A, C, P > 0.05). By contrast, the majority (10/13) exhibited a prominent depression, to 64.8 ± 5.0 % of control mIPSC amplitude using identical stimulation protocols (n = 10, P < 0.05, Fig 6.10 C). Due to the opposite polarity, we named this novel form of plasticity, rebound depression (RD).

In Fig 6.11 A, the superimposed scaled average mIPSCs verified RP and RD from the two populations of PCs in $\gamma2^{Y365,\ 367F}$ +/- animals (traces were taken from one representative cell of each population). The heterozygous mice may have adopted a mixed electrophysiological phenotype, the outcome of which may rely on the relative ratio of wt $\gamma2$ and mutant $\gamma2^{Y365,\ 367F}$ +/- protein expressed in the given PC.

DSI remained unaffected by the mutations (Fig 6.11C), displaying frequency reductions of 77.5 ± 6.7 %, 79.8 ± 3.3 %, and 64.9 ± 3.1% for wt, heterozygous RP group, and heterozygous RD group respectively (P > 0.05 ANOVA)

6.11

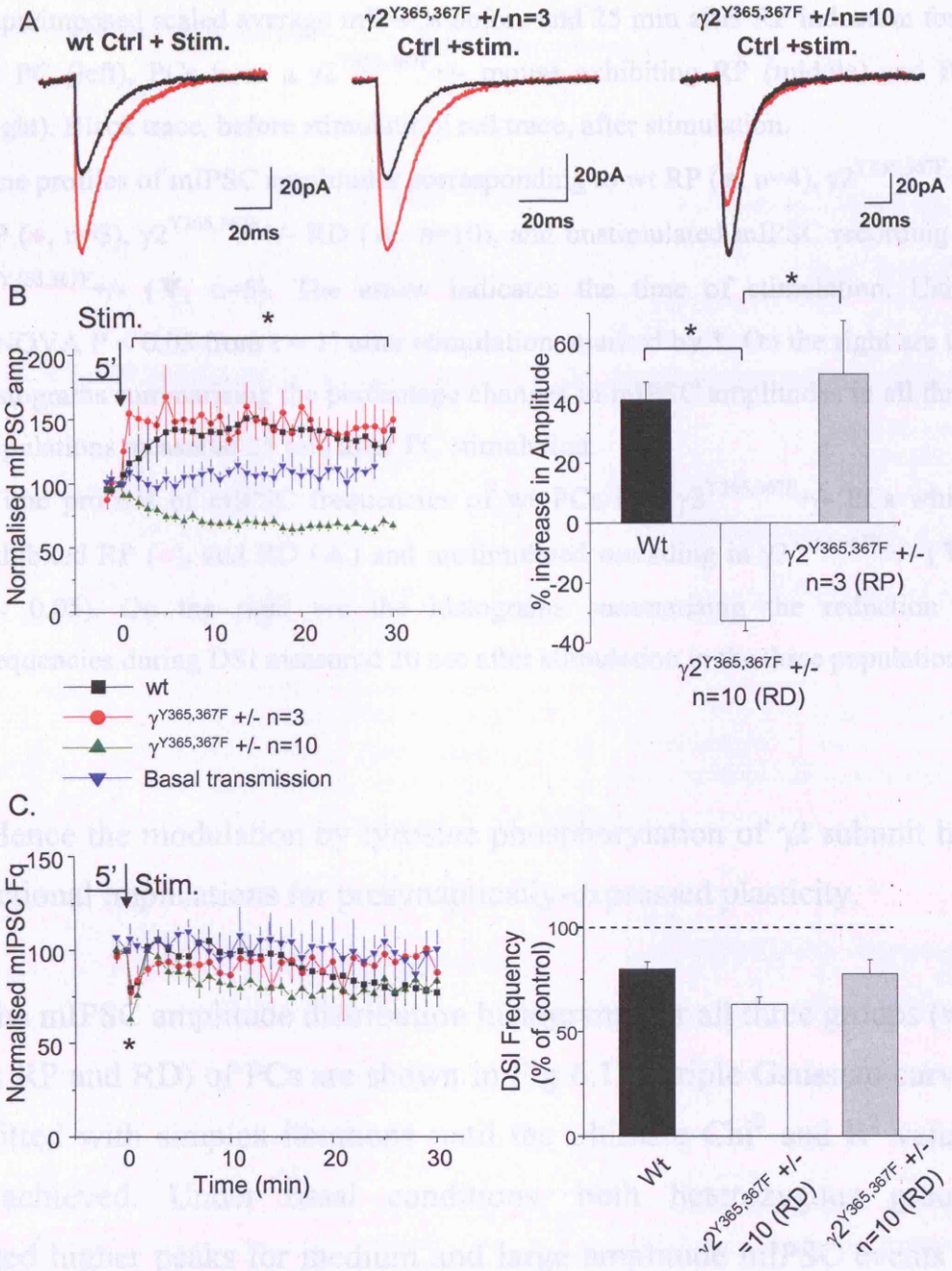
A
wt Ctrl + Stim.
γ2Y365,367F +/-n=3
Ctrl +stim.
γ2Y365,367F +/-n=10
Ctrl +stim.
20pA
20ms
20pA
20ms
20pA
20ms
B
Stim.
5'
*
Normalised mIPSC amp
200
150
100
50
0
0
10
20
30
wt
γY365,367F +/- n=3
γY365,367F +/- n=10
Basal transmission
*
*
% increase in Amplitude
60
40
20
0
-20
-40
Wt
γ2Y365,367F +/-
n=3 (RP)
γ2Y365,367F +/-
n=10 (RD)
C.
Normalised mIPSC Fq
150
100
50
0
5'
Stim.
*
0
10
20
30
Time (min)
DSI Frequency
(% of control)
100
50
0
Wt
γ2Y365,367F +/-
=10 (RD)
γ2Y365,367F +/-
n=10 (RD)

Fig 6.11 RP and DSI in $\gamma2^{Y365,367F}$+/- mice.

A). Superimposed scaled average mIPSCs before and 25 min after RP induction for a wt PC (left), PCs from a $\gamma2^{Y365,367F}$+/- mouse exhibiting RP (middle) and RD (right). Black trace, before stimulation; red trace, after stimulation.

B). Time profiles of mIPSC amplitudes corresponding to wt RP (■, n=4), $\gamma2^{Y365,367F}$+/- RP (●, n=3), $\gamma2^{Y365,367F}$+/- RD (▲, n=10), and unstimulated mIPSC recording in $\gamma2^{Y365,367F}$+/- (▼, n=5). The arrow indicates the time of stimulation. Using ANOVA $P < 0.05$ from t = 1' after stimulation, marked by *. On the right are the histograms summarising the percentage changes in mIPSC amplitudes in all three populations measured 25 min after PC stimulation.

C). Time profiles of mIPSC frequencies of wt PCs (■), $\gamma2^{Y365,367F}$+/- PCs which exhibited RP (●), and RD (▲) and unstimulated recording in $\gamma2^{Y365,367F}$+/- (▼* $P< 0.05$). On the right are the histograms summarising the reduction in frequencies during DSI measured 20 sec after stimulation in the three populations.

RD). Hence the modulation by tyrosine phosphorylation of γ2 subunit has no functional implications for presynaptically-expressed plasticity.

The mIPSC amplitude distribution histograms for all three groups (wt, mutant RP and RD) of PCs are shown in Fig 6.12. Triple Gaussian curves were fitted with simplex iterations until the ultimate Chi^2 and R^2 values were achieved. Under basal conditions, both heterozygous groups exhibited higher peaks for medium and large amplitude mIPSC events in comparison to the wt group (Fig 6.12). After stimulation, the peaks and width of the medium and large amplitude subpopulations in wt increased (to match that of the heterozygous in control conditions), accompanied

with a reduction in the frequency of small events. Intriguingly, the three populations of the heterozygous RP group

6.12

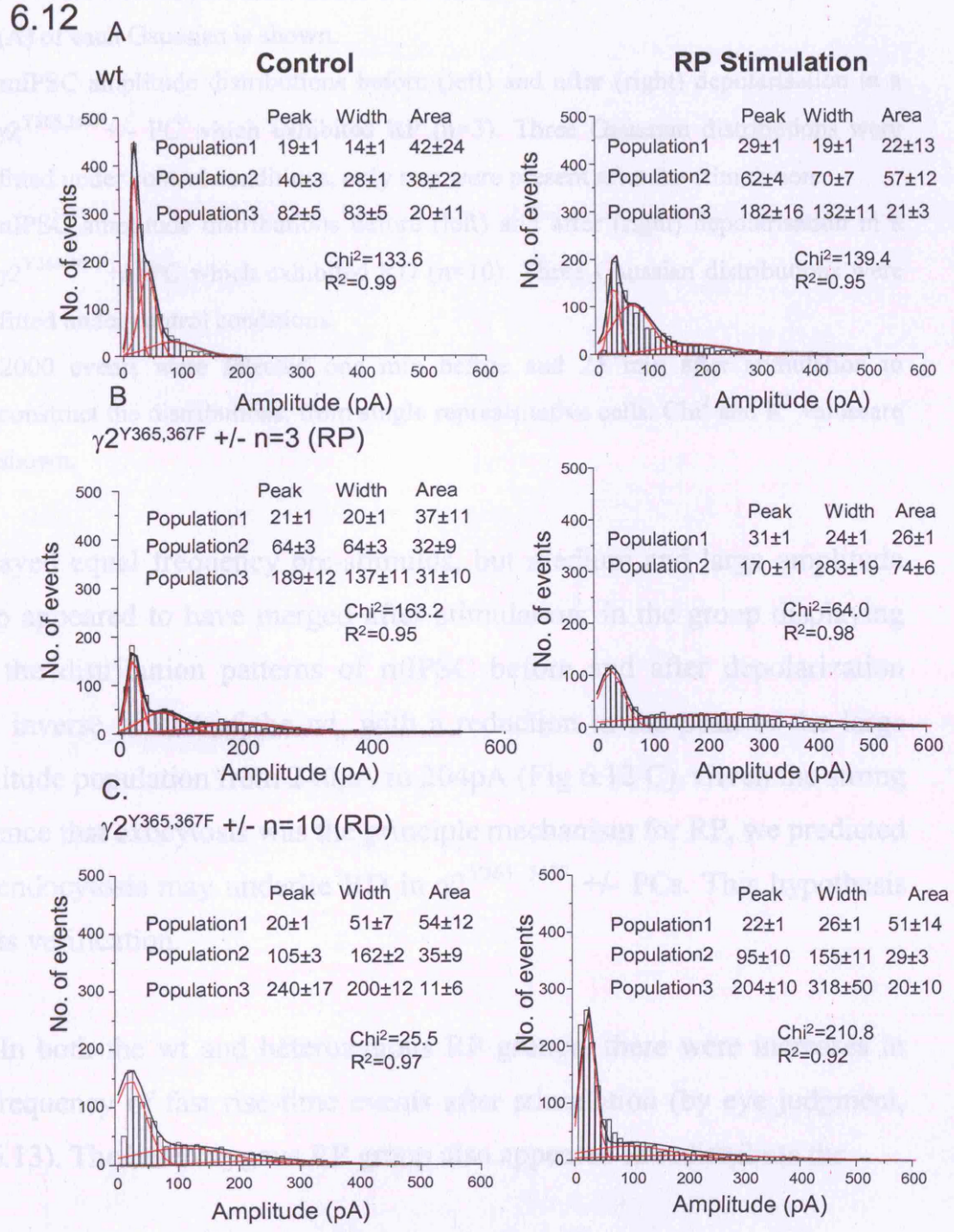

Fig 6.12 mIPSC amplitude distributions before and after stimulation in wt and $\gamma2^{Y365,367F}$+/- PCs.

A). mIPSC amplitude distributions before (left) and after (right) depolarisation in a wt PC. Three Gaussian distributions were fitted. The peak (P), width (W) and area (A) of each Gaussian is shown.

B). mIPSC amplitude distributions before (left) and after (right) depolarisation in a $\gamma2^{Y365,367F}$+/- PC which exhibited RP (n=3). Three Gaussian distributions were fitted under control conditions, only two were present after the stimulation.

C). mIPSC amplitude distributions before (left) and after (right) depolarisation in a $\gamma2^{Y365,367F}$+/- PC which exhibited RD (n=10). Three Gaussian distributions were fitted under control conditions.

~2000 events were selected one min before and 25 min after stimulation to construct the distributions, from single representative cells. Chi^2 and R^2 valuesare shown.

displayed equal frequency pre-stimulus, but medium and large amplitude group appeared to have merged after stimulation; in the group displaying RD, the distribution patterns of mIPSC before and after depolarization were inverse of that of the wt, with a reduction in the peak of the large amplitude population from 240pA to 204pA (Fig 6.12 C). Given the strong evidence that exocytosis was the principle mechanism for RP, we predicted that endocytosis may underlie RD in $\gamma2^{Y365,\ 367F}$ +/- PCs. This hypothesis awaits verification.

In both the wt and heterozygous RP groups, there were increases in the frequency of fast rise-time events after stimulation (by eye judgment, Fig 6.13). The heterozygous RP group also appeared to redistribute the

6.13

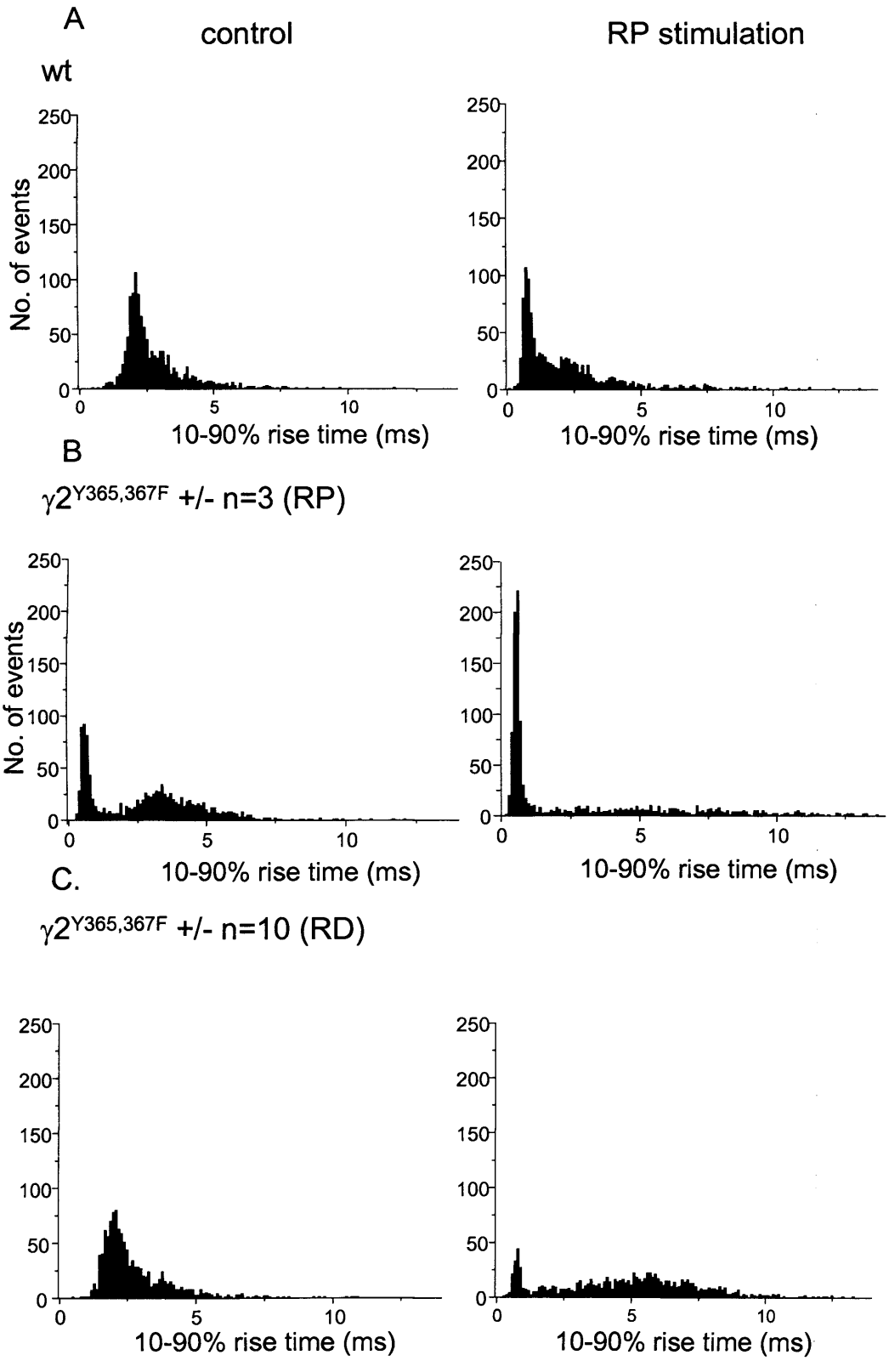
A
control
RP stimulation
wt
No. of events
250
200
150
100
50
0
0
5
10
10-90% rise time (ms)
B
γ2Y365,367F +/- n=3 (RP)
C.
γ2Y365,367F +/- n=10 (RD)

Fig 6.13 mIPSC rise-time (10~90%) distributions and after stimulation in wt, and $\gamma2^{Y365,367F}$+/- PCs.

A). mIPSC rise-time distributions, of mIPSC before (left) and after (right) depolarisation in a wt PC.

B). mIPSC rise-time distributions, of mIPSC before (left) and after (right) depolarisation in a $2^{Y365,367F}$+/- PC which exhibited RP (n=3).

C). mIPSC rise-time distributions, of mIPSC before (left) and after (right) depolarisation in a $\gamma2^{Y365,367F}$+/- PC which exhibited RD (n=10).

~2000 events were selected one min before and 25 min after stimulation to construct all the relationships, from single representative cells.

slower rise time events over a broader time-scale. In the heterozygous RD group, the slower population (peak of ~ 7ms) substantially exceeded the faster population (~1ms) after stimulation.

Scatter-plots of mIPSC amplitude *vs* rise time demonstrated a clear preferential increase in the frequency of fast rise time-large amplitude mIPSC events in wt and heterozygous RP groups after stimulation (Fig 6.14 A). The opposite was observed for $\gamma2^{Y365,\ 367F}$ +/- RD group, as the fast rise-time–large amplitude population was eclipsed by the slow rise time–small amplitude population after stimulation. This implies $\gamma2^{Y365,\ 367F}$ +/- RD may utilise reversal mechanisms from RP to achieve the reduction in synaptic strength.

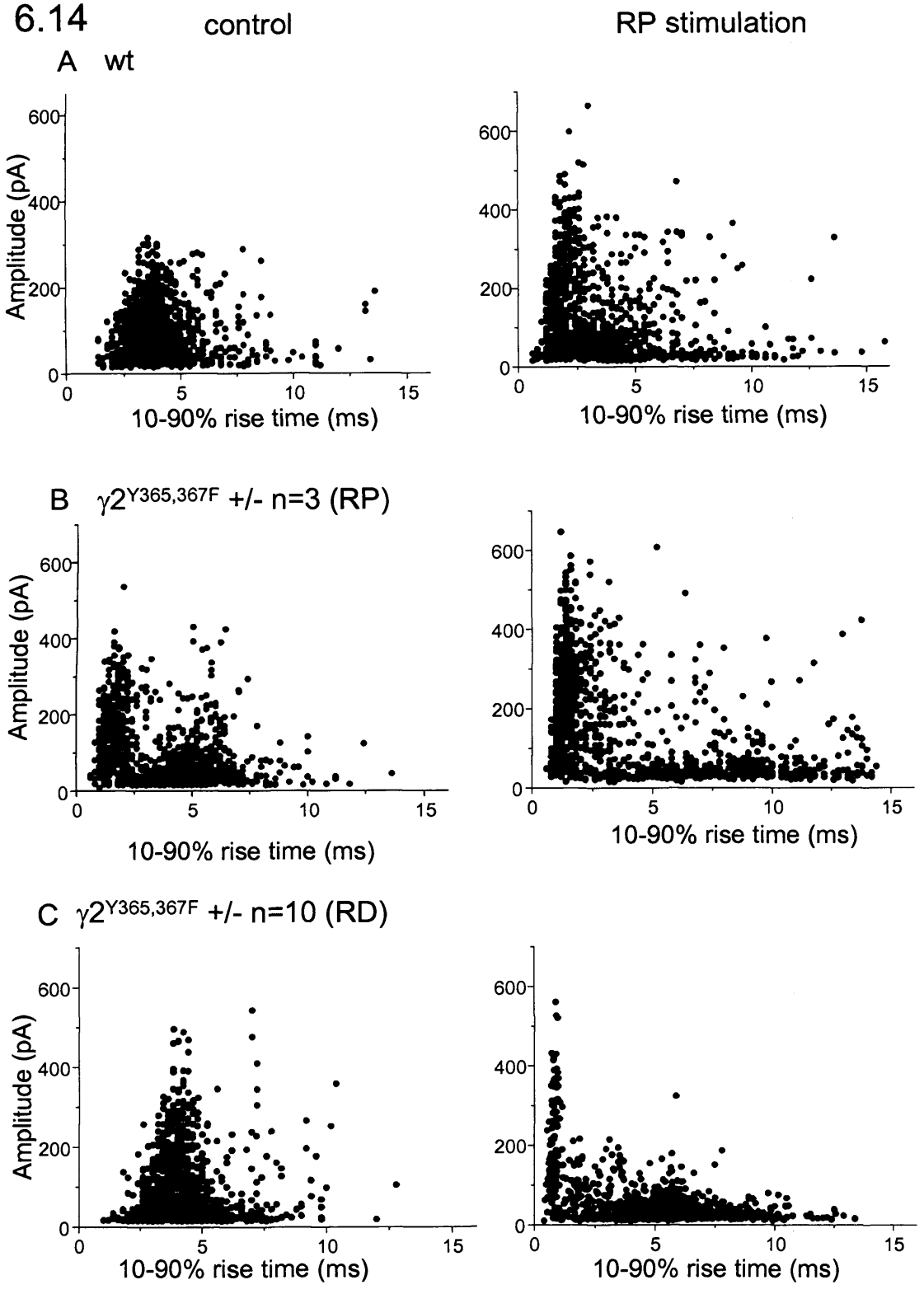
6.14
control
RP stimulation
A wt
Amplitude (pA)
10-90% rise time (ms)
B γ2Y365,367F +/- n=3 (RP)
C γ2Y365,367F +/- n=10 (RD)

Fig 6.14 Scatter-plots of mIPSC amplitude against rise-time before and after stimulation in wt, and $\gamma2^{Y365,367F}$+/- PCs.

A). mIPSC scatter-plots of amplitude *vs* rise-time before (left) and after (right) depolarisation in a wt PC.

B). mIPSC scatter-plots before (left) and after (right) depolarisation in a $\gamma2^{Y365,367F}$+/- PC which exhibited RP (n = 3).

C). mIPSC scatter-plots before (left) and after (right) depolarisation in a $\gamma2^{Y365,367F}$+/- PC which exhibited RD (n = 10).

~2000 events were selected one min before and 25 min after stimulation to construct all The relationships, from single representative cells.

Given that a change in the number of cell surface receptors is proposed to alter synaptic strength, the three groups were analysed using PS-NSNA (Fig 6.15) to test whether a reduction in N_p can account for the occurrence of RD. Under basal (unstimulated) conditions, $\gamma2^{Y365,\ 367F}$ +/- RD group exhibited an N_p value almost 3-fold higher than the wt group. The heterozygous RP group also displayed a 2-fold increase in N_p value compared to wt group (RD group 79.9 ± 13.4, RP group 43.6 ±3.3, wt 23.7 ±4.3, $P < 0.05$ ANOVA test, Table 6.2). After stimulation, wt-N_p increased to 51.2 ± 18.6 ($n = 4$, $P < 0.05$), while $\gamma2^{Y365,\ 367F}$ +/- (RD)-N_p decreased to 42.7 ± 8.4 ($n = 10$, $P < 0.05$), and the $\gamma2^{Y365,\ 367F}$ +/- RP group showed an increase from 43.6 ± 3.3 to 73.5 ± 5.9 ($n = 3$, $P < 0.05$; Table 6.2).

The higher basal N_p values in both $\gamma2^{Y365,\ 367F}$ +/- groups paralleled the increase in the surface staining of receptors from immunohistochemistrical study. Hence RP may have already occurred in $\gamma2^{Y365,\ 367F}$ +/- mice (*in vivo* RP), to occlude further potentiation. Of interest, stimulation of PCs under *in vivo* RP may then elicit an inverse regulation leading to internalisation

of receptors and thus RD. Hence these two tyrosine residues in the γ2 subunit may serve as critical factors for the trafficking of $GABA_A$Rs in response to stimuli.

6.15

wt
n = 4

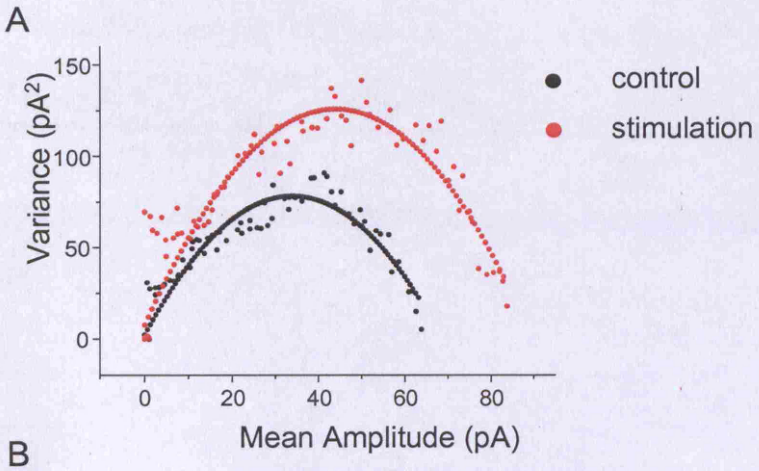

$\gamma 2^{Y365,367F}$ +/-
n=3 (RP)

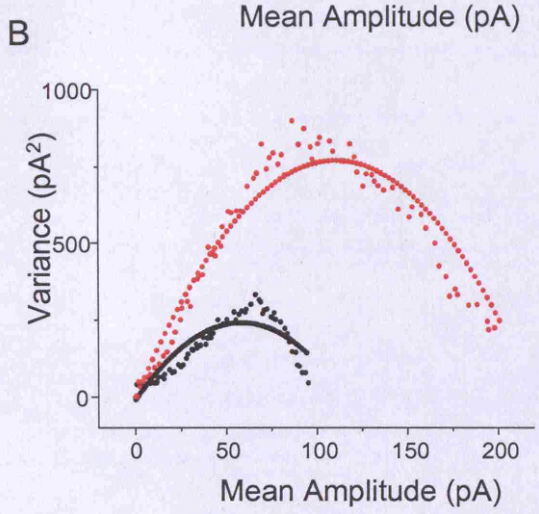

$\gamma 2^{Y365,367F}$ +/-
n=10 (RD)

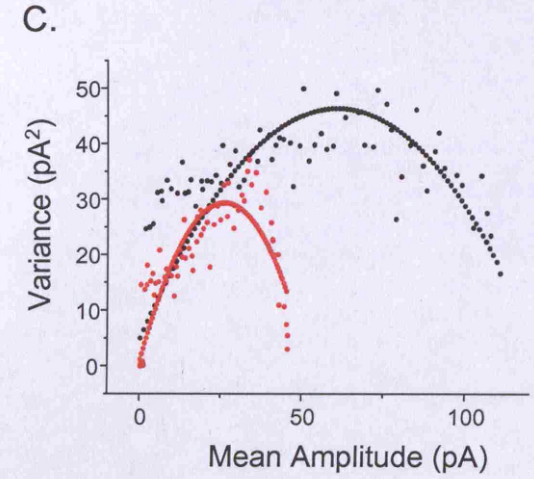

Fig 6.15 Peak-scaled non-stationary noise analysis of mIPSCs before and min after depolarising the wt and the $\gamma2^{Y365,367F}$+/- PCs.

A). mIPSC current variance against mean current amplitude before (black) and after (red) depolarisation in a wt PC. 100 consecutive single mIPSC events were taken from one min before and 25 min after stimulation, from a single representative cell, then selected, filtered and fitted using the peak scale method.

B). Current-variance plots before (black) and after (red) depolarisation in a PC exhibiting RP from a $\gamma2^{Y365,367F}$+/- slice.

C). Current-variance plots before (black) and after (red) depolarisation in a PC exhibiting RP from a $\gamma2^{Y365,367F}$+/- slice.

6.3 Discussion

6.3.1 Role of α1 subunits in inhibitory neurotransmission in PCs

In the first part of this chapter, we characterized the staining pattern of various $GABA_AR$ α and β subunits in the cerebellum. The paradoxical viability of α1 and β2 knockout mice contrasted with the lethality and serious epileptic seizures observed in β3 and γ2 knockout mice (Gunther et al., 1995; Homanics et al., 1997). This implies the occurrence of extensive compensatory mechanisms in the α1-/- and β2-/- mice. The expression of α1 and α3 subunits were both observed in wt PCs. The predominant α1 subunit staining covered the majority of the cell surface from soma to distal dendrites. α3 subunit staining was observed mainly on the dendrites. No compensatory upregulation of α3 or α5 subunits was seen in the α1-/- mice. If any such mechanisms were operative, they were most likely terminated in later generations of this transgenic line.

Curiously, α1-/- mice did not exhibit any miniature inhibitory synaptic currents, in agreement with previous reports of impairment of responses to exogenous GABA (Sur et al., 2001). The residual exogenous GABA currents noted in a proportion of PCs suggested the existence of α2/3 containing receptors or β2γ2 receptors, in response to high GABA concentration (1mM), as confirmed by a reduction in zolpidem mediated potentiation, but not chlordiazepoxide (Sur et al., 2001). Hence α1 subunits are indispensable for the clustering of functional postsynaptic $GABA_ARs$, and for mediating spontaneous inhibition in PCs. Although α2/3 subunits upregulation was thought to be maximal in the early generations, it only compensated for 55% of the total $GABA_ARs$ compared to wt. It was

thought the detrimental effect of retaining the predominantly embryonic α2/3 subunits during development forced this compensation to be annulled in later generations (Sur et al., 2001). One study identified increased tonic inhibition in cerebellar granule cells to balance the loss of phasic inhibition in α1-/- mice, by reducing $GABA_AR$ uptake transporter GAT-1 activity (Ortinski et al., 2006). This provides a novel compensatory mechanism of tonic inhibition substituting for phasic inhibition in order to restore neuronal homeostasis. Another compensatory solution may entail changes in membrane potential regulating ion channels to allow normal inhibition in the absence of α1 subunits. Identification of a transcriptional fingerprint, with cDNA microarray, revealed diverse adaptive transcriptional changes affecting inhibitory tone in α1-/- mice brains. Genes involved in neuronal plasticity in the α1-/- mice were the early growth response 1 (Egr1), small GTP binding protein Rac1 (Rac1), neurogranin (Nrgn), sodium channel ss 4 subunit (Scn4b), and potassium voltage-gated Kv4.2 channel (Kcnd2). Astrocytes Bergmann gila may also play an active role in adjusting the neuronal plasticity incurred by the deletion of the α1 subunit (Ponomarev et al., 2006).

6.3.2 The β2 subunit and its association with RP

The expression of β subunits was also examined in this study. β1/2/3 subunits expressions were observed in the wt. In the β2-/- mice, the mIPSC amplitude was reduced but not ablated. Zolpidem potentiation was less susceptible to β2 subunit deletion than α1 subunit, indicative of a mixed population of α1βxγ2 and α2/3βxγ2 receptors (x is most likely the β3 subunit). β1 subunit did not exhibit upregulation in the absence of β2 subunit, as confirmed by the lack of effect of the β1 subunit selective

inhibitor SCS. In accord with published studies, etomidate potentiation of the remaining mIPSCs in the β2-/- mice suggested that the principle β isoform mediating inhibition in the β2-/- mouse was the β3 subunit (Sur et al., 2001). Previous evidence also unveiled equivalent expressions of β2 and β3 subunits in PCs, which may account for the less drastic effect on mIPSCs of deleting β2 subunits, compared to the complete loss of mIPSCs in α1-/- mice (α1 being the predominant α isoform in the PC) (Fritschy and Mohler, 1995; Wisden et al., 1992). However, β3 subunit staining was not detected in the β2-/- mice in our studies, but difficulty in detecting β subunits immunofluorscence is common to many studies (Gutierrez et al., 1994d; Somogyi, 1989). Hence, we placed greater emphasis on complementary electrophysiological data to obviate the insufficient sensitivity in detecting β subunit expression on PCs by immunofluorescence.

The reduction in mIPSC amplitude in β2-/- mice was associated with the loss of fast rise-time events. These large amplitude miniature events are a unique characteristic of PCs owing to the presence of presynaptic ryanodine sensitive Ca^{2+} stores, orchestrating multivescular release of GABA onto the postsynaptic PCs (Llano et al., 2000). These ryanodine-sensitive stores are particularly enriched in the somatic basket cell terminals, innervating soma and proximal dendrites of PCs (Conti et al., 2004). They also govern PC mIPSC frequency in the absence of presynaptic firing (Galante and Marty, 2003). The disappearance of large amplitude fast rise-time events in the β2-/- animals, coupled with a reduction of mIPSC frequency, implies that basket cell inputs are particularly susceptible to the deletion of β2 subunit. Hence in wt animals,

basket cell-PC synapses may accommodate the majority of β2 subunit containing $GABA_A$Rs. Afferent dependent regulation of area-specific expression of $GABA_A$R α1 subunits has been demonstrated during development of the rat cortex, by thalamic inputs (Paysan et al., 1997). This raised the possibility that the expression of β2 and β3 subunits on the postsynaptic PCs may be specifically induced by basket cell and stellate cell inputs.

The β2 subunits were essential to the expression of RP, as RP was impaired in the β2-/- animals, with reduced magnitude and a shortened duration. The etomidate potentiation and ineffectiveness of SCS verified β3 as the sole β isoform mediating the mIPSCs in the β2-/- animal, thus the residual potentiation is manifested by the β3 subunit-containing receptors. The lack of effect of CaMKIINtide and genistein suggests that CaMKII and PTK have no functional importance to RP in the β2-/- PCs, phosphorylation and downstream effects of these kinases may be exclusive to β2 subunit-containing receptors in RP.

Compelling evidence suggested that phosphorylation of β3 subunits by various kinases has more profound functional consequences over β2 subunits (Brandon et al., 2000; Houston and Smart, 2006; Houston et al., 2007). One may then expect the β3 subunit-containing receptors to be better candidates for functional phosphorylation in RP than β2-subunit containing receptors. The paradoxical impairment of RP, and failure of CaMKIINtide and genistein to inhibit residual potentiation in β2-/- mice, where most inhibition was mediated by β3 subunit-containing receptors, may be a result of distinct subcellular protein kinase localizations. Despite

the prominent Ca^{2+} elevation induced by PC depolarisation in the distal dendrites of PCs (Kano et al., 1992), synapses at these locations may lack the machinery for sequestration CaMKII/PTK upon stimulation, or the kinases do not translocate to these distal sites for their actions to take place.

The preferential potentiation of the fast rise-time, basket cell inputs in wt animals after stimulation (also see chapter 3), taken together with the evidence presented in this chapter, suggest that RP might be an input specific synaptic plasticity, hence it is likely that specific subcellular targeting of $GABA_AR$ subunits may contribute to RP as well as the actual subunit composition present.

As RP is thought to involve an insertion of receptors into the membrane, it is of interest that $\beta 2$ subunit phosphorylation has been established to increase receptor numbers (Wan et al., 1997b). CaMKII has been described to phosphorylate of $\beta 2$ on Ser 410 (McDonald and Moss, 1997); PTK phosphorylation of $\beta 2$ subunits was also demonstrated in both HEK293 cells and neuronal cultures (Moss et al., 1995; Wan et al., 1997a). Whether RP relies on direct CaMKII phosphorylation of S410 on $\beta 2$ subunits, and/or PTK phoshphorylation of $\beta 2/\gamma 2$ subunits, is as yet unknown.

6.3.3 Mutation of two tyrosine residues on the γ2 subunit reverses the polarity of plasticity at IN-PC synapses

γ2 subunit is the predominant γ isoform expressed in PCs, with implications in the trafficking of $GABA_A$Rs. One major role is to increase the endocytotic capacity of $GABA_A$Rs, thereby regulating cell surface number (Connolly et al., 1999; Kittler et al., 2000; Kittler et al., 2008).

Tyrosine phosphorylation of γ2 subunits on adjacent residues Y365, Y367 can be unmasked upon the removal of tyrosine phosphatase activity by the inhibitor orthovanadate (Brandon et al., 2001), to enhance channel function by increasing the channel opening probability and prolonging the opening duration (Moss et al., 1995).

With the mutation of the two tyrosine residues in the γ2 subunits, the first prominent observation was a 50% increase in the mIPSC amplitude, presumably by an increase in receptor numbers as immunohistochemistry study suggested. PTK phosphorylation of Y365, Y367 suppresses the interaction between γ2 subunits and the μ2 subunits of the AP2 complex which instigates the clathrin-dependent removal of γ2 containing $GABA_A$Rs from synapses. In particular, the second tyrosine at position 367 is indispensable, as a part of a Yxxø type tyrosine motif $Y^{367}ECL^{370}$, to enable high affinity binding of γ2 subunits to AP2 (within the 30 amino acids on the AP2 carboxyl-terminal). Inhibition of this binding by dialysis of a γ2 YECL peptide resulted in enhancement the mIPSC amplitude by increasing number of surface receptors. Y367 and L370 form the basic chemical pocket interaction, while upstream Y365 conveys further binding

specificity with a third hydrophobic pocket, creating a highly stable 'three-pin-plug' conformation (Kittler et al., 2008). Src phosphorylation of either Y365, Y367 reduced AP2 binding, while phosphorylation of both ablated AP2 interaction with the γ2 subunit, thereby increasing surface $GABA_AR$ numbers, as also achieved by inhibition of tyrosine phosphatases with orthovanadate. Prior evidence has demonstrated that β3-AP2 binding has an additive effect on mIPSC enhancement when co-applied with γ2- YECL peptide. Similar to the γ2 binding to AP2, the β3-AP2 interaction is also negatively-regulated by phosphorylation at S408, S409.

The presence of two regulatory mechanisms of $GABA_AR$ internalisation via two separate subunits which converge at the level of subunit phosphorylation, providing multiple regulations of γ2 and/or β3 subunit containing receptors by different classes of kinases (serine/theronine and protein tyrosine kinases). As a consequence of the high binding affinity of γ2-AP2, and the prerequisite of γ2 subunits for most synaptic $GABA_ARs$, the γ2 subunits regulated mechanism may be a major determinant of surface $GABA_AR$ internalisation, whereas the β3 subunits mediated regulation will only affect the endocytosis of β3 subunit-containing receptors (Kittler et al., 2005; Kittler et al., 2008). The atypical AP2 binding motif, incorporating the serine phoshphorylation site, is present on the major ICL of all β subunits, potentially enabling phosphorylation-dependent interactions with AP2. In addition the β2 subunit also contains a unique AP2 binding di-leucine (LL at 343, 344) motif which initiates dynamin-dependent endocytosis of $GABA_AR$ (Herring et al., 2003). Hence, the majority of $GABA_ARs$ in PCs can potentially undergo multiple internalisation routes regulated by β and γ2

subunits, to govern the number of surface receptors on PCs, which may also dynamically control the polarity of synaptic plasticity.

In $\gamma2^{Y365,367F}$ +/- mice, an increase in surface numbers of receptors can be interpreted as a disruption in the binding of $\gamma2$ subunits to $\mu2$-AP2 due to the absence of the YECL motif in the $\gamma2$ subunits, leading to reduced endocytosis and accumulation of receptors on the surface. This implies that the inclusion of YECL-peptide in wt would effectively occlude RP. However, the appearance of RD suggests the existence of another separate mechanism. One explanation is that in heterozygous mice, the increase in surface receptor number has reached saturation, in effect expressing RP *in vivo*. Further stimulation may trigger a similar kinase cascade, to generate a trafficking signal that leads to a reversed modulation of inhibitory transmission, switching off *in vivo* RP to reset the synaptic strength. This *in vivo* RP was thought to be present in the GluRδ2 knockout mouse. GluRδ2 is a novel subunit of glutamate receptors, specifically expressed at PF-PC synapses. This strain of mice exhibited deficits in motor coordination and learning, in connection with the impairment of PF LTD. The enhanced CF activity characterised in these mice ultimately led to an increment in inhibitory transmission in PCs, i.e. *in vivo* RP (saturated). Further depolarisation failed to elicit RP in these animals, though they did not exhibit RD upon stimulation (Ohtsuki et al., 2004).

The mechanism of RD is unclear, although endocytosis may be a possibility. However, mIPSCs following RD induction exhibited different patterns of amplitude and rise-time distributions from control mIPSC events, which may imply different subcellular locations of $GABA_AR$

subtypes after RD modulation. This could also entail lateral movement of receptors in the plasma membrane, presumably away from the soma to more distal dendritic regions.

6.4 Conclusion

We have confirmed that in PCs, the presence of α1 subunits is obligatory for functional inhibitory neurotransmission, as established by previous studies (Sur et al., 2001). The manifestation of RP requires β2 subunits, which contain the for CaMKII target S410, with potential significance to the induction of RP. The γ2 subunits contain two tyrosine residues, which may determine the polarity of synaptic plasticity through the PTK activity. This provides a cross-link between β2 and γ2 subunits, emphasising their coordinated roles in RP. The precise mechanism of RD is still elusive, whether it is via lateral movement of receptors, or internalisation, is unknown. The two tyrosine residues in the γ2 subunits are directly involved in the regulation of surface receptor numbers of $GABA_AR$ on PCs, hence the PTK phosphorylation of Y365 and Y367 might act as trafficking regulators in response to upstream CaMKII activation. Further experimental verification is required to elucidate the specific role of S410 on β2 subunits and the understanding of phosphorylation and RP.

Chapter 7

General Discussion

7.1 Synaptic plasticity at Purkinje Cell synapses: the potential physiological role of RP in cerebellar function

As the principal neurons of the cerebellum, PCs output to the DCN neurons, utilising the inhibitory neurotransmitter GABA to code and convey information. They integrate vast amounts of input signals, transmitted from various synaptic contacts in the circuit and thus shape the firing pattern in DCN cells as stored memory traces. The precise conduction of coordinated behaviour is enabled by the capability of PCs to undergo plasticity at virtually every synapse, in response to global or focal stimuli.

PCs are sometimes considered as the 'side-loops' of the cerebellar circuit, arising from MFs as 'teaching signals' with regard to motor control. The purpose of the MF–PC 'side loops' was thought to detect abnormal neuronal firing as external feedback during erratic movements, to compare with the internal feedback signals that coded for the correct intended movement. By using feedback and feedforward control on descending motor centres, the neuronal circuit involving the PC intiates corrections of the aberrant movements. This is evident for parallel fibre LTD, where precisely timed firing of PFs and CFs suppressed excitatory transmission between PFs and PCs, modulating the gain of DCN cells to create a trace for motor learning (Hansel et al., 2001). PF LTD was considered to be reversible as the occurrence of postsynaptic PF LTP has

been identified (Lev-Ram et al., 2002; Salin et al., 1996). This restoration of synaptic strength creates capacity for regenerative memory storage. Mossy fibre-granule cell synapses, and CF-PC synapses can also undergo bidirectional plasticity, creating more upstream modification of PC outputs (Hansel et al., 2001). The CF-PC synapses, thought to be the strongest excitatory synapses in the CNS, exhibit homosynaptic LTD, upon simultaneous activation of inhibitory transmission from stellate cells, to reduce further Ca^{2+} influx (Callaway et al., 1995; Weber et al., 2003). This restrains the induction of further plasticity modifications and induces metaplasticity amongst PC synapses (Hansel and Linden, 2000).

By comparison, the plasticity of inhibitory transmission between interneurons and PCs may provide a more subtle tuning of the cerebellar circuit. RP and DPI will dampen the excitability of PCs and increase their firing intervals, effectively synergising with PF-LTD to disinhibit and increase the firing rate of DCN cells. In particular, RP may facilitate LTD and LTP at PC-DCN synapses, by increasing the amplitude of IPSCs (rebound depolarisation) as a trigger for plasticity at PC-DCN synapses (Aizenman et al., 1998). It is therefore likely that RP will shape the output of the cerebellum and contribute substantially to cerebellar functions such as correcting erratic motor behaviour.

In this study, we have uncovered new findings about rebound potentiation. Primarily, it is a $GABA_AR$ $\beta 2$ subunit-mediated long term potentiation of inhibitory synaptic transmission, between cerebellar interneurons and Purkinje cells. The manifestation of RP relies on both CaMKII and PTK activity, through downstream cell surface insertion of

postsynaptic $GABA_ARs$, to enhance the strength of inhibition at PCs, and shape the output of cerebellum, potentially influencing motor learning.

7.2 Regulation of inhibitory synaptic plasticities at cerebellar IN-PC synapses

Multiple array of heterosynaptically regulated inhibitory synaptic plasticities occurs between interneurons and PCs in response to CF stimulation (Duguid and Smart, 2004; Kano et al., 1992; Llano et al., 1991). Repetitive firing of CF triggers a potent depolarisation of PCs through the activation of AMPARs, resulting in an extensive Ca^{2+} transient. The origin of this initial Ca^{2+} current was thought to occur via VGCC followed by intracellular Ca^{2+} release, though recent evidence suggests the presence of the NMDAR NR2A and 2B subunits in 3 weeks old mouse PCs may mediate parts of the CF-EPSCs (Piochon et al., 2007; Renzi et al., 2007), which may contribute to this Ca^{2+} surge. Activation of postsynaptic mGluR1s elicit slow EPSCs and coincident Ca^{2+} currents in PCs, thus may add to Ca^{2+} entry to promote the expression of inhibitory plasticity (Hartmann and Konnerth, 2005; Jin et al., 2007; Netzeband and Gruol, 2008; Yuan et al., 2007). These mGluR1s may have a specific facilitatory role in RP, by counteracting the activation of $GABA_BR$, to downregulate the phophatase, PP1, hence promoting CaMKII activity (Sugiyama et al., 2008); however, another study reported that inhibition of postsynaptic mGluR1s did not influence RP induction (Duguid et al., 2007).

Subsequent to the PC Ca^{2+} elevation, various second messenger systems are activated to alter the strength of inhibitory transmission. DSI

and DPI are both presynaptically-expressed inhibitory plasticities, utilising retrograde messenger transmission between PCs and INs (Duguid and Smart, 2004; Glitsch et al., 2000). DSI is thought to entail Ca^{2+} dependent endocannabinoid production from postsynaptic PCs, crossing the synaptic cleft to activate the presynaptic CB1 receptors, resulting in a transient reduction in presynaptic GABA release (Diana et al., 2002; Kreitzer and Regehr, 2001). DPI is apparent after the cessation of DSI, causing a prolonged rebound increase in presynaptic GABA release far up to 20 min. DPI requires retrograde activation of presynaptic NMDARs on the interneurons, following Ca^{2+} dependent glutamate release from stimulated PCs. This NMDAR activation initiates the release of Ca^{2+} from presynaptic ryanodine-sensitive Ca^{2+} stores, thus enhancing exocytosis of GABA (Duguid and Smart, 2004).

Rebound potentiation was described as the long term potentiation of $GABA_AR$ responsiveness between INs and PCs (Kano et al., 1992; Kano et al., 1996). Its postsynaptic origin was reflected by the increment in mIPSC amplitudes, but not frequencies. RP is induced simultaneously with DSI and DPI, to achieve a synchronised net increase in inhibitory transmission onto PCs. The short duration of DSI (20 s ~1 min) coincides with the induction of RP. By transiently reducing GABA release, DSI minimises the activation of postsynaptic $GABA_BR$ to ensure the efficient onset of RP (Kawaguchi and Hirano, 2000). DPI occurs after the induction of RP, exceeding the time window for $GABA_BR$ mediated suppression. Hence DPI amplifies the sustained potentiation of inhibitory transmission by simultaneously increasing presynaptic GABA release to complement the RP-induced increase in postsynaptic responsiveness of $GABA_ARs$.

Curiously, using different stimulation latencies after forming the whole-cell configuration, the appearance of early RP and late RP emerged, separated by a transient depotentiation of mIPSCs. The source of the depotentiation is unidentified, though a disruption to kinases/phosphatases inside PCs, due to a 'wash-out' effect, may contribute to this. Another observation is that the time window of the depotentiation coincided with the switching time point between DSI and DPI (Duguid and Smart, 2004), further insinuating the coordination between pre- and postsynaptically expressed plasticity. To summarise, DSI, DPI and RP might be components of a complex plasticity resulting from the same CF signal, causing a profound potentiation of inhibition at PCs. The net outcome is expected to be a dis-inhibition of the cerebellar neuronal network and increased excitability of the output deep cerebellar nuclei cells.

7.3 Rebound potentiation: phosphorylation and trafficking

For over two decades, many studies have worked to identify the signalling cascades and mechanisms underlying the onset and maintenance of RP (Kano et al., 1996; Kawaguchi and Hirano, 2000). The prime cellular pathway resembled the kinase(CaMKII)/phosphatase(PP1) switch reported for hippocampal LTP in CA1 and CA3 neurons (Hedou and Mansuy, 2003; Lisman and Zhabotinsky, 2001). In the cerebellum, the adaptor protein DARPP-32 is postulated to be an intermediate protein to modulate the level of PP1 and CaMKII (Kawaguchi and Hirano, 2002). The present study focused on the downstream cellular events from CaMKII activation and the underlying mechanism of RP. Using a highly selective CaMKII peptide inhibitor, we discovered that CaMKII was required not just for the induction but also for the maintenance of RP. The binding of

CaMKII to $GABA_AR$ also appeared to be crucial for RP, although whether this is an intermediate step for subsequent events such as structural changes of GABARAP, or direct receptor phosphorylation affecting $GABA_AR$ channel function, remain unresolved.

A direct role for protein tyrosine kinases in RP was also identified for the first time in this study, working in conjunction with CaMKII activity. Inhibiting either kinase completely ablated late RP, reflecting a degree of functional convergence. Intriguingly, enhancing either kinase individually with selective phosphatase antagonists, while inhibiting the other kinase, led to complete reinstatement of RP. In particular, the protein tyrosine phosphatase (PTP) inhibitor, sodium orthovanadate, restored the depotentiation between early and late RP, observed with the 12' stimulation latency protocol. Orthovanadate also enhanced basal mIPSC amplitudes, reflecting a high level of endogenous PTP activity in PCs. These experiments suggested the availability of multiple signalling pathways for RP induction. A dominating pathway may be operative under normal conditions, inhibition of this major pathway could compel the PC to employ a secondary cascade, which is normally dormant, and only manifest by inhibition of phosphatase activity. Following previous reports on CaMKII induced PTK phosphorylation of $GABA_AR$ $\gamma 2$ subunits (Houston et al., 2007), we also discovered that the downstream PTK activity could result from αCaMKII activity in PCs, as RP-like enhancement of mIPSCs by direct injection of preactivated αCaMKII was reversed by PTK inhibition with genistein. This led to the conclusion that PTK activity may have a more direct role on the induction of RP. The interaction between CaMKII, PTK and RP expression was further explored

with transgenic mice, to dissect the significance of each $GABA_AR$ subunit and their phospho-residues.

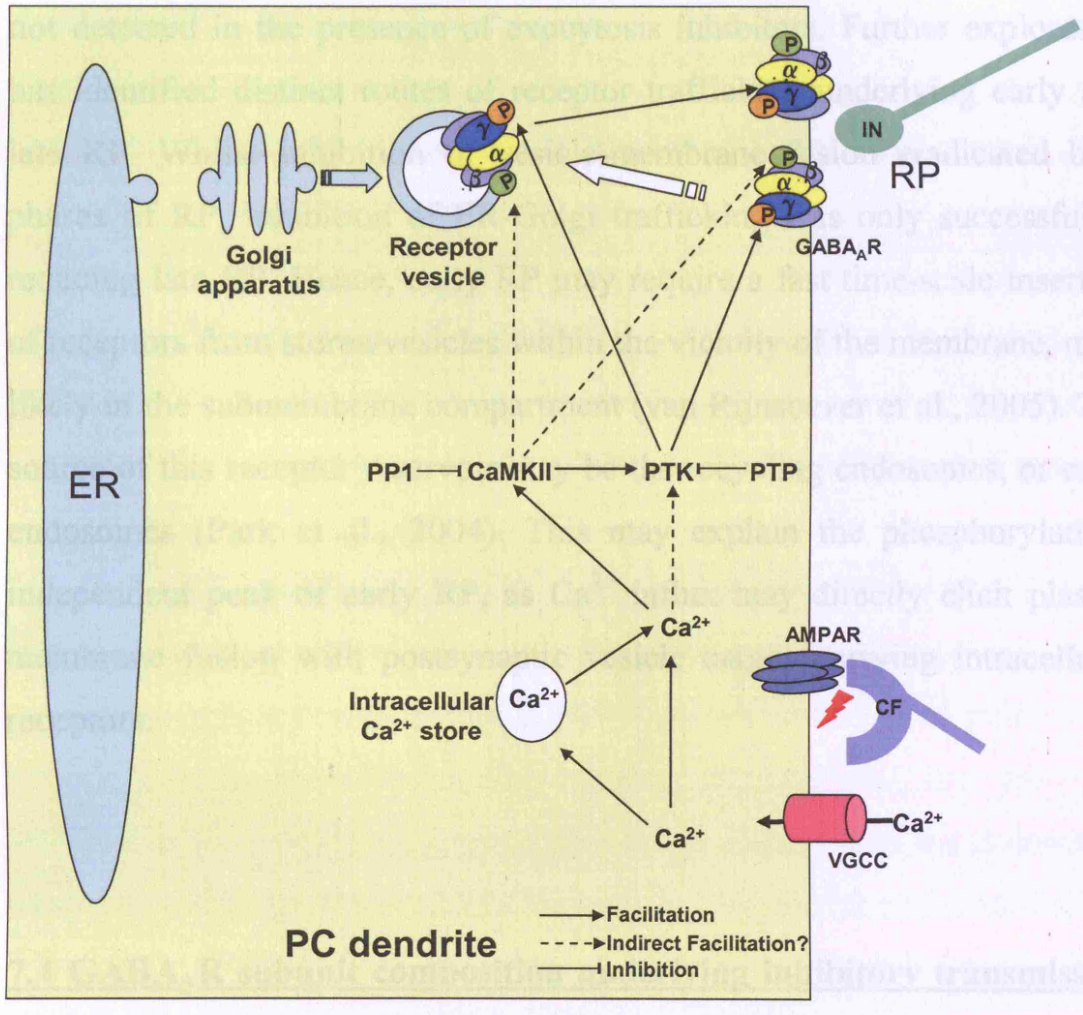

7.1 Schematic diagram of the manifestation of RP constructed from our data.
Upon Ca^{2+} entry and Ca^{2+} intracellular release, both CaMKII and PTK are recruited; PTK activity is putatively downstream of CaMKII. This may result in the phosphorylation of β2S410 by CaMKII, or γ2Y365, 367 by PTK to enhance $GABA_AR$ channel function. CaMKII and PTK activity are suppressed by endogenous PP1 and PTP. Intracellular trafficking vesicles are also recruited by the RP induced CaMKII/PTK signal, to deliver $GABA_AR$ to inhibitory synapses from ER/Golgi network, or from recycling endosomes to increase the number of surface receptors and enhance inhibition.

Evidence from our study supports postsynaptic receptor insertion as the key mechanism underlying RP expression. In agreement with these data, PS-NSNA also indicated an increase in N_p in control RP, which was not detected in the presence of exocytosis inhibitors. Further exploration has identified distinct routes of receptor trafficking underlying early and late RP. Whilst inhibition of vesicle-membrane fusion eradicated both phases of RP, inhibition of ER-Golgi trafficking was only successful in reducing late RP. Hence, early RP may require a fast time-scale insertion of receptors from stores/vesicles within the vicinity of the membrane, most likely in the submembrane compartment (van Rijnsoever et al., 2005). The source of this receptor reservoir may be the recycling endosomes, or early endosomes (Park et al., 2004). This may explain the phosphorylation-independent peak of early RP, as Ca^{2+} influx may directly elicit plasma membrane fusion with postsynaptic vesicle cargos carrying intracellular receptors.

7.4 $GABA_AR$ subunit composition underlying inhibitory transmission and RP in PCs

In agreement with previously work (Sur et al., 2001), inhibitory transmission was substantially lost in either α1 or β2 knockout mice. mIPSCs were completely absent from PCs of α1-/- mice without obvious consequence for the viability of the mice, indicating the presence of extensive compensatory mechanisms. This adaptation process may entail the reorganisation of the entire neuronal circuit, rather than upregulation of other $GABA_AR$ α isoforms to replace the synaptic α1 subunit-containing

receptors. For example, enhanced tonic inhibition is apparent in α1-/- cerebellar granules cells (Ortinski et al., 2006). An increase in shunt inhibition and changes in membrane potential could raise the threshold of firing and rewire neuronal network activity in order to adapt to the loss of phasic inhibition (Ortinski et al., 2006). A loss of β2 subunits was not as catastrophic to phasic inhibition as the deletion of the α1-/- subunit gene, suggesting that β3 subunits may compensate for the absence of β2 subunits, and carry part of the phasic inhibition in wt animals. However, β3 subunit-containing receptors exhibited an impaired RP, reflecting either a difference in their susceptibility to modulation by protein kinases, or distinct synaptic locations from β2 subunit containing receptor subtypes.

Our data revealed a consistent population specific enhancement of mIPSC events in RP, with particular emphasis on the fast rise-time (somatodendritic) events, over the slower events arising from more distal dendritic locations. Fluorescence imaging demonstrated that the Ca^{2+} transient subsequent to PC depolarisation was global, with distal dendritic sites displaying a more profound increase in Ca^{2+} than the somatic regions (Kano et al., 1992). Thus the subdued RP in distal dendrites cannot be a result of an insufficient Ca^{2+} transient. One significant difference between the somatic and dendritic segments of PCs, is that they are innervated by basket cells and stellate cells, respectively. Basket cells are enriched with ryanodine-sensitive Ca^{2+} stores, capable of orchestrating multivesicular transmitter release evoking large amplitude mIPSCs in PCs with fast onset (Conti et al., 2004). The biased potentiation of large amplitude fast rise-time mIPSCs, suggested that basket cell inputs are preferentially enhanced, raising the prospect that RP is input specific. Further evidence from β2-/-

mice implied differential subcellular distribution of receptor subtypes, with the β2 and β3 subunit-containing receptors localised at proximal basket cell and distal stellate cell inputs, respectively. Hence, the inability of β3 containing receptors to undergo RP may be explained by differences in the exocytotic machinery at somatic and dendritic synapses of PCs. Regardless of the presence of the β2 subunits, β3 subunit expression on the soma is rarely seen, possibly due to the failure of the β3 subunits to associate with somatic exocytotic apparatus. In addition, β3 subunit interactions with NSF and AP2, both cause a decreased surface expression of β3 subunits by promoting endocytosis (Goto et al., 2005; Kittler et al., 2000).

The sustained late phase RP appeared to require ER-Golgi trafficking, from perinuclear sites where newly synthesed receptors are assembled and sorted into specific vesicles. Immunofluorescence of the β3 subunits was detected mainly as intracellular aggregates. ER retention of the β3 subunit-containing receptors may be the reason behind their inability to express RP, although published reports suggested accessibility of β3 subunits to the membrane surface is significantly greater than that of β2 subunits in Madin-Darby canin kidney (MDCK) cells (Connolly et al., 1996). The 4 amino acids, glycine 171, lysine 173, glutamate 179, and arginine 180 in the β2 subunits serve as retention signals, which prevent homo-oligomerized β2 subunits from exiting the ER; on the other hand, the β3 homomers were detected at the cell surface with spontaneous gating properties (Connolly et al., 1996; Taylor et al., 1999; Wooltorton et al., 1997). Once the trafficking limitation was removed upon binary assembly formation with α1 subunits, α1β1, α1β2, α1β3 displayed differential distribution (unaffected by the presence of γ2 subunits): α1β1 exhibited

non-polarisation immunofluorscence; $\alpha 1\beta 2$ were targeted to the basolateral surface of MDCK cells, analogous to the somatodendritic membrane of neurons; $\alpha 1\beta 3$ were preferentially detected in the apical surface (5 hours after transfection), bearing resemblance to the axonal membranes of neurons. However, within 24 hours after the initial detection of $\alpha 1\beta 3$, the immunofluorscence migrated to the basolateral surface through possible transcytosis (Connolly et al., 1996). Using this paradigm, newly recruited $\beta 3$ subunit-containing receptors may be initially targeted to the axonal surfaces. Hence, in synaptic inhibition or RP they may have a limited role. Over time that exceeds our recording duration, $\beta 3$ subunit-containing receptors may transcytose to synaptic sites and then participate in the late phase of RP.

By contrast to the β subunits, the $\gamma 2$ subunit appears to have a 'housekeeping' role in RP. Its function may be to act as a downstream regulator of $GABA_AR$ exocytosis, in response to numerous signals, such as RP, or dephosphorylation, to recruit AP2 to surface $GABA_ARs$ (Kittler et al., 2008). The identification of the two near-adjacent tyrosine residues, with affinity for PTK phosphorylation, revealed a $\gamma 2$ subunit-dependent modulation of $GABA_AR$ function (Brandon et al., 2001; Houston et al., 2007; Moss et al., 1995). Phosphorylation of these two residues increased the opening probability of $GABA_AR$ channels; interfered with the recruitment of AP2 to the synaptic receptors and subsequent clathrin-dependent endocytosis, thereby stabilizing surface receptors (Kittler et al., 2008). Reduced endocytosis may account for the increase in surface receptor numbers and mIPSC amplitude observed in the $\gamma 2^{Y365,367F}$ +/- mice. Increments in surface receptor numbers appeared to occlude the

expression of RP, whilst revealing a new form of plasticity, rebound depression, using the same depolarisation protocol that induced RP in wt animals. It appears that tyrosine phosphorylation of the γ2 subunits provides a bidirectional switch to inhibitory synaptic plasticity. Previous work also identified pre-existing RP in mice lacking the GluRδ2 subunit (Ohtsuki et al., 2004). Although RD has not yet been described in normal physiological systems, the reversibility of RP may serve to help store synaptic memory transiently, and provide regenerative storage for new neuronal memory. Consequently, it is plausible to speculate, under physiological conditions, that RD could be elicited with a second depolarisation stimuli to cells with maximal RP, to reset the inhibition level, in a similar fashion to the bidirectional control of excitatory plasticity in cerebellum and other brain structures (Hansel et al., 2001; Lev-Ram et al., 2002; Lisman, 1989).

7.5 Future directions: is RP input specific? Is direct CaMKII-phosphorylation of β2 S410 required for RP? What is the role of early endosomes

Many questions remain to be addressed with further experiments. Particularly, the input specificity of RP can be studied using paired recordings to selectively stimulate a single presynaptic interneuron (evoked IPSC) to exam how subcellular synaptic location affects the extent of RP. Basket cell-PC and stellate cell-PC paired recordings will allow comparison between somatic and distal synapses and their responses to RP induction. According to the preliminary data presented here, it is likely that the basket cell evoked IPSCs will exhibit a more profound potentiation over the stellate cell evoked IPSCs by PC depolarisation.

The data gathered so far inferred that the role of β2 subunits in RP may be concerned with the CaMKII phosphorylation site within the major ICL, S410 (McDonald and Moss, 1994). Mutation of this residue to an alanine will prevent the CaMKII phosphorylation. Using lenti-viral vectors (Torashima et al., 2006), this mutant β2S410A can be transfected into the β2-/- mice *in vivo*, to compare with wt β2 subunit-transfected β2-/- slices. These experiments can be conducted to elucidate the importance of this residue, as phosphorylation of β2 subunit has been reported to recruit $GABA_A$Rs to the membrane surface (Wan et al., 1997a; Wan et al., 1997b).

Thirdly, we established early RP does not entail ER-Golgi trafficking, potentially implicating a faster route such as the recycling endosomes. Selective disruption of the recycling pathways can be achieved by overexpression of mutant GTPase Rab11a-S25N, or the mutant Rme1-G429R (Park et al., 2004). These experiments will also benefit our understanding of early RP, but require lenti viral *in vivo* transfection of neuron for the expression of mutant proteins.

Reference

Aguayo,L.G., Espinoza,F., Kunos,G., and Satin,L.S. (1998). Effects of intracellularcalcium on $GABA_A$ receptors in mouse cortical neurons. Pflugers Archiv-European Journal of Physiology *435*, 382-387.

Aizenman,C.D., Manis,P.B., and Linden,D.J. (1998). Polarity of long-term synaptic gain change is related to postsynaptic spike firing at a cerebellar inhibitory synapse. Neuron *21*, 827-835.

Akiyama,T., Ishida,J., Nakagawa,S., Ogawara,H., Watanabe,S., Itoh,N., Shibuya,M., and Fukami,Y. (1987). Genistein, A Specific Inhibitor of Tyrosine-Specific Protein-Kinases. Journal of Biological Chemistry *262*, 5592-5595.

Alger,B.E., Pitler,T.A., Wagner,J.J., Martin,L.A., Morishita,W., Kirov,S.A., and Lenz,R.A. (1996). Retrograde signalling in depolarization-induced suppression of inhibition in rat hippocampal CA1 cells. Journal of Physiology-London *496*, 197-209.

Alldred,M.J., Mulder-Rosi,J., Lingenfelter,S.E., Chen,G., and Luscher,B. (2005). Distinct $\gamma 2$ subunit domains mediate clustering and synaptic function of postsynaptic $GABA_A$ receptors and gephyrin. Journal of Neuroscience. *25*, 594-603.

Amin,J. and Weiss,D.S. (1993). $GABA_A$ receptor needs two homologous domains of the β-subunit for activation by GABA but not by pentobarbital. Nature *366*, 565-569.

Angelotti,T.P. and MacDonald,R.L. (1993). Assembly of $GABA_A$ receptor subunits: α_1 β_1 and α_1 β_1 γ_{2S} subunits produce unique ion channels with dissimilar single- channel properties. Journal of Neuroscience. *13*, 1429-1440.

Armstrong,C.L. and Hawkes,R. (2000). Pattern formation in the cerebellar cortex. Biochemistry and Cell Biology-Biochimie et Biologie Cellulaire *78*, 551-562.

Auger,C., Kondo,S., and Marty,A. (1998). Multivesicular release at single functional synaptic sites in cerebellar stellate and basket cells. Journal of Neuroscience. *18*, 4532-4547.

Baer,K., Essrich,C., Benson,J.A., Benke,D., Bluethmann,H., Fritschy,J.M., and Luscher,B. (1999). Postsynaptic clustering of γ-aminobutyric acid type A receptors by the γ3 subunit *in vivo*. Proc.Natl.Acad.Sci.U.S.A *96*, 12860-12865.

Barnard,E.A., Skolnick,P., Olsen,R.W., Mohler,H., Sieghart,W., Biggio,G., Braestrup,C., Bateson,A.N., and Langer,S.Z. (1998). International Union of Pharmacology. XV. Subtypes of gamma-aminobutyric acid($_A$) receptors: Classification on the basis of subunit structure and receptor function. Pharmacological Reviews *50*, 291-313.

Barnard,E.A., Darlison,M.G., and Seeburg,P. (1987). Molecular biology of $GABA_A$ receptor: the receptor/channel superfamily. TINS *10*, 502-509.

Barr,J.R., Moura,H., Boyer,A.E., Woolfitt,A.R., Kalb,S.R., Pavlopoulos,A., McWilliams,L.G., Schmidt,J.G., Martinez,R.A., and Ashley,D.L. (2005). Botulinum neurotoxin detection and differentiation by mass spectrometry. Emerging Infectious Diseases *11*, 1578-1583.

Batchelor,A.M., Madge,D.J., and Garthwaite,J. (1994). Synaptic Activation of Metabotropic Glutamate Receptors in the Parallel Fiber-Purkinje Cell Pathway in Rat Cerebellar Slices. Neuroscience *63*, 911-915.

Bedford,F.K., Kittler,J.T., Muller,E., Thomas,P., Uren,J.M., Merlo,D., Wisden,W., Triller,A., Smart,T.G., and Moss,S.J. (2001). $GABA_A$ receptor cell surface number and subunit stability are regulated by the ubiquitin-like protein Plic-1. Nature Neuroscience. *4*, 908-916.

Belmeguenai,A. and Hansel,C. (2005). A role for protein phosphatases 1, 2A, and 2B in cerebellar long-term potentiation. Journal of Neuroscience *25*, 10768-10772.

Ben Ari,Y. (2002). Excitatory actions of GABA during development: the nature of the nurture. Nature Review Neuroscience. *3*, 728-739.

Bergersen,L., Ruiz,A., Bjaalie,J.G., Kullmann,D.M., and Gundersen,V. (2003). GABA and $GABA_A$ receptors at hippocampal mossy fibre synapses. European Journal of Neuroscience. *18*, 931-941.

Bialojan,C. and Takai,A. (1988). Inhibitory Effect of A Marine-Sponge Toxin, Okadaic Acid, on Protein Phosphatases - Specificity and Kinetics. Biochemical Journal *256*, 283-290.

Bier,M., Kits,K.S., and Borst,J.G. (1996). Relation between rise times and amplitudes of GABAergic postsynaptic currents. Journal of Neurophysiology. *75*, 1008-1012.

Boileau,A.J., Pearce,R.A., and Czajkowski,C. (2005). Tandem subunits effectively constrain $GABA_A$ receptor stoichiometry and recapitulate receptor kinetics but are insensitive to $GABA_A$ receptor-associated protein. Journal of Neuroscience. *25*, 11219-11230.

Bonnert,T.P., McKernan,R.M., Farrar,S., Le Bourdelles,B., Heavens,R.P., Smith,D.W., Hewson,L., Rigby,M.R., Sirinathsinghji,D.J., Brown,N., Wafford,K.A., and Whiting,P.J. (1999). ρ, a novel γ-aminobutyric acid type A receptor subunit. Proc.Natl.Acad.Sci.U.S.A *96*, 9891-9896.

Bormann,J. (2000). The 'ABC' of GABA receptors. Trends in Pharmacological Science *21*, 16-19.

Boxall,A.R. (2000). GABAergic mIPSCs in rat cerebellar purkinje cells are modulated by TrkB and mGluR1-mediated stimulation of Src. Journal of Physiology *524 Pt 3*, 677-684.

Boxall,A.R.& Marty,A. (1997) A critical time-window for the potentiation of synaptic GABA responses in rat cerebellar Purkinje cells. *Society for Neuroscience abstract* **23,** 2006.

Brandon,N.J., Jovanovic,J.N., Colledge,M., Kittler,J.T., Brandon,J.M., Scott,J.D., and Moss,S.J. (2003). A-kinase anchoring protein 79/150 facilitates the phosphorylation of $GABA_A$ receptors by cAMP-dependent protein kinase via selective interaction with receptor beta subunits. Molecule and Cell Neuroscience. *22*, 87-97.

Brandon,N.J., Jovanovic,J.N., Smart,T.G., and Moss,S.J. (2002a). Receptor for activated C kinase-1 facilitates protein kinase C-dependent phosphorylation and functional modulation of $GABA_A$ receptors with the activation of G-protein-coupled receptors. Journal of Neuroscience *22*, 6353-6361.

Brandon,N., Jovanovic,J., and Moss,S. (2002b). Multiple roles of protein kinases in the modulation of g-aminobutyric $acid_A$ receptor function and cell surface expression. Pharmacology and Therapeutics. *94*, 113-122.

Brandon,N.J., Delmas,P., Hill,J., Smart,T.G., and Moss,S.J. (2001). Constitutive tyrosine phosphorylation of the $GABA_A$ receptor gamma 2 subunit in rat brain. Neuropharmacology *41*, 745-752.

Brandon,N.J., Delmas,P., Kittler,J.T., McDonald,B.J., Sieghart,W., Brown,D.A., Smart,T.G., and Moss,S.J. (2000). $GABA_A$ receptor phosphorylation and functional modulation in cortical neurons by a protein kinase C-dependent pathway. Journal of Biological Chemistry *275*, 38856-38862.

Brandon,N.J., Uren,J.M., Kittler,J.T., Wang,H., Olsen,R., Parker,P.J., and Moss,S.J. (1999). Subunit-specific association of protein kinase C and the receptor for activated C kinase with GABA type A receptors. Journal of Neuroscience. *19*, 9228-9234.

Brenowitz,S.D., Best,A.R., and Regehr,W.G. (2006). Sustained elevation of dendritic calcium evokes widespread endocannabinoid release and suppression of synapses onto cerebellar Purkinje cells. Journal of Neuroscience *26*, 6841-6850.

Brickley,S.G., Cull-Candy,S.G., and Farrant,M. (1999). Single-channel properties of synaptic and extrasynaptic $GABA_A$ receptors suggest differential targeting of receptor subtypes. Journal of Neuroscience. *19*, 2960-2973.

Brown,T.C., Correia,S.S., Petrok,C.N., and Esteban,J.A. (2007). Functional compartmentalization of endosomal trafficking for the synaptic delivery of AMPA receptors during long-term potentiation. Journal of Neuroscience *27*, 13311-13315.

Brunig,I., Scotti,E., Sidler,C., and Fritschy,J.M. (2002a). Intact sorting, targeting, and clustering of g-aminobutyric $acid_A$ receptor subtypes in hippocampal neurons in vitro. Journal of Comparative Neurology *443*, 43-55.

Brunig,I., Suter,A., Knuesel,I., Luscher,B., and Fritschy,J.M. (2002b). GABAergic terminals are required for postsynaptic clustering of dystrophin but not of $GABA_A$ receptors and gephyrin. Journal of Neuroscience *22*, 4805-4813.

Brunig,I., Penschuck,S., Berninger,B., Benson,J., and Fritschy,J.M. (2001). BDNF reduces miniature inhibitory postsynaptic currents by rapid

downregulation of $GABA_A$ receptor surface expression. European Journal of Neuroscience *13*, 1320-1328.

Brussaard,A.B., Kits,K.S., Baker,R.E., Willems,W.P.A., Leyting-Vermeulen,J.W., Voorn,P., Smit,A.B., Bicknell,R.J., and Herbison,A.E. (1997). Plasticity in fast synaptic inhibition of adult oxytocin neurons caused by switch in $GABA_A$ receptor subunit expression. Neuron *19*, 1103-1114.

Bureau,M. and Olsen,R.W. (1990). Multiple Distinct Subunits of the Gamma-Aminobutyric Acid-A Receptor Protein Show Different Ligand-Binding Affinities. Molecular Pharmacology *37*, 497-502.

Callaway,J.C., Lasserross,N., and Ross,W.N. (1995). IPSPs Strongly Inhibit Climbing Fiber-Activated $[Ca^{2+}]$, Increases in the Dendrites of Cerebellar Purkinje Neurons. Journal of Neuroscience *15*, 2777-2787.

Caraiscos,V.B., Elliott,E.M., You,T., Cheng,V.Y., Belelli,D., Newell,J.G., Jackson,M.F., Lambert,J.J., Rosahl,T.W., Wafford,K.A., MacDonald,J.F., and Orser,B.A. (2004). Tonic inhibition in mouse hippocampal CA1 pyramidal neurons is mediated by $\alpha 5$ subunit-containing g-aminobutyric acid type A receptors. Proc.Natl.Acad.Sci.U.S.A *101*, 3662-3667.

Chandra,D., Korpi,E.R., Miralles,C.P., De Blas,A.L., and Homanics,G.E. (2005). $GABA(_A)$ receptor gamma(2) subunit knockdown mice have enhanced anxiety-like behaviour but unaltered hypnotic response to benzodiazepines. Bmc Neuroscience *6,* 1141-1153.

Chang,B.H., Mukherji,S., and Soderling,T.R. (2001). Calcium/calmodulin-dependent protein kinase II inhibitor protein: Localization of isoforms in rat brain. Neuroscience *102*, 767-777.

Chang,B.H., Mukherji,S., and Soderling,T.R. (1998). Characterization of a calmodulin kinase II inhibitor protein in brain. Proc.Natl.Acad.Sci.U.S.A *95*, 10890-10895.

Chardin,P. and McCormick,F. (1999). Brefeldin A: the advantage of being uncompetitive. Cell *97*, 153-155.

Charych,E.I., Yu,W., Miralles,C.P., Serwanski,D.R., Li,X., Rubio,M., and De Blas,A.L. (2004). The brefeldin A-inhibited GDP/GTP exchange factor

2, a protein involved in vesicular trafficking, interacts with the beta subunits of the GABA receptors. Journal of Neurochemistry. *90*, 173-189.

Chen,L., Wang,H., Vicini,S., and Olsen,R.W. (2000). the γ-aminobutyric acid type A ($GABA_A$) receptor- associated protein (GABARAP) promotes $GABA_A$ receptor clustering and modulates the channel kinetics. Proc.Natl.Acad.Sci.U.S.A *97*, 11557-11562.

Chen,Z.W. and Olsen,R.W. (2007). $GABA_A$ receptor associated proteins: a key factor regulating $GABA_A$ receptor function. Journal of Neurochemistry *100*, 279-294.

Chen,Z.W., Chang,C.S., Leil,T.A., Olcese,R., and Olsen,R.W. (2005). $GABA_A$ receptor-associated protein regulates $GABA_A$ receptor cell-surface number in *Xenopus laevis* oocytes. Molecular Pharmacology *68*, 152-159.

Cheng,Q. and Yeh,H.H. (2005). PLCγ signaling underlies BDNF potentiation of Purkinje cell responses to GABA. Journal of Neuroscience Research *79*, 616-627.

Cheng,Q. and Yeh,H.H. (2003). Brain-derived neurotrophic factor attenuates mouse cerebellar granule cell $GABA_A$ receptor-mediated responses via postsynaptic mechanisms. Journal of Physiology-London *548*, 711-721.

Christie,S.B., Miralles,C.P., and De Blas,A.L. (2002). GABAergic innervation organizes synaptic and extrasynaptic $GABA_A$ receptor clustering in cultured hippocampal neurons. Journal of Neuroscience. *22*, 684-697.

Churn,S.B. and DeLorenzo,R.J. (1998). Modulation of GABAergic receptor binding by activation of calcium and calmodulin-dependent kinase II membrane phosphorylation. Brain Research. *809*, 68-76.

Cinar,H. and Barnes,E.M., Jr. (2001). Clathrin-independent endocytosis of $GABA_A$ receptors in HEK 293 cells. Biochemistry *40*, 14030-14036.

Connolly,C.N., Kittler,J.T., Thomas,P., Uren,J.M., Brandon,N.J., Smart,T.G., and Moss,S.J. (1999a). Cell surface stability of γ-aminobutyric acid type A receptors. Dependence on protein kinase C activity and subunit composition. Journal of Biological Chemistry *274*, 36565-36572.

Connolly,C.N., Uren,J.M., Thomas,P., Gorrie,G.H., Gibson,A., Smart,T.G., and Moss,S.J. (1999b). Subcellular localization and endocytosis of homomeric gamma2 subunit splice variants of gamma-aminobutyric acid type A receptors. Molecular and Cell Neuroscience *13*, 259-271.

Connolly,C.N., Wooltorton,J.R., Smart,T.G., and Moss,S.J. (1996). Subcellular localization of gamma-aminobutyric acid type A receptors is determined by receptor beta subunits. Proc.Natl.Acad.Sci.U.S.A *93*, 9899-9904.

Conti,R., Tan,Y.P., and Llano,I. (2004). Action potential-evoked and ryanodine-sensitive spontaneous Ca^{2+} transients at the presynaptic terminal of a developing CNS inhibitory synapse. Journal of Neuroscience. *24*, 6946-6957.

Coyle,J.E., Qamar,S., Rajashankar,K.R., and Nikolov,D.B. (2002). Structure of GABARAP in two conformations: Implications for $GABA_A$ receptor localization and tubulin binding. Neuron *33*, 63-74.

Danglot,L., Triller,A., and Bessis,A. (2003). Association of gephyrin with synaptic and extrasynaptic $GABA_A$ receptors varies during development in cultured hippocampal neurons. Molecular and Cell Neuroscience *23*, 264-278.

Daniel,H., Levenes,C., and Crepel,F. (1998). Cellular mechanisms of cerebellar LTD. TINS. *21*, 401-407.

De Koninck,Y. and Mody,I. (1994). Noise analysis of miniature IPSCs in adult rat brain slices: properties and modulation of synaptic $GABA_A$ receptor channels. Journal of Neurophysiology *71*, 1318-1335.

Diana,M.A., Levenes,C., Mackie,K., and Marty,A. (2002). Short-term retrograde inhibition of GABAergic synaptic currents in rat Purkinje cells is mediated by endogenous cannabinoids. Journal of Neuroscience. *22*, 200-208.

Dino,M.R., Schuerger,R.J., Liu,Y.B., Slater,N.T., and Mugnaini,E. (2000). Unipolar brush cell: A potential feedforward excitatory interneuron of the cerebellum. Neuroscience *98*, 625-636.

Drew,C.A., J.G.A.R.W.R.P. (1984). Bicuculline-insensitive GABA receptors: studies on the binding of baclofen to rat cerebellar membranes. Neuroscience Letters *52*, 317-321.

Drexler,B., Roether,C.L., Jurd,R., Rudolph,U., and Antkowiak,B. (2005). Opposing actions of etomidate on cortical theta oscillations are mediated by different gamma-aminobutyric acid type A receptor subtypes. Anesthesiology *102*, 346-352.

Duguid,I.C., Pankratov,Y., Moss,G.W., and Smart,T.G. (2007). Somatodendritic release of glutamate regulates synaptic inhibition in cerebellar Purkinje cells via autocrine mGluR1 activation. Journal of Neuroscience. *27*, 12464-12474.

Duguid,I.C. and Smart,T.G. (2004). Retrograde activation of presynaptic NMDA receptors enhances GABA release at cerebellar interneuron-Purkinje cell synapses. Nature Neuroscience. *7*, 525-533.

Dutar,P. and Nicoll,R.A. (1988). A Physiological-Role for $GABA_B$ Receptors in the Central Nervous-System. Nature *332*, 156-158.

Eccles,J.C., Llinas,R., and Sasaki,K. (1966). Intracellularly Recorded Responses of Cerebellar Purkinje Cells. Experimental Brain Research *1*, 161-168.

Edgerton,J.R. and Reinhart,P.H. (2003). Distinct contributions of small and large conductance Ca^{2+}-activated K^+ channels to rat Purkinje neuron function. Journal of Physiology-London *548*, 53-69.

Edwards,F.A., Konnerth,A., Sakmann,B., and Busch,C. (1990). Quantal Analysis of Inhibitory Synaptic Transmission in the Dentate Gyrus of Rat Hippocampal Slices - A Patch-Clamp Study. Journal of Physiology-London *430*, 213-249.

Enslen,H. and Soderling,T.R. (1994). Roles of Calmodulin-Dependent Protein-Kinases and Phosphatase in Calcium-Dependent Transcription of Immediate-Early Genes. Journal of Biological Chemistry *269*, 20872-20877.

Essrich,C., Lorez,M., Benson,J.A., Fritschy,J.M., and Luscher,B. (1998). Postsynaptic clustering of major $GABA_A$ receptor subtypes requires the $\gamma 2$ subunit and gephyrin. Nature Neuroscience *1*, 563-571.

Everitt,A.B., Luu,T., Cromer,B., Tierney,M.L., Birnir,B., Olsen,R.W., and Gage,P.W. (2004). Conductance of recombinant $GABA_A$ channels is increased in cells co-expressing $GABA_A$ receptor-associated protein. Journal of Biological Chemistry *279*, 21701-21706.

Faber,D.S., Young,W.S., Legendre,P., and Korn,H. (1992). Intrinsic Quantal Variability Due to Stochastic Properties of Receptor-Transmitter Interactions. Science *258*, 1494-1498.

Farrant,M. and Nusser,Z. (2005). Variations on an inhibitory theme: phasic and tonic activation of GABAA receptors. Nature Review Neuroscience. *6*, 215-229.

Fierro,L. and Llano,I. (1996). High endogenous calcium buffering in Purkinje cells from rat cerebellar slices. Journal of Physiology-London *496*, 617-625.

Fritschy,J.-M. and Mohler,H. (1995). $GABA_A$ receptor heterogeneity in the adult rat brain: differential regional and cellular distribution of seven major subunits. Journal of Comparative Neurology *359*, 154-194.

Fritschy,J.M., Benke,D., Mertens,S., Oertel,W.H., Bachi,T., and Mohler,H. (1992). Five subtypes of type A γ-aminobutyric acid receptors identified in neurons by double and triple immunofluorescence staining with subunit-specific antibodies . Proc.Natl.Acad.Sci.U.S.A. Aug 1;*89(15)*:6726-30.

Fuentes,C.T. and Bastian,A.J. (2007). 'Motor cognition' - what is it and is the cerebellum involved? Cerebellum *6*, 232-236.

Fukunaga,K., Muller,D., and Miyamoto,E. (1996). CaM kinase II in long-term potentiation. Neurochemistry International *28*, 343-358.

Fukunaga, K. (1993). The role of Ca^{2+}/calmodulin-dependent protein kinase II in the cellular signal transduction. Nippon Yakurigaku Zasshi. *102(6),* 355-369

Gaiarsa,J.L., Caillard,O., and Ben Ari,Y. (2002). Long-term plasticity at GABAergic and glycinergic synapses: mechanisms and functional significance. TINS. *25*, 564-570.

Galante,M. and Marty,A. (2003). Presynaptic ryanodine-sensitive calcium stores contribute to evoked neurotransmitter release at the basket cell-Purkinje cell synapse. Journal of Neuroscience. *3*, 11229-11234.

Ghez C (1991) The cerebellum, in Principles of Neural Science, 3rd edition, edited by Kandel ER, Schwartz JH. Elsevier, pp 626–646

Giese,K.P., Fedorov,N.B., Filipkowski,R.K., and Silva,A.J. (1998). Autophosphorylation at Thr286 of the alpha calcium-calmodulin kinase II in LTP and learning. Science *279*, 870-873.

Glickstein,M. (2007). What does the cerebellum really do? Current Biology *17*, R824-R827.

Glitsch,M., Parra,P., and Llano,I. (2000). The retrograde inhibition of IPSCs in rat cerebellar Purkinje cells is highly sensitive to intracellular Ca^{2+}. European Journal of Neuroscience *12*, 987-993.

Goto,H., Terunuma,M., Kanematsu,T., Misumi,Y., Moss,S.J., and Hirata,M. (2005). Direct interaction of N-ethylmaleimide-sensitive factor with $GABA_A$ receptor beta subunits. Molecular and Cell Neuroscience *30*, 197-206.

Grosche,J., Kettenmann,H., and Reichenbach,A. (2002). Bergmann glial cells form distinct morphological structures to interact with cerebellar neurons. Journal of Neuroscience Research *68*, 138-149.

Grosshans,B.L., Ortiz,D., and Novick,P. (2006). Rabs and their effectors: Achieving specificity in membrane traffic. Proc.Natl.Acad.Sci.U.S.A *103*, 11821-11827.

Gunther,U., Benson,J., Benke,D., Fritschy,J.M., Reyes,G., Knoflach,F., Crestani,F., Aguzzi,A., Arigoni,M., and Lang,Y. (1995). Benzodiazepine-insensitive mice generated by targeted disruption of the γ_2 subunit gene of γ-aminobutyric acid type A receptors. Proc.Natl.Acad.Sci.U.S.A *92*, 7749-7753.

Gutierrez,A., Khan,Z.U., and Deblas,A.L. (1994). Immunocytochemical Localization of Gamma-(2) Short and Gamma-(2) Long Subunits of the $GABA(_A)$ Receptor in the Rat-Brain. Journal of Neuroscience *14*, 7168-7179.

Haines,D.E. (1997) Fundamental neuroscience 1st edition Edinburgh, Churchill Livingstone.

Hansel,C., de Jeu,M., Belmeguenai,A., Houtman,S.H., Buitendijk,G.H.S., Andreev,D., De Zeeuw,C.I., and Elgersma,Y. (2006). alpha CaMKII is essential for cerebellar LTD and motor learning. Neuron *51*, 835-843.

Hansel,C. (2005). When the B-team runs plasticity: GluR2 receptor trafficking in cerebellar long-term potentiation. Proc.Natl.Acad.Sci.U.S.A. *102*, 18245-18246.

Hansel,C., Linden,D.J., and D'Angelo,E. (2001). Beyond parallel fiber LTD: the diversity of synaptic and nonsynaptic plasticity in the cerebellum. Nature Neuroscience *4*, 467-475.

Hansel,C. and Linden,D.J. (2000). Long-term depression of the cerebellar climbing fiber-Purkinje neuron synapse. Neuron *26*, 473-482.

Hanson,P.I. and Schulman,H. (1992). Inhibitory Autophosphorylation of Multifunctional Ca^{2+} Calmodulin-Dependent Protein-Kinase Analyzed by Site-Directed Mutagenesis. Journal of Biological Chemistry *267*, 17216-17224.

Hartmann,J. and Konnerth,A. (2005). Determinants of postsynaptic Ca^{2+} signaling in Purkinje neurons. Cell Calcium *37*, 459-466.

Harvey,R.J., Morando,L., Rasetti,R., and Strata,P. (2005). Spontaneous electrical activity and dendritic spine size in mature cerebellar Purkinje cells. European Journal of Neuroscience *21*, 1777-1784.

Harvey,V.L., Duguid,I.C., Krasel,C., and Stephens,G.J. (2006). Evidence that GABA ρ subunits contribute to functional ionotropic GABA receptors in mouse cerebellar Purkinje cells. Journal of Physiology *577*, 127-139.

Hashimoto,T., Ishii,T., and Ohmori,H. (1996). Release of Ca^{2+} is the crucial step for the potentiation of IPSCs in the cultured cerebellar Purjinke cells of the rat. Journal of Physiology *497*, 611-627.

Hashimoto,Y., Schworer,C.M., Colbran,R.J., and Soderling,T.R. (1987). Autophosphorylation of Ca^{2+}-Calmodulin-Dependent Protein Kinase-Ii - Effects on Total and Ca^{2+}-Independent Activities and Kinetic-Parameters. Journal of Biological Chemistry *262*, 8051-8055.

Hayashi,Y., Shi,S.H., Esteban,J.A., Piccini,A., Poncer,J.C., and Malinow,R. (2000). Driving AMPA receptors into synapses by LTP and CaMKII: Requirement for GluR1 and PDZ domain interaction. Science *287*, 2262-2267.

Hedou,G. and Mansuy,I.M. (2003). Inducible molecular switches for the study of long-term potentiation. Philosophical Transactions of the Royal Society of London Series B-Biological Sciences *358*, 797-804.

Herring,D., Huang,R., Singh,M., Robinson,L.C., Dillon,G.H., and Leidenheimer,N.J. (2003). Constitutive $GABA_A$ receptor endocytosis is dynamin-mediated and dependent on a dileucine AP2 adaptin-binding motif within the $\beta 2$ subunit of the receptor. Journal of Biological Chemistry *278*, 24046-24052.

Heynen,A.J., Quinlan,E.M., Bae,D.C., and Bear,M.F. (2000). Bidirectional, activity-dependent regulation of glutamate receptors in the adult hippocampus in vivo. Neuron *28*, 527-536.

Homanics,G.E., DeLorey,T.M., Firestone,L.L., Quinlan,J.J., Handforth,A., Harrison,N.L., Krasowski,M.D., Rick,C.E., Korpi,E.R., Makela,R., Brilliant,M.H., Hagiwara,N., Ferguson,C., Snyder,K., and Olsen,R.W. (1997). Mice devoid of γ-aminobutyrate type A receptor $\beta 3$ subunit have epilepsy, cleft palate, and hypersensitive behavior. Proc.Natl.Acad.Sci.U.S.A *94*, 4143-4148.

Houston,C.M., Lee,H.H.C., Hosie,A.M., Moss,S.J., and Smart,T.G. (2007). Identification of the Sites for CaMK-II-dependent Phosphorylation of $GABA_A$ Receptors. Journal of Biological Chemistry *282*, 17855-17865.

Houston,C.M. and Smart,T.G. (2006). CaMK-II modulation of $GABA_A$ receptors expressed in HEK293, NG108-15 and rat cerebellar granule neurons. European Journal of Neuroscience *24*, 2504-2514.

Hudmon,A. and Schulman,H. (2002). Neuronal Ca^{2+}/calmodulin-dependent protein kinase II: The role of structure and autoregulation in cellular function. Annual Review of Biochemistry *71*, 473-510.

Isaac,J.T.R., Ashby,M., and Mcbain,C.J. (2007). The role of the GluR2 subunit in AMPA receptor function and synaptic plasticity. Neuron *54*, 859-871.

Ito,M., (2001). Cerebellar plasticity. Encyclopedia of Life sciences. pp1-8

Jalilian Tehrani,M.H. and Barnes,E.M.Jr. Sequestration of γ-aminobutyric acid$_A$ receptors on Clathrin-coated vesicles during chronic benzodiazepine administration *in vivo*. Journal of Pharmacology and Experimental Therapeutics 283, 384-390. 1997.

Jiang,J.X., Suppiramaniam,V., and Wooten,M.W. (2006). Posttranslational modifications and receptor-associated proteins in AMPA receptor trafficking and synaptic plasticity. Neurosignals *15*, 266-282.

Jin,Y.J., Kim,S.J., Kim,J., Worley,P.F., and Linden,D.J. (2007). Long-term depression of mGluR1 signaling. Neuron *55*, 277-287.

Johnson,J., Bierle,B.M., Gallicano,G.I., and Capco,D.G. (1998). Calcium/calmodulin-dependent kinase II and calmodulin: Regulators of the meiotic spindle in mouse eggs. Molecular Biology of the Cell *9*, 437A.

Jones,A., Korpi,E.R., McKernan,R.M., Pelz,R., Nusser,Z., Makela,R., Mellor,J.R., Pollard,S., Bahn,S., Stephenson,F.A., Randall,A.D., Sieghart,W., Somogyi,P., Smith,A.J., and Wisden,W. (1997). Ligand-gated ion channel subunit partnerships: GABA$_A$ receptor α_6 subunit gene inactivation inhibits delta subunit expression. Journal of Neuroscience. *17*, 1350-1362.

Jones,M.V. and Westbrook,G.L. (1997). Shaping of IPSCs by endogenous calcineurin activity. Journal of Neuroscience. *17*, 7626-7633.

Jones,M.V. and Westbrook,G.L. (1995). Desensitized states prolong GABA$_A$ channel responses to brief agonist pulses. Neuron *15*, 181-191.

Jovanovic,J.N., Thomas,P., Kittler,J.T., Smart,T.G., and Moss,S.J. (2004). Brain-derived neurotrophic factor modulates fast synaptic inhibition by regulating GABA$_A$ receptor phosphorylation, activity, and cell-surface stability. Journal of Neuroscience. *24*, 522-530.

Kakegawa,W. and Yuzaki,M. (2005). A mechanism underlying AMPA receptor trafficking during cerebellar long-term potentiation. Proc.Natl. Acad.Sci.U.S.A.*102*, 17846-17851.

Kanematsu,T., Fujii,M., Mizokami,A., Kittler,J.T., Nabekura,J., Moss,S.J., and Hirata,M. (2007). Phospholipase C-related inactive protein is implicated in the constitutive internalization of GABA$_A$ receptors mediated by clathrin and AP2 adaptor complex. Journal of Neurochemistry *101*, 898-905.

Kano,M., Kano,M., Fukunaga,K., and Konnerth,A. (1996). Ca^{2+}-induced rebound potentiation of γ-aminobutyric acid-mediated currents requires activation of Ca^{2+}/calmodulin-dependent kinase II. Proc.Natl.Acad.Sci.U.S.A *93*, 13351-13356.

Kano,M. and Konnerth,A. (1992). Potentiation of GABA-mediated currents by cAMP-dependent protein kinase. NeuroReport *3*, 563-566.

Kapur,J. and MacDonald,R.L. (1996). Cyclic AMP-dependent protein kinase enhances hippocampal dentate granule cell $GABA_A$ receptor currents. Journal of Neurophysiology. *76*, 2626-2634.

Kawaguchi,S.Y. and Hirano,T. (2007). Sustained Structural Change of $GABA_A$ Receptor-Associated Protein Underlies Long-Term Potentiation at Inhibitory Synapses on a Cerebellar Purkinje Neuron. Journal of Neuroscience *27*, 6788-6799.

Kawaguchi,S.Y. and Hirano,T. (2006). Integrin alpha3beta1 suppresses long-term potentiation at inhibitory synapses on the cerebellar Purkinje neuron. Molecular Cell Neuroscience *31*, 416-426

Kawaguchi,S. and Hirano,T. (2002). Signaling cascade regulating long-term potentiation of $GABA_A$ receptor responsiveness in cerebellar Purkinje neurons. Journal of Neuroscience *22*, 3969-3976.

Kawaguchi,S. and Hirano,T. (2000). Suppression of inhibitory synaptic potentiation by presynaptic activity through postsynaptic $GABA_B$ receptors in a Purkinje neuron. Neuron *27*, 339-347.

Kellenberger,S., Malherbe,P., and Sigel,E. (1992). Function of the α1 β2 γ2S γ-aminobutyric acid type A receptor is modulated by protein kinase C via multiple phosphorylation sites. Journal of Biological Chemistry. *267*, 25660-25663.

Keller,C.A., Yuan,X., Panzanelli,P., Martin,M.L., Alldred,M., Sassoe-Pognetto,M., and Luscher,B. (2004). The γ2 subunit of $GABA_A$ receptors is a substrate for palmitoylation by GODZ. Journal of Neuroscience. *24*, 5881-5891.

Khaliq,Z.M. and Raman,I.M. (2005). Axonal propagation of simple and complex spikes in cerebellar Purkinje neurons. Journal of Neuroscience *25*, 454-463.

Khan,Z.U., Gutierrez,A., and De Blas,A.L. (1996a). The α_1 and α_6 subunits can coexist in the same cerebellar $GABA_A$ receptor maintaining their individual benzodiazepine-binding specificities [published erratum appears in J Neurochem 1996 May;66(5):2221]. Journal of Neurochemistry. *66*, 685-691.

Khan,Z.U., Gutierrez,A., Miralles,C.P., and De Blas,A.L. (1996b). The γ subunits of the native $GABA_A$/ benzodiazepine receptors. Neurochemical Research 147-159.

Kirsch,J., Langosch,D., Prior,P., Littauer,U.Z., Schmitt,B., and Betz,H. (1991). The 93-kDa glycine receptor-associated protein binds to tubulin. Jounral of Biological Chemistry. *266*, 22242-22245.

Kitazawa,S. and Wolpert,D.M. (2005). Rhythmicity, randomness and synchrony in climbing fiber signals. TINS *28*, 611-619.

Kittler,J.T., Chen,G., Kukhtina,V., Vahedi-Faridi,A., Gu,Z.L., Tretter,V., Smith,K.R., McAinsh,K., Arancibia-Carcamo,I.L., Saenger,W., Haucke,V., Yan,Z., and Moss,S.J. (2008). Regulation of synaptic inhibition by phospho-dependent binding of the AP2 complex to a YECL motif in the $GABA_A$ receptor gamma 2 subunit. Proc.Natl.Acad.Sci.U.S.A. *105*, 3616-3621.

Kittler,J.T., Chen,G., Honing,S., Bogdanov,Y., McAinsh,K., Arancibia-Carcamo,I.L., Jovanovic,J.N., Pangalos,M.N., Haucke,V., Yan,Z., and Moss,S.J. (2005). Phospho-dependent binding of the clathrin AP2 adaptor complex to $GABA_A$ receptors regulates the efficacy of inhibitory synaptic transmission. Proc.Natl.Acad.Sci.U.S.A *102*, 14871-14876.

Kittler,J.T., Thomas,P., Tretter,V., Bogdanov,Y.D., Haucke,V., Smart,T.G., and Moss,S.J. (2004). Huntingtin-associated protein 1 regulates inhibitory synaptic transmission by modulating γ-aminobutyric acid type A receptor membrane trafficking. Proc.Natl.Acad.Sci.U.S.A *101*, 12736-12741.

Kittler,J.T. and Moss,S.J. (2003). Modulation of $GABA_A$ receptor activity by phosphorylation and receptor trafficking: implications for the efficacy of synaptic inhibition. Current Opinion in Neurobiology. *13*, 341-347.

Kittler,J.T., Delmas,P., Jovanovic,J.N., Brown,D.A., Smart,T.G., and Moss,S.J. (2000a). Constitutive endocytosis of $GABA_A$ receptors by an

association with the adaptin AP2 complex modulates inhibitory synaptic currents in hippocampal neurons. Journal of Neuroscience. *20*, 7972-7977.

Kittler,J.T., Wang,J., Connolly,C.N., Vicini,S., Smart,T.G., and Moss,S.J. (2000b). Analysis of $GABA_A$ receptor assembly in mammalian cell lines and hippocampal neurons using gamma 2 subunit green fluorescent protein chimeras. Molecular and Cell Neuroscience *16*, 440-452.

Khvotchev,M.V., Ren,M.D., Takamori,S., Jahn,R., and Sudhof,T.C. (2003). Divergent functions of neuronal Rab11b in Ca^{2+}-regulated versus constitutive exocytosis. Journal of Neuroscience *23*, 10531-10539.

Klann,E., Chen,S.J., and Sweatt,J.D. (1991). Persistent Protein-Kinase Activation in the Maintenance Phase of Long-Term Potentiation. Journal of Biological Chemistry *266*, 24253-24256.

Klausner,R.D., Donaldson,J.G., and Lippincott-Schwartz,J. (1992). Brefeldin A: insights into the control of membrane traffic and organelle structure. Journal of Biological Chemistry *116*, 1071-1080.

Kneussel,M., Brandstatter,J.H., Gasnier,B., Feng,G., Sanes,J.R., and Betz,H. (2001). Gephyrin-independent clustering of postsynaptic $GABA_A$ receptor subtypes. Molecular and Cell Neuroscience *17*, 973-982.

Kneussel,M., Brandstatter,J.H., Laube,B., Stahl,S., Muller,U., and Betz,H. (1999). Loss of postsynaptic $GABA_A$ receptor clustering in gephyrin-deficient mice. Journal of Neuroscience. *19*, 9289-9297.

Knight,D.E. (2002). Calcium-dependent transferrin receptor recycling in bovine chromaffin cells. Traffic *3*, 298-307.

Knuesel,I., Mastrocola,M., Zuellig,R.A., Bornhauser,B., Schaub,M.C., and Fritschy,J.M. (1999). Altered synaptic clustering of $GABA_A$ receptors in mice lacking dystrophin (mdx mice). European Journal of Neuroscience *11*, 4457-4462.

Konnerth,A. and Eilers,J. (1994). Synaptic Plasticity and Calcium Dynamics in Cerebellar Purkinje Neurons. Biomedical Research-Tokyo *15*, 73-77.

Konnerth,A., Llano,I., and Armstrong,C.M. (1990). Synaptic Currents in Cerebellar Purkinje-Cells. Proc.Natl.Acad.Sci.U.S.A. *87*, 2662-2665.

Korpi,E.R., Grunder,G., and Luddens,H. (2002). Drug interactions at $GABA_A$ receptors. Progress in Neurobiology *67*, 113-159.

Kreitzer,A.C. and Regehr,W.G. (2001). Cerebellar depolarization-induced suppression of inhibition is mediated by endogenous cannabinoids. Journal of Neuroscience *21*, RC174.

Krishek,B.J., Xie,X., Blackstone,C., Huganir,R.L., Moss,S.J., and Smart,T.G. (1994). Regulation of $GABA_A$ receptor function by protein kinase C phosphorylation. Neuron *12*, 1081-1095.

Laurie,D.J., Seeburg,P.H., and Wisden,W. (1992a). The Distribution of 13-GABA-A Receptor Subunit Messenger-RNAs in the Rat-Brain .II. Olfactory-Bulb and Cerebellum. Journal of Neuroscience *12*, 1063-1076.

Laurie,D.J., Wisden,W., and Seeburg,P.H. (1992b). The distribution of thirteen $GABA_A$ receptor subunit mRNAs in the rat brain. III. Embryonic and postnatal development. Journal of Neuroscience. *12*, 4151-4172.

Lee,H.K., Barbarosie,M., Kameyama,K., Bear,M.F., and Huganir,R.L. (2000). Regulation of distinct AMPA receptor phosphorylation sites during bidirectional synaptic plasticity. Nature *405*, 955-959.

Leil,T.A., Chen,Z.W., Chang,C.S., and Olsen,R.W. (2004). $GABA_A$ receptor-associated protein traffics $GABA_A$ receptors to the plasma membrane in neurons. Journal of Neuroscience. *24*, 11429-11438.

Lev-Ram,V., Wong,S.T., Storm,D.R., and Tsien,R.Y. (2002). A new form of cerebellar long-term potentiation is postsynaptic and depends on nitric oxide but not cAMP. Proc.Natl.Acad.Sci.U.S.A. *99*, 8389-8393.

Levi,S., Logan,S.M., Tovar,K.R., and Craig,A.M. (2004). Gephyrin is critical for glycine receptor clustering but not for the formation of functional GABAergic synapses in hippocampal neurons. Journal of Neuroscience *24*, 207-217.

LeDoux,J., Chartier,D., and Leblanc,N. (1999). Inhibitors of calmodulin-dependent protein kinase are nonspecific blockers of voltage-dependent K^+ channels in vascular myocytes. Journal of Pharmacology and Experimental Therapeutics *290*, 1165-1174.

Lengyel,I., Voss,K., Cammarota,M., Bradshaw,K., Brent,V., Murphy,K.P.S.J., Giese,K. P., Rostas,J.A. P., and Bliss,T.V.P. (2004). Autonomous activity of CaMKII is only transiently increased following the induction of long-term potentiation in the rat hippocampus. European Journal of Neuroscience. *20(11),* 3063-3072

Lisman,J., Schulman,H., and Cline,H. (2002). The molecular basis of CaMKII function in synaptic and behavioural memory. Nature Reviews Neuroscience *3*, 175-190.

Lisman,J.E. and Zhabotinsky,A.M. (2001). A model of synaptic memory: A CaMKII/PP1 switch that potentiates transmission by organizing an AMPA receptor anchoring assembly. Neuron *31*, 191-201.

Lisman,J. (1989). A Mechanism for the Hebb and the Anti-Hebb Processes Underlying Learning and Memory. Proc.Natl.Acad.Sci.U.S.A. *86*, 9574-9578.

Lissin,D.V., Carroll,R.C., Nicoll,R.A., Malenka,R.C., and von Zastrow,M. (1999). Rapid, activation-induced redistribution of ionotropic glutamate receptors in cultured hippocampal neurons. Journal of Neuroscience *19*, 3275.

Llano,I., Gonzalez,J., Caputo,C., Lai,F.A., Blayney,L.M., Tan,Y.P., and Marty,A. (2000). Presynaptic calcium stores underlie large-amplitude miniature IPSCs and spontaneous calcium transients. Nature Neuroscience. *3*, 1256-1265.

Llano,I., Leresche,N., and Marty,A. (1991). Calcium entry increases the sensitivity of cerebellar Purkinje cells to applied GABA and decreases inhibitory synaptic currents. Neuron. 1991 Apr; *6(4)*:565-74.

Lledo,P.M., Zhang,X.Y., Sudhof,T.C., Malenka,R.C., and Nicoll,R.A. (1998). Postsynaptic membrane fusion and long-term potentiation. Science *279*, 399-403.

Llinas,R., Sugimori,M., Hillman,D.E., and Cherksey,B. (1992). Distribution and Functional-Significance of the P-Type, Voltage-Dependent Ca^{2+} Channels in the Mammalian Central-Nervous-System. TINS *15*, 351-355.

Llinas,R. and Sugimori,M. (1980). Electro-Physiological Properties of Invitro Purkinje-Cell Somata in Mammalian Cerebellar Slices. Journal of Physiology-London *305*, 171-195.

Lorez,M., Benke,D., Luscher,B., Mohler,H., and Benson,J.A. (2000). Single-channel properties of neuronal $GABA_A$ receptors from mice lacking the $\gamma 2$ subunit. Journal of Physiology *527*, 11-31.

Losonczy,A., Makara,J.K., and Magee,J.C. (2008). Compartmentalized dendritic plasticity and input feature storage in neurons. Nature *452*, 436-441.

Lu,W.Y., Man,H.Y., Ju,W., Trimble,W.S., MacDonald,J.F., and Wang,Y.T. (2001). Activation of synaptic NMDA receptors induces membrane insertion of new AMPA receptors and LTP in cultured hippocampal neurons. Neuron *29*, 243-254.

Luddens,H., Korpi,E.R., and Seeburg,P.H. (1995). Neurotransmitter Receptors III. $GABA_A$/Benzodiazepine receptor heterogeneity: Neurophysiological implications. Neuropharmacology *34*, 245-254.

Luscher,B. and Keller,C.A. (2004). Regulation of $GABA_A$ receptor trafficking, channel activity, and functional plasticity of inhibitory synapses. Pharmacology and Therapeutics *102*, 195-221.

Luscher,C., Xia,H.H., Beattie,E.C., Carroll,R.C., von Zastrow,M., Malenka,R.C., and Nicoll,R.A. (1999). Role of AMPA receptor cycling in synaptic transmission and plasticity. Neuron *24*, 649-658.

Luu,T., Gage,P.W., and Tierney,M.L. (2006). GABA Increases both the Conductance and Mean Open Time of Recombinant $GABA_A$ Channels Co-expressed with GABARAP. Journal of Biological Chemistry *281*, 35699-35708.

Maas,C., Tagnaouti,N., Loebrich,S., Behrend,B., Lappe-Siefke,C., and Kneussel,M. (2006). Neuronal cotransport of glycine receptor and the scaffold protein gephyrin. Journal of Cell Biology. *172*, 441-451.

Maeda,H., Ellis-Davies,G.C.R., Ito,K., Miyashita,Y., and Kasai,H. (1999). Supralinear Ca^{2+} signaling by cooperative and mobile Ca^{2+} buffering in Purkinje neurons. Neuron *24*, 989-1002.

Maejima,T., Oka,S., Hashimotodani,Y., Ohno-Shosaku,T., Aiba,A., Wu,D., Waku,K., Sugiura,T., and Kano,M. (2005). Synaptically driven endocannabinoid release requires Ca^{2+}-assisted metabotropic glutamate receptor subtype 1 to phospholipase C $\beta 4$ signaling cascade in the cerebellum. Journal of Neuroscience. *25*, 6826-6835.

Malinow,R., Schulman,H., and Tsien,R.W. (1989). Inhibition of Postsynaptic PKC or CaMKII Blocks Induction But Not Expression of LTP. Science *245*, 862-866.

Marsden,K.C., Beattie,J.B., Friedenthal,J., and Carroll,R.C. (2007). NMDA Receptor Activation Potentiates Inhibitory Transmission through GABA Receptor-Associated Protein-Dependent Exocytosis of $GABA_A$ Receptors. Journal of Neuroscience *27*, 14326-14337.

Martin,J.H. (1996). Neuroanatomy: Text and altas Chapter 10 cerebellum pp291-320

McAinsh,K., Jovanovic,J.N., Moss,S.J. (2003) CaM Kinase II-dependent phosphorylation of neuronal $GABA_A$ receptors. *Society of neuroscience abstract* 68

Mccormick,D.A. and Thompson,R.F. (1984). Cerebellum - Essential Involvement in the Classically-Conditioned Eyelid Response. Science *223*, 296-299.

McDonald,B.J., Amato,A., Connolly,C.N., Benke,D., Moss,S.J., and Smart,T.G. (1998). Adjacent phosphorylation sites on $GABA_A$ receptor β subunits determine regulation by cAMP-dependent protein kinase. Nature Neuroscience *1*, 23-28.

McDonald,B.J. and Moss,S.J. (1997). Conserved phosphorylation of the intracellular domains of $GABA_A$ receptor $\beta 2$ and $\beta 3$ subunits by cAMP-dependent protein kinase, cGMP-dependent protein kinase protein kinase C and Ca^{2+}/calmodulin type II-dependent protein kinase. Neuropharmacology *36*, 1377-1385.

McDonald,B.J. and Moss,S.J. (1994). Differential phosphorylation of intracellular domains of γ- aminobutyric acid type A receptor subunits by calcium/calmodulin type 2- dependent protein kinase and cGMP-dependent protein kinase. Journal of Biological Chemistry *269*, 18111-18117.

McKay,B.E. and Turner,R.W. (2005). Physiological and morphological development of the rat cerebellar Purkinje cell. Journal of Physiology *567*, 829-850.

McKernan,R.M. and Whiting,P.J. (1996). Which $GABA_A$ -receptor subtypes really occur in the brain? TINS *19*, 139-143.

Mehta,A.K. and Ticku,M.K. (1999). An update on $GABA_A$ receptors. Brain Research Brain Research Review *29*, 196-217.

Meyer,G., Kirsch,J., Betz,H., and Langosch,D. (1995). Identification of a gephyrin binding motif on the glycine receptor β subunit. Neuron *15*, 563-572.

Middleton,F.A. and Strick,P.L. (1998). The cerebellum: an overview. TINS *21*, 367-369.

Mielke,J.G. and Wang,Y.T. (2005). Insulin exerts neuroprotection by counteracting the decrease in cell-surface $GABA_A$ receptors following oxygen-glucose deprivation in cultured cortical neurons. Journal of Neurochemistry *92*, 103-113.

Millward,T.A., Zolnierowicz,S., and Hemmings,B.A. (1999). Regulation of protein kinase cascades by protein phosphatase 2A. Trends in Biochemical Sciences *24*, 186-191.

Mittmann,W., Koch,U., and Hausser,M. (2005). Feed-forward inhibition shapes the spike output of cerebellar Purkinje cells. Journal of Physiology-London *563*, 369-378.

Mizoguchi,Y., Ishibashi,H., and Nabekura,J. (2003a). The action of BDNF on $GABA_A$ currents changes from potentiating to suppressing during maturation of rat hippocampal CA1 pyramidal neurons. Journal of Physiology-London *548*, 703-709.

Mizoguchi,Y., Kanematsu,T., Hirata,M., and Nabekura,J. (2003b). A rapid increase in the total number of cell surface functional $GABA_A$ receptors induced by brain-derived neurotrophic factor in rat visual cortex. Journal of Biological Chemistry *278*, 44097-44102.

Mizokami,A., Kanematsu,T., Ishibashi,H., Yamaguchi,T., Tanida,I., Takenaka,K., Nakayama,K.I., Fukami,K., Takenawa,T., Kominami,E., Moss,S.J., Yamamoto,T., Nabekura,J., and Hirata,M. (2007). Phosholipase

C-Related Inactive Protein Is Involved in Trafficking of γ2 Subunit-Containing GABAA Receptors to the Cell Surface. Journal of Neuroscience *27*, 1692-1701.

Mohler,H., (2000) Pharmacology of GABA and Glycine Neurotransmission

Mollenhauer,H.H., Morre,D.J., and Rowe,L.D. (1990). Alteration of Intracellular Traffic by Monensin - Mechanism, Specificity and Relationship to Toxicity. Biochimica et Biophysica Acta *1031*, 225-246.

Morishita,W., Kirov,S.A., Pitler,T.A., Martin,L.A., Lenz,R.A., and Alger,B.E. (1997). N-ethylmaleimide blocks depolarization-induced suppression of inhibition and enhances GABA release in the rat hippocampal slice in vitro. Journal of Neuroscience *17*, 941-950.

Moss,S.J. and Smart,T.G. (1996). Modulation of amino acid-gated ion channels by protein phosphorylation. International Review Neurobiology *39*, 1-52.

Moss,S.J., Gorrie,G.H., Amato,A., and Smart,T.G. (1995). Modulation of $GABA_A$ receptors by tyrosine phosphorylation. Nature *377*, 344-348.

Moss,S.J., Doherty,C.A., and Huganir,R.L. (1992a). Identification of the cAMP-dependent protein kinase and protein kinase C phosphorylation sites within the major intracellular domains of the β_1, γ_{2S}, and γ_{2L} subunits of the g-aminobutyric acid type A receptor. Journal of Biological Chemistry *267*, 14470-14476.

Moss,S.J., Smart,T.G., Blackstone,C.D., and Huganir,R.L. (1992b). Functional modulation of $GABA_A$ receptors by cAMP-dependent protein phosphorylation. Science *257*, 661-665.

Nadler,L.S., Guirguis,E.R., and Siegel,R.E. (1994). $GABA_A$ Receptor Subunit Polypeptides Increase in Parallel But Exhibit Distinct Distributions in the Developing Rat Cerebellum. Journal of Neurobiology *25*, 1533-1544.

Neher,E. and Stevens,C.F. (1977). Conductance Fluctuations and Ionic Pores in Membranes. Annual Review of Biophysics and Bioengineering *6*, 345-381.

Netzeband,J.G. and Gruol,D.L. (2008). mGluR1 agonists elicit a Ca^{2+} signal and membrane hyperpolarization mediated by apamin-sensitive potassium channels in immature rat Purkinje neurons. Journal of Neuroscience Research

Nusser,Z., Sieghart,W., and Mody,I. (1999). Differential regulation of synaptic $GABA_A$ receptors by cAMP-dependent protein kinase in mouse cerebellar and olfactory bulb neurones. Journal of Physiology-London *521 t 2*, 421-435.

Nusser,Z., Sieghart,W., and Somogyi,P. (1998a). Segregation of different $GABA_A$ receptors to synaptic and extrasynaptic membranes of cerebellar granule cells. Journal of Neuroscience *18*, 1693-1703.

Nusser,Z., Hajos,N., Somogyi,P., and Mody,I. (1998b). Increased number of synaptic $GABA_A$ receptors underlies potentiation at hippocampal inhibitory synapses. Nature *395*, 172-177.

Nymann-Andersen,J., Wang,H.B., and Olsen,R.W. (2002). Biochemical identification of the binding domain in the $GABA_A$ receptor-associated protein (GABARAP) mediating dimer formation. Neuropharmacology *43*, 476-481.

O'Sullivan,G.A., Kneussel,M., Elazar,Z., and Betz,H. (2005). GABARAP is not essential for $GABA_A$ receptor targeting to the synapse. European Journal of Neuroscience *22*, 2644-2648.

Obata,K., Oide,M., and Tanaka,H. (1978). Excitatory and Inhibitory Actions of GABA and Glycine on Embryonic Chick Spinal Neurons in Culture. Brain Research *144*, 179-184.

Olsen,R.W., Mccabe,R.T., and Wamsley,J.K. (1990). $GABA_A$ Receptor Subtypes - Autoradiographic Comparison of GABA, Benzodiazepine, and Convulsant Binding-Sites in the Rat Central-Nervous-System. Journal of Chemical Neuroanatomy *3*, 59-76.

Ohtsuki,G., Kawaguchi,S.Y., Mishina,M., and Hirano,T. (2004). Enhanced inhibitory synaptic transmission in the cerebellar molecular layer of the GluRδ2 knock-out mouse. Journal of Neuroscience. *24*, 10900-10907.

Ortinski,P.I., Turner,J.R., Barberis,A., Motamedi,G., Yasuda,R.P., Wolfe,B.B., Kellar,K.J., and Vicini,S. (2006). Deletion of the $GABA_A$

receptor α1 subunit increases tonic $GABA_A$ receptor current: a role for GABA uptake transporters. Journal of Neuroscience. *26*, 9323-9331.

Otis,T.S., De Koninck,Y., and Mody,I. (1994). Lasting potentiation of inhibition is associated with an increased number of γ-aminobutyric acid type A receptors activated during miniature inhibitory postsynaptic currents. Proc.Natl.Acad.Sci.U.S.A *91*, 7698-7702.

Otmakhov,N., Griffith,L.C., and Lisman,J.E. (1997). Postsynaptic inhibitors of calcium/calmodulin-dependent protein kinase type II block induction but not maintenance of pairing-induced long-term potentiation. Journal of Neuroscience *17*, 5357-5365.

Palizvan,M.R., Sohya,K., Kohara,K., Maruyama,A., Yasuda,H., Kimura,F., and Tsumoto,T. (2004). Brain-derived neurotrophic factor increases inhibitory synapses, revealed in solitary neurons cultured from rat visual cortex. Neuroscience *126*, 955-966.

Park,M., Penick,E.C., Edwards,J.G., Kauer,J.A., and Ehlers,M.D. (2004). Recycling endosomes supply AMPA receptors for LTP. Science *305*, 1972-1975.

Patterson,S.L., Abel,T., Deuel,T.A.S., Martin,K.C., Rose,J.C., and Kandal,E.R. (1996). Recombinant BDNF rescues deficits in basal synaptic transmission and hippocampal LTP in BDNF knockout mice. Neuron *16*, 1137-1145.

Paysan,J., Kossel,A., Bolz,J., and Fritschy,J.M. (1997). Area-specific regulation of g-aminobutyric acid type A receptor subtypes by thalamic afferents in developing rat neocortex. Proc.Natl.Acad.Sci.U.S.A *94*, 6995-7000.

Peng,Z., Hauer,B., Mihalek,R.M., Homanics,G.E., Sieghart,W., Olsen,R.W., and Houser,C.R. (2002). $GABA_A$ receptor changes in δ subunit-deficient mice: altered expression of α4 and γ2 subunits in the forebrain. Journal of Comparative Neurology. *446*, 179-197.

Pickard,L., Noel,J., Duckworth,J.K., Fitzjohn,S.M., Henley,J.M., Collingridge,G.L., and Molnar,E. (2001). Transient synaptic activation of NMDA receptors leads to the insertion of native AMPA receptors at hippocampal neuronal plasma membranes. Neuropharmacology *41*, 700-713.

Piochon,C., Irinopoulou,T., Brusciano,D., Bailly,Y., Mariani,J., and Levenes,C. (2007). NMDA receptor contribution to the climbing fiber response in the adult mouse Purkinje cell. Journal of Neuroscience *27*, 10797-10809.

Pirker,S., Schwarzer,C., Wieselthaler,A., Sieghart,W., and Sperk,G. (2000). $GABA_A$ receptors: immunocytochemical distribution of 13 subunits in the adult rat brain. Neuroscience *101*, 815-850.

Poisbeau,P., Cheney,M.C., Browning,M.D., and Mody,I. (1999). Modulation of synaptic $GABA_A$ receptor function by PKA and PKC in adult hippocampal neurons. Journal of Neuroscience. *19*, 674-683.

Poltl,A., Hauer,B., Fuchs,K., Tretter,V., and Sieghart,W. (2003). Subunit composition and quantitative importance of $GABA_A$ receptor subtypes in the cerebellum of mouse and rat. Journal of Neurochemistry. *87*, 1444-1455.

Ponomarev,I., Maiya,R., Harnett,M.T., Schafer,G.L., Ryabinin,A.E., Blednov,Y.A., Morikawa,H., Boehm,S.L., Homanics,G.E., Berman,A., Lodowski,K.H., Bergeson,S.E., and Harris,R.A. (2006). Transcriptional signatures of cellular plasticity in mice lacking the alpha 1 subunit of $GABA_A$ receptors. Journal of Neuroscience *26*, 5673-5683.

Pearce,R.A. (1993). Physiological evidence for two distinct $GABA_A$ responses in rat hippocampus. Neuron *10*, 189-200.

Porter,N.M., Twyman,R.E., Uhler,M.D., and Macdonald,R.L. (1990). Cyclic AMP-dependent protein kinase decreases $GABA_A$ receptor current in mouse spinal neurons. Neuron *5*, 789-796.

Pregenzer,J.F., Im,W.B., Carter,D.B., and Thomsen,D.R. (1993). Comparison of Interactions of [H-3] Muscimol, T-Butylbicyclophosphoro[S-35]Thionate, and [H-3] Flunitrazepam with Cloned Gamma-Aminobutyric $Acid_A$ Receptors of the $\alpha 1\beta 2$ and $\alpha 1\beta 2\gamma 2$ Subtypes. Molecular Pharmacology *43*, 801-806.

Rapoport,M., van Reekum,R., and Mayberg,H. (2000). The role of the cerebellum in cognition and behavior: A selective review. Journal of Neuropsychiatry and Clinical Neurosciences *12*, 193-198.

Renzi,M., Farrant,M., and Cull-Candy,S.G. (2007). Climbing-fibre activation of NMDA receptors in Purkinje cells of adult mice. Journal of Physiology-London *585*, 91-101.

Rico,B., Xu,B.J., and Reichardt,L.F. (2002a). TrkB receptor signaling is required for establishment of GABAergic synapses in the cerebellum. Nature Neuroscience *5*, 225-233.

Robinson,D.A. (1976). Adaptive Gain Control of Vestibuloocular Reflex by Cerebellum. Journal of Neurophysiology *39*, 954-969.

Roberson,E.D., English,J.D., and Sweatt,J.D. (1996). A biochemist's view of long-term potentiation. Learning & Memory *3*, 1-24.

Ruiz,A., Fabian-Fine,R., Scott,R., Walker,M.C., Rusakov,D.A., and Kullmann,D.M. (2003). $GABA_A$ receptors at hippocampal mossy fibers. Neuron *39*, 961-973.

Salin,P.A., Malenka,R.C., and Nicoll,R.A. (1996). Cyclic AMP mediates a presynaptic form of LTP at cerebellar parallel fiber synapses. Neuron *16*, 797-803.

Sanhueza,M., McIntyre,C.C., and Lisman,J.E. (2007). Reversal of synaptic memory by Ca^{2+}/calmodulin-dependent protein kinase II inhibitor. Journal of Neuroscience *27*, 5190-5199.

Sassoe-Pognetto,M., Panzanelli,P., Sieghart,W., and Fritschy,J.M. (2000). Colocalization of multiple $GABA_A$ receptor subtypes with gephyrin at postsynaptic sites. Journal of Comparative Neurology *420*, 481-498.

Schiavo,G., Matteoli,M., and Montecucco,C. (2000). Neurotoxins affecting neuroexocytosis. Physiology Review. *80*, 717-766.

Schmidt,H., Stiefel,K.M., Racay,P., Schwaller,B., and Eilers,J. (2003). Mutational analysis of dendritic Ca^{2+} kinetics in rodent Purkinje cells: role of parvalbumin and calbindin D-28k. Journal of Physiology-London *551*, 13-32.

Schmolesky,M.T., Weber,J.T., De Zeeuw,C.I., and Hansel,C. (2002). The making of a complex spike: Ionic composition and plasticity. Cerebellum: Recent Developments in Cerebellar Research *978*, 359-390.

Schofield,P.R., Darlison,M.G., Fujita,N., Burt,D.R., Stephenson,F.A., Rodriguez,H., Rhee,L.M., Ramachandran,J., Reale,V., Glencorse,T.A.,

Seeburg,P.H., and Barnard,E.A. (1987). Sequence and functional expression of the $GABA_A$ receptor shows a ligand-gated receptor super-family. Nature *328*, 221-227.

Schweizer,C., Balsiger,S., Bluethmann,H., Mansuy,I.M., Fritschy,J.M., Mohler,H., and Luscher,B. (2003). The gamma 2 subunit of $GABA_A$ receptors is required for maintenance of receptors at mature synapses. Molecular and Cellular Neuroscience *24*, 442-450.

Shen,K. and Meyer,T. (1999). Dynamic control of CaMKII translocation and localization in hippocampal neurons by NMDA receptor stimulation. Science *284*, 162-166.

Shen,Y., Hansel,C., and Linden,D.J. (2002). Glutamate release during LTD at cerebellar climbing fiber-Purkinje cell synapses. Nature Neuroscience *5*, 725-726.

Shepherd,J.D. and Huganirl,R.L. (2007). The cell biology of synaptic plasticity: AMPA receptor trafficking. Annual Review of Cell and Developmental Biology *23*, 613-643.

Sieczkarski,S.B. and Whittaker,G.R. (2002). Dissecting virus entry via endocytosis. Journal of General Virology *83*, 1535-1545.

Sigel,E., Baur,R., Kellenberger,S., and Malherbe,P. (1992). Point mutations affecting antagonist affinity and agonist dependent gating of $GABA_A$ receptor channels. EMBO Journal. *11*, 2017-2023.

Sigel,E., Baur,R., Trube,G., Mohler,H., and Malherbe,P. (1990). The effect of subunit composition of rat brain $GABA_A$ receptors on channel function. Neuron *5*, 703-711.

Sigworth,F.J. (1980). The variance of sodium current fluctuations at the node of Ranvier. Journal of Physiology *307*, 97-129.

Simat,M., Parpan,F., and Fritschy,J.M. (2007). Heterogeneity of glycinergic and gabaergic interneurons in the granule cell layer of mouse cerebellum. Journal of Comparative Neurology *500*, 71-83.

Smart,T.G., (1998) Electrophysiology of $GABA_A$ receptors, Amino acid neurotransmission, edited by Stephenson,F.A., Turner,A. pp37-63

Smart,T.G., Moss,S.J., Xie,X., and Huganir,R.L. (1991). $GABA_A$ receptors are differentially sensitive to zinc: dependence on subunit composition. British Journal of Pharmacology *103*, 1837-1839.

Smith,G.B. and Olsen,R.W. (1995). Functional domains of $GABA_A$ receptors. Trends in Pharmacological Sciences *16*, 162-168.

Smith,G.B. and Olsen,R.W. (1994). Identification of a [^{3}H]muscimol photoaffinity substrate in the bovine $GABA_A$ receptor α subunit. Journal of Cell Biology *269*, 20380-20387.

Soderling,T.R., Chang,B., and Brickey,D. (2001). Cellular signaling through multifunctional Ca^{2+}/calmodulin-dependent protein kinase II. Journal of Biological Chemistry *276*, 3719-3722.

Soderling,T.R. and Derkach,V.A. (2000). Postsynaptic protein phosphorylation and LTP. TINS *23(2),* 75-80

Sola,C., Tusell,J.M., and Serratosa,J. (1999). Comparative study of the distribution of calmodulin kinase II and calcineurin in the mouse brain. Journal of Neuroscience Research *57*, 651-662.

Soler-Llavina,G.J. and Sabatini,B.L. (2006). Synapse-specific plasticity and compartmentalized signaling in cerebellar stellate cells. Nature Neuroscience *9*, 798-806.

Somogyi,P., Fritschy,J.M., Benke,D., Roberts,J.D., and Sieghart,W. (1996). The γ2 subunit of the $GABA_A$ receptor is concentrated in synaptic junctions containing the α1 and β2/3 subunits in hippocampus, cerebellum and globus pallidus. Neuropharmacology *35*, 1425-1444.

Somogyi,P. (1989). Synaptic organization of GABAergic neurons and $GABA_A$ receptors in the lateral geniculate nucleus and visual cortex. Neural Mechanisms of Visual Perception 35-62.

Stell,B.M., Brickley,S.G., Tang,C.Y., Farrant,M., and Mody,I. (2003). Neuroactive steroids reduce neuronal excitability by selectively enhancing tonic inhibition mediated by δ subunit-containing $GABA_A$ receptors. Proc.Natl.Acad.Sci.U.S.A *100*, 14439-14444.

Stell,B.M. and Mody,I. (2002). Receptors with different affinities mediate phasic and tonic $GABA_A$ conductances in hippocampal neurons. Journal of Neuroscience. *22*, RC223.

Stephenson, F.A. (1998). Molecular structure of $GABA_A$ Receptors, Amino acid neurotransmission, edited by Stephenson,F.A., Turner,A.J. pp65-92

Strack,S., Barban,M.A., Wadzinski,B.E., and Colbran,R.J. (1997). Differential inactivation of postsynaptic density-associated and soluble Ca^{2+}/calmodulin-dependent protein kinase II by protein phosphatases 1 and 2A. Journal of Neurochemistry *68*, 2119-2128.

Strata,P. and Rossi,F. (1998). Plasticity of the olivocerebellar pathway. TINS *21*, 407-413.

Stuart,G. and Hausser,M. (1994). Initiation and Spread of Sodium Action-Potentials in Cerebellar Purkinje-Cells. Neuron *13*, 703-712.

Sudhof,T.C. (1997). Function of Rab3 GDP-GTP exchange. Neuron *18*, 519-522.

Sudhof,T.C. (1995). The Synaptic Vesicle Cycle - A Cascade of Protein-Protein Interactions. Nature *375*, 645-653.

Sugiyama,Y., Kawaguchi,S.Y., and Hirano,T. (2008). mGluR1-mediated facilitation of long-term potentiation at inhibitory synapses on a cerebellar Purkinje neuron. European Journal of Neuroscience *27*, 884-896.

Sumi,M., Kiuchi,K., Ishikawa,T., Ishii,A., Hagiwara,M., Nagatsu,T., and Hidaka,H. (1991). The Newly Synthesized Selective Ca^{2+}/Calmodulin Dependent Protein Kinase-II Inhibitor KN-93 Reduces Dopamine Contents in Pc12H Cells. Biochemical and Biophysical Research Communications *181*, 968-975.

Sur,C., Wafford,K.A., Reynolds,D.S., Hadingham,K.L., Bromidge,F., Macaulay,A., Collinson,N., O'Meara,G., Howell,O., Newman,R., Myers,J., Atack,J.R., Dawson,G.R., McKernan,R.M., Whiting,P.J., and Rosahl,T.W. (2001). Loss of the major $GABA_A$receptor subtype in the brain is not lethal in mice. Journal of Neuroscience. *21*, 3409-3418.

Suzuki,T. (1994). Protein-Kinases Involved in the Expression of Long-Term Potentiation. International Journal of Biochemistry *26*, 735-744.

Szabo,B., Urbanski,M.J., Bisogno,T., Di Marzo,V., Mendiguren,A., Baer,W.U., and Freiman,I. (2006). Depolarization-induced retrograde

synaptic inhibition in the mouse cerebellar cortex is mediated by 2-arachidonoylglycerol. Journal of Physiology-London *577*, 263-280.

Takayama,C. and Inoue,Y. (2004). Transient expression of $GABA_A$ receptor $\alpha 2$ and $\alpha 3$ subunits in differentiating cerebellar neurons. Developmental Brain Research. *148*, 169-177.

Tanaka,T., Saito,H., and Matsuki,N. (1997). Inhibition of $GABA_A$ synpatic responses by brain-derived neurotrophic factor (BDNF) in rat hippocampus. Journal of Neuroscience *17*, 2959-2966.

Taylor,P.M., Thomas,P., Gorrie,G.H., Connolly,C.N., Smart,T.G., and Moss,S.J. (1999). Identification of amino acid residues within $GABA_A$ receptor β subunits that mediate both homomeric and heteromeric receptor expression. Journal of Neuroscience. *19*, 6360-6371.

Tempia,F., Konnerth,A. (1994) Calcium requirement of long-term depression and rebound potentiation in cerebellar Purkinje neurons. Cell Biology. Vol 5, 243-250.

Terunuma,M., Jang,I.S., Ha,S.H., Kittler,J.T., Kanematsu,T., Jovanovic,J.N., Nakayama,K.I., Akaike,N., Ryu,S.H., Moss,S.J., and Hirata,M. (2004). GABAA receptor phospho-dependent modulation is regulated by phospholipase C-related inactive protein type 1, a novel protein phosphatase 1 anchoring protein. Journal of Neuroscience. *24*, 7074-7084.

Thomas,P., Mortensen,M., Hosie,A.M., and Smart,T.G. (2005). Dynamic mobility of functional $GABA_A$ receptors at inhibitory synapses. Nature Neuroscience. *8*, 889-897

Thompson,S.A., Wheat,L., Brown,N.A., Wingrove,P.B., Pillai,G.V., Whiting,P.J., Adkins,C., Woodward,C.H., Smith,A.J., Simpson,P.B., Collins,I., and Wafford,K.A. (2004). Salicylidene salicylhydrazide, a selective inhibitor of b1-containing $GABA_A$ receptors. British Journal of Pharmacology *142*, 97-106.

Tokumitsu,H., Chijiwa,T., Hagiwara,M., Mizutani,A., Terasawa,M., and Hidaka,H. (1990b). KN-62, 1-[N,O-Bis(5-Isoquinolinesulfonyl)-N-Methyl-L-Tyrosyl]-4-Phenylpiperazine, A Specific Inhibitor of Ca^{2+}/Calmodulin-Dependent Protein Kinase-Ii. Journal of Biological Chemistry *265*, 4315-4320.

Torashima,T., Okoyama,S., Nishizaki,T., and Hirai,H. (2006). *In vivo* transduction of murine cerebellar Purkinje cells by HIV-derived lentiviral vectors. Brain Research. *1082*, 11-22.

Traynelis,S.F., Silver,R.A., and Cull-Candy,S.G. (1993). Estimated Conductance of Glutamate-Receptor Channels Activated During EPSCs at the Cerebellar Mossy Fiber-Granule Cell Synapse. Neuron *11*, 279-289.

Tretter,V., Jacob,T.C., Mukherjee,J., Fritschy,J.M., Pangalos,M.N., and Moss,S.J. (2008). The clustering of $GABA_A$ receptor subtypes at inhibitory synapses is facilitated via the direct binding of receptor alpha 2 Subunits to gephyrin. Journal of Neuroscience *28*, 1356-1365.

Tretter,V., Hauer,B., Nusser,Z., Mihalek,R.M., Hoger,H., Homanics,G.E., Somogyi,P., and Sieghart,W. (2001). Targeted disruption of the $GABA_A$ receptor delta subunit gene leads to an up-regulation of $\gamma 2$ subunit-containing receptors in cerebellar granule cells. Journal of Biological Chemistry *276*, 10532-10538.

van Rijnsoever,C., Sidler,C., and Fritschy,J.M. (2005). Internalized GABA-receptor subunits are transferred to an intracellular pool associated with the postsynaptic density. European Journal of Neuroscience *21*, 327-338.

Vest,R.S., Davies,K.D., O'Leary,H., Port,J.D., and Bayer,K.U. (2007) Dual Mechanism of a Natural CaMKII Inhibitor. Molecular Biology of the Cell. *18(12),* 5024-5033

Vetiska,S.M., Ahmadian,G., Ju,W., Liu,L., Wymann,M.P., and Wang,Y.T. (2007). GABAA receptor-associated phosphoinositide 3-kinase is required for insulin-induced recruitment of postsynaptic $GABA_A$ receptors. Neuropharmacology *52*, 146-155.

Vincent,P. and Marty,A. (1996). Fluctuations of inhibitory postsynaptic currents in Purkinje cells from rat cerebellar slices. Journal of Physiology-London *494*, 183-199.

Vincent,P., Armstrong,C.M., and Marty,A. (1992). Inhibitory synaptic currents in rat cerebellar Purkinje cells: modulation by postsynaptic depolarization. Journal of Physiology-London *456*, 453-471.

Vicini,S., Ferguson,C., Prybylowski,K., Kralic,J., Morrow,A.L., and Homanics,G.E. (2001). $GABA_A$ receptor α1 subunit deletion prevents developmental changes of inhibitory synaptic currents in cerebellar neurons. Journal of Neuroscience. *21*, 3009-3016.

Voogd,J. and Glickstein,M. (1998). The anatomy of the cerebellum. TINS *21*, 370-375.

Wan,Q., Man,H.Y., Braunton,J., Wang,W., Salter,M.W., Becker,L., and Wang,Y.T. (1997a). Modulation of $GABA_A$ receptor function by tyrosine phosphorylation of β subunits. Journal of Neuroscience. *17*, 5062-5069.

Wan,Q., Xiong,Z.G., Man,H.Y., Ackerley,C.A., Braunton,J., Lu,W.Y., Becker,L.E., MacDonald,J.F., and Wang,Y.T. (1997b). Recruitment of functional $GABA_A$ receptors to postsynaptic domains by insulin. Nature *388*, 686-690.

Wang,H. and Olsen,R.W. (2000). Binding of the $GABA_A$ receptor-associated protein (GABARAP) to microtubules and microfilaments suggests involvement of the cytoskeleton in GABARAP-$GABA_A$ receptor interaction. Journal of Neurochemistry. *75*, 644-655.

Wang,H.B., Bedford,F.K., Brandon,N.J., Moss,S.J., and Olsen,R.W. (1999). $GABA_A$-receptor-associated protein links $GABA_A$ receptors and the cytoskeleton. Nature *397*, 69-72.

Wang,J., Liu,S., Haditsch,U., Tu,W., Cochrane,K., Ahmadian,G., Tran,L., Paw,J., Wang,Y., Mansuy,I., Salter,M.M., and Lu,Y. (2003a). Interaction of calcineurin and type-A GABA receptor γ2 subunits produces long-term depression at CA1 inhibitory synapses. Journal of Neuroscience. *23*, 826-836.

Wang,Q., Liu,L., Pei,L., Ju,W., Ahmadian,G., Lu,J., Wang,Y., Liu,F., and Wang,Y.T. (2003b). Control of synaptic strength, a novel function of Akt. Neuron *38*, 915-928.

Wang,R.A., Cheng,G., Kolaj,M., and Randic,M. (1995). α-subunit of calcium/calmodulin-dependent protein kinase II enhances γ-aminobutyric acid and inhibitory synaptic responses of rat neurons in vitro. Journal of Neurophysiology *73*, 2099-2106.

Wang,S.S.H., Denk,W., and Hausser,M. (2000). Coincidence detection mediated by supralinear calcium signals in dendritic spines of cerebellar Purkinje cells. Biophysical Journal *78*, 15A.

Wang,Y.T. and Linden,D.J. (2000). Expression of cerebellar long-term depression requires postsynaptic clathrin-mediated endocytosis. Neuron *25*, 635-647.

Weber,J.T., De Zeeuw,C.I., Linden,D.J., and Hansel,C. (2003). Long-term depression of climbing fiber-evoked calcium transients in Purkinje cell dendrites. Proc.Natl.Acad.Sci.U.S.A. *100*, 2878-2883.

Wei,J., Zhang,M., Zhu,Y., and Wang,J.H. (2004). Ca^{2+}-calmodulin signalling pathway up-regulates GABA synaptic transmission through cytoskeleton-mediated mechanisms. Neuroscience *127*, 637-647.

Whiting,P.J., Bonnert,T.P., McKernan,R.M., Farrar,S., Le Bourdelles,B., Heavens,R.P., Smith,D.W., Hewson,L., Rigby,M.R., Sirinathsinghji,D.J.S., Thompson,S.A., and Wafford,K.A. (1999). Molecular and functional diversity of the expanding $GABA_A$ receptor gene family. Molecular and Functional Diversity of Ion Channels and Receptors *868*, 645-653.

Whiting,P.J., McKernan,R.M., and Wafford,K.A. (1995). Structure and pharmacology of vertebrate $GABA_A$ receptor subtypes. International Review of Neurobiology *38*, 95-138.

Wisden,W., Korpi,E.R., and Bahn,S. (1996). The cerebellum: a model system for studying $GABA_A$ receptor diversity. Neuropharmacology *35*, 1139-1160.

Wisden,W., Laurie,D.J., Monyer,H., and Seeburg,P.H. (1992). The distribution of 13 $GABA_A$ receptor subunit mRNAs in the rat brain. I. Telencephalon, diencephalon, mesencephalon. Journal of Neuroscience. *12*, 1040-1062.

Wooltorton,J.R., Moss,S.J., and Smart,T.G. (1997). Pharmacological and physiological characterization of murine homomeric $\beta 3$ $GABA_A$ receptors. European Journal of Neuroscience. *9*, 2225-2235.

Yakushiji,T., Shirasaki,T., Munakata,M., Hirata,A., and Akaike,N. (1993). Differential properties of type I and type II benzodiazepine receptors in mammalian CNS neurones. British Journal of Pharmacology *109*, 819-825.

Yoshida,T., Hashimoto,K., Zimmer,A., Maejima,T., Araishi,K., and Kano,M. (2002). The cannabinoid CB1 receptor mediates retrograde signals for depolarization-induced suppression of inhibition in cerebellar Purkinje cells. Journal of Neuroscience *22*, 1690-1697.

Yuan,Q., Qiu,D.L., Weber,J.T., Hansel,C., and Knopfel,T. (2007). Climbing fiber-triggered metabotropic slow potentials enhance dendritic calcium transients and simple spike firing in cerebellar Purkinje cells. Molecular and Cellular Neuroscience *35*, 596-603.

Zempel,J.M. and Steinbach,J.H. (1995). Neonatal rat cerebellar granule and Purkinje neurons in culture express different $GABA_A$ receptors. European Journal of Neuroscience *7*, 1895-1905.

Zezula,J., Slany,A., and Sieghart,W. (1996). Interaction of allosteric ligands with $GABA_A$ receptors containing one, two, or three different subunits. European Journal of Pharmacology *301*, 207-214.

Zhang,J.H., Sato,M., and Tohyama,M. (1991). Different postnatal development profiles of neurons containing distinct $GABA_A$ receptor β subunit mRNAs (b_1, b_2, and b_3) in the rat forebrain. Journal of Comparative Neurology. *308*, 586-613.